Remote force application to the T cell receptor modulates $CD4^+$ T cell activation



Joseph Clarke

Institute of Healthcare Technologies

School of Chemical Engineering

University of Birmingham

A thesis submitted for the degree of

Doctor of Philosophy

January 2023

UNIVERSITY OF
BIRMINGHAM

University of Birmingham Research Archive

e-theses repository

This unpublished thesis/dissertation is copyright of the author and/or third parties. The intellectual property rights of the author or third parties in respect of this work are as defined by The Copyright Designs and Patents Act 1988 or as modified by any successor legislation.

Any use made of information contained in this thesis/dissertation must be in accordance with that legislation and must be properly acknowledged. Further distribution or reproduction in any format is prohibited without the permission of the copyright holder.

Abstract

Whilst T cell receptor (TCR) signalling pathways become increasingly well understood, the precise mechanism by which TCR triggering is achieved remains elusive. Models of TCR triggering surrounding TCR aggregation or segregation from inhibitory phosphatases have provided compelling insight, but these models have their limitations and fail to fully address how the TCR is able to trigger upon recognition of cognate antigen. Recent studies propose that the TCR is able to function as a mechanosensor, whereby it can directly interpret the mechanical cues it encounters and translate these into internal biochemical signals. However, whilst these studies are mechanistically revealing, they fail to address if force application to the TCR can achieve robust T cell activation and modulate T cell phenotype.

Here, we utilise small magnetic nanoparticles (MNPs, 0.25-1μm diameter) functionalised with anti-CD3 antibodies to transfer forces to the TCR in the presence of external dynamic magnetic fields. We show that force application to the TCR increases TCR signal strength to reach the thresholds required for T cell activation. We find that these thresholds are reached through force mediated membrane remodelling of the TCR complex and subsequent accumulation of downstream signalling intermediates. Interestingly, force application to MNPs functionalised with higher levels of antibody, which provide a higher TCR signal strength in the absence of force, dampened T cell activation and induced co-inhibitory receptor expression, suggestive of additional negative feedback thresholds set higher than thresholds for T cell activation.

The data presented in this thesis thus supports a concept whereby force application to the TCR promotes TCR signalling, membrane TCR remodelling and has further consequences on downstream CD4+ T cell activation.

Acknowledgements

Firstly, I would like to extend sincere thanks to Professor David Wraith, for his constant encouragement and support not only throughout the course of this PhD, but in encouraging me to pursue a PhD to begin with. Thank you for sharing your experiences, scientific insight, knowledge, and of course numerous incredible anecdotes over the past 5 and a half years that I have been part of the Wraith lab. Thank you to Professor Alicia El Haj and all members of the El Haj lab for continuous support, guidance and laughs over the past 3 years!

Thank you to all members of the Wraith lab for their support, advice, and insight, together with providing fascinating discussion and continuous laughter throughout this PhD. You have made my time within the lab incredibly fun and enjoyable. Special thanks to Heather for showing me the ropes within the lab back in 2017 and always providing help on a daily basis. Additional special thanks to Sky for fascinating discussion surrounding this project and for sparing so much time to help design, build and operate several pieces of kit!

A huge thank you to my parents for their continual support and belief in me, and constant encouragement to push myself. Thank you for everything that you have done for me (and indeed continue to do for me!)

Finally, no thanks are enough for my partner Samantha. I simply would not have made it through the past 3 years without your unconditional support, love and encouragement to keep going. Our lives have changed and developed quite amazingly over the past 3 years, through some of the strangest times that we are likely to experience! I look forward to our future together!

List of Contents

Abstract 1

Acknowledgements 2

Table of contents 3

List of figures and tables 8

List of abbreviations 13

Table of Contents

CHAPTER 1 22

1 Introduction 22

1.1 T Cell Development and Subsets 22

1.2 T Cell Function 24

1.3 T Cell Receptor Structure 28

1.4 T Cell Receptor Signalling and Cell Activation 30

1.5 Checkpoint Inhibitor Signalling and T Cell Anergy 34

1.6 Immune Synapse Formation 39

1.7 T Cell Receptor Triggering Models 43

1.7.1 Aggregation Based Models 44

1.7.2 Segregation Based Models 47

1.7.3 The Kinetic Proofreading Model 50

1.7.4 Conformational Change Based Models 53

1.7.5 Mechanosensing Based Models 58

1.8 Introduction to Mechanosensing 64

1.8.1 Integrin mechanosensing 65

1.8.2 Piezo Mechanosensing 68

1.8.3 TRPV4 Mechanosensing 69

1.8.4 TREK Mechanosensing 70

1.9 Mechanosensing in the Immune System 71

1.10 Project Aims 76

1.11 Future Work 78

CHAPTER 2 80
2 Materials and Methods 80
2.1 Mice 80
2.2 Tissue Culture 82
2.3 Isolation of CD4 or CD11c cells 82
2.4 Magnetic Particle Functionalisation Buffers 83
2.5 Magnetic Particle Functionalisation Protocol 83
2.6 Treatment of CD4 T cells with Functionalised MNPs 87
2.7 Magnetic Force Application Experiments - MICA 87
2.8 T Cell Activation Assays 89
2.8.1 Activation Marker Expression at 4 hours post Magnetic Force Application 89
2.8.2 Proliferation and Cytokine Production Assays 90
2.8.3 Signalling Protein Phosphorylation Experiments 90
2.9 Flow Cytometry 91
2.9.1 Surface staining for T cell activation, T cell phenotype and TCR expression 91
2.9.2 Intracellular Staining for Cytokine Production 93
2.9.3 Phospho-protein Staining 94
2.9.4 MNP Quality Control Staining 94
2.9.5 Surface vs Cycling vs Total TCR analysis 95
2.9.6 Transcription Factor Staining, and FoxP3/IL-10 Dual Staining 96
2.10 Confocal Microscopy 97
2.10.1 Confocal Microscopy for Membrane CD3 Distribution - Protocol 97
2.10.2 Confocal Microscopy for Membrane CD3 Distribution – Acquisition and Analysis 98
2.10.3 Confocal Microscopy for CD45 Localisation – Protocol 99
2.10.4 Confocal Microscopy for CD45 Localisation – Analysis 100
2.11 Production of a Halbach Array for Shear Force Application 101
2.11.1 Halbach Array Design 101
2.11.2 Halbach Array Magnetic Field Profiles and Force Calculations 102
2.11.3 Calcium Signalling Experiments 103
2.12 Single Molecule Localisation Microscopy 105
2.13 $CD4^+$ T Cell Restimulation and Phenotype Assessment 106
2.13.1 Co-Inhibitory Receptor Blockade 107
2.14 Enzyme Linked Immunosorbent Assays 107

2.15 Immune Suppression Assays 109
2.15.1 Inhibition of Naïve CD4+ T cell Proliferation 109
2.15.2 DC – Putative Suppressor Co-Cultures 111
2.16 *In vitro* Th1 Polarisation 112
2.17 Data Representation and Statistical Analysis 113
CHAPTER 3 114
3 External Force Application to the TCR to Influence TCR Triggering 114
3.1 Introduction 114
3.2 Optimisation of 250nm MNPs for External Force Application 117
3.2.1 Force application to 250nm MNPs upregulated Nr4a3 expression 117
3.2.2 Force application for 1hour is required to upregulate Nr4a3 expression 119
3.2.3 Functionalisation with activating antibodies is required to drive TCR signalling 120
3.2.4 Activation markers CD69 and CD25 are also upregulated with 1 hour magnetic force application to 250nm MNPs 122
3.3 Effect of Co-stimulation on Responses to 250nm MNPs 124
3.4 Increased anti-CD3/CD28 Loading on 250nm MNPs Negates Effect of Magnetic Force 127
3.5 Optimisation of 1µm MNPs for External Magnetic Force Application 128
3.6 Effect of Magnetic Force on T Cell Activation in Transgenic Mouse Models 135
3.6.1 Tg4 vs RTO vs B10.PL 135
3.7 T Cell Activation in Response to Functionalised MNPs are TCR Triggering Specific 139
3.8 External Magnetic Force Drives Nuclear Accumulation of Transcription Factors . 141
3.9 Effect of Magnetic Force Application on CD4+ T Cell Proliferation and Cytokine Production 149
3.9.1 250nm MNPs 150
3.9.2 1µm MNPs 152
3.10 Discussion 155
3.10.1 Force Application for T Cell Activation 155
3.10.2 Correlation between TCR engagement and T cell activation 161
3.10.3 TCR Signalling Thresholds for T Cell Activation 162
3.10.4 Concluding Remarks 165
CHAPTER 4 167

4 TCR Mobilisation and Clustering – A Potential Mechanism of Action for Magnetic Force Induced TCR Triggering 167
4.1 Introduction 167
4.2 Force Application Induces TCR Downregulation 168
4.2.1 TCR Downregulation occurs under the same conditions as force induced TCR triggering 168
4.2.2 Magnetic force induced TCR downregulation acts through manipulation of the TCR-CD3 complex 170
4.2.3 TCR downregulation occurs in a magnetic force directional manner 172
4.2.4 Alteration of signal 1 strength on 1µm MNPs correlates with the degree of TCR downregulation 176
4.3 Cycling TCR Staining Protocols Catch TCR Downregulation in the act 179
4.4 TCR Downregulation Occurs Concurrently with TCR Triggering 184
4.4.1 TCRhi/TCRlo analyses and expression of TCR signalling markers 184
4.5 Cytoskeletal Dynamics Control TCR Downregulation 191
4.6 Blockade of Active TCR Signalling Prevents TCR Downregulation 193
4.7 Force Application Induces CD45 Segregation from Particle-Membrane Contact Zones 196
4.8 Single Molecule Microscopy Reveals the Presence of Force Induced TCR Clustering 201
4.9 Discussion 207
4.9.1 Force Induced TCR Re-Organisation as a Mechanism of Promoting T Cell Activation 209
4.9.2 Mechanical Activation of the TCR to promote TCR-MC formation 211
4.9.3 Comparisons of Normal and Shear Motion Applications 213
4.9.4 Concluding Remarks and Future Experimentation 215
CHAPTER 5 217
5 Force Modulated Signal 1 Strength – Effect on $CD4^+$ T Cell Phenotype and Function .. 217
5.1 Introduction 217
5.2 Force Modulation of Activation Marker and Co-Inhibitory Receptor Expression . 220
5.3 Exogenous IL-2 Fails to Reverse the High Signal 1 Strength Induced Anergic Phenotype 228
5.4 Co-Inhibitory Blockade Fails to Reverse the High Signal 1 Strength Induced Anergic Phenotype 230
5.5 Increased Antigenic Dose Reveals High Signal 1 Strength Induced Antigenic Insensitivity Upon Restimulation 234

5.5.1 Persistent TCR Downregulation Mediates the Antigen Insensitivity Phenotype 236
5.6 Immune Suppression Studies 237
5.6.1 Co-inhibitory receptor high $CD4^+$ T cells stimulated with $1\mu m^{Hi}$ MNPs fail to induce immune suppression at day 3 237
5.6.2 Treatment of $CD4^+$ T cells with CAL101 induces a $FoxP3^-$ $IL\text{-}10^+$ suppressive population by day 7 242
5.7 Discussion 251
5.7.1 Signal 1 strength modulation of $CD4^+$ T cell phenotype 251
5.7.2 Distinct mechanisms of immune suppression linked to TCR signal strength . 253
CHAPTER 6 257
6 General Discussion 257
6.1 Introduction 257
6.2 Force application to the TCR modulates TCR signalling strength and commits cells to T cell activation 259
6.2.1 Force application induces specific TCR triggering, reaching thresholds required for T cell activation 259
6.2.2 Force application serves to modulate TCR signal strength 264
6.3 Pseudo Immune Synapse formation likely mediates the effects of magnetic force 268
6.3.1 Particle size is a key determinant in promoting TCR signalling 268
6.3.2 Hallmarks of immune synapse formation – Concurrent TCR downregulation and activation, and CD45 exclusion 270
6.4 Force modulation of $CD4^+$ T cell phenotype and therapeutic outlook 274
CHAPTER 7 277
7 References 277
CHAPTER 8 299
8 Appendix 299
8.1 TCR Downregulation Kinetics with $1\mu m^{Mid}$ MNPs 299
8.2 Inhibition of Calmodulin with Cyclosporin A Does Not Inhibit TCR Downregulation 300
8.3 Halbach Array Calcium Signalling Experiments 300
8.4 Magnetic Force Application to Tg4 Th1 cells Fails to Upregulate T Cell Activation Marker CD69 303
8.5 Surface Expression of Antigen Presentation Machinery Proteins by PL8 Cells 304

8.6 Blockade of CTLA-4 and PD-1 does not reverse the anergic phenotype observed in 1μm^{Hi} MNP stimulated cells 305

8.7 Surface Phenotype of CD4^{+} FoxP3- T cells in Suppression Assays 306

8.8 Pulsatile Magnetic Force Application to 1μm^{Hi} MNPs Appears to Prevent CTLA-4 Upregulation..... 307

List of Figures and Tables

Figure 1.1 - CD4$^+$ T cell differentiation subsets, master transcription factor expression and subset effector function. 27
Figure 1.2 - TCR and CD28 Signalling Events Promoting T Cell Activation.. 32
Table 1.1 – Summary of main co-inhibitory receptors and their mechanism of action. 38
Figure 1.3 - Summary of CD4 T cell activation phenotype based on differential activation or deactivation signalling pathway initiation. 39
Figure 1.4 – Summary of proposed TCR triggering models. 44
Figure 1.5 - Aggregation based models of TCR triggering. 47
Figure 1.6 - The segregation model of TCR triggering. 50
Figure 1.7 - The kinetic proofreading model of TCR triggering. 53
Figure 1.8 – Catch Bond Mediated TCR Signalling – A Unified Model of TCR Triggering..... 64
Table 1.2 - Evidence for Integrin Catch Bond Behaviour 67
Table 2.1 - Antibodies used to phenotype Tg4 and Tg4 CD45.1 mice. 81
Table 2.2 – Antibodies used for MNP Functionalisation. 85
Equations 2.1 - Calculations for number of antibodies added per surface area unit. 86
Table 2.3 - Levels of antibody per surface area unit for particle used. 86
Figure 2.1 - Direction of force application to individual TCRs with MICA. 88
Equation 2.2 - Force calculations for MNPs on a MICA bioreactor.. 89
Table 2.4 - Magnetic Forces for Functionalised MNPs on a MICA bioreactor.. 89
Table 2.5 - Surface antibodies used for flow cytometry 93
Table 2.6 - Antibodies used for intracellular cytokine staining..... 93
Table 2.7 - Antibodies used in phospho-protein staining 94
Table 2.8 - Staining antibodies used for surface vs cycling vs total TCR analysis 95
Table 2.9 – Intracellular antibodies used for transcription factor staining. 96
Table 2.10 - Staining procedure used in CD3 membrane localisation experiments. 98
Figure 2.2 – Birds eye view of the magnet arrangement within the Halbach array. 102
Figure 2.3 - Modelling of halbach array field profiles through one full rotation. 102
Table 2.11 – ELISA Reagents..... 109
Table 2.12 - Antibodies used for surface staining in DC – putative suppressor co-culture assays. 111
Figure 3.1 – Optimisation of 250nm^{Mid} MNP concentration for TCR signalling studies. .. 118
Figure 3.2 – Force application for 1 hour drives an upregulation of Nr4a3 expression. ... 119
Figure 3.3 – Functionalisation of 250nm MNPs with non-activating antibodies fails to promote upregulation of Nr4a3 expression. 121
Figure 3.4 - CD69 and CD25 are also upregulated with 1 hour of Magnetic Force Application...... 123
Figure 3.5 - Effect of Co-stimulation on Responses to 250nm^{Mid} MNPs. 126
Figure 3.6 - Optimisation of Surface Antibody Concentration on 250nm MNPs...... 127
Figure 3.7 - Increasing Surface Antibody Concentration on 250nm MNPs Bypasses Magnetic Force Induced T Cell Activation.. 128
Equation 3.1 - Surface Area Calculations for 1µm and 250nm MNPs. 129

Figure 3.8 - Optimisation of particle concentration for 1µm MNPs. 131
Figure 3.9 - Force application to 1µm^{Hi} or 1µm^{Mid} MNPs induces differential effects on TCR signalling. 133
Figure 3.10 - Surface CD3 on functionalised 250nm and 1µm MNPs. 134
Figure 3.11 - Effects of Magnetic Force on TCR Signalling - Tg4 vs RTO Experiments. 137
Figure 3.12 - Effect of Magnetic Force Application on TCR Signalling in B10.PL Mice. 138
Figure 3.13 - PP2 Blockade Inhibits Magnetic Force Induced TCR Signalling to 250nm^{Mid} anti-CD3 MNPs. 140
Figure 3.14 - PP2 Blockade Inhibits Magnetic Force Induced TCR Signalling to 1µm^{Mid} CD3 MNPs. 141
Figure 3.15 - Magnetic Force Application Does Not Specifically Influence TCR Signalling Pathways. 143
Figure 3.16 - Schematic of Force Induced Signal Accumulation Experimental Protocol. 144
Figure 3.17 - Pulsatile Magnetic Force Treatment Leads to an Accumulation of Nr4a3 Expression. 145
Figure 3.18 - Cyclosporin A (CsA) Addition to Probe Nuclear Accumulation of NFAT. 147
Figure 3.19 - Pulsatile Magnetic Force Treatment Drives Nuclear NFAT Accumulation. 148
Figure 3.20 - Representative CTV traces for 250nm MNP stimulated CD4$^+$ Tg4 T cells. 150
Figure 3.21 - CTV Analysis from 250nm MNP proliferation experiments. 151
Figure 3.22 - ICCS analysis of IFNγ and IL-2 production in response to 250nm MNPs and magnetic force. 152
Figure 3.23 - Representative CTV traces from 1µm MNP proliferation assays. 153
Figure 3.24 – CTV analysis from 1µm MNP proliferation experiments. 154
Figure 3.25 – ICCS analysis of IFNγ and IL-2 production in response to 1µm functionalised MNPs and magnetic force. 155
Figure 3.26 - Calcium Signals Induced Downstream of the TCR. 156
Figure 3.27 - Src kinase inhibition proves TCR signalling responses to functionalised MNPs are TCR specific. 157
Table 3.1 - Correlation between antibodies per surface area unit on the particle surface and T cell activation with magnetic force application. 161
Figure 3.28 – Summary illustration of magnetic force (MF) induced accumulation of signalling intermediates along the TCR-NFAT pathway, which promotes robust T cell activation. 166
Figure 4.1 – Force induced TCR downregulation occurs under the same conditions with which force induces T cell activation. 169
Figure 4.2 – Influence of co-stimulation on TCR downregulation kinetics. 170
Figure 4.3 - TCR downregulation accumulates over the time course of magnetic force application reaching a maximum at 1 hour of force application. 172
Figure 4.4 - Membrane distribution of TCR-CD3 complex with magnetic force treatment. 173
Figure 4.5 – TCR-CD3 downregulation occurs in a magnetic field dependent directional manner (A) and accumulates across the time course of force application (B). 174
Figure 0.1 - TCR expression in response to force application to anti-CD3 functionalised 1µm MNPs… 176

Figure 4.7 - Representative TCR histograms from 1µm MNP experiments. 178
Figure 4.8 – TCR downregulation kinetics in response to 1µm^{Mid} MNPs and force application show that TCR downregulation accumulates across the time course. 179
Figure 4.9 - Surface vs Cycling vs Total TCR staining protocols for 250nm MNPs Reveals TCR Internalisation. 181
Figure 4.10 – Surface vs Cycling vs Total TCR Expression for 1µm^{Mid} MNP stimulated CD4^{+} T cells. 182
Figure 4.11 - Surface vs Cycling vs Total TCR Analysis for 250nm^{Mid} anti-CD3 MNPs. 183
Figure 4.12 - Surface vs Cycling vs Total TCR Analysis for 1µm^{Mid} MNPs. 183
Figure 4.13 - Magnetic Force Induces TCR Downregulation and Activation Marker Expression Concurrently in Response to 250nm MNPs. 185
Figure 4.14 - Magnetic force Application Induces TCRlo Nr4a3+, CD69+ and CD25+ cells in Response to 1µm^{Mid} MNPs. 186
Figure 4.15 – Normal Force Application Induces TCRlo Nr4a3^{+} CD4^{+} Phenotypes – 250nm^{Mid} MNPs. 189
Figure 4.16 – Normal Force Application to 1µm^{Mid} MNPs induces TCRlo Nr4a3^{+} CD4^{+} Phenotypes. 190
Figure 4.17 - Blockade of the actin cytoskeleton with Latrunculin A blocks TCR downregulation. 192
Figure 4.18 - Inhibition of TCR downregulation with Latrunculin A Prevents Nr4a3 Expression. 193
Figure 4.19 - Blockade of active TCR signalling by treatment with 10µM PP2 prevents force induced TCR downregulation. 195
Figure 4.20 - PP2 Treatment Prevents Force Induced TCR Downregulation. 196
Figure 4.21 - Representative Images from CD45 Confocal Microscopy Experiments. 198
Figure 4.22 - Force application to 250nm^{Mid}and 1µm^{Mid} anti-CD3 MNPs induce CD45 exclusion from particle-membrane contact zones. 199
Figure 4.23 - Force induced CD45 exclusion relies on actin polymerisation and active TCR-CD3 phosphorylation. 200
Figure 4.24 – Representative images from STORM experiments mapping surface TCR organisation with magnetic field stimulation. 202
Figure 4.25 - Single molecule cluster maps from STORM Image Analysis. 204
Figure 4.26 – Force application induces TCR cluster formation with 5 and 15 minutes. 205
Figure 4.27 – TCR cluster formation is dependent on TCR phosphorylation. 207
Figure 4.28 - Hypothesis for differential signalling responses with normal and shear force application. 214
Figure 5.1 - High signal 1 strength MNPs induce an anergic phenotype upon restimulation through the TCR. 220
Figure 5.2 – Stimulation with 1µm^{Hi} MNPs alters IL-2 and IFNγ secretion upon rechallenge with APC and peptide. 222
Figure 5.3 – Co-inhibitory receptor expression on CD4^{+} T cells stimulated with 250nm anti-CD3 MNPs is dependent on peptide concentration at the point of restimulation. 223
Figure 5.4 – Stimulation of CD4^{+} T cells with 1µm^{Mid} MNPs fails to induce robust co-inhibitory receptor expression. 224

Figure 5.5 – Stimulation of CD4$^+$ T cells with 1µm^{Hi} MNPs induces robust co-inhibitory receptor expression which is further upregulated by force application. 226
Figure 5.6 – Force application to 1µm^{Hi} MNPs increases co-expression of CTLA-4 and Tigit. 227
Figure 5.7 – PD-1 expression gated on CTLA-4$^+$ Tigit$^+$ CD4$^+$ T cells identifies that PD-1 expression correlates with T cell activation. 228
Figure 5.8 - Provision of exogenous IL-2 does not reverse the high signal 1 strength induced anergic phenotype. 230
Figure 5.9 - CTLA-4 blockade does not restore ability to respond to restimulation through the TCR. 232
Figure 5.10 - CTLA-4 blockade does not restore IFNg or IL-2 production in response to TCR stimulation. 233
Figure 5.11 - CD69 expression via TCR stimulation is recovered by increased antigenic strength at restimulation in CD4$^+$ T cells stimulated with 1µm^{Hi} MNPs. 235
Figure 5.12 – Increased peptide concentration recovers IFNγ and IL-2 secretion in 1µm^{Hi} MNP stimulated CD4$^+$ T cells. 235
Figure 5.13 – TCR downregulation persists out to 72 hours in CD4$^+$ T cells stimulated with 1µm^{Hi} MNPs. 236
Figure 5.14 – Co-culture with 1µm:1µg stimulated putative suppressors mediates moderate immune suppression of naïve Tg4 CD45.1$^+$ CD4$^+$ T cells. 238
Figure 5.15 – FoxP3$^+$ expression, and surface phenotype of FoxP3$^+$ CD4$^+$ T cells at day 3 upon stimulation with 1µm^{Mid} or 1µm^{Hi} MNPs. 239
Figure 5.16 - Addition of exogenous IL-2 appears to partially reverse the observed immune suppression. 240
Figure 5.17 - Treatment with CAL101 fails to restore FoxP3 expression in 1µm^{Hi} stimulated CD4$^+$ T cells. 241
Figure 5.18 - CAL101 treatment fails to enhance immune suppression when putative suppressors are used at 72 hours. 242
Figure 5.19 - 1µm anti-CD3 MNP stimulated putative suppressors secrete low levels of IL-10 when used at 72 hours. 242
Figure 5.20 – Day 7 FoxP3 expression and surface phenotype of FoxP3$^+$ CD4$^+$ T cells in response to 1µm anti-CD3 MNP stimulation. 243
Figure 5.21 - Treatment of CD4$^+$ T cells with CAL-101 fails to restore FoxP3 expression by day 7. 244
Figure 5.22 – 1µm^{Hi} and CAL101 treated putative suppressors induce robust immune suppression when used at day 7. 245
Figure 5.23 – 1µm^{Hi} and CAL101 treated putative suppressors secrete the highest levels of IL-10. 246
Figure 5.24 – ICCS analysis reveals the Vβ8$^+$ CD45.1$^-$ CD4$^+$ putative suppressor population as the producers of IL-10 in immune suppression co-culture assays. 247
Figure 5.25 – Emergence of a FoxP3$^-$ IL-10$^+$ population correlates with TCR signal 1 strength and is increased by CAL101 treatment to 1µm^{Hi} stimulated CD4$^+$ T cells. 248
Figure 5.26 - Representative FACS plots from FoxP3 and IL-10 co-staining experiments described in figure 5.25. 249

Figure 5.27 – Co-culture of 1µm^{Hi} and CAL101 treated putative suppressors with B10.PL CD11c^{+} DCs at day 7 modulates DC surface expression of CD80 and CD86. 251
Figure 6.1 - Force application modulates TCR signal strength.. 265
Figure 6.2 - Proposed threshold involved in TCR signalling and T cell activation...... 266
Figure 6.3 – A proposed mechanism of action for force mediated TCR signalling. 273
Figure 8.1 - TCR downregulation kinetics in response to 1µm^{Mid} MNPs and magnetic force application.. 299
Figure 8.2 - Blockade of the NFAT pathway with CsA does not prevent force induced TCR downregulation. 300
Figure 8.3 – Calcium signalling with shear force application – 250nm^{Mid} MNPs. 302
Figure 8.4 – Calcium signalling with shear force application – 1µm MNPs. 302
Figure 8.5 - Magnetic force application to Tg4 Th1 cells fails to induce upregulation of CD69.. 303
Figure 8.6 - Cell surface expression of proteins involved in the antigen presentation machinery by PL8 cells. 304
Figure 8.7 - PD-1 blockade or dual CTLA-4 and PD-1 blockade does not restore TCR dependent CD69 expression.. 305
Figure 8.8 - Cell surface co-inhibitory receptor expression on 1µm MNP stimulated FoxP3^{-} CD4^{+} T cells at 72 hours.. 306
Figure 8.9 - Cell surface co-inhibitory receptor expression on 1µm MNP stimulated FoxP3^{-} CD4^{+} T cells at day 7.. 306
Figure 8.10 - Pulsatile magnetic force application to 1µm^{Hi} MNPs prevents upregulation of CTLA-4.. 307

List of Abbreviations

$1\mu m^{Mid}$	1µm MNPs functionalised with a total quantity of 1µg anti-CD3 antibody
$1\mu m^{Hi}$	1µm MNPs functionalised with a total quantity of 10µg anti-CD3 antibody
AF488/555/647	Alexa fluor (488/555/647)
AFM	Atomic force microscopy
Aire	Autoimmune regulator gene
APC	Antigen presenting cell
BAC	Bacterial artificial chromosome
BAPN	Beta-aminopropionitrile
BAPTA/Ni^{2+}	1,2-bis(o-aminophenoxy)ethane-N,N,N',N'-tetraacetic acid
BCR	B cell receptor
BFP	Biomembrane force probe
BMDCs	Bone marrow derived dendritic cells
BMSU	Biomedical services unit
BRS	Basic residue sequences
BSA	Bovine serum albumin
Ca^{2+}	Calcium ion
CAR	Chimeric antigen receptor
Cbl	Casitas B-lineage lymphoma
CD	Cytoplasmic domain
CDR	Complementarity-determining regions
CP	Connecting peptide

CRAC	Calcium release activated calcium channels
CRISPR	Clustered regularly interspaced short palindromic repeats
Cas9	CRISPR associated protein 9
CsA	Cyclosporin A
cSMAC	Central supramolecular activation complex
CTLA-4	Cytotoxic T lymphocyte associated protein 4
CTV	Cell trace violet
DAG	Diacylglycerol
DAPI	4’,6-Diamidino-2-Phenylindole
DCs	Dendritic cells
DMSO	Dimethyl sulfoxide
DOX	Doxycycline
dSMAC	Distal supramolecular activation complex
DUSPs	Dual specificity phosphatases
ECD	Ectodomain
ECM	Extracellular matrix
EDAC	N-(3-Dimethylaminopropyl)-N’-ethylcarbodiimide
EGF	Epidermal growth factor
eGFP	Enhanced green fluorescent protein
ELISA	Enzyme linked immunosorbent assay
ER	Endoplasmic reticulum
ERK	Extracellular signal-regulated kinase (ERK)
ESCRT	Endosomal sorting complex required for transport

FACS	Fluorescence associated cell sorting
FCS	Fetal calf serum
FKBP	FK506-binding protein
FoxP3	Forkhead box P3
FRB	FKBP12-rapamycin-binding domain
FRET	Förster resonance energy transfer
GM-CSF	Granulocyte-macrophage colony-stimulating factor
HIV	Human immunodeficiency virus
HRP	Horseradish peroxidase
IC	Intracellular
ICAM-1	Intracellular adhesion molecule 1
ICCS	Intracellular cytokine staining
IFN	Interferon
IL	Interleukin
iNOS	Inducible nitric oxide synthase
IP_3	Inositol 1,4,5-trisphosphate
IS	Immune synapse
ISGs	Interferon stimulated genes
ITAM	Immunoreceptor tyrosine-based activation motif
Itk	IL-2 inducible T cell kinase
KO / dKO	Knockout / Double Knockout
KPR	Kinetic proofreading
Lag3	Lymphocyte activation gene 3

LAT	Linker of activated T cells
Lat A	Latrunculin A
LBPA	Lysobisphosphatidic acid
Lck	Lymphocyte specific tyrosine kinase
LFA-1	Leukocyte functional antigen – 1
LOV2	Light oxygen voltage sensing domain 2
LOX	Lysyl oxidase
LPS	Lipopolysaccharide
LSM	Laser scanning microscopy
MAPK	Mitogen-activated protein kinase
MBP	Myelin basic protein
MCC	Moth cytochrome c
MEA	Mercaptoethilamine
MES	4-morpholinoethanesulfonic acid
MF	Magnetic force
MFI	Mean fluorescence intensity
MHC	Major Histocompatibility Protein
MICA	Magnetic ion channel activation
MNP	Magnetic nanoparticles
MSCs	Mesenchymal stem cells
mTOR	Mammalian target of rapamycin
NFAT	Nuclear factor of activated T cells
NF-κβ	Nuclear factor κβ

NHS	N-hydroxysuccinimide
Ni^{2+}	Nickel ion
NMR	Nuclear magnetic resonances
Nr4a3-FT	Nr4a3 – fluorescent timer
Opto-CAR	Optically controlled CAR
OVA	Ovalbumin
PAF	Platelet activating factor
PBS	Phosphate buffered saline
PBS-T	PBS – Tween
PD-1	Programmed death 1
PD-L1	Programmed death 1-ligand 1
PDMS	Polydimethylsiloxane
PEG-PDLLA	Poly(ethylene-glycol)-block-poly(D,L-lactide)
PFA	Paraformaldehyde
PI	PMA-Ionomycin
PI3K	Phosphoinositide 3-kinase
PIGS	PI + GolgiStop
PIP_2 / PIP_3	Phosphatidylinositol-4,5-bisphosphate / Phosphatidylinositol-3,4,5-trisphosphate
PKCθ	Protein kinase C θ
PLCγ	Phospholipase C γ
PLL	Poly-l-lysine
PMA	Phorbol 12-myristate 13-acetate

pMHC	Peptide-MHC
PP2	4-amino-5-(4-chlorophenyl)-7-(t-butyl) pyrazolo[3,4-d]pyrimidine)
PRS	Proline rich sequence
pSMAC	Peripheral supramolecular activation complex
PTEN	Phosphatase and tensin homolog
pTreg	Peripheral Treg
RAG	Recombination Activating Gene
RAS-GRP	RAS – Guanyl nucleotide-releasing protein
SDFL	Site directed fluorescence labelling
SEV9	Sendai virus derived peptide
SFK	Src family kinases
SH2 / SH3	Src homology domain 2 / Src homology domain 3
SHP-1	Src homology region 2 domain containing phosphatase 1
SLB	Supported lipid bilayer
SMLM	Single molecule localisation microscopy
STORM	Stochastic optical reconstruction microscopy
TAG	SV40 large T antigen epitope 1
Tbet	T-box expressed in T cells
TCR	T Cell Receptor
TCR-MCs	TCR microclusters
TdT	Terminal deoxynucleotidyl transferase
TEC	Thymic epithelial cells
Tfh	T follicular helper cell

TGFβ	Transforming growth factor β
Th	T helper cell
TIRF	Total internal reflection fluorescence
TM / TMD	Transmembrane / Transmembrane domain
TMB	3,3’,5,5’-Tetramethylbenzidine
TNFα	Tumour necrosis factor α
Tox	Thymocyte selection-associated HMG box
Treg	Regulatory T cell
TREK1	Twik-related potassium channel 1
TRPV	Transient receptor potential vanilloid-type ion channels
TSG101	Tumour susceptibility gene 101
UD	Unique domain
VCAM-1	Vascular adhesion molecule 1
WASP	Wiskott-Aldrich Syndrome protein
WIP	WASP interacting protein
WT	Wild type
ZAP-70	Zeta chain associated protein 70kDa

CHAPTER 1

1 Introduction

1.1 T Cell Development and Subsets

T cells, aptly named as a consequence of their development in the thymus, are critical mediators of the adaptive immune response. Central to their function is their ability to recognise antigenic peptides, presented in complex with major histocompatibility proteins (MHC, loaded with peptide to become pMHC) mostly commonly presented by a specialised group of cells known as antigen presenting cells. In the healthy individual, this process occurs with exquisite sensitivity where any given T cell expresses a clonal T cell receptor (TCR) specific for an individual pMHC molecule. This TCR not only mediates recognition of cognate pMHC but also must remain inert to the sea of closely related self-pMHC molecules, recognition of which would permit auto-immune responses against the body's own tissues.

T cell development in the thymus produces the pool of TCRs released to the periphery that are then responsible for mounting immune responses against foreign antigens or cancer associated neoantigens. Within the thymus, T cell progenitors that lack expression of either a CD4 or CD8 co-receptor, undergo somatic rearrangement of the TCR α and β chain loci as a first step in gene-rearrangements that permit an extraordinarily large number of different αβTCRs to be expressed, estimated to be in the range of 10^{15} different αβTCRs[1,2]. TCRα chains are made up via recombination of variable (V) and joining (J) gene regions, whilst β chains are made up of V, diversity (D) and J regions. Expression of a wide range of different variations of each gene segment provides the basis for combinatorial diversity in the wide variety of αβTCR clones through recombination activating gene (RAG) mediated

VDJ gene recombination[2–4]. Adding to this diversity is the process of junctional diversity, where random addition of nucleotides at joining regions between these gene segments, mediated by the enzyme terminal deoxynucleotidyl transferase (TdT), results in the presence of amino acids in the TCRα and β chains that are not encoded for in the germline[5].

Production of this TCR repertoire is then tested within the thymus before these T cells are released to the periphery. The thymus is a highly specialised organ whose structure is specifically adapted to allow for this screening of the TCR repertoire to take place. Initially within the thymic cortex, expression of MHC proteins (either MHC class I or II) by cortical thymic epithelial cells (cTEC) allows for presentation of pMHC molecules to these TCRs[6,7]. Here, developing T cells express a pre-TCR, which consists of a re-arranged β chain paired with an invariant precursor α chain. Signalling through a functional pre-TCR induces the arrest of β chain gene rearrangement, permits α chain rearrangement, and expression of both CD4 and CD8 co-receptors, resultant in a double positive (DP, $CD4^+$ $CD8^+$) T cell population[3,4,6]. These developing T cells then migrate to the thymic medulla, where they undergo positive and negative selection processes mediated by antigen presentation by medullary thymic epithelial cells (mTEC)[8,9]. Expression of the autoimmune regulator gene (Aire) by mTEC provides the ability to express various self-antigens, that would otherwise be absent within the thymus[9,10], against which rearranged TCRs are tested.

Ultimately, a large number of TCRs will be non-productive and unable to bind pMHC complexes and die by neglect as a result[6]. Many TCRs, however, will bind with high affinity and would be unsuitable for release to the periphery. T cells bearing these TCRs receive apoptotic signals and are subsequently deleted by negative selection[6,8]. However, those cells bearing TCRs that bind with an intermediate affinity are permitted to develop and are

released to the periphery following positive selection[9]. Positive selection processes drive differentiation of these developing DP T cells into $CD4^+$ or $CD8^+$ single positive (SP) T cells with a functional TCR dependent on whether positive selection was induced by antigen presentation via MHC class I or II, for CD8+ or $CD4^+$ SP T cells respectively[11]. Finally, recognition of self-antigens with an affinity between the positive and negative selection thresholds, where TCR avidity is sufficiently high to pass positive selection but is just below the threshold for negative selection, is known to be involved in differentiation of natural regulatory T cells (Treg) within the thymus[12,13]. Thymic derived Treg cells, characterised by expression of the Forkhead box P3 (FoxP3) transcription factor, are then released to the periphery and are capable of mediating immune suppression as a mechanism of establishing peripheral tolerance against self-antigen[12,13].

Single positive CD4 or CD8 T cells are then released to the periphery in a non-activated state known as 'naïve'. These cells then patrol the body via the lymphatic system in search of their cognate antigen that their newly expressed αβTCR is specific for. In secondary lymphoid organs (i.e., the spleen or lymph nodes) antigen presenting cells present antigen via MHC proteins to naïve T cells to permit their activation as discussed later[14]. In brief, protein degradation (either foreign or self-derived) results in short peptide fragments that are loaded onto MHC proteins, which are then expressed on the cell surface of APCs to permit pMHC recognition by TCRs[15]. Antigen recognition by T cells induces robust activation, differentiation, clonal expansion, and effector function as discussed next.

1.2 T Cell Function

Following activation in the secondary lymphoid organs, primed T cells migrate from the lymphatics to the periphery to carry out their effector function. In brief, $CD8^+$ T cells are

cytotoxic T cells which mediate killing of cells displaying cognate pMHC-I molecules on their cell surface. $CD8^+$ T cells can induce their effector functions through the production of effector molecules such as perforin and granzyme B, which act together to induce apoptosis within the target cell[16]. Perforin is a pore forming protein that permits entry of granzyme B, a pro-apoptotic serine protease that rapidly induces apoptosis within the target cell[17]. $CD8^+$ T cells can also induce apoptosis on target cells through activation induced upregulation of Fas/FasL (CD95/CD95L) on their cell surface[18]. Finally, $CD8^+$ T cells also produce pro-inflammatory cytokines such as IFNγ and TNFα, which are known to induce upregulation of MHC-I molecules can therefore act to promote a robust $CD8^+$ T cell response[19,20].

$CD4^+$ T cell activation and effector function is somewhat more complicated than that of their $CD8^+$ cytotoxic counterparts. $CD4^+$ T cells are termed 'helper' T cells (Th), owing to their ability to orchestrate the immune response, and are activated in the lymphatics in a similar manner to $CD8^+$ T cells, with the key difference being antigen presentation in complex with MHC-II proteins as opposed to MHC-I. The differentiation of naïve $CD4^+$ cells gives rise to various different Th subsets, which confer the ability of the body to handle the wide variety of pathogens it may encounter. The key determinant for entry to these various differentiation pathways is the cytokine milieu within which antigen recognition initially occurs[20]. The key polarising cytokines that induce various $CD4^+$ T cell differentiation fates, and their differing effector functions are summarised in figure 1.1.

In brief, Th1 cells play a key role in clearance of intracellular pathogens through secretion of IFNγ and IL-2. IFNγ promotes expression of IFNγ stimulated genes (ISGs) by innate immune cells[21], whilst IL-2 promotes robust T cell expansion to promote the ongoing immune response. Th2 cells mediate immune responses to extracellular parasites by

production of IL-4, which triggers production of pro-inflammatory mediators IL-6 and GM-CSF as well as inducing antibody class switching[20,22], whilst Th17 cells produce IL-17 as an effector cytokine to promote pro-inflammatory cytokine production at mucosal or epithelial barrier sites[22,23]. T follicular helper (Tfh) cells mainly produce IL-21 as an effector cytokine and provide key T cell help signals to antigen primed B cells in germinal centres, crucial for their differentiation into antibody secreting plasma cells[20]. Finally, Treg cells are key mediators of peripheral tolerance against self-antigens through production of soluble factors such as IL-10, but also through cell signalling mediated mechanisms through the expression of multiple co-inhibitory receptors[20,22,23].

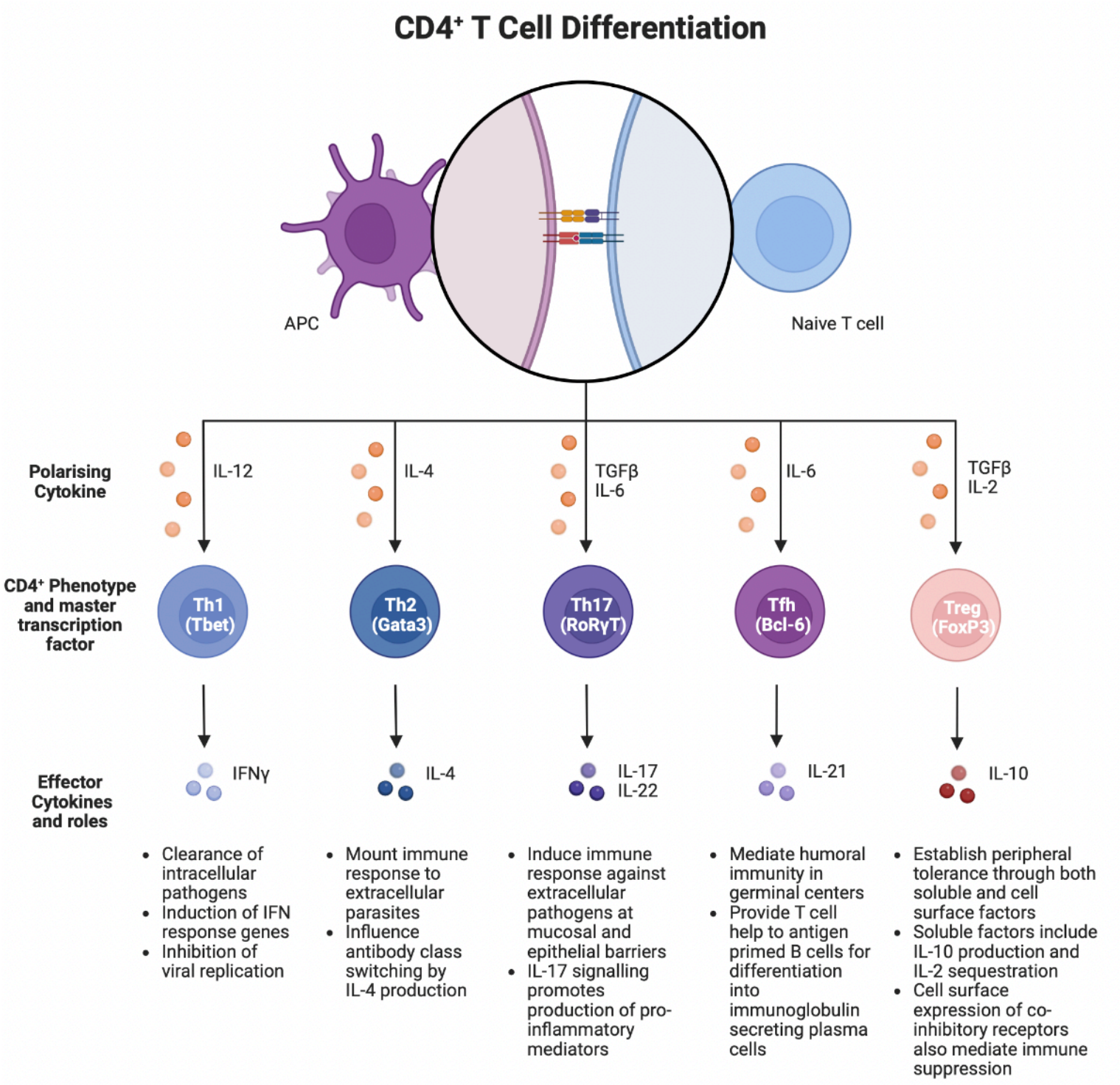


Figure 1.1 - CD4⁺ T cell differentiation subsets, master transcription factor expression and subset effector function. Naïve CD4⁺ T cells are primed against pMHC-II molecules in secondary lymphoid organs to induce differentiation into a wide variety of CD4⁺ T cells subsets. The cytokine milieu within which priming takes place dictates naïve CD4⁺ differentiation. Each CD4⁺ subset have distinct roles, mediated by production of differing effector cytokines to provide the ability to orchestrate the immune response against a variety of infectious agents (Th1, Th2 Th17, Tfh) whilst also inducing immune suppression to maintain peripheral tolerance to self-antigens (Treg). Image created in BioRender.

1.3 T Cell Receptor Structure

The TCR is a multimeric transmembrane complex consisting most commonly of disulphide linked α and β chains [24,25], except in the far less frequent case of the γδTCR which consist of γ and δ chains in place of αβ. T cells bearing a γδTCR have been termed non-conventional T cells, since they are expressed by a relatively small fraction of human peripheral blood T cells (estimates range from 5% [26], to anywhere from 0.5-16% [27]) and do not follow the same classical rules of T cell activation by peptide loaded major histocompatibility (MHC) proteins on the surface of antigen presenting cells (APCs). Due to these factors, the biology of γδTCR activation lies beyond the scope of this research, and thus all reference to the TCR from this point refers to the αβTCR.

The TCR ectodomain consists of constant and variable regions termed CαCβ and VαVβ. Whilst all TCRs share their constant regions, each clonotypic TCR expresses a distinct variable region that mediates antigen recognition. This is a direct result of VJ or VDJ gene recombination as previously described[3,4,28–30], as there is no post expression editing of the TCR to provide diversity in the antigen recognition repertoire as there is for B cell receptors by somatic hypermutation[31]. Three looped structures known as complementarity-determining regions (CDRs) within the variable regions of both the α and β chain (i.e., 6 CDRs in total) confer recognition of individual pMHC molecules[32]. Both α and β chains of the heterodimer contain membrane proximal connecting peptide (CP), transmembrane (TM) and short intracellular regions [24,33–36], yet despite this the TCR itself harbours no intracellular signalling capacity. Therefore, the TCR makes use of cell surface co-expression with immunoreceptor tyrosine-based activation motif (ITAM) expressing CD3 proteins in order to propagate an intracellular biochemical signal upon antigen recognition[33,36,37].

CD3 proteins ε, δ and γ form heterodimers of CD3εγ and CD3εδ with rigid ectodomains and one intracellular ITAM motif per CD3 chain[33,38,39], whilst the CD3ζ chain forms a CD3ζζ homodimer which has a relatively small ectodomain and three ITAM motifs per chain[38–40]. The fully assembled TCR therefore harbours ten ITAM motifs to initiate signal propagation, arising from the 1:1:1:1 stoichiometry with which the completed protein complex is expressed (TCRαβ:CD3εγ:CD3εδ:CD3ζζ)[24,36,38,41]. Following successful assembly within the endoplasmic reticulum, where acidic residues within the CD3 dimer TM regions associate with basic residues within TCRαβ TM regions thereby preventing exposure of ionisable residues within the protein structure, permitting integration into the lipid bilayer hence preventing degradation, the fully assembled complex is integrated into the lipid membrane where antigen recognition and signal propagation can be conferred by the TCRαβ dimer and the CD3 dimers respectively[42,43]. A recent cryo-electron microscope (cryo-EM) structure of the ectodomain, CP and TM regions of the fully assembled TCR-CD3 complex outlined the importance of the TM regions for proper assembly of the complex, reflected in the far greater buried surface for these regions when compared with the ectodomain (3207 $Å^2$ vs 1038 $Å^2$)[24]. An additional cryo-EM resolved TCR structure further indicated the importance of the TM region in TCR-CD3 assembly, where the presence of sterol lipids in the TM region was suggested to promote stabilisation of the TCR-CD3 complex[44]. This cryo-EM structure, of the GPa3b17 TCR in complex with its ligand (gp100 antigen in the context of HLA-A2), also highlighted the importance of membrane proximal cystine residues in the connecting peptide regions in promoting the stability of the interaction between the TCR and the CD3εδ and εγ heterodimers[44]. Interactions between the TM regions of the TCR-CD3 dimers also provide the basis for organisation of the ectodomains, where interactions between TCRα and CD3εδ, and TCRβ and CD3εγ respectively ensure that the TCRαβ heterodimer exists in

the middle of the CD3εγ and CD3εδ ectodomains, with CD3εδ on the side of TCRα and CD3εγ on the side of TCRβ[24,38,41].

1.4 T Cell Receptor Signalling and Cell Activation

Upon pMHC ligation, the first true biochemical event induced in the TCR signalling cascade can be considered the phosphorylation of the dual tyrosine residues within the ITAM motifs motifs (YxxL/I-X_{6-8}-YxxL/I)[45,46] by Src family kinases (SFKs) such as Lck and Fyn[46]. Other TCR signalling events that occur within seconds, such as calcium influx, have been shown to be blocked by the use of the Src kinase inhibitor PP2 and therefore are ITAM phosphorylation dependent[47]. Following ITAM phosphorylation, the zeta chain associated protein of 70kDa (ZAP-70) is recruited to the TCR-CD3 complex, where its SH2 domains bind favourably to the phosphorylated dual tyrosines within the ITAM residues[37]. This interaction permits Src kinase driven ZAP-70 phosphorylation and activation, ultimately resulting in the recruitment of linker of activated T cells (LAT) proximal to the membrane and formation of the LAT signalosome around the membrane tethered LAT molecule[48–50]. LAT possesses many tyrosine residues within its large cytoplasmic domain which become phosphorylated as part of the ongoing TCR signalling cascade and thus serve as docking sites for other adaptor proteins and henceforth mediate their activation[49,51,52]. These proteins include IL-2 inducible T cell kinase (Itk) and phospholipase Cγ (PLCγ) [48,49,52]. Itk activation by Lck[53] allows for Itk mediated PLCγ phosphorylation and activation[48], which cleaves the membrane phosphatidylinositol 4,5-bisphosphate (PIP_2), at which point secondary messengers inositol (1,4,5)-trisphosphate (IP_3) and diacylglycerol (DAG) for signalling pathway initiation are produced[48,53].

IP_3 then triggers the release of intracellular calcium stores from the endoplasmic reticulum (ER), raising the intracellular calcium concentration and opening the calcium release activated channels (CRAC) in the T cell membrane[54,55]. These large calcium influxes into the cell typical of TCR triggering then allows for the progression of the calcineurin-calmodulin pathway which converges on the dephosphorylation of the nuclear factor of activated T cells (NFAT) transcription factor, permitting its entry to the nucleus[48].

DAG initiates two signalling pathways via activation of protein kinase C θ (PKCθ) and RAS-GRP, activating the NF-κβ and MAPK-ERK pathways respectively, ultimately allowing nuclear entry for these transcription factors thus influencing transcription and T cell fate[48,55]. Finally, robust T cell activation is known to occur when TCR ligation occurs concurrently with the activation of co-stimulatory pathways, most commonly achieved through CD28 ligation on the T cell membrane with the B7 ligands CD80/CD86 on the antigen presenting cell. Phosphorylation of the cytoplasmic tail of the CD28 molecule induces recruitment of phosphatidyl-3-kinase (PI3K) which converts PIP_2 to PIP_3. Production of PIP_3 can induce activation of many other signalling proteins involved in the TCR signalling cascase, including Itk, PLCγ1 and AKT[56]. Thus, co-stimulatory signalling pathways synergise with TCR signalling pathways to promote robust T cell activation. These signalling events responsible for T cell activation are summarised in figure 1.2.

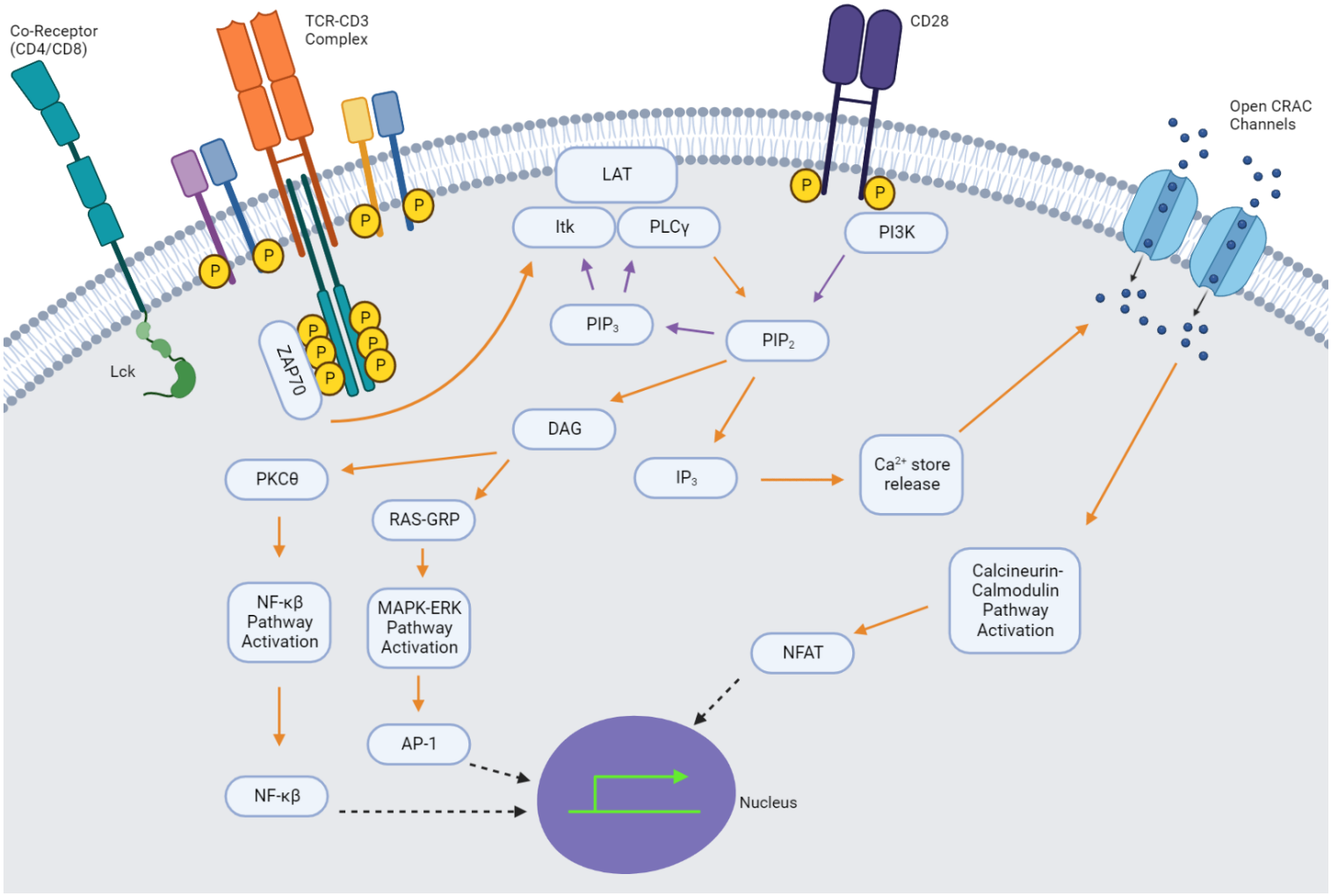


Figure 1.2 - TCR and CD28 Signalling Events Promoting T Cell Activation. Solid arrows represent positive activating events from protein to protein during the signalling cascade. Orange lines indicate signalling events initiated by the TCR-CD3 complex, whilst purple lines indicate signalling downstream of CD28 ligation. Dashed arrows indicate nuclear translocation of various transcription factors to promote gene transcription. Image created in BioRender.

However, signalling pathways induced downstream of the TCR are not universally activatory events. Many negative feedback protein signalling pathways exist, where phosphorylation of various proteins downstream of TCR ligation induce activation of proteins known to dephosphorylate activating signalling proteins and thus act to tune TCR signalling[57]. It is the balance between these phosphorylation/dephosphorylation events that controls and tunes TCR signalling as later discussed for CD45 (see 1.7.2). One such protein is the SH2 domain-containing protein tyrosine phosphatase 1 (SHP-1)[58,59], which is activated

by Lck via phosphorylation at tyrosine residue Y564 in SHP-1. SHP-1 has also been shown to be further phosphorylated at Y536, and phosphorylation at this site has been shown to greatly increase its phosphatase activity. Expression of SHP-1 proteins with phosphotyrosine mimetics (F_2Pmp) at positions 536 and 564 showed an 8 fold increase in phosphatase activity for F_2Pmp incorporation at position 536 compared with a 1.6-fold increase at 564[60]. Additionally, phosphorylation at the serine residue 591 (S591) in SHP-1 has been shown to attenuate SHP-1 phosphatase activity[61,62], reflecting the complex role for phosphorylation of various SHP-1 sites in controlling SHP-1 phosphatase activity. However, phosphatase activity by SHP-1 is still widely appreciated to induce Lck dephosphorylation at Y394, thus providing negative feedback on Lck activity and subsequently tuning TCR signalling[63]. Many other non-membrane tethered phosphatases are involved in tuning TCR signalling, including the dual specificity phosphatases (DUSPs) which are known to inactivate ERK proteins[64,65]. Transfection of HeLa with ERK proteins harbouring a D319N mutation to prevent DUSP binding resulted in enhanced ERK activation in response to the ERK2 activators epidermal growth factor and phorbol 12,13-dibutyrate[64]. Additionally, in studies of inflammatory bowel disease (IBD), IL-10$^{-/-}$ knockout mice are known to develop spontaneous chronic enterocolitis[65]. DUSP6$^{-/-}$ knockouts exhibit increased ERK1/2 activation upon TCR stimulation, and dual IL-10$^{-/-}$ DUSP6$^{-/-}$ knockouts develop accelerated and exacerbated disease which is reversed by use of the ERK1/2 inhibitor PD0325901[65]. These results indicate the important role of DUSP proteins in modulation of the TCR signalling pathways. Other cytosolic proteins involved in modulating the TCR signalling cascade include the lipid phosphatase and tensin homolog (PTEN)[56,66], which dephosphorylates PIP_3 to form PIP_2 and thus serves to counteract the activity of PI3K[66,67].

Other mechanisms aside from phosphatase activity exist to tune TCR signalling responses. These include the use of various ubiquitin pathways which serve to degrade ubiquitinated target proteins. Ubiquitination is initiated when E1 ubiquitin activating enzymes convert ubiquitin to an active state. Active ubiquitin is then transferred to E2 ubquitin-conjugating enzymes and finally E3 ubiquitin ligases mediate the attachment of the ubiquitin molecule to the substrate to be tagged for degradation[56,68]. Many E3 ligases including Itch, Deltex and proteins belonging to the Casitas B-lineage lymphoma (Cbl) family have been shown to be involved in the regulation of TCR signalling through the targeted degradation of proteins involved in TCR signalling including CD3ζ, PKCθ, ZAP-70, PLCγ1 and PI3K[56]. The Cbl family of proteins has 3 mammalian members (c-Cbl, Cbl-b and Cbl-3) which have distinct roles in modulation of T cell activation[69]. Both Cbl and Cbl-b are co-expressed but to different levels in thymocytes and mature T cells, with Cbl-b expression being elevated vs Cbl in mature T cells as compared to thymocytes, and vice versa[69]. Cbl-b has been shown to directly ubiquitinate the p85 subunit of PI3K, which in turn prevents its association with the TCR[70,71]. To this end, Cbl-b is a known mediator of T cell anergy by targeting phosphorylated signaling molecules for degradation by the proteasome[72,73]. In line with this, it has been shown that stimulation of CD4 and CD8 T cells from Cbl-b$^{-/-}$ mice hyperproliferate upon TCR stimulation alone, and mice bearing the Cbl-b$^{-/-}$ deletion are at significant risk of autoimmunity[74,75].

1.5 Checkpoint Inhibitor Signalling and T Cell Anergy

As described, robust T cell activation is achieved through activation of both the TCR and the co-stimulatory pathways. Ligation of the TCR alone in the absence of co-stimulatory pathway activation has long been known to induce a non-responsive T cell state known as anergy[76–78]. The earliest evidence of this phenotype arose from the discovery that

stimulation of murine Th1[79] or human T cell clones[80] through the TCR alone induced a state of non-responsiveness in these stimulated cells. The term anergy simply refers to this dysfunctional non-responsive state, which has been broadly broken down further into two classifications: clonal anergy and adaptive tolerance. In its simplest form, clonal anergy refers to the hyporesponsive state in which T cells that have been stimulated by their TCR in the absence of co-stimulation, or by low affinity antigen stimulation (with or without co-stimulation), are unable to produce IL-2 and proliferate upon subsequent TCR stimulation[76]. These cells are known to mount a moderate response to the initial TCR stimuli, through CD69 and CD25 expression and small amounts of proliferation; however, they are then rendered hyporesponsive upon rechallenge[81]. However, they are still able to express the IL-2 receptor and therefore this anergic state can often be reversed to varying degrees either by other IL-2 producing cells, or exogenous IL-2 addition *in vitro*[77,82]. Despite this seemingly straightforward clonal anergy phenotype, it has also been reported that anergy induced *in vitro* can also exist in a state that is not simply reversed by addition of IL-2. In these experiments, stimulation of $CD4^+$ T cells with anti-CD3 antibodies in the presence of endogenous B7 stimulation (i.e, endogenous co-stimulation) showed that despite CD69 expression at 24 hours by >97% of cells, 30% of these cells failed to proliferate. Isolation of these undivided cells showed that they were unable to proliferate when re-stimulated, despite IL-2 production in response to rechallenge by 30% of the $CD4^+$ cells in this sorted undivided population. Addition of exogenous IL-2 consequently had no effect on the ability of these cells to proliferate to rechallenge. However, blockade of co-stimulatory pathways during the first round of stimulation by addition of soluble CTLA-4 (CTLA-Ig, which binds B7 molecules and thus will block CD28 ligation on the $CD4^+$ T cells) showed that the undivided population from these conditions then displayed a 'classical' clonal anergy phenotype which

was readily reversed by addition of exogenous IL-2[83]. Therefore, in these experiments co-stimulation did not prevent the induction of an anergic phenotype but did mediate this phenotype as these anergic cells were then refractory to IL-2 addition. Given the observations when B7 molecules were blocked by CTLA-4-Ig addition, the authors tested whether CTLA-4 expression by $CD4^+$ T cells may promote this phenotype. Addition of anti-CTLA-4 Fab fragments to block CTLA-4 on $CD4^+$ T cells prevented the establishment of this IL-2 independent anergic response upon restimulation, and instead these cells returned to appearing to be typically clonally anergic (i.e., they once again proliferated upon rechallenge only in the presence of IL-2)[83]. These data suggest that anergic phenotypes can develop even in response to 'full' T cell stimulation (i.e., both TCR and CD28 activation) but that there appears to be levels to these anergic phenotypes such that they are no longer simply reversed by IL-2 signalling and instead are mediated via signalling through other inhibitory receptors.

Adaptive tolerance, sometimes referred to as *in vivo* anergy, is somewhat similar to clonal anergy with a key difference being that maintenance of the phenotype requires antigen persistence[76]. This is not the case for clonal anergy, which has been shown to persist for weeks after the removal of antigen and APC from the culture[76]. Descriptions of adaptive tolerance as a mechanism of anergy induction have shown that upon transfer of TCR transgenic T cells on a $Rag2^{-/-}$ background into a $CD3\varepsilon^{-/-}$ recipient expressing the pigeon cytochrome c antigen, these transferred T cells underwent classical clonal expansion followed by a reduction in their numbers ultimately producing a population of anergic cells after this round of stimulation. These cells were shown to remain in this anergic state for as long as 5 months, yet when transferred to a second $CD3\varepsilon^{-/-}$ mouse not expressing the pigeon

cytochrome c antigen, these cells lost their anergic phenotype and once again became responsive to *in vivo* peptide treatment[84].

Finally, other T cell surface receptors than the TCR play a role in controlling TCR signalling and promoting tolerant T cell phenotypes. These receptors, known as co-inhibitory receptors or checkpoint receptors, have been shown to 'apply the brakes' to T cell activation through various mechanisms including activation of negative signalling regulatory proteins such as SHP-1[85], providing competition for co-stimulatory ligands CD80 and CD86[86,87], and promoting upregulation of ubiquitin ligases including Cbl-b known to target TCR-CD3 signalling proteins for ubiquitylation[88]. Modulation of these receptors have proven extremely successful therapeutically, where blockade of both CTLA-4 and PD-1 has been shown to re-invigorate the T cell anti-tumour response[89,90]. For instance, PD-1 blockade has revolutionised cancer immunotherapy through restoration of anti-tumour T cell immunity. However, many patients remain non-responsive to PD-1 blockade, outlining the complexity of the tumour environment and mechanisms involved in tumour immune escape[90]. Some of the main inhibitory receptors studied to date and their mechanisms of action are summarised in table 1.1, and the effects of negative signalling on T cell activation and tolerance is briefly summarised in figure 1.3.

Receptor	Target	Function	Reference
CTLA-4	B7 molecules CD80/CD86	Competition with CD28 for CD80/CD86 binding, thus tuning availability of co-stimulatory signals[86,87,91].	Schwartz et al 2001, Stamper et al 2001, Rowshanravan et al 2018[86,87,91]
PD-1	PD-L1	Negatively impacts TCR signalling pathways through activation of negative signalling regulators SHP-1 and SHP-2[92], and promoting expression of ubiquitin ligases including Cbl-b[88].	Arasanz et al 2017, Qin et al 2019, Yokosuka et al 2012, Sharpe et al 2018[88,92–94]
Tigit	Nectin family molecules CD155, CD112 and CD113 (binds CD155 with higher affinity vs CD112/113)[95].	Ligation of CD155 on T cells induces inhibitory signalling through SHP-1 recruitment and activation[85]. Ligation of CD155 on APCs triggers IL-10 production and decreased production of IL-12[96].	Yu et al 2008, Liu et al 2013, Harjunpää, H. & Guillerey 2020, Chauvin and Zarour 2020[85,95–97]
Lag3	MHC-II molecules	Binds stable pMHC-II molecules and induces inhibitory signalling downstream of ligation[98,99]. Lag3 recruitment to the immune synapse (IS) localises this inhibitory signalling to the site of active TCR signalling[98].	Graydon et al 2021, Maruhashi et al 2022, Workman et al 2002, Workman et al 2005[98–101]

Table 1.1 – Summary of main co-inhibitory receptors and their mechanism of action.

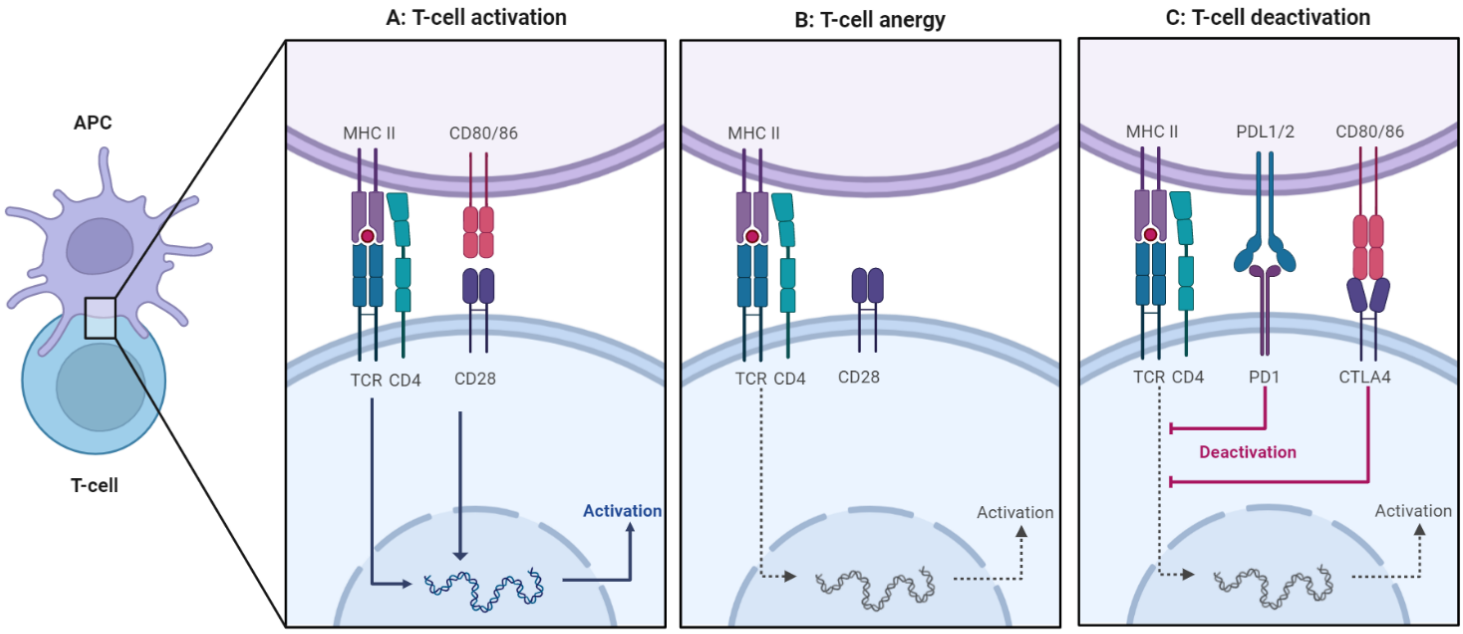


Figure 1.3 - Summary of CD4 T cell activation phenotype based on differential activation or deactivation signalling pathway initiation. **A)** Engagement of TCR and CD28 by pMHC-II and CD80/86 molecules respectively triggering activating signalling pathways, resulting in robust T cell activation. **B)** Engagement of TCR alone in the absence of CD28 ligation induces a dysfunctional activated phenotype known as T cell anergy. **C)** Triggering of co-inhibitory receptors such as PD-1 and CTLA-4 (others not shown) alongside TCR triggering can modulate TCR signalling pathways preventing T cell activation in response to cognate pMHC molecules. Image created in BioRender.

1.6 Immune Synapse Formation

Engagement of the TCR with its specific pMHC on the surface of an APC leads to the formation of an immunological synapse (IS) between the two cells, where radical reorganisation of both cell surface proteins and intracellular signalling proteins allows for the integration of signalling pathways permitting T cell activation. The IS was initially identified as a classical bulls-eye structure[102,103], where proteins were found to be re-organised into distinct supramolecular activation clusters (SMAC). This structure was found to exist as a central SMAC (cSMAC) made up of TCR-CD3 complexes and signalling associated proteins, surrounded by a ring of LFA-1 and cytoskeletal associated proteins that act to stabilise the synapse in the peripheral SMAC (pSMAC). Inhibitory phosphatases with large

rigid ectodomains such as CD45 were found to be excluded to the most distal regions (dSMAC) of the structure on the basis of their size, and hence permitted segregation of phosphatase events from the area of engaged TCRs.

However, understanding of the structure has advanced since this early work, and it is now appreciated that the TCR-CD3 complex exists in distinct TCR microclusters (TCR-MCs) on the cell surface[104–107], which can originate in the p/dSMAC but accumulate in the cSMAC. These microclusters have been suggested to contain approximately 100 TCR molecules and can be readily formed upon TCR engagement through merging of smaller pre-existing TCR nanoclusters[108], suggested to contain 2-20 TCR molecules[107,109]. TCR-MCs have been suggested as the site of TCR signalling[105,110], supported by the findings that they are associated with TCR signalling proteins such as ZAP70, Lck and LAT in the pSMAC, but migrate along a flow of actin polymerisation toward the cSMAC[111] where they ultimately accumulate[105]. As TCRs within these microclusters migrate toward the cSMAC their association with these signalling proteins is lost, and instead these TCRs then exist in what can be considered a 'signalling inactive' cSMAC region[104], which is devoid of TCR-CD3 complexes associated with phosphorylated signalling molecules[108]. Therefore, the pSMAC has been suggested as the site of actively signalling TCR-CD3 complexes[111], whilst the cSMAC has since been proposed to serve as a site of TCR recycling from the cell surface through internalisation and degradation[108].

These proposals are supported by the fact that proteins involved in TCR internalisation and degradation are found to localise within the cSMAC[104]. These proteins include Cbl-b[104,112] and c-Cbl, ubiquitin ligase proteins responsible for targeting proteins for proteasome mediated degradation[56]. Depletion of both c-Cbl and Cbl-b has been shown to induce a

hyperresponsive phenotype in double knock-out mice (dKO) in response to anti-CD3 stimulation[113]. Authors in these studies found that TCR signalling pathways in the dKO mice were not altered, but instead T cells from the dKO mice were unable to downregulate their TCR in response to ligand binding and thus resulted in sustained TCR signalling[113], indicating the involvement of these proteins in termination of TCR signalling and TCR downregulation. For degradation of ubiquitinylated proteins, these proteins are first sorted into multivesicular bodies (MVBs) by protein family members of the endosomal sorting complex required for transport (ESCRT), which are then ultimately translocated to the proteasome for degradation[114]. Interestingly, not only has c-Cbl and Cbl-b enrichment within the cSMAC been described, but markers of MVB formation (lysobisphosphatidic acid, LBPA)[111] and proteins within the ESCRT pathway (namely E3 variant (UEV) domain of tumor suppressor gene 101, TSG101) have also been shown to be enriched within the cSMAC[112]. Vardhana and colleagues have described that *in vitro* siRNA mediated depletion of TSG101 in AND TCR transgenic primary T cells prevents cSMAC formation and TCR downregulation in response to stimulation with strong agonist pMHC molecules via a planar lipid bilayer[112]. Interestingly however, in response to weak agonist pMHC molecules, TCR MCs were formed but dissociated within the cSMAC without the requirement for internalisation by TSG101 mediated mechanisms[112]. This therefore suggests that cSMAC formation and function varies in response to TCR signal strength, where in response to strong signals TCRs are readily downregulated to prevent hyperstimulation, yet in response to weak signals TCR signalling is terminated through TCR MC dissociation within the membrane without the need for internalisation.

TCR downregulation has also been shown via an additional clathrin-independent pathway, in which the authors provide evidence that internalised TCRs also take with them

bound pMHC molecules via trogocytosis[115]. Here, Martinez-Martin and colleagues identify that the Rras subfamily GTPase TC21 colocalises with the TCR in the cSMAC, and mediates TCR internalisation in a mechanism dependent on the small GTPase RhoG. In experiments utilising peptide pulsed APCs, authors were able to show that TC21- and RhoG-dependent phagocytosis also permits the internalisation of pMHC molecules from the APC with these internalised TCRs[115]. These findings propose an interesting question as to whether internalised TCR-CD3 complexes are 'signalling-dead' or if, in fact, signalling can continue and accumulate with internalised endosomes. This strikes an important parallel with findings reported by Yudushkin and Vale where internalised, plasma membrane derived CD3ζ molecules were shown to remain co-localised with active Lck on internalised endosomes, which may promote continual CD3ζ phosphorylation[116]. Authors found that endosomal CD3ζ was more heavily phosphorylated than plasma membrane CD3ζ[116], yet whether these phosphorylation events were mediated by Lck as a former-membrane bound CD3ζ protein, or whether they continually occur in the endosomes remains to be seen. Additionally, internalisation of antigen engaged TCRs has been shown to also result in internalisation of other non-engaged, 'bystander' TCR molecules[117], which may potentially aid mechanisms of endosomal signalling.

Whether IS formation is a cause or consequence of initial triggering of a TCR remains to be fully elucidated. Some groups have reported that stable synapse formation is drastically hindered upon blocking of internal calcium signalling[105], suggesting that TCR signalling is inherently required to drive IS formation, whilst others have suggested that formation of TCR-MCs fails to be blocked by use of the Src kinase inhibitor PP2, thus implying TCR-MC formation independent of TCR-CD3 phosphorylation[118]. The discrepancy between these two findings may arise from the differing experimental methods employed (live T cell-APC

imaging with GFP tagged proteins in the former[105], vs planar lipid bilayers in the latter[118]). However, the ability of IS formation to promote sustained signalling required for robust T cell activation is unequivocal.

1.7 T Cell Receptor Triggering Models

Despite the fact that TCR signalling pathways are becoming increasingly well understood and manipulated for therapeutic benefit, the exact mechanism by which the TCR is triggered still remains elusive. Any TCR triggering model must answer the paradoxical nature by which TCR triggering takes place, where the TCR must be able to respond with exquisite sensitivity to as little as one specific peptide-MHC (pMHC) molecule, whilst remaining inert to the ocean of non-specific, yet extremely structurally similar pMHC molecules also displayed on the surface of antigen presenting cells (APCs), where estimates suggest that approx. 100,000 copies of non-specific pMHC may be presented for every copy of specific pMHC[25,119–121]. Adding to the complexity, is the fact that TCRs binding to pMHC molecules on the surface of APCs typically has a very low affinity, and thus fast off-rate, when compared with other receptor ligand pairings[14,122].

The main concepts underpinning TCR triggering models are summarised in figure 1.4. Early models of TCR triggering centred around aggregation of TCRs or CD4/8 co-receptors in order to bring the TCR-CD3 ITAMs in closer proximity to co-receptor associated (or in other reports, lipid raft anchored[123]) Lck, thus shifting the kinase-phosphatase balance in the favour of receptor activation[124–126]. Segregation models also propose a similar mechanism, where exclusion of phosphatase molecules with large rigid ectodomains such as CD45, are forced out from the regions of close contact between TCR and pMHC. This is owing to the much greater size of the CD45 ectodomain when compared with the physical size of the

membrane-membrane distance between T cell and APC, (estimated to be in the range of 14nm[44]), determined by the TCR-pMHC interactions, which ultimately again shifts the balance of kinase-phosphatase activity at the site of engaged TCRs in favour of activating kinases[127–129].

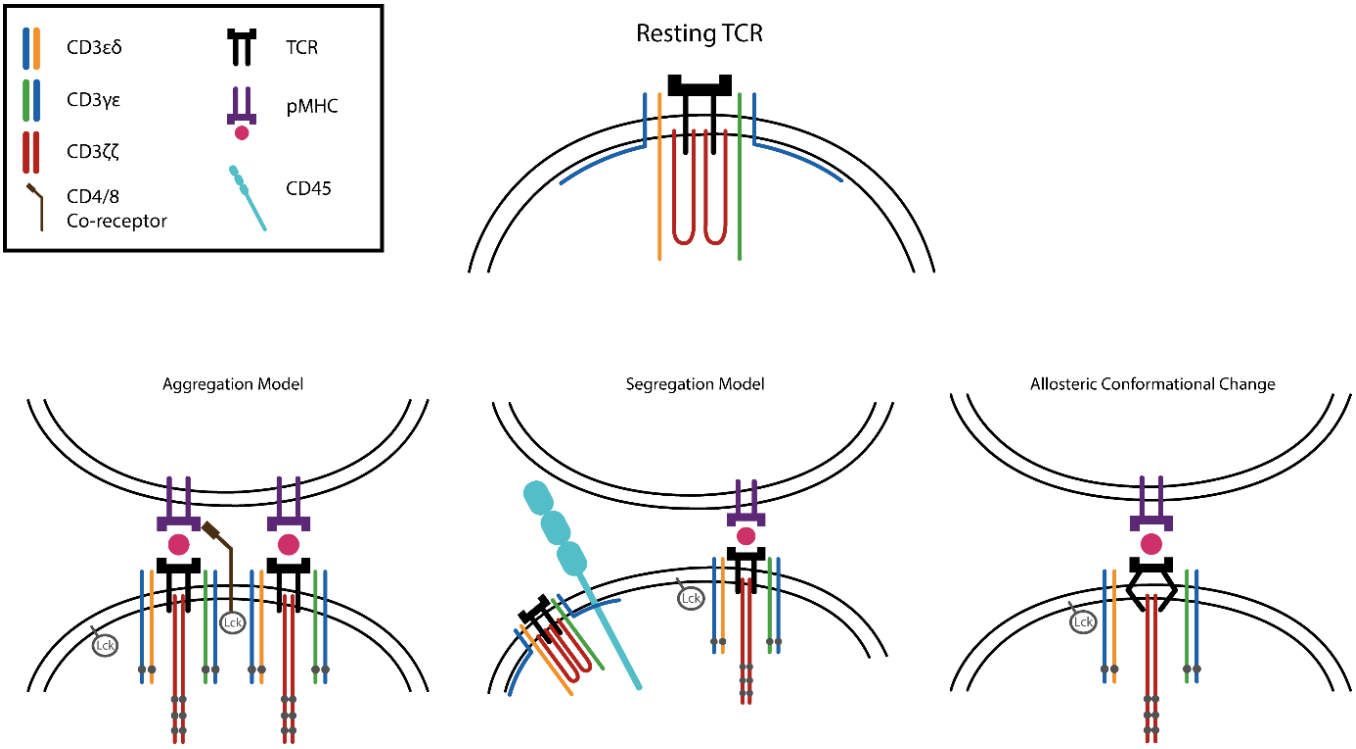


Figure 1.4 – Summary of proposed TCR triggering models. Aggregation models postulate that clustering of TCR-CD3 complexes increases its proximity with Lck, thus promoting TCR phosphorylation. Segregation models also centre around a kinase/phosphatase balance but propose that exclusion of large phosphatases such as CD45 from the site of engaged TCRs shifts the balance in favour of receptor phosphorylation. Finally, conformational change based models imply that pMHC binding by TCR induces a conformational change in the receptor, permitting ITAM accessibility by intracellular activating kinases.

1.7.1 Aggregation Based Models

Aggregation based models of TCR triggering initially stem from the observation that soluble multimeric pMHC molecules or antibodies against the TCR-CD3 complex are capable of inducing TCR triggering, whilst monomeric pMHC molecules or Fab fragments are not[125,130]. In these models (summarised in figure 1.5), ligation of multiple TCRs either by the multimeric pMHC molecules, bivalent antibodies, or indeed by pMHC molecules on the APC

surface serves to cluster the TCR on the T cell surface and as a result is able to manipulate the kinase-phosphatase balance between activating kinases such as Lck, and inhibitory phosphatases such as CD45, shifting the balance away from the equilibrium of a resting TCR in favour of kinase activity and thus receptor phosphorylation and TCR signalling[126].

The co-receptor model of TCR triggering proposes that since CD4 and CD8 molecules are also capable of binding MHC-II or MHC-I molecules respectively, at a site not related to antigen recognition by the TCR, and that these co-receptors are intracellularly associated with membrane tethered Lck, that antigen recognition by the TCR occurring concurrently with the CD4/8-pMHC interaction serves to facilitate Lck mediated ITAM phosphorylation[124,125]. Whilst it is clear that co-receptors play a critical role in the specificity of TCR triggering, where they are able to stabilise the TCR-pMHC interaction and are therefore of particular importance in the context of low affinity pMHC molecules, the model fails to explain how TCR triggering is able to occur in the complete absence of co-receptor recruitment to the site of actively engaged TCRs[125,130,131].

The pseudodimer model postulates that the vast amount of non-specific pMHC molecules on the APC surface still serve a role in achieving TCR triggering for a given clonal TCR[132–135]. Thymic selection processes inherently produce a repertoire of TCRs that are able to bind to self-pMHC molecules to some degree, where positive selection ensures the survival of T cells bearing TCRs that bind self pMHC molecules with an 'optimal' intermediate affinity, whilst negative selection processes ensure deletion of those TCRs that bind self pMHC with too high of an affinity that release of these TCRs to the periphery would render an individual at risk of developing autoimmunity[130]. T cells that bear TCRs that either

do not engage self pMHC or engage with too weak an affinity are also deleted from the repertoire as these cells die by neglect.

It is this property of the TCR repertoire, set by thymic selection processes, that forms the basis of the pseudodimer model of TCR triggering. Here, it is proposed that one specific TCR-pMHC interaction can temporally dimerise with a TCR-self pMHC molecule at the same time and same recognition site through a shared co-receptor. Here, the cognate antigen serves as an initiator as this strong TCR-pMHC interaction together with the coreceptor-pMHC interaction serves to drive phosphorylation of both the TCR specific for the cognate pMHC molecule, and any nearby TCRs loosely interacting with self pMHC molecules on the surface of the APC[130,135]. Such a phenomena is an appealing model of TCR triggering as it would certainly allow for phosphorylation of multiple TCRs in response to extremely low copy numbers of cognate pMHC molecules on the APC surface, and indeed evidence has suggested that self pMHC molecules are able to enhance agonist pMHC recognition at low density of cognate ligand[132]. Additionally, substantial recruitment of endogenous pMHC molecules into sites of active TCR – cognate pMHC recognition has been observed[136]. However, mutation of the co-receptor binding site on specific pMHC molecules, but not on self-pMHC molecules[135], has been found to severely impair T cell activation. This therefore implies heavy dependence on the co-receptor, and again fails to explain how the TCR can trigger in the absence of any CD4/8 co-receptor. In addition, monomeric TCRs have since been identified as the drivers of TCR signalling, observations which are in stark contrast to models that propose TCR aggregation as the true initiating event of TCR triggering[137].

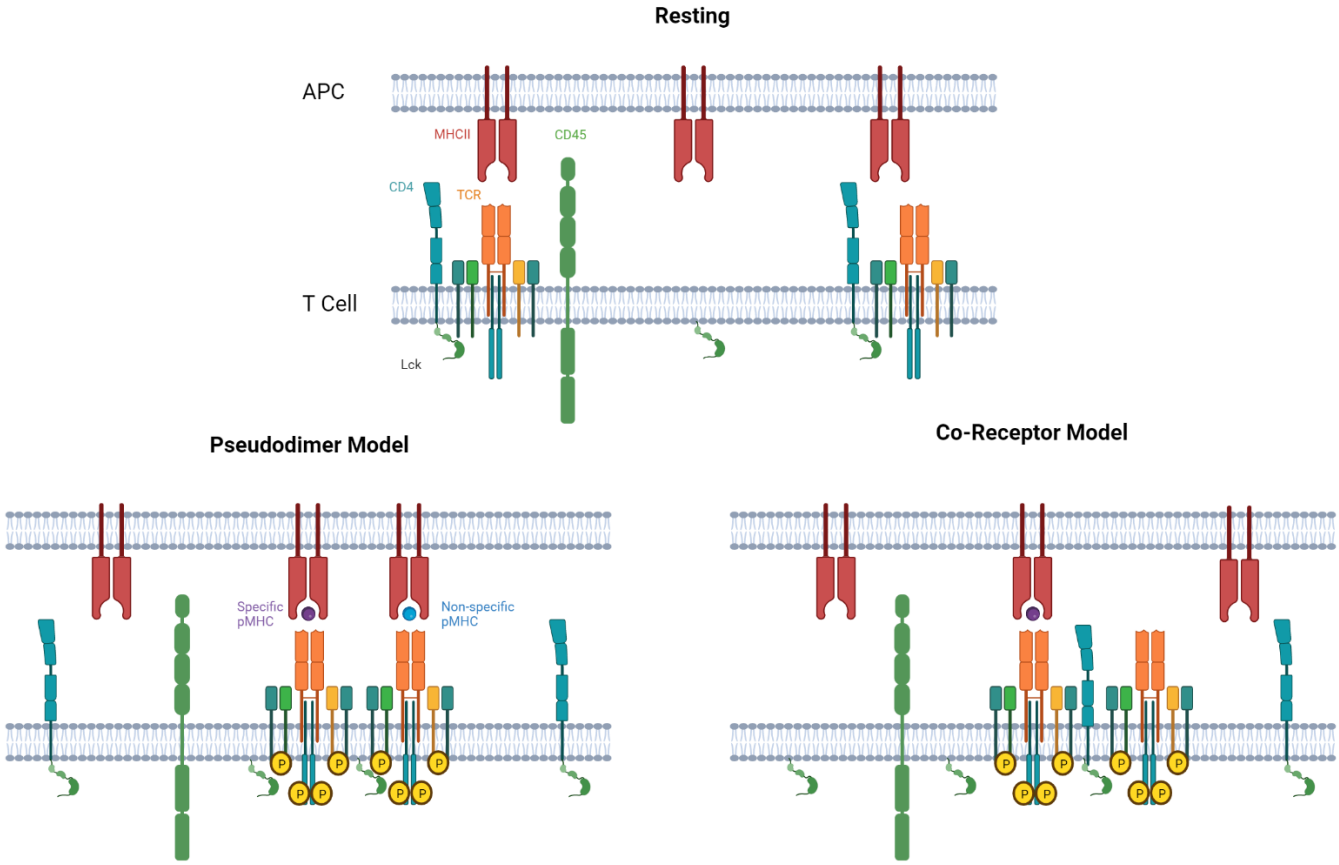


Figure 1.5 - Aggregation based models of TCR triggering. In the resting state, TCRs are kept in a non-phosphorylated equilibrium through the contrasting actions of Lck and CD45. In the pseudodimer model, low affinity interactions of TCRs with self pMHC serves to bring these TCRs into proximity with TCRs engaged with cognate pMHC molecules. The co-receptor model proposes that a shared co-receptor bound to the MHC molecule facilitates phosphorylation of multiple TCRs. In both proposals, the kinase/phosphatase balance is shifted in favour of receptor phosphorylation. Image created in BioRender.

1.7.2 Segregation Based Models

Whilst aggregation models of TCR triggering centre around increased proximity of the TCR-CD3 complex with activating kinases thus shifting the balance of kinase-phosphatase activity in favour of receptor phosphorylation, this can also be achieved through exclusion of phosphatases from the region of actively engaged TCRs. The TCR-CD3 complex has indeed been shown to alter its position within the cell membrane with respect to other membrane proteins[125,130], and the physical characteristics of a developing immune synapse between T

cell and APC may physically favour certain interactions over others. It is these properties that form the basis of the kinetic segregation model of TCR triggering[128,138].

Tyrosine phosphatases CD45 and CD148 exist as membrane embedded proteins in T cells with large rigid ectodomains[139,140], and given the finding that a large proportion of Lck has been shown to be constitutively active in resting T cells[141], it is reasonable to consider that the action of membrane embedded tyrosine phosphatases serves to keep the TCR-CD3 complex in a non-phosphorylated resting state. In favour of this, treatment of T cells with the pan-tyrosine phosphatase inhibitor pervanadate alone is enough to induce TCR signalling[142,143], supporting the notion of a kinase-phosphatase balance in the context of a resting TCR.

The physical distance across which pMHC recognition by the TCR must take place is governed by the distance between the opposing membranes, which has been estimated to be approximately 14-15nm[44,128,144,145], and this close apposition of the two cellular membranes involved in T cell activation has been shown to be enough to modulate rearrangement of protein distribution within these close contact regions[139]. To this end, CD45 has been repeatedly shown to localise at more distal regions of the IS (where it is found enriched within the distal supramolecular activation cluster, dSMAC), confirming its exclusion from the sites of active TCR engagement and signalling (which occur within the central and peripheral supramolecular activation clusters, c/pSMAC)[146]. In line with these findings, expression of forms of CD45 and CD148 in T cell hybridomas in which the ectodomain has been truncated inhibited TCR triggering. However, expression of endogenous CD45 and CD148 with large ectodomains prevented their inhibitory effect on

TCR triggering when stimulated with TCR ligands either in the form of plate bound anti-CD3ε or stimulation with peptide and APC[147].

In addition, elongation of TCR ligands, serving to prevent exclusion of large phosphatases from the sites of engaged TCRs, has been shown to abolish TCR triggering[47,138,145,148]. In experiments utilising supported lipid bilayers (SLBs) and Jurkat T cell lines, the anti-CD3ε antibody UCHT1 was tethered to the extracellular region of CD45RO both with and without a polyhistidine tag (UFabROH6 and UfabRO respectively). Given its large extracellular domain of approximately 21nm, TCRs engaging UfabRO were shown to be excluded from the sites of close contact between the T cell and SLB. However, owing to the polyhistidine tag which is capable of binding to nickel conjugated lipids in the SLB and thus reducing the physical size over which the UFabROH6-TCR interaction takes place, TCRs engaging with UfabRoH6 are not excluded from the close contact regions to the same extent as those engaging UfabRO. Importantly, TCRs engaging more physiological ligands such as SLB tethered Fab fragments of UCHT1 alone, or SLB tethered pMHC molecules were also not excluded from close contact zones as expected. Correlating this manipulation of TCR distribution within the membrane with the ability of these TCRs to trigger, found that engagement of UfabRO greatly prevented the ability of TCRs to trigger, which was restored when engaging UFabROH6[145]. Taken together, these experiments show that size-based segregation of actively engaged TCRs from tyrosine phosphatases CD45 and CD148 is sufficient to drive TCR signalling and that manipulation of either the TCR ligand or the tyrosine phosphatases to alter this segregation is sufficient to inhibit TCR triggering upon stimulation. These models of TCR triggering are summarised in figure 1.6.

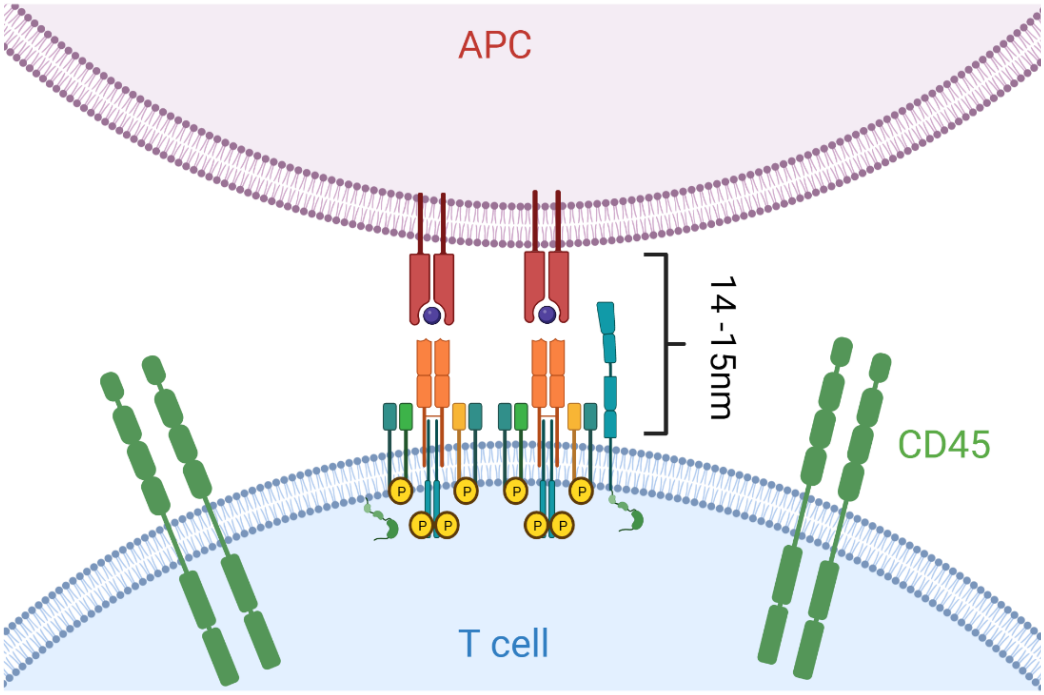


Figure 1.6 - The segregation model of TCR triggering. The large extracellular domain of CD45 prevents its localisation within sites of engaged TCR molecules based on the physical properties of the TCR-pMHC interaction (size across the intramembrane space estimated to be approx. 14-15nm). Exclusion of CD45 thus prevents phosphatase activity on the TCR and shifts the kinase/phosphatase balance in favour of TCR phosphorylation. Image created in BioRender.

Despite the compelling evidence for the kinetic segregation model of TCR triggering, it has since been shown that application of shear and normal forces to elongated ligand-TCR interactions in a micropipette based experiment is able to induce TCR triggering[47]. Given that the elongation of this interaction served to prevent CD45 exclusion and thus inhibited TCR triggering in the absence of force application, it can be argued that other TCR triggering mechanisms exist.

1.7.3 The Kinetic Proofreading Model

Every TCR-pMHC interaction has an affinity determined by the strength of binding between the TCR and the given pMHC molecule that it is interacting with. This affinity

determines the half-life of the TCR-pMHC bond, and thus mediates the lifetime of each TCR-pMHC complex. The kinetic proofreading (KPR, summarised in figure 1.7) model of TCR triggering proposes that once a TCR is engaged with pMHC, a sufficient window of time must be allowed to elapse to allow for a certain number of rapidly reversible steps, such as ITAM and signalling protein phosphorylation, to take place and initiate an internal biochemical signal[149,150]. The KPR model proposes that only those TCR-pMHC interactions of a sufficiently high affinity, and thus with a sufficiently long life-time allow such a window of time to elapse, and that those TCR-pMHC interactions of affinities below this undergo bond dissociation before these events can allowed to occur, after which any steps along this cascade are rapidly reversed before robust signalling has been able to occur. Therefore, the KPR model proposes an affinity/bond-life time mediated basis of ligand discrimination by the TCR. In agreement with this model, multiple reports have shown that increasing the bond lifetime between TCR and ligand through the use of altered peptide ligands of decreasing/increasing affinities is a key parameter for TCR signalling and T cells activation[151–153]. These studies have shown that an optimal TCR-pMHC bond lifetime, sometimes referred to as dwell-time or receptor confinement time, exists for robust T cell activation and that mutations that either increase or decrease the bond half-life can decrease the observed response[154,155].

In the KPR model, the time between receptor occupancy by pMHC and bond dissociation is known as the proofreading time, and previous mathematical modelling has suggested that 2-3 signalling events must occur during this proofreading time in order to commit a T cell to TCR signalling pathway progression[156]. In line with this, a key molecular event in ligand discrimination by the TCR has been shown to not to be ZAP-70 recruitment, but phosphorylation of the kinase at Y492. Therefore, in this scenario ITAM phosphorylation and

ZAP-70 recruitment will have occurred (steps 1 and 2) prior to full ZAP-70 activation by phosphorylation at Y492, phosphorylation of which completely prevents autoinhibition of ZAP-70[157,158]. In these experiments, the phospho-proteome of OT-1 T cells, stimulated with altered peptide ligands whilst controlling for levels of receptor occupancy was determined[159]. Here, it was found that CD3 ITAM phosphorylation and recruitment of ZAP-70 to the TCR-CD3 complex was unaffected by decreasing peptide affinity for the OT-1 TCR. However, phosphorylation of ZAP-70 at Y492 was only found to occur in response to high affinity ligands[159], indicating this event as a key molecular switch in ligand discrimination by the TCR. Interestingly, formation of the CD6 signalosome, which involves the recruitment of phosphatases UBASH3A and UBASH3B, was found to occur in response to peptides of all affinities tested yet had a greater impact on dampening TCR signalling events in response to low affinity peptides[158,159].

The KPR model therefore provides compelling evidence for how the TCR may discriminate between specific and non-specific pMHC molecules and initiate a TCR signalling cascade only in response to cognate antigen. However, factors upstream of signalling protein phosphorylation may modulate TCR-pMHC bond lifetimes thereby altering the proofreading time for a given pMHC-TCR interaction. These factors include force application to the TCR-pMHC bond, which has been shown to modulate TCR-pMHC bond lifetime through the formation of catch or slip bonds as discussed later (see 1.7.5). Therefore, the KPR model itself may not provide the full picture as to how the TCR discriminates between ligands and induces the TCR trigger.

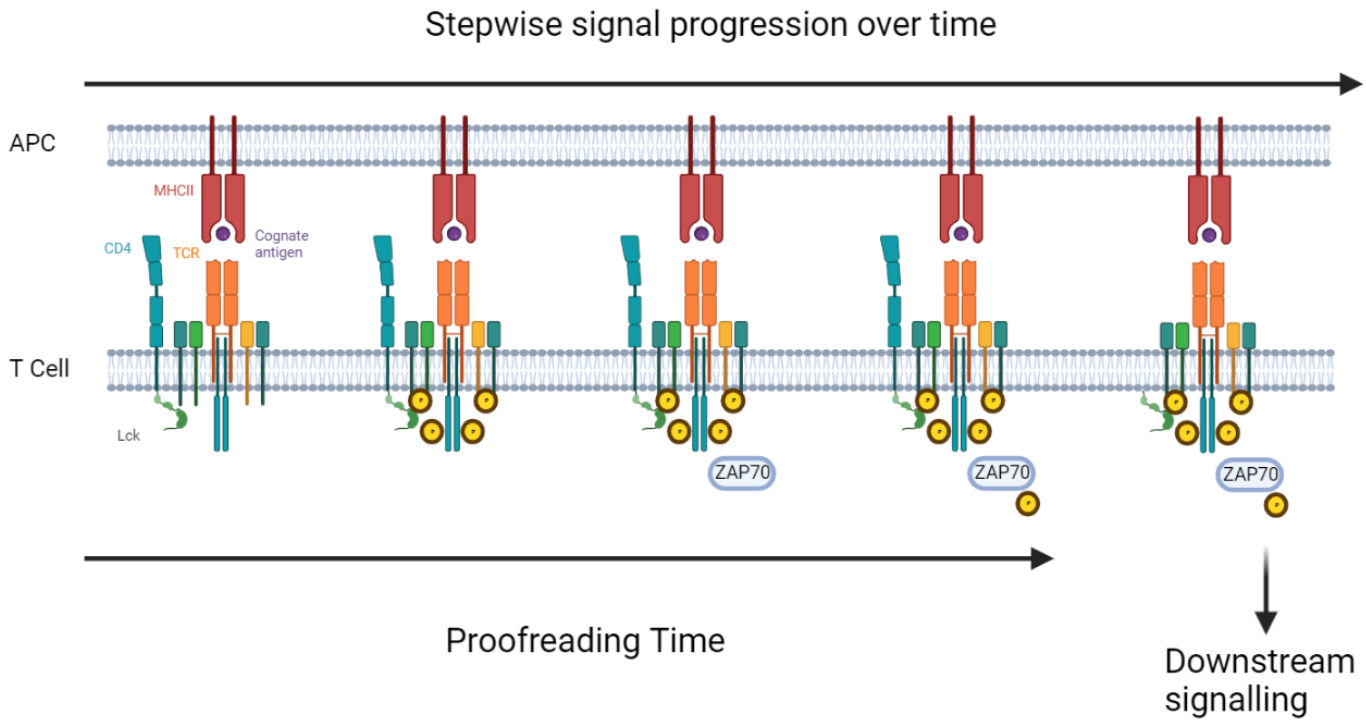


Figure 1.7 - The kinetic proofreading model of TCR triggering. The kinetic proofreading (KPR) model of TCR triggering postulates that the pMHC-TCR bond must persist for a given period of time, known as the proofreading time, to permit for several reversible steps in TCR signalling to take place and induce downstream signalling. These steps include CD3 phosphorylation, ZAP-70 recruitment and ZAP-70 phosphorylation, as shown in steps 2, 3 and 4 during the proof-reading time. Bond dissociation within the proofreading time results in the resetting these events, ensuring that these short-lived pMHC-TCR bonds do not induce downstream signalling. Image created in BioRender.

1.7.4 Conformational Change Based Models

Conformational change models of TCR triggering also aim to solve the enigma of how antigen binding is translated to internal biochemical signal. Antigen ligation has been identified to induce conformational changes in the complementary determining regions (CDRs) of the TCR[32], but until recently these changes were not thought to progress beyond these regions.

Analysis of several independent TCRs has begun to highlight conformational changes in distal regions of the TCR-CD3 complex, providing a basis for a model of TCR triggering by dynamic allosteric conformational regulation. However, this model of TCR triggering can be

considered one of the most controversial, as other recent cryo-EM resolved structures of the TCR in complex with bound ligand reported no conformational change in the receptor[44]. Nevertheless, independent nuclear magnetic resonance (NMR)[160] and site directed fluorescence labelling (SDFL)[161] analysis of human anti-viral TCRs A6 (specific for Tax-HLA-A2) and LC13 (specific for FLR-HLA-B8)[162] both identified conformational change within the AB loop of the Cα domain of the TCR upon pMHC binding. Importantly, in the $CD8^+$ LC13 TCR, expression of an AB loop-mutant LC13 TCR significantly inhibited CD69 upregulation upon pMHC mediated T cell activation, highlighting the functional significance of this region in TCR triggering[162].

Conformational changes were observed at regions outside of the Cα AB loop in the ligated A6 TCR, including residues located in the Vα/Vβ, Vβ/Cβ and Cα/Cβ interfaces[160]. Residues within the Cα/Cβ interface of the TCRαβ heterodimer have been suggested to be in proximity with CD3 subunit docking sites[41,160,163], thus providing a potential pathway of conformational change relay through the TCR-CD3 complex. In addition, analysis of the B4.2.3 TCR, which recognises P18-I10 antigen from human immunodeficiency virus type 1 (HIV-1) in complex with $H2\text{-}D^d$ also implicated conformational change in residues local to these docking sites[163], which could perhaps suggest a conserved mechanism of allosteric conformational change relay from antigen docking through to the CD3 subunits for signal propagation. Single alanine mutagenesis for each residue in the B4.2.3 TCR proved functional importance for these regions in TCR surface expression and TCR triggering, yet importantly proved unimportant for pMHC-TCR interaction at the distal antigen binding domain[163].

Conformational changes were reported at residues mapping to the Vβ/Cβ interface, yet not the Vα/Cα interface, of the A6 TCR which may suggest more of a role for the TCRβ chain in conformational change relay through the TCR-CD3 complex. In support of this idea is the finding of a far greater buried surface within the Vβ/Cβ interface when compared with that of the Vα/Cα (1007 $Å^2$ vs 539 $Å^2$)[160], a feature that is true of all TCR structures characterised to date[164]. This may be of particular importance when considering intra-thymic T cell development processes, where the pre-TCR expressed by developing thymocytes consists of the TCRβ chain, genes for which have been successfully rearranged, paired with an invariant α chain, expression of which precedes TCRα gene rearrangement[46]. Signalling through this pre-TCR complex is essential for β-selection, the progression from the $CD4^-CD8^-$ (double negative, DN) to the $CD4^+CD8^+$ (double positive, DP) stage of thymocyte development[165,166].

The TCRβ chain also contains a conserved, unusually long insertion that protrudes from the Vβ/Cβ interface known as the FG loop[167–170], which accounts for approximately one third of the interface buried surface. Interestingly, this loop has been shown to rigidify upon pMHC binding in the aforementioned TCRs[160] and is intriguingly positioned above the CD3εγ heterodimer[167]. Intrachain disulphide bonds toward the ectodomains of both chains of the CD3εγ heterodimer, and extensive hydrophobic interactions between the parallel beta sheets of the heterodimer provide an extremely rigid structure that could conceivably function in a 'piston like' manner to transmit conformational change of the TCR-CD3 extracellular domains through the membrane to intracellular CD3 ITAMs, via the FG loop – CD3εγ heterodimer axis[167]. Therefore, during immunosurveillance where TCRs sample pMHC molecules on the surface of an APC with both cells physically crawling in respect to one another, shear force induced conformational changes or bending of the TCR may induce TCR triggering by the FG loop – CD3εγ axis. Indeed, deletion of the FG loop has been shown

to severely impair proliferation and cytokine production in naïve T cells upon pMHC challenge[171]. Further promise for this axis of conformational change induced TCR triggering is garnered from the notion that emergence of the FG loop and expression of distinct CD3 heterodimer forming subunits appear to have co-evolved, where mammalian jawed vertebrates (Gnathostomata) possess both factors, whilst non-mammalian members of the Gnathostomata family possess FG loop devoid TCRs and a single CD3-precursor gene (CD3p)[167,172].

Regardless of the reported conformational changes in the various regions of TCR:CD3 ECDs, for conformational change to be considered a true mechanism of TCR triggering these conformational changes must be passed to the intracellular signalling machinery of the CD3 proteins. To this end, various conformational changes for the intracellular cytoplasmic domains (CD) of the CD3 chains have been observed. Mediated by basic residue sequences (BRS) in their CDs[173,174], and by an additional proline rich sequence (PRS) in the CD3ε CD[175–177], both CD3ε[175–178] and CD3ζ[173,174] have been shown to bind acidic phospholipids and thus associate with the inner leaflet of the plasma membrane in a resting T cell[179]. This has been proposed as a potential mechanism to keep the unligated TCR-CD3 complex in a non-phosphorylated resting state, yet since both human CD3δ and CD3γ chains do not contain BRS or PRS regions[175], it is questionable as to why the ITAM residues within these chains are not phosphorylated at rest by constitutively active Lck[141]. One answer may be the observation that only the CD3ε chain is able to recruit Lck to the TCR-CD3 complex, which is achieved by interaction between the CD3ε BRS region and a unique domain (UD) within the Lck protein. Therefore, it is conceivable that in a resting TCR, Lck recruitment is not permitted due to the sequestering on the CD3ε BRS in the phospholipid membrane. Of

course, the action of CD45 in a resting T cell may also act to keep the ITAMs of the CD3δ/CD3γ chains in a non-phosphorylated state.

Excitingly, both CD3ε and CD3ζ have been shown to dissociate from the membrane upon T cell activation with both pMHC and anti-CD3 monoclonal antibodies[174,179]. Additionally, in the case of CD3ζ, both tyrosine to phenylalanine mutations within the ITAM residue and use of the Src kinase inhibitor PP2 confirmed the release of this chain from the membrane to be phosphorylation dependent[174]. Since this does not appear to be the case for CD3ε and taken together with the proposed CD3ε BRS – Lck UD interaction, this suggests a critical role for the CD3ε chain in the initiation of ITAM phosphorylation.

Additional atomic force microscopy studies have since identified that the CD3ε – plasma membrane interaction can exist in a variety of conformations, based on the association of both its BRS and PRS with the membrane[33,177]. Applying a reductionist view, these interactions provide the basis for 3 CD3ε conformations; 'fully closed' (state 1, both BRS and PRS bound to the membrane), 'fully open' (state 3, both BRS and PRS regions dissociated from the membrane) and an intermediate 'partially open' state (state 2, BRS bound, PRS dissociated)[177]. These CD3ε conformational states can conceivably allow for modulation of TCR signalling.

Experimentally, the functional importance of this CD3ε-membrane interaction is not fully understood. Conflicting reports have suggested both positive and negative evidence for this axis of TCR triggering. Mutation of the positively charged residues within the membrane interacting regions of the CD3ε CD have rendered the molecule unable to induce TCR-CD3 phosphorylation[180], whilst other independent reports have shown reduced thymic cellularity and reduced tyrosine phosphorylation upon TCR stimulation in CD3ε BRS deficient

transgenic mice[181]. However, in the latter study, the reduced TCR phosphorylation at early time points (10mins) in BRS deficient mice did not translate through to altered T cell proliferative responses[181]. Therefore, the shielding of the cytoplasmic domains of the CD3 chains in the plasma membrane of the resting T cell remains unclear as a mechanism to keep the resting TCR in a non-phosphorylated state[182].

1.7.5 Mechanosensing Based Models

Mechanosensory activity by the TCR may also shed light on how the TCR initially triggers. Mechanosensors are a group of receptors that interpret mechanical information and cues and translate them into biochemical signals. The initial observation of TCR signalling in response to external forces came from the laboratory of Ellis Reinherz, where application of an oscillatory external force of approximately 50pN to antibody functionalised protein-G dynabeads was able to drive TCR calcium signalling[183]. In these experiments, anti-CD3ε antibody 145-2C11 was able to drive calcium signalling within minutes independent of force application, whilst anti-CD3εγ 17A2 required application of external force to drive TCR signalling. The differential binding topologies of these two anti-CD3 monoclonal antibodies may shed light on how the TCR may function as a mechanosensor, with 145-2C11 binding in an orthogonal fashion whilst 17A2 binds with a more 'classic' perpendicular mode[172,183]. The authors thus suggest that binding induced torque in the 145-2C11 interaction may be translated across the membrane and can thus influence triggering, but that this is largely absent in the 17A2 interaction and requires external force application to drive such an effect[172,183].

However, the differential binding topologies of these antibodies may also influence TCR triggering by other factors. It has been shown in the past that some clones of anti-CD28

antibodies are indeed agonistic to T cell activation independent of TCR-CD3 stimulation and are able to induce robust T cell proliferation[184]. This phenomenon has been attributed to the binding topology of these antibodies, where the agonistic clones of anti-CD28 antibody have been shown to bind with a more orthogonal binding topology owing to a slightly altered binding site on the CD28 ectodomain[185–187]. The result of this alteration may be a failure to properly exclude CD45 from regions of antibody binding, hereby inducing differential levels of TCR triggering. Therefore, it is conceivable that a similar scenario may take place when T cells were presented with protein G dynabeads beads functionalised with either 145-2C11 or 17A2 in the Reinherz experiment. This would however suggest that force application to the 17A2 interaction was able to overcome the inhibitory effects of CD45 on TCR signalling and shift the balance in the favour of receptor phosphorylation. In line with this, other independent studies have made use of elongated TCR ligands to bind the TCR, thus increasing the intermembrane space between T cell and SLB preventing size based exclusion from the areas of actively engaged TCRs, thus inhibiting TCR signalling[47,138,145,148]. However, micropipette based shear force application to these elongated interactions was shown to rescue TCR signalling within 3-4mins as measured by Ca^{2+} flux, again suggesting that force application may overcome the inhibitory effects of CD45 on TCR signalling[47].

In addition to these seminal studies, the same laboratory has identified that mechanosensing by the TCR may enhance its sensitivity for antigen and thus alter the threshold for initiation of TCR signalling. Optical trap based approaches, utilising N15-TCR transgenic T cells, specific for the VSV8 peptide, high levels of pMHC molecules on the bead surface (approx. $2x10^4$) induced TCR calcium signalling irrelevant of external force application. However, when using pMHC surface coatings that better represent what a T cell may typically engage physiologically (copy number of approximately 29 and 2 pMHC

molecules), calcium signalling was absent. Force application (again achieved via oscillating the optical trap with respect to the immobilised T cell) of approximately 10-20pN was able to drive TCR calcium signalling within 4-5 minutes at low pMHC copy numbers where signalling was not observed in the absence of force application[188]. Importantly, calcium signalling was again not observed when using an irrelevant SEV9 peptide. Therefore, force interpretation by the TCR was suggested to be able to fine tune TCR signalling and thus permit signalling in response to fewer pMHC numbers. Of notable interest is the observation that the TCR may act with a degree of anisotropy, where the receptor appears to favour application of tangential force over normal forces when beads were functionalised with 29 copies of pMHC molecules. However, since rescuing of a TCR signal via force application was achieved with both normal and tangential forces[47,189], it remains to be seen whether the TCR does indeed behave as an anisotropic mechanosensor, or whether the TCR can interpret different modes of mechanical cues in a different manner.

In spite of this, application of tangential forces does form a promising scenario, where any conformational change in the receptor in the form of receptor bending in response to tangential forces will likely allow for the TCRβ FG loop to impinge on the CD3εγ heterodimer, potentially initiating CD3 ITAM release as previously described[167]. Physiologically, this is an attractive proposal as it suggests that T cells can harness mechanical energy generated upon crawling of a T cell over an APC during immunosurveillance, where TCRs are sampling pMHC molecules in search of cognate antigen[183]. Importantly, and consistent with the notion that TCRβ may be more involved in conformational change relay than TCRα, the differing CP lengths (24 residues for TCRα, 14 for TCRβ)[167] of the TCRαβ chains may provide a bias where TCRβ experiences greater

mechanical load than TCRα ensuring bending of the receptor toward the β chain, supporting the FG loop axis.

T cells have also been shown to be mechanically responsive in a variety of other settings including the utilisation of force exertion at the IS to potentiate target cell killing by $CD8^+$ T cells[190,191], and the modulation of IL-2 secretion and proliferation by $CD4^+$ T cells in response to the stiffness of PDMS/polyamine gel substrate they were cultured on[192–194]. However, perhaps the most fascinating and significant observation of mechanical force interpretation by the TCR is the formation of catch and slip bonds[170,195–197].

Catch bonds, defined as bonds that display an increased bond lifetime with force application[195,196,198,199], may answer how the TCR is able to achieve such high levels of sensitivity to its cognate antigen whilst remaining functionally inert in response to non-specific pMHC molecules[25,170]. Structural analysis has revealed that the application of normal force to the 2C TCR in complex with antigen increases the amount of hydrogen bonds formed between the CDR loops of the TCR and the arginine residues within the P4 pocket of the peptide binding groove of the pMHC molecule[198]. Utilising a biomembrane force probe (BFP), OT1 $CD8^+$ T cells specific for the OVA peptide presented by H2-K^b (OVA-H2-K^b)[196,197] showed an increase in bond lifetime, correlating with increased calcium flux, upon force application of 10pN to this interaction[196]. Altered peptide ligands of the OVA peptide of a hierarchical decrease in potency showed a correlation between antigenic potency and catch bond behaviour, where the least antigenic and non-specific peptide controls showed slip bond behaviours (bonds which exhibit a decrease in bond lifetime under force, thus dissociating under force application)[196].

Of clinical importance, catch bond engineering has been shown to be a potential promising therapeutic approach, enriching for specific T cell activation in the field of cancer immunotherapy[199]. A common drawback in adoptive cell transfer therapy for cancer treatment is the fact that many tumour-antigen specific TCRs have a low affinity for tumour associated antigens and thus only achieve weak T cell activation. One way to avert this issue is to increase the affinity of the TCR for the given tumour associated pMHC prior to infusion. However, affinity matured TCRs are then at risk of exhibiting cross-reactivity with other pMHC molecules in the body and have indeed shown significant off target effects including lethal cross-reactivity with a cardiac peptide from the TITIN protein by TCRs specific for MAGE-A3 in complex with HLA-A:01[200,201]. It has since been shown that greater sensitivity to tumour-associated antigens whilst avoiding potentially lethal cross-reactivity can be achieved through engineering TCRs to display catch bond behaviour[199]. For this, the same TCR as the aforementioned trial was used: TCR-A3, specific for MAGE-A3. Based on the resolved crystal structure of the A3 TCR in complex with HLA-A1- MAGE-A3, residues within the CDR loops of both the TCRα and TCRβ chain were chosen for mutation since they are located close to the pMHC but do not directly contact the pMHC molecule in the crystal structure (thus making them candidates to mediate increased bond lifetimes when under force). SKW3 T cell lines were transduced with mutant TCR libraries, and following stimulation through their TCR, cells were sorted based on a CD69 high tetramer low staining strategy (thus selecting cells displaying strong responses via their TCR with low peptide affinity). This gave rise to 8 distinct high sensitivity mutant transduced clones that displayed similar responsiveness to MAGE-A3 peptide as the affinity matured A3A TCR, and enhanced responsiveness over WT TCR. Importantly, 4 mutants showed no cross-reactivity with the TITIN peptide, and 4 displayed very weak activation by TITIN peptide compared with TCR-

A3. This was followed up with biomembrane force probe (BFP) studies of 2 mutant clones that displayed no cross-reactivity to TITIN peptides (namely 94α-14 and 20α-18), alongside the affinity matured A3 TCR and WT TCR. All 4 TCRs formed catch bonds with HLA-A1-MAGE-A3 when subjected to approximately 10pN of force. Peak bond lifetime correlated well with maximal CD69 MFI, and it is noteworthy that the engineered 94α-14 TCR showed both highest maximal CD69 MFI and longest peak bond lifetime. BFP experiments with the 94α-14 and 20α-18 TCRs in complex with HLA-A1-TITIN showed only slip bond behaviour under force, consistent with the loss of cross-reactivity to TITIN for these TCRs. Finally, human primary T cells transduced with the 94α-14 or 20α-18 were shown to be capable of killing the HLA-A1-MAGE-A3 expressing melanoma cell line A375, and the HLA-A1-MAGE-A3^{+} colon cancer cell line HCT-116. Coculture of these transduced human primary T cells with either TITIN pulsed or MAGE-A3 pulsed APCs provided further evidence of functional responses to MAGE-A3 peptide whilst maintaining a state of functional inertia to TITIN peptides[199].

The mounting detailed evidence of catch bond/slip bond formations by the TCR under force load proposes a clear scenario as to how the TCR may achieve exquisite sensitivity to specific antigen whilst remaining non-responsive to structurally similar but non-specific antigens. As illustrated in figure 1.8, if an allosteric conformational change through the TCR was to set in motion ITAM release and initiate TCR-CD3 phosphorylation, it is plausible that force regulated catch bond dynamics may only allow specific peptides to hold the complex in an 'active' conformation and permit receptor phosphorylation. Decreasing ligand potencies correlating with weaker catch bonds may then only permit either partial conformational changes or a shorter time frame for existence of this conformational change and thus may allow for mediation of the TCR signal. Non-specific peptides which then form

slip bonds with the TCR will rupture before relay of conformational change through the membrane and thus not initiate TCR signalling. Indeed, these proposals also feed directly into the proofreading time postulated within the KPR model of TCR triggering as described in 1.7.3.

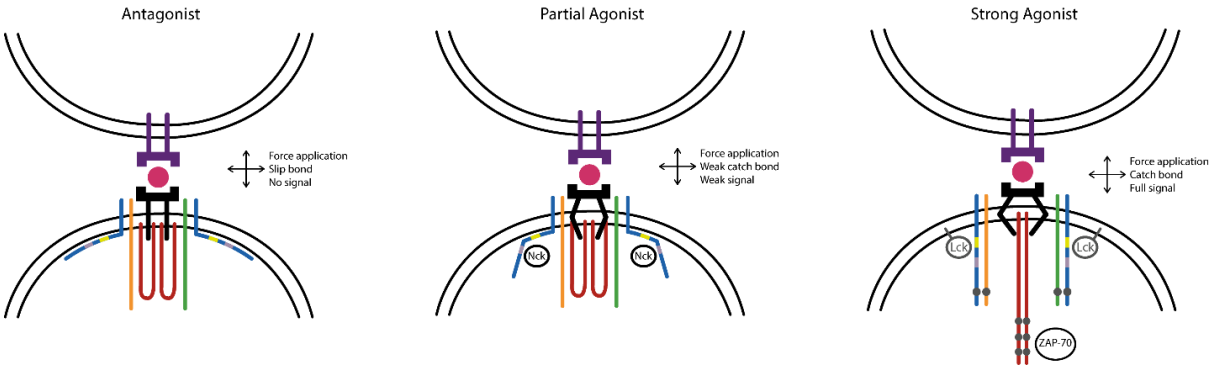


Figure 1.8 – Catch Bond Mediated TCR Signalling – A Unified Model of TCR Triggering – Catch vs slip bond formation under force application may provide a mechanism by which the TCR is able to trigger. Upon encountering low affinity / antagonist pMHC molecules, force application to the TCR-pMHC bond will induce slip bond formation, whereby bond lifetimes are shortened in response to force application leading to bond dissociation and a lack of signalling. Force application to partial agonists however may induce weak catch bonds which increase bond lifetimes under force application and permit weak signals to transmit from the TCR. Finally, force application to high affinity TCR-pMHC interactions will induce robust catch bond formation, hereby promoting an increased bond lifetime that may fulfil the proofreading time required for all reversible signalling events required for the TCR trigger to occur as postulated by the kinetic proofreading model.

1.8 Introduction to Mechanosensing

Mechanosensing has not only been described in the context of the TCR. Many other cell surface receptors and ion channels have been shown to be sensitive to mechanical cues. Mechanotransduction pathways are known to control key cellular process including proliferation, differentiation and migration[202], as well as providing key components in the biochemical signalling behind touch, pressure sensing, proprioception, hearing and muscle stretch[203]. The following section aims to detail the current landscape for mechanosensing by other non-TCR receptors and ion channels.

1.8.1 Integrin mechanosensing

Integrin molecules are key mediators of cell adhesion, spreading and migration, and have long been suggested to function as mechanosensors, whereby they are critical interpreters of force transmission from the ECM across the cell membrane via focal adhesions. The initial observation of integrin-mediated mechanosensing was published 29 years ago, where endothelial cells were shown to stiffen in response to mechanical twisting of ligand functionalised beads bound to β1 integrins[204]. The integrin family is made up of 24 different αβ heterodimeric transmembrane receptors, each making use of 18 different α and 8 different β subunits[205]. Each subunit consists of an N-terminal ectodomain, containing a large 'head' which houses the ligand binding site, a single pass transmembrane domain (TMD) and a short C-terminal cytoplasmic tail[206,207]. In the resting state, integrins are known to exist in a bent conformation with a closed head piece. However, upon activation the integrin molecule undergoes a series of conformational changes to result in a signalling process known of 'outside-in' signalling[207].

These conformational changes include ectodomain extension and opening of both the headpiece and the α and β chains throughout the ectodomain, transmembrane region and cytoplasmic tail[207]. The opening of the headpiece permits high affinity ligand binding, whilst the separated cytoplasmic tail then allows for association with cytoskeletal related signalling proteins such as talin and kindlin to permit signal transduction[208]. Therefore, it is clear how force application arising from hemodynamic blood flow to integrin-ligand bonds during processes such a leukocyte adhesion can aid in stronger integrin bonds via headpiece opening, and subsequent downstream signalling. It is, therefore, unsurprising that catch bond behaviours under force have also been identified for several integrin-ligand

interactions as detailed in table 1[207,209]. Integrins have also been shown to display features of a signalling process known as 'inside-out' signalling, where signal generation originating from other cell receptors are relayed by the integrin molecule from the cytoplasmic tail to the headpiece, to induce headpiece opening and induce high-affinity ligand binding[207,208].

Integrin and cell type	**Ligand**	**Force Applied**	**Result**	**Reference**
α5β1, cell free system.	Fibronectin	10-30pN via atomic force microscopy. Plastic coated integrin molecules brought into contact with cantilevers coated with fibronectin fragments.	Prolonged bond lifetimes associated with headpiece activation	Kong et al 2009[206]
αLβ2 (LFA-1), Jurkat T cells	ICAM-1	0-30pN via biomembrane force probe (BFP)	Bond lifetimes peaking with 10-15pN force application. Slip bond behaviour/bond dissociation beyond 15pN force.	Chen et al 2010[210]
α4β1, developing $CD4^+CD8^+$ murine thymocytes	VCAM-1	10-40pN via BFP	Bond lifetimes peaking with approx. 15pN force application. Slip bond/bond dissociation beyond this.	Choi et al 2014[211]
αMβ2 (Macrophage-1 antigen, MAC-1). Murine neutrophils	ICAM-1	10-30pN via BFP	Bond lifetimes peaking with approx. 10-15pN force application. Slip bond/bond dissociation beyond this. Responses abolished with R77H mutation in β propeller (located within the headpiece region).	Rosetti et al 2015[212]
αVβ3, murine lung endothelial cell lines	fibronectin	0-60pN via BFP	Bond lifetimes peaking with approx. 20pN force application. Slip bond/dissociation beyond this.	Chen et al 2016[213]; Elosegui-Artola et al 2016[214]

Table 1.2 - Evidence for Integrin Catch Bond Behaviour

As detailed in table 1.2, targeting of integrins for force manipulation has commonly been performed using a biomembrane force probe (BFP) approach. However, integrin molecules have also been targeted using magnetic nanoparticles (MNPs) functionalised with antibodies to target α2 and β1 subunits[215,216]. Force application through exposure of these MNPs with external magnetic fields has been shown to induce calcium signalling dependent anchoring of tyrosine phosphorylated proteins to the cytoskeleton and an increase in mitogen activated protein kinase (MAPK) phosphorylation in response to force application in the U2OS osteosarcoma cell line[215,216].

1.8.2 Piezo Mechanosensing

Piezo ion channels are a group of mechanically activated non-selective cation channels expressed in a wide variety of tissues, and highly expressed in the bladder, lung, vascular endothelium and skin of adult mice[217,218]. Most vertebrates express 2 different piezo paralogs (Piezo 1 and Piezo 2), which only share approximately 42% sequence homology yet have highly similar structures[203,219]. Global knockouts of either Piezo1 or Piezo2 were shown to result in murine embryonic lethality. Both Piezo 1 and 2 are homotrimeric channels, consisting of three large curved extracellular 'blades' beneath a cap region. Each blade is anchored at a transmembrane central pore region, which forms the ion accessible pathway. This pathway is covered by a dome-like C-terminal extracellular domain, and sensing of membrane tension by Piezo 1 is sufficient to induce deformations within the ion channel to permit ion entry[220,221]. To this end, force exerted on Piezo1 perpendicularly to the cellular membrane via atomic force microscopy (AFM) has been shown to induce a flattening deformation of this dome structure covering the ion channel, which reverses upon removal of this force application[222]. In line with this, Piezo1 activity has been shown to respond to

fluid flow, thus indicating that the channel is able to directly interpret mechanical stimuli into a biochemical signal. Given this finding and taken together with the high expression of Piezo1 in the vasculature, it is perhaps unsurprising that perturbation of Piezo1 in mice erythrocytes showed symptoms of anaemia and abnormal erythrocyte morphology. Additionally, mutations within human Piezo1 are known to lead to dehydrated stomatocytosis[223] and lymphatic dysplasia[224,225], outlining the physiological importance of mechanosensing through this ion channel.

1.8.3 TRPV4 Mechanosensing

The transient receptor potential vanilloid-type 4 (TRPV4) ion channel belongs to the TRPV family of 6 ion channels (i.e., TRPV1-6) and is another example of a non-selective cation channel[226], which has been proposed to act as a mechanosensor in response to shear forces, stretch-associated membrane tensions and osmotic swelling[227] and heat (in the case of TRPV1-4)[228]. Activation of TRPV4 is known to mediate influx of Ca^{2+} ions, hereby inducing intracellular signalling responses upon sensing of mechanical input. It has been suggested that not only can TRPV4 be directly mechanically activated as a result of subjecting the cellular membrane to various forces, but the channel can also be activated in an in-direct manner downstream of other mechanosensing events such as integrin activation[227], in an example of outside-in signalling by integrins relaying to other mechanically responsive ion channels. Targeting of TRPV4 with MNPs has been shown to specifically induce Ca^{2+} signalling in HEK293T cells[229]. In this approach, a 6xHis tag was inserted into an extracellular loop of the TRPV4 channel, which was then targeted with MNPs functionalised with anti-His antibodies. Application of external magnetic fields to induce a force upon these

functionalised MNPs showed a field strength dependent increase in TRPV4 mediated calcium signalling the HEK293T cells[230]

TRPV4 is expressed at high levels in the vasculature and by a variety of immune cells including neutrophils and macrophages[227], and has been proposed to play an important role in mechanosensing in the innate immune response[231]. This is through reported effects on both vascular permeability and cell adhesion. TRPV4 has been indicated to be a potential mediator of ventilator-induced lung injury, characterised by an increase in lung vasculature permeability. Experiments utilising TRPV4-/- and TRPV4 +/+ mice showed that increase in lung vasculature permeability (as measured by the filtration coefficient) in response to periods of 30 minutes of high pressure ventilation was specifically associated with TRPV4 expression and activation[232]. These findings indicate that TRPV4 activation is able to modulate membrane permeability, which has been proposed to function through disintegration of cellular junctions[233]. However, TRPV4 has also been shown to be crucial for neutrophil adhesion to LPS stimulated lung microvascular endothelial cells and reactive oxygen species production in response to pro-inflammatory stimuli (stimulation with platelet activating factor, PAF)[234]. Together, these findings suggest that TRPV4 plays a key role in neutrophil extravasation both by mediated neutrophil adhesion and barrier permeability in endothelial cells[227,231].

1.8.4 TREK Mechanosensing

Finally, another well studied mechanosensitive ion channel is the Twik-related potassium channel 1 (TREK1), which has also been shown to be responsive to changes in temperature and pH[202,203]. TREK1 is expressed at high levels in cells of the nervous system, heart and smooth muscle and is known to play a role in controlling the resting cell membrane

potential of TREK1 expressing cells[235]. Remote stimulation of TREK1 channels has been shown again using an anti-His functionalised MNP approach, targeting TREK1 proteins in which a 6xHis repeat is engineered with an extracellular loop of the TREK1 channel[236]. Whole cell electrophysiology approaches showed that force application to these His targeted MNPs induced detectable current flow through the TREK1 channel. A similar approach, where TREK1 targeting using MNPs functionalised with TREK1 antibodies are again subjected to forces via external magnetic fields, showed an increase in calcium deposition and mineralisation from human mesenchymal stem cells (hMSCs), indicating a role for TREK1 mechanosensing in osteogenic differentiation[237,238].

Additionally, targeting of TREK1 in osteogenic differentiation has also been reported *in vivo*[239]. In these experiments, ovine mesenchymal stem cells (oMSCs) were labelled with MNPs functionalised with anti-TREK1 antibodies and were placed in a 3D collagen hydrogel. These hydrogels were then implanted into ovine hind legs at sites of induced defects (defects created in the cancellous bone region of the medial femoral condyle), and mechanically activated by the application of external magnetic fields[239]. Enhanced bone repair was observed at 13 weeks when comparing mechanically activated conditions versus no mechanical activation controls. In these cases, micro-CT analyses displayed clear enhanced bone growth when implanted constructs were mechanically stimulated[239].

1.9 Mechanosensing in the Immune System

Given that numerous pathophysiological environments are associated with an altered mechanical environment, the ability of T cells to modulate their behaviour within each environment is of significant importance but is often overlooked. Whilst the role that force can play in controlling TCR triggering and T cell activation by mediation of bond lifetime is

coming to light, the physiological relevance of these force interactions *in vivo* remains an important question. Classical T cell activation *in vitro* often involves the study of somewhat 'stable' T cell cultures, where T cells are often activated on plastic/glass bound antibodies. However, whilst useful for *in vitro* study of T cell behaviours, these conditions poorly replicate the environment a T cell would likely encounter *in vivo* when undergoing antigen recognition and activation in lymphoid organs.

To address this, many groups have investigated T cell activation on hydrogels presenting either anti-CD3 and anti-CD28 antibodies, or pMHC molecules[240]. Production of hydrogels with a stiffness from 2-25kPa showed a stiffness dependent titration of levels of $CD8^+$ T cell activation, as measured by activation marker expression and cell proliferation[240]. Interestingly, increasing the hydrogel stiffness up to 12-25kPa promoted more robust $CD8^+$ T cell activation, yet when ligands were simply presented on tissue culture plastic (a much stiffer surface than the 25kPa hydrogel, tissue culture plastic estimated to be in the range of 100,000kPa[26]) T cell activation was poorer at limiting antigen concentrations vs the 12/25kPa hydrogels[240]. This, therefore, suggests the existence of a 'sweet spot' in the stiffness of the mechanical landscape for optimal T cell activation. Additional independent studies also report a correlation between enhanced T cell activation and increasing surface stiffness, where use of alginate-based hydrogels of 4 and 40kPa show enhanced $CD4^+$ T cell proliferation and CD25 expression on 40kPa hydrogels vs 4kPa[241]. Authors within the same study also measure the stiffness of inguinal and brachial lymph nodes over the course of 14 days in the context of LCMV infection. Stiffness of the lymph nodes increased from a baseline of approximately 1-3kPa to approximately 30kPa at day 3, and peaked at approximately 40kPa 7 days post infection. Tissue stiffness of the lymph node returned to baseline by 10- and 14-days post-infection[241]. These measurements of tissue stiffness during

on-going infection, together with the parallel findings of enhanced $CD4^+$ T cell activation on 40kPa hydrogels provide an intriguing scenario where remodelling of lymphoid tissue during the course of infection can modulate the immune response. In line with this, $CD8^+$ cytotoxic T cells have been shown to mount a stronger killing response in response to stiffer target cells[190,242]. Taken together with reports of metastatic cancer cells being softer than their primary tumour counterparts, an interesting scenario arises where modulation of their mechanical properties may form a mechanism of immune escape by metastatic cancer cells[243,244]. These studies also highlight that whilst at a tissue level cancerous organs are generally stiffer than their healthy counterparts, this is reversed at a single cell level[243]. This suggests an intriguing possibility where increased stiffness of the tumour extracellular matrix (ECM) may serve as a mechanism to modulate the T cell response, whilst remaining softer on a cellular level may aid immune escape.

Indeed, increased stiffness of the tumour ECM has been shown to negatively impact the T cell response, where stiff tumour ECM has been shown to reduce $CD8^+$ T cell motility. This was recovered with LOX inhibition as a means to decrease the stiffness of the tumour ECM[245]. Interrogation of the global stiffness of these tumours revealed numerous regions exceeding 40kPa, which was reduced upon LOX inhibition via treatment with beta-aminopropionitrile (BAPN)[245]. The existence of these regions exceeding 40kPa again may suggest a sweet spot within the mechanical landscape exists for robust T cell activation. BAPN treatment resulted in enhanced T cell infiltration into the tumour; however, tumour growth was only significantly reduced by combination therapy of BAPN treatment and PD-1 blockade[245]. These results indicate that ECM stiffness is an important factor able to manipulate T cell behaviour, but also reflects the complexity of other factors within the tumour microenvironment also capable of modulating T cell activation.

Other immune cell types have shown similar dependence on substrate stiffness for robust activation, where multiple groups report a beneficial mechanical landscape for dendritic cell (DC) priming and function. In similar stiffness sensing experiments, it has been shown that activation of bone marrow derived DCs (BMDCs) by LPS stimulation on high stiffness hydrogels (50kPa) produced an increase in DC activation and proliferation compared with softer hydrogels of 2kPa[246]. Furthermore, the stiffer hydrogels also induced DC to adopt a more pro-inflammatory profile evidenced by increased expression of proteins involved in antigen presentation (MHC-II, CD80 and CD86) and pro-inflammatory cytokines TNFα, IL-1α, IL-1β, IL-6 and IL-12[246]. Additionally, other groups have shown that an increase in DC stiffness can arise as a consequence of DC maturation. Perturbation of the cytoskeleton of these DCs, thereby reducing maturation associated stiffness, has been linked to quality of T cell activation achieved by these DCs[240]. In these experiments, use of the actin polymerisation inhibitor Latrunculin A (Lat A) reversed the increase in DC stiffness upon LPS induced maturation. These results were replicated in matured DCs from Wiskott-Aldrich Syndrome protein (WASP, a protein involved in actin cytoskeletal remodelling downstream of receptor signalling)-KO mice, and these DCs were shown to be poorer activators of $CD8^+$ T cells at limiting antigen doses[240]. Taken together, these results indicate that the mechanical landscape within which immune responses take place is able to physically manipulate the quality of these responses.

Behaviour of many other innate immune cells have been reported to be sensitive to mechanical cues. It has previously been established that adhesion of macrophages to substrates of varied stiffness promotes distinct macrophage phenotypes. Use of stiffer substrates for *in vitro* macrophage culture has been shown to enhance TNFα production upon LPS stimulation, across stiffness ranges of 1/20/280kPa[247]. Additionally, use of rigid

polystyrene hydrogels induces increased TNFα and IL-6 in response to LPS, when compared with production from the same cells cultured on softer fibrin hydrogels, whilst also reducing IL-10 production[247,248]. Clearly, this indicates that the mechanical environment in which macrophage activation takes place can modulate the production of both pro-inflammatory and anti-inflammatory cytokines. Mechanosensing by macrophages through Piezo-1 has also been shown to modulate macrophage activity and phenotype. By depleting Piezo-1 expression on bone marrow derived macrophages (BMDMs), Piezo-1 was shown to play an important role in production of pro-inflammatory cytokines in response to inflammatory stimuli (i.e., BMDM stimulation with IFNγ/LPS), where a significant decrease in expression of the inflammatory marker inducible nitric oxide synthase (iNOS) was observed vs Piezo-1 expressing controls[249]. On top of this, stimulation of Piezo-1 depleted BMDMs with pro-healing cytokines IL-4/IL-13 showed a significant increase in expression of arginase-1 (ARG-1), a pro-healing marker[249]. Furthermore, the authors report that culturing of BMDMs on stiff substrates (280kPa polyacrylamide gels) promotes increased Piezo-1 expression when compared with softer substrate (1kPa)[249]. Finally, BMDMs on these stiffer substrates also showed enhanced calcium signalling signatures in response to the Piezo-1 agonist Yoda-1. These reports indicate how mechanosensing of substrate stiffness via Piezo-1 can modulate macrophage activation and phenotype[249].

Mechanosensing in innate immune cells has also been shown to occur in response to shear forces, where neutrophils under shear flow have been shown to upregulate calcium signalling through mechanosensing by LFA-1[250]. There is, therefore, a growing body of evidence for mechanosensing by immune cells, utilising varied cell receptors and ion channels to modulate their response determined by the mechanical environment of the ongoing immune response.

1.10 Project Aims

This project aims to approach the question as to whether signalling through the TCR can be modulated by external force application, and to interrogate the mechanisms by which the TCR can interpret mechanical forces. Within this, we aimed to investigate further the characteristics of how TCRs can interpret external forces, in terms of force magnitude, directionality and duration of force application. Given the vast therapeutic benefits of modulating $CD4^+$ T cell behaviour, we chose in this study to focus on the manipulation of TCRs on $CD4^+$ T cells.

Our approach utilises antibody functionalised superparamagnetic nanoparticles (MNPs) directed against the TCR-CD3 complex, which translate force to the complex when exposed to remote magnetic fields. This approach has been extensively used by El Haj and colleagues for the mechanical manipulation of various ion channels (TREK[236,237,239], Piezo1[251] and TRPV4 amongst others) both *in vitro* and *in vivo*[239]. Therefore, use of MNPs is not only beneficial from a mechanistic point of view to interrogate the mechanism of action of mechanosensors but is also promising from a therapeutic standpoint where cellular behaviours can be controlled remotely.

It should be noted that whilst other systems do exist for applying forces to ligand-receptor interactions, we chose to utilise the approach consisting of functionalised MNPs and external magnetic fields to generate forces throughout the course of this study. Other approaches include atomic force microscopes (AFMs), where cantilever tips on the AFM can be functionalised with antibodies[252,253] to target the TCR, which can then be presented to TCRs to interrogate the TCR-ligand interaction under force. This approach has already been applied to the study of T cells[252–254] yet unless the AFM instrument is part of a specialised

set up that allows for live imaging, for instance calcium imaging[252], this approach fails to provide information on the activation of the cells interrogated. Optical tweezers[183,188], magnetic tweezers[207,255] and biomembrane force probes (BFPs)[196,199] are all examples of other methodologies that have been applied to studying force application to the TCR-ligand interaction. However, these approaches again fail to provide information on the activation state of the cells in question unless utilised as part of a specialised set up. Additionally, all 4 of the approaches mentioned are single cell approaches, and therefore are not entirely compatible with studying TCR signalling and T cell activation upon force application at scale. Since the MICA instrument utilised within the El Haj laboratory is able to apply forces to MNPs on the surface of T cells at scale (i.e., applying forces to up to 10^5-10^6 cells per condition, determined by the user), and that these cells are then recoverable for downstream analysis, we chose to utilise this approach to investigate whether external force application to the TCR can influence signalling and T cell activation.

Chapter 3 describes a system for how external force application via MNPs can work in the context of the TCR and provides insights as to how this approach impacts TCR signalling. The experiments described herein provide evidence that force application specifically induces TCR signalling and T cell activation. Chapter 4 begins to shed light on the mechanism behind force induced $CD4^+$ T cell activation, by identifying that TCR membrane reorganisation in response to force application is critical for force induced TCR signalling. Finally, chapter 5 begins to probe how force modulation of TCR signalling can impact $CD4^+$ T cell phenotype and assesses whether force induced phenotypic differences are able to produce differential functional responses.

1.11 Future Work

Whilst the data presented within this thesis outline how force application to the TCR can influence T cell activation, further experimentation is required in some parts. Within chapter 3, we identify that pulsatile force application to the TCR promotes signal accumulation, reaching the threshold required for T cell activation (figures 3.16 – 3.19). Further to this, we identify that when TCR signalling strength is sufficiently high to induce the expression of co-inhibitory receptors in the presence of force application, pulsatile application of this force input prevents upregulation of these markers (appendix figure 8.10). These results suggest the existence of negative feedback loops or alternative negative signalling pathways that may be triggered when TCR signalling strength reaches too high of a level, as discussed in chapter 6 (see figure 6.2). Further investigation should look for the existence of these negative signalling pathways, whereby study of the phosphoproteomics of $CD4^+$ T cells under the conditions tested (i.e., those where force application induces upregulation of activation markers, yet pulsatile force application prevents this) may indicate which regulators of T cell signalling pathways are mediating this effect.

Additionally, within chapter 4 we identify that a potential driving mechanism for force induced T cell activation in our protocol centres around force induced re-organisation of the TCR within the cell membrane. Here, we outline that force application the TCR induces the formation of TCR clusters (as identified by single molecule localisation microscopy, figures 4.24 – 4.25), and subsequent TCR downregulation. Importantly, we show that it is those cells that downregulate their TCR in response to force application that are indeed triggered by force application, evidenced through expression of Nr4a3, CD69 and CD25 (figures 4.13 – 4.14). An important question that requires further investigation from this work is whether downregulated TCRs continue to contribute to the TCR signalling cascade once they are internalised. Other groups have shown that internalisation of engaged TCRs also results in the internalisation of nearby non-engaged, 'bystander' TCRs[117]. It is conceivable that if activating kinases are also internalised in the same endosome, then TCR-CD3 phosphorylation can continue to occur and allow for continued signalling and enhance signal accumulation. Whilst complex, further investigation with live, multi-colour single molecule localisation microscopy utilising fluorescently tagged particles together with

labelled TCR and Lck (or other activating kinases) may be able to shed light on this potential mechanism. If indeed this phenomenon is found to take place, it may answer how engagement of a single TCR is able to induce robust T cell activation.

Finally, the true initiating mechanism of the TCR trigger is still inconclusive. Whilst it is unlikely that any one mechanism fully explains how the TCR functions, mounting evidence suggests that force application may play a role. Of upmost importance are the findings that under force, the TCR can form catch or slip bonds, which correlate with functional output for those given T cells[196,199]. It is tempting to consider that formation of these bonds under force may be an event upstream of any of the key events currently postulated to induce TCR triggering in the various triggering models. For instance, since catch or slip bond formation under force regulates the lifetime of the TCR-pMHC bond, does alter the length of the proofreading time postulated in the kinetic proofreading model, and hence act upstream of intracellular signalling molecule phosphorylation? Furthermore, in the kinetic segregation model whereby phosphatases such as CD45 are excluded from zones of TCR-pMHC contact[128,145], is this only permitted to occur at sites where catch bonds are formed, allowing for longer lived TCR-pMHC interactions? Since catch and slip bonds can be imaged using biomembrane force probes (BFP), development of this technique to incorporate live fluorescent imaging will allow for the investigation of these questions. Here, BFP experiments using T cells engaging altered peptide ligands of hierarchal affinities for the TCR (for example, the OVA system used in the Evavold catch vs slip bond experiments[196]), will allow for the identification of catch bonds in response to high affinity ligands, and the temporal relationship between these events and intracellular signalling protein phosphorylation and phosphatase exclusion.

CHAPTER 2

2 Materials and Methods

2.1 Mice

All experimental mice were maintained under specific pathogen free conditions by the Biomedical Services Unit (BMSU) at the University of Birmingham. All experiments were performed in accordance with the UK Home Office Project Licence held by Professor David Wraith for Tg4/B10.PL/RTO/Tg4 CD45.1 mice (current licence, P17E7ABFB) or Dr David Bending for Nr4a3-fluoescent timer (Nr4a3-FT) reporter 'tocky' mice (current licence, P18A92E0A (0135)).

Tg4 and Tg4 CD45.1 TCR transgenic mice express a Vβ8.2 TCR on 95% of $CD4^+$ T cells, specific for the myelin basic protein (MBP) peptide, MBP Ac1-9, in the context of MHC-II H-$2A_u^{256}$. Mice were phenotyped in house by analysis of tail vein bleeds taken by BMSU staff after weaning. Antibodies used to phenotype these mice are shown in table 2.1.

Tg4 Phenotyping Antibodies			
Target	**Clone**	**Dilution**	**Supplier**
TCR Vβ8.1/8.2 FITC	KJ16-133.18	1:200	Biolegend
CD4 PerCP-Cy5.5	RM4-5	1:200	Biolegend
CD19 APC	eBio1D3	1:200	Thermo Fisher
MHC-II PE	OX-6	1:500	Biolegend
Tg4 CD45.1 Phenotyping Antibodies			
Target	**Clone**	**Dilution**	**Supplier**
TCR Vβ8.1/8.2 FITC	KJ16-133.18	1:200	Biolegend
CD4 PeCy7	GK1.5	1:200	Biolegend
CD45.1 APC	A20	1:200	Biolegend
CD45.2 PerCP-Cy5.5	104	1:200	Biolegend

Table 2.1 - Antibodies used to phenotype Tg4 and Tg4 CD45.1 mice.

B10.PL mice are H-2A^{u} positive and were thus utilised as a source of antigen presenting cell for T cell activation assays of T cells from Tg4 mice. B10.PL mice also form the background of the Tg4 transgenics[256] and were thus used as a wild type (WT) control for Tg4 studies. B10.PL mice were originally obtained from the Jackson Laboratory and since maintained as part of the Wraith laboratory colonies within the BMSU.

RTO mice express the Tg4 TCR on a Rag$^{-/-}$ background meaning CD4^{+} T cells from RTO mice express only the Tg4 TCR, due to an inability of developing thymocytes to properly undergo VDJ gene-rearrangement.

Nr4a3-FT timer of cell kinetics and activity, or Nr4a3-FT 'tocky' (henceforth referred to as Nr4a3-FT) mice were kindly provided by the laboratory of Dr David Bending. Nr4a3-FT mice

express a BAC containing the FT Fast mCherry mutant under the influence of Nr4a3 regulatory regions on the C57BL/6 background[257]. Briefly, the FT mCherry mutant is initially expressed in a blue fluorescent form with a half-life of approximately 4 hours, detectable in the BV421 channel. This blue form decays to a red fluorescent form with a longer half-life (estimated to be 20hours)[257] which permits the interrogation of TCR signalling kinetics.

Single cell suspensions were produced from spleens harvested from these mice by disruption of the spleen and passing of the resulting suspension through a 40µm cell strainer (Greiner BioOne, 542040). Following centrifugation for 5 minutes at 1800rpm at 4°C, cell suspensions were resuspended in 1mL red blood lysis buffer (Sigma-Aldrich, R7757) for 4 minutes prior to addition of 9mL complete RPMI + 10% fetal calf serum (FCS, Sigma-Aldrich, F9665) to quench the RBS lysis step. Resulting suspensions were washed twice in 15mL complete RPMI + 10% FCS by centrifugation as described, and cell number was determined, with cell purification processes carried out afterwards if required as described.

2.2 Tissue Culture

All tissue culture was performed in complete RPMI-1640 (Sigma-Aldrich, R0883). Complete RPMI was supplemented with final concentrations of 4mM L-glutamine (Sigma-Aldrich, G7513), 1000U/mL penicillin and 1mg/mL streptomycin (Sigma-Aldrich, P4333), 20mM HEPES (Sigma-Aldrich, H0887), 50µM β-mercaptoethanol (Gibco, 31350-010) and 10% FCS (Sigma-Aldrich, F9665). Weeklong cultures were supplemented with a final concentration of 20U/mL IL-2 (R&D Systems, 202-IL) at D3 and D5.

2.3 Isolation of CD4 or CD11c cells

Following production of a single cell suspension, $CD4^+$ T cells or $CD11c^+$ cells were purified using the following kits as per the manufacturer's instructions. $CD4^+$ T cell isolation kit:

Invitrogen magnisort negative selection kit (8804-6821-74). $CD11c^+$ cell isolation kit: Miltenyi $CD11c^+$ microbeads (130-125-835).

2.4 Magnetic Particle Functionalisation Buffers

The following buffers were used to functionalise magnetic nanoparticles as described in 2.5. 0.1M and 0.5M MES buffer (Sigma Aldrich, M3671) was dissolved in PBS (Sigma-Aldrich, D8537) and pH adjusted to 6.3 by the dropwise addition of 2M Na_2CO_3 (Sigma-Aldrich, S2127). For activation of particles, EDAC/NHS (approximately 31mM/104mM respectively) solution was produced by dissolving 12mg and 24mg of EDAC (Sigma Aldrich, 03449) and NHS (Sigma Aldrich, 130672) in 2mL of 0.5M MES buffer which was then sterile filtered. 25mM glycine (Sigma Aldrich, G8898) in PBS was used to stop the antibody binding reaction. Finally, blocking/storage buffer consisted of 0.1% BSA (Sigma-Aldrich, A7906) in PBS. All particles were functionalised, stored at 4°C and used in an experiment within 1 week.

2.5 Magnetic Particle Functionalisation Protocol

Commercially available superparamagnetic nanoparticles particles (MNPs) were functionalised with antibodies via standard carbodiimide chemistry. Briefly, 1mg of 250nm (micromod, Nanomag-D 250nm MNPs, 09-02-252) or 1µm (chemicell, SiMAG-carboxyl MNPs, 1402-1) MNPs in 100µL were activated by addition of 20µL EDAC/NHS solution for 1 hour under constant rotation (final concentrations of EDAC/NHS were 5mM and 17mM respectively). MNPs were then washed three times in 200µL 0.1M MES buffer by magnetic separation, before resuspension in 100µL and addition of capture antibody as per tables 2.2-2.3. MNPs with capture antibody were incubated overnight at 4°C with constant rotation, before being washed three times as previous and resuspended in 100µL 0.1M MES buffer.

Target antibody was then added as per tables 2.2 and 2.3 and incubated at room temperature for 3 hours under constant rotation. Free antibody was then quenched by addition of 10µL 25mM glycine under constant rotation at room temperature for 30 minutes (achieving a final concentration of approximately 2.3mM), before three washes in 200µL 0.1% BSA. Functionalised MNPs were then resuspended in 1mL 0.1% BSA (producing final concentrations of 1mg/mL of functionalised particles). Functionalised MNPs were stored at 4°C and used within 1 week of functionalisation. For non-functionalised MNP controls, all described steps were followed but addition of antibodies was omitted.

It should be noted that quantity of target antibody used to functionalise MNPs are as indicated in table 2.3. In brief, amount of target antibody for positive effects of magnetic force was optimised to an addition of a total of 1µg target antibody for both 250nm and 1µm MNPs. This was increased to 10µg total antibody to investigate a negative effect of magnetic force application for 1µm MNPs. In every case, amount of capture antibody used in functionalisation was 2X quantity of target antibody used (i.e., for 1µg total target antibody, 2µg total capture antibody was used. For 10µg total target antibody, 20µg total capture antibody was used). Assuming a 100% efficiency of antibody loading onto the particle surface during the functionalisation process, levels of antibody per particle and hence antibodies per surface area unit could be calculated as per equations 2.1 below. The results of these calculations are shown in table 2.3.

Particle Size	Target	Secondary Antibody	Primary Antibody
250nm	Anti-CD3ε (145-2C11)	AffiniPure Goat anti-Armenian Hamster IgG (Jackson Immunoresearch, catalogue number: 127-005-099).	Anti-mouse CD3ε (Invitrogen, 145-2C11, catalogue number: 16-0031-82)
250nm	Anti-CD3εγ (17A2)	Mouse anti-Rat IgG2B (Biolegend, MRG2b, catalogue number: 408205)	Anti-mouse CD3εγ (Biolegend, 17A2, catalogue number: 100201)
250nm	Anti-TCRβ (H57-597)	AffiniPure Goat anti-Armenian Hamster IgG (Jackson Immunoresearch, catalogue number: 127-005-099)	Anti-mouse TCRβ (Biolegend, H57-597, catalogue number: 1092901)
250nm	Anti-MHCI	Rat anti-mouse IgG2a (Biolegend, RMGa-62, catalogue number: 407105)	Anti-mouse H-2K^{b} (Biolegend, Af6-88.5, catalogue number: 116501)
250nm	Anti-CD28	AffiniPure Goat anti-Armenian Hamster IgG (Jackson Immunoresearch, catalogue number: 127-005-099)	Anti-mouse CD28 (Invitrogen, 37.51, catalogue number: 16-0281-82)
250nm	Anti-CD3/CD28	AffiniPure Goat anti-Armenian Hamster IgG (Jackson Immunoresearch, catalogue number: 127-005-099)	Anti-mouse CD3ε (Invitrogen, 145-2C11, catalogue number: 16-0031-82) Anti-mouse CD28 (Invitrogen, 37.51, catalogue number: 16-0281-82)
1µm	Anti-CD3ε (1µg)	AffiniPure Goat anti-Armenian Hamster IgG (Jackson Immunoresearch, catalogue number: 127-005-099)	Anti-mouse CD28 (Invitrogen, 37.51, catalogue number: 16-0281-82)
1µm	Anti-CD3ε (10µg)	AffiniPure Goat anti-Armenian Hamster IgG (Jackson Immunoresearch, catalogue number: 127-005-099)	Anti-mouse CD28 (Invitrogen, 37.51, catalogue number: 16-0281-82)
1µm	Anti-MHCI	Rat anti-mouse IgG2a (Biolegend, RMGa-62, catalogue number: 407105)	Anti-mouse H-2K^{b} (Biolegend, Af6-88.5, catalogue number: 116501)
1µm	Anti-CD28	AffiniPure Goat anti-Armenian Hamster IgG (Jackson Immunoresearch, catalogue number: 127-005-099)	Anti-mouse CD28 (Invitrogen, 37.51, catalogue number: 16-0281-82)

Table 2.2 – Antibodies used for MNP Functionalisation.

$$Antibody\ molecular\ weight(Hamster\ IgG) = 150kDa$$

$$150kDa\ =\ 150{,}000g/mol$$

$$Amount\ of\ antibody\ added(g) \div 150{,}000 = Number\ of\ moles$$

$$Number\ of\ moles\ \times\ avagadros\ constant\ =\ Number\ of\ antibody\ molecules\ added$$

$$Particle\ surface\ area\ =\ 4\pi r^2$$

$$Number\ of\ antibody\ molecules\ per\ surface\ area\ unit$$

$$=\ Number\ of\ antibody\ molecules\ added\ \div\ particle\ surface\ area$$

Equations 2.1 - Calculations for number of antibodies added per surface area unit.

Particle	Amount of 145-2C11 added (quantity)	Total number of antibody molecules added	Amount of particles functionalised to (quantity)	Stock particle concentration	Antibodies per particle	Particle surface area	Antibodies per surface area unit
1µm^{Hi}	10µg	4.01476x10^{13}	1mg	1.8x10^{9}/mg	22304	3.14µm^2	7103/µm^2
1µm^{Mid}	1µg	4.01476x10^{12}	1mg	1.8x10^{9}/mg	2230.4	3.14µm^2	710.3/µm^2
1µm^{Lo}	0.1µg	4.01476x10^{11}	1mg	1.8x10^{9}/mg	223.04	3.14µm^2	71.03/µm^2
250nm^{Hi}	10µg	4.01476x10^{13}	1mg	4.9x10^{10}/mg	819	0.2µm^2	4095/µm^2
250nm^{Mid}	1µg	4.01476x10^{12}	1mg	4.9x10^{10}/mg	81.9	0.2µm^2	409.5/µm^2

Table 2.3 - Levels of antibody per surface area unit for particle used. Predicted numbers of antibodies added during the functionalisation process could be determined based on equations 2.1. Numbers of particles/mg could be determined from SDS information sheets from the particle manufacturers, allowing for the determination of numbers of antibody per particle, and hence numbers of antibody/µm^2 based on the equations shown in 2.1.

Levels of anti-CD3 antibodies for each given particle are shown in table 2.3 above. Titrating the level of total antibody added during the functionalisation process produced a titration of antibodies per surface area unit as shown. Particles with >1000 antibodies/µm^2 were termed were predicted to induce high levels of TCR signalling, and hence termed 1µm^{Hi} or 250nm^{Hi}. Particles with 100-1000 antibodies/µm^2 were predicted to induce intermediate levels of TCR signalling, and hence were termed 1µm^{Mid} or 250nm^{Mid}, whilst particles with 10-100 antibodies/µm^2 were predicted to induce little to no levels of TCR signalling and are hence termed 1µm^{Lo}. Particles are henceforth referred to as 1µm^{Hi}/^{Mid}/^{Lo}

or 250nm^{Hi}/^{Mid} throughout the text, referring to their levels of antibody per surface area unit as per table 2.3.

2.6 Treatment of CD4 T cells with Functionalised MNPs

Purified CD4$^+$ T cells were treated with functionalised MNPs on ice for 30 minutes, with end cell concentrations being maintained at 5x10^5/mL during the treatment process. Initially, the final concentration of functionalised MNPs required to observe an effect on TCR signalling was determined experimentally (as per figure 3.1 and 3.8) and maintained at treatment with a final concentration of 50µg/mL of functionalised MNPs. Cells were then washed three times in at least 20mL of PBS by centrifugation at 300g, 4°C for 5 minutes to pellet cells only. Cells bound with functionalised particles were then resuspended at 1x10^6/mL and used in experiments as described.

2.7 Magnetic Force Application Experiments - MICA

CD4$^+$ T cells treated with functionalised particles as per 2.6 were plated at 4x10^5/well in a final volume of 800µL in 24 well plates. Magnetic force (MF) application was applied for time frames described using a computer programmable oscillating magnetic bioreactor, termed magnetic ion channel activation (MICA, MICA Biosystems Ltd)[237,258], which applies normal force (i.e., perpendicular to the tissue culture plate) to functionalised MNPs. Therefore, individual TCRs on any given T cell will experience forces in different directions, as illustrated in figure 2.1, due to the nature of MF application from under neath a tissue culture plate containing a suspension of MNP labelled CD4$^+$ T cell.

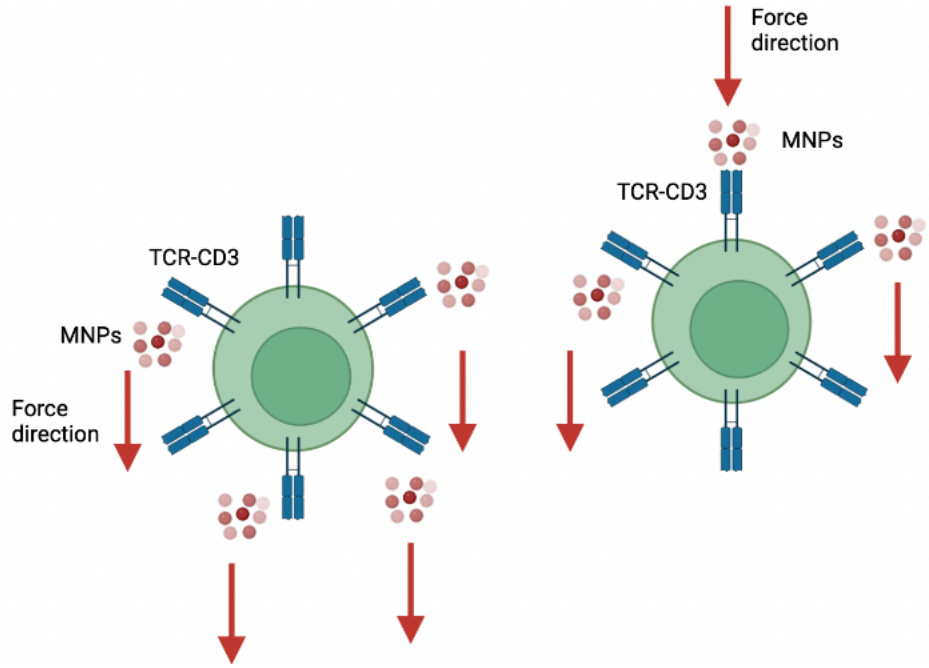


Figure 2.1 - Direction of force application to individual TCRs with MICA. TCRs on $CD4^+$ T cells are labelled in suspension with anti-CD3 functionalised MNPs, as described in 2.6. As a result, individual TCRs can experience forces in different directions to one another and hence can either be pulled perpendicular to the membrane, experience shear forces along the membrane, as well as possibly being pushed into the membrane. Image produced in BioRender.

The MICA instrument is housed within a 37°C 5% CO_2 incubator, and was equipped with a 24 well magnet array, that mimics the layout of a 24 well plate. Therefore, each well in the plate is subjected to the same magnetic field, as evidenced previously using an automated 3D magnetic field scanner[258]. Computer programming of the MICA instrument allows for the magnetic array to cycle back and forth between an 'on' and 'off' position with a frequency of 1Hz, to provide a constant exposure to magnetic forces. In the on position, the magnetic array was positioned approximately 5mm from the cells + MNPs, providing a magnetic field strength and field gradient of approximately 0.213T and 40.106Tm^{-1} respectively. In the off position, the magnetic array is positioned more than 15cm away from the cells + MNPs and exerts no measurable magnetic field on the MNPs at this position. Force magnitudes transferred to each particle at these magnetic field strengths were calculated as per equation 2.2 below[259] and are summarised in table 2.4.

$$F = S \times MNPvol \times (1/P) \times B \times \Delta B$$

Equation 1.2 - Force calculations for MNPs on a MICA bioreactor. F; force (Newtons, N) = S (susceptibility) x MNPvol; particle volume (meters, m) x P (magnetic permeability of free space) x B; magnetic field strength (Tesla, T) x ΔB; magnetic field gradient (Tesla, Tm^{-1}).

Particle	Force Transferred with MICA
250nm	0.009pN
1µm	0.59pN

Table 2.4 - Magnetic Forces for Functionalised MNPs on a MICA bioreactor. Forces shown are calculated using equation 1 with field strength and field gradient values as described in 2.7.

2.8 T Cell Activation Assays

2.8.1 Activation Marker Expression at 4 hours post Magnetic Force Application

As described, purified $CD4^+$ T cells were pre-treated with functionalised MNPs and subjected to magnetic force (MF) as per 2.6 for time frames indicated. Unless otherwise stated, this time frame was optimised to and most commonly set at 1 hour. After MF application, cells were maintained in a 37°C 5% CO_2 incubator for 4 hours to allow for protein translation from the Nr4a3-FT reporter and cell surface activation marker expression. Cell suspensions were then surface stained for activation markers as per 2.9.1. Where experiments were performed in Nr4a3-FT mice, the BV421 channel was kept free to allow for acquisition of the blue form of the fluorescent protein. Where indicated, PP2 (Sigma-Aldrich, P0042) and cyclosporin A (CsA, Cell guidance systems, SM43) were used at final concentrations of 10µM and 1µM respectively. The actin polymerisation inhibitor Latrunculin A (Tocris, 3973) was also used as shown to final concentrations of 0.25 and 1µM. For all inhibitor use, DMSO controls to the appropriate concentrations were performed at the same time. Stimulation of $CD4^+$ T cells with phorbol 12-myristate 13-acetate (PMA, Sigma-Aldrich, P1585) – ionomycin (Sigma-Aldrich, I3909) (PI) at final concentrations of

5ng/mL and 500ng/mL respectively was often included as a positive control for timer protein expression.

2.8.2 Proliferation and Cytokine Production Assays

$CD4^+$ T cells from Tg4 mice were first loaded with cell trace violet (CTV) proliferation dye (Invitrogen, C34557). Cells were first resuspended in pre-warmed (37°C) PBS at $5x10^6$/mL before addition of CTV at 1:1000 to achieve an end concentration of 5µM. Cells were loaded with CTV in a 37°C incubator for 20 minutes before addition 5X volumes of RPMI 10% FCS to quench the reaction. Cells were rested in a 37°C incubator for a further 5 minutes, before 3 standard centrifugation washes at 1800rpm for 5 minutes in RPMI + 10% FCS, after which cells were ready to use. Cells were treated with functionalised MNPs and subjected to 1 hour MF as described in 2.6 and 2.7 respectively and supplemented with a final concentration of 20U/mL IL-2.

At day 3, $CD4^+$ cell cultures were transferred to a 96 well round bottomed plate and re-stimulated for 4 hours with PI as described (2.8.5) plus GolgiStop (henceforth known as PIGS) (BD Bioscience, 554724) at a final dilution factor of 1:100. Cells were then surface stained as described in 2.9.1, and fixed in 200µL IC fixation buffer (Invitrogen, 00-8222-49) for 30 minutes at 4°C. Cells were then permeabilized in 100µL 1X permeabilization buffer (Invitrogen, 00-8333-56) at 4°C for 15minutes, prior to intracellular staining as described in 2.9.2.

2.8.3 Signalling Protein Phosphorylation Experiments

Purified $CD4^+$ T cells were treated with MNPs and stimulated with MF for time frames indicated as described in 2.6 and 2.7 respectively. It should be noted that to allow for

immediate fixation, cells were kept in PBS as opposed to RPMI+10% FCS for these experiments. At each time point, cells were fixed by addition of paraformaldehyde (PFA) (Thermo Scientific, 28906) to a final concentration of 4%. Cells were fixed at 4°C for 20 minutes, washed at least three times in PBS (1800rpm, 5 minutes), and surface stained for CD4 as described in 2.9.1. Cells were then resuspended in 1mL of 90% methanol (VWR, 20847.307) pre-chilled to -20°C. Addition of methanol was performed in a slow drop-wise manner whilst the sample was kept under constant agitation on a vortex to prevent the formation of aggregates. Cells were permeabilized in methanol over night at -20°C, washed three times as described in FACS buffer and stained for intracellular phosphorylated signalling proteins as described in 2.9.3.

2.9 Flow Cytometry

2.9.1 Surface staining for T cell activation, T cell phenotype and TCR expression

Antibodies shown in table 2.5 were diluted to their appropriate dilution factors in FACS buffer (PBS + 2mM EDTA (Sigma-Aldrich, E7889) and 2% FCS). All samples were stained in 100µL of staining mastermix for 25 minutes at 4°C in the dark. Samples were then washed three times for 5 minutes by centrifugation at 1800rpm in 1mL FACs buffer, and ultimately resuspended in 200µL FACS buffer prior to acquisition on an LSR-Fortessa-X20 flow cytometer (BD Biosciences).

Target	Fluorophore	Clone	Dilution	Supplier
TCRβ	FITC	H57-597	1:200	Biolegend
TCR Vβ8.1/8.2	FITC	KJ16-133.18	1:200	Biolegend
TCR Vβ8	PE	F23.1	1:400	BD Pharmigen
CD4	AF700	RM4-5	1:200	Biolegend
CD69	PeCy7	H1.2F3	1:400	Biolegend
CD25	APC	PC61	1:200	Biolegend
CD25	BV605	PC61	1:300	Biolegend
CD25	BV650	PC61	1:300	Biolegend
Fixable viability dye	ef780 (APC-Cy7)	N/A	1:1000	Thermo Fisher
CD45.1	APC	A20	1:200	Biolegend
CD45.1	PerCP Cy5.5	A20	1:200	eBioscience
Tigit	PE	1G9	1:200	Biolegend
CTLA-4	PeCy7	UC10-4B9	1:200	Biolegend
PD-1	BV711	29F.1A12	1:200	Biolegend
Lag 3	PerCP Cy5.5	C9B7W	1:200	Biolegend
Tim3	ef450	8B.2C12	1:200	Invitrogen
CD73	PeCy7	eBioTY/11.8	1:400	Invitrogen
FR4	PerCP Cy5.5	12A5	1:200	Biolegend
CD39	APC	Duha59	1:200	Biolegend
NRP-1	BV421	3E12	1:200	Biolegend
CD44	PerCp Cy5.5	IM7	1:200	Biolegend

CD62L	PE	MEL-14	1:400	Biolegend
PDL1	BV421	10F.9G2	1:200	Biolegend

Table 2.5 - Surface antibodies used for flow cytometry

For correlation analyses between TCR downregulation and activation marker expression, experiments were set up as per 2.8.1 before surface staining 4 hours post force application as described above. Post sample acquisition, cells were analysed using FlowJo software v.9 or 10 (FlowJo LLC, TreeStar), where each sample was appropriately gated into TCRhi or TCRlo populations. Expression of T cell activation markers Nr4a3, CD69 and CD25 was then assessed within both TCRhi and TCRlo population to assess the relationship between TCR downregulation and activation marker expression.

2.9.2 Intracellular Staining for Cytokine Production

Antibodies shown in table 2.6 were diluted as shown in 1X FoxP3 kit permeabilization buffer (Invitrogen, 00-833-56), and permeabilized cells were incubated in 100µL staining mastermix for 30 minutes at 4°C in the dark. Samples were washed x2 in 200µL permeabilization buffer in a 96 well round bottom plate by centrifugation for 2 minutes at 2000rpm, before a further wash in 100µL FACS buffer and ultimately resuspended in 200µL FACS buffer prior to acquisition of an LSR-Fortessa-X20 flow cytometer.

Target	**Fluorophore**	**Clone**	**Dilution**	**Supplier**
IFNg	PeCy7	XMG1.2	1:500	Biolegend
IL-2	PE	JES6-5H4	1:200	Biolegend
IL-10	APC	JES5-16E3	1:100	Biolegend

Table 2.6 - Antibodies used for intracellular cytokine staining

2.9.3 Phospho-protein Staining

Samples were prepared as per 2.8.3 and stained as per the staining strategies for each phospho-protein target as per table 2.7. Samples were stained in 100µL of antibody mix at all times.

Target	Primary Antibody	Primary Staining Procedure	Secondary Antibody	Secondary Staining Procedure
Phosphorylated ERK (pERK)	Anti-Phospho-p44/42 MAPK (Erk1/2). Cell signalling, 9101.	1:50 in FACs buffer, 1hr @ RT	Anti-Rabbit IgG Alexa Fluor 647. Thermo Fisher, A21245.	1:500 in FACs buffer. 30min @ RT
Phosphorylated Lck (pLck)	PE conjugated anti-Lck (Phospho Tyr394). Biolegend, A18002D, Catalogue number 933103.	1:25 in FACs buffer, 30min @ RT	N/A	N/A
Phosphorylated SHP-1 (pSHP-1)	FITC conjugated anti-SHP-1 (Phospho Tyr536). Invitrogen, MA5-37130.	1:25 in FACs buffer, 30min @ RT	N/A	N/A

Table 2.7 - Antibodies used in phospho-protein staining

2.9.4 MNP Quality Control Staining

To assess the level of CD3 antibody bound to the surface of MNPs post-functionalisation, 50µL of functionalised MNPs were taken and resuspended in 100µL of FITC conjugated anti-Hamster IgG (Biolegend, Poly4055, 405502) at a 1:100 dilution. MNPs were stained for 20 minutes at 4°C in the dark, before 3 standard centrifugation washes (5 minutes, 1800rpm) in 1mL FACs buffer. Ultimately, stained particles were resuspended in 200µL FACs buffer prior to data acquisition as previously described.

2.9.5 Surface vs Cycling vs Total TCR analysis

Purified $CD4^+$ T cells from either Nr4a3-FT or Tg4 transgenic mice were stimulated with functionalised MNPs and subjected to external magnetic force as described. For surface TCR analysis, cells were stained with 100µL antibody mastermix diluted to their appropriate dilution factors in FACS buffer as per 2.9.1. Antibodies for this analysis are shown in table 2.8. All staining steps were performed for 25 minutes at 4°C in the dark.

Target	**Fluorophore**	**Clone**	**Dilution**	**Supplier**
TCRβ	FITC	H57-597	1:200	Biolegend
CD4	AF700	RM4-5	1:200	Biolegend
Fixable viability dye	ef780 (APC-Cy7)	N/A	1:1000	Thermo Fisher

Table 2.8 - Staining antibodies used for surface vs cycling vs total TCR analysis

For cycling TCR analysis, cells were immediately surface stained with 100µL anti-TCRβ alone as per table 2.8, for 2 hours at 37°C. After this, cells were washed three times as described and surface stained for CD4 together with fixable viability dye as described. Cells were then washed three times (1800rpm, 5 minutes), fixed in 200µL BD cytofix (BD Bioscience, 554655) at 4°C for 20 minutes, before a further three washes and resuspension in 200µL FACS buffer.

For total TCR analysis, cells were surface TCR stained as described earlier, with a mastermix containing all antibodies shown in table 2.8. Following surface staining, washing, and fixation in BD cytofix as described, cells were permeabilized in 1X permeabilization buffer (Invitrogen, 00-8333-56) at 4°C for 15 minutes. Cells were then stained intracellularly

for TCR at 4°C for 25 minutes, with the antibody made up in permeabilization buffer to a final volume of 200µL per sample. Following intracellular staining, cells were washed once (1800rpm, 5 minutes) in permeablization buffer, and twice in FACS buffer before resuspension in 200µL FACS buffer. All surface / cycling / total TCR stained samples were acquired together on a LSR-Fortessa-X20 flow cytometer (BD Bioscience).

2.9.6 Transcription Factor Staining, and FoxP3/IL-10 Dual Staining

For transcription factor staining without co-staining for cytokines, the following protocol was followed. At the appropriate time point, cells were surface stained as required as per 2.9.1, and fixed in 100µL BD cytofix/cytoperm (BD Biosciences, 554722) for 40 minutes at 4°C. Cells were washed three times in 200µL FACS buffer in 96 well round bottomed plates by centrifugation at 2000rpm for 2 minutes at 4°C, before permeabilization for 20 minutes in 200µL 1X FoxP3 kit permeabilzation buffer (Invitrogen, 00-8333-56) at 4°C. Cells were washed in permeabilization buffer, and incubated in 100µL of intracellular staining mastermix containing antibodies as shown in table 2.9 for 30 minutes. Intracellular mastermixes were made up in 1X permeabilization buffer. Following intracellular staining, cells were washed twice (2000rpm, 5 minutes) in permeabilization buffer, and once in FACS buffer before resuspension in 200µL FACS buffer and acquisition on a LSR-Fortessa-X20 flow cytometer (BD Biosciences).

Target	**Fluorophore**	**Clone**	**Dilution**	**Supplier**
FoxP3	PE eFluor 610	FKJ-16s	1:200	Invitrogen
Tbet	PerCP Cy5.5	4B10	1:200	Biolegend
Tox	APC	TXRX10	1:200	Invitrogen

Table 2.9 – Intracellular antibodies used for transcription factor staining.

For dual staining of FoxP3 and IL-10 expression the following protocol was followed. At the appropriate time points, cells were plated into a 96 well round bottomed plate at $1x10^5$/well and restimulated with PI as per 2.8.1, for 1 hour. Cells were then pelleted and resuspended in 1X PIGS (made as per 2.9.2) with the addition of Brefeldin A (eBioscience, 00-4506-51) at a final dilution factor of 1:2000 for a further 3 hours. Cells were then surface stained as required as per 2.9.1 and fixed in 100µL BD cytofix/cytoperm for 1 hour at 4°C. Cells were then washed three times in 200µL FACS buffer by centrifugation at 2000rpm for 2 minutes, before overnight incubation in 100µL intracellular staining mastermix containing antibodies shown in tables 2.6 and 2.9 for IL-10 and FoxP3 respectively. Intracellular staining mastermixes were made up in 1X FoxP3 kit permeabilization buffer. The following day, cells were washed twice as described in 200µL 1X permeabilization buffer, and once in FACS buffer before resuspension in 200µL FACS buffer prior to immediate acquisition on an LSR-Fortessa-X20 flow cytometer (BD Biosciences).

2.10 Confocal Microscopy

2.10.1 Confocal Microscopy for Membrane CD3 Distribution - Protocol

Purified $CD4^+$ T cells from Tg4 mice were treated with $250nm^{Mid}$ anti-CD3 functionalised MNPs are described in 2.6. Cells were then plated into a 24 well plate as described in 2.7, except a glass cover slip was added to the bottom of the well prior to cell addition, and cells were kept in PBS for the experiment to allow for immediate fixation. Plates were kept on ice for 10 minutes to allow for cells to settle within the well. Magnetic force was then applied for 15, 30 or 60 minutes as described in 2.7, and at the end of each time point, cells were fixed by the addition of PFA to a final concentration of 4%. Cells were left unstimulated for negative controls. Cells were fixed on ice for 20 minutes and washed 3 three times by the

addition of 500µL PBS. Cells were blocked for 1 hour at room temperature in PBS + 5% BSA, before three further washes and incubation in an antibody staining mastermix for 1 hour. Antibody mastermix was made up as per table 2.10 in PBS, and cells were stained in a total volume of 250µL per well. Cells were then washed three times in PBS, and coverslips were retrieved from the well and mounted onto microscopy slides using 1 drop of fluoromount (Sigma-Aldrich, F4680). Coverslips were left in the dark for >2 hours to allow the fluoromount to dry, before the edge of the coverslip was carefully sealed using clear nail polish. Coverslips were left to dry at room temperature in the dark overnight and were imaged within 48 hours.

Target / Stain	**Fluorophore**	**Clone**	**Dilution**	**Supplier**
CD3εγ	AF647	17A2	1:100	Biolegend
Nucleic acids (DAPI)	DAPI	N/A	1:2000	Sigma-Aldrich (D9542)

Table 2.10 - Staining procedure used in CD3 membrane localisation experiments.

2.10.2 Confocal Microscopy for Membrane CD3 Distribution – Acquisition and Analysis

For membrane CD3 distribution, z-stack images were taken on an Olympus IX81 Fluoview FV1000 confocal microscope, at 60X magnification (NA 1.2) under oil immersion. Z-stacks were taken at a scan speed of 40µs/pixel and incorporated the full cell volume with a step size of 0.2µm between each slice. All samples within any given experiment were imaged using identical imaging parameters. Following image acquisition, z-stacks were reconstructed in Imaris v9.7 to visualise membrane CD3 distribution.

Reconstructed z-stacks were analysed in two ways. Firstly, open-source ICY software was used to determine surface CD3 intensity across the entire z-stack for each cell. Here, each individual cell was gated as an individual region of interest (ROI), before the sum of the intensity was measured in the CD3 channel. Secondly, for analysis of CD3 signal detection throughout each slice of the z-stack, the particle analysis plug-in was used in FIJI (ImageJ). Here, particle analysis parameters were set to 10-1000µm, which permitted the software to distinguish each individual cell as one 'particle'. This was therefore used a method to segment each individual cell. Applying these segmentations to the entire z stack then allowed for the determination of CD3 intensity with each slice of the z stack, and hence allows for the investigation of where the CD3 signal is present throughout the entire cell body.

2.10.3 Confocal Microscopy for CD45 Localisation – Protocol

Purified $CD4^+$ T cells from the Tg4 mouse were treated with $250nm^{Mid}$ anti-CD3 MNPs, or $1\mu m^{Mid}$ CD3 MNPs as described in 2.6, and subjected to magnetic force for 60 minutes as per 2.7. Where indicated, cells were treated with 10µM PP2 or 1µM Latrunculin A during the particle treatment steps, and inhibitor concentrations were maintained throughout all particle wash and force application steps. For these experiments, cells were kept in PBS to allow for immediate fixation of the cells post force application. Cells were plated in glass bottomed imaging chambers (Ibidi, 80807), and following force application cells were fixed for 20 minutes at 4°C by the addition of PFA to a final concentration of 4%. Cells were either left unstimulated (i.e., no particle addition) or were stimulated with anti-mouse CD3/CD28 dynabeads to a 1:1 ratio for 15 minutes for negative and positive controls respectively.

Post fixation, cells were washed three times by the addition of 200µL PBS + 0.1% tween (PBS-T), before blocking in 200µL PBS + 5% BSA for 1 hour at room temperature. Cells were then again washed three times in PBS-T and stained over-night at 4°C in 200µL biotinylated anti-CD45 (Clone 30-F11, Thermo Fisher, 13-0451-82) at 1:200 in PBS-T. The following day, cells were washed three times in PBS-T and stained for 1 hour at room temperature with streptavidin conjugated Alexa Fluor (AF) 555 (Invitrogen, S21381) and anti-hamster IgG AF488 (Invitrogen, A11055), both at 1:1000, made up in PBS-T to a staining volume of 200µL per well. Streptavidin 555 detects CD45, whilst anti-hamster IgG AF488 binds to the CD3ε antibody on the particle surface and thus detects localisation of the functionalised MNPs. Following the secondary staining step, cells were washed three times in PBS-T and ultimately kept in 200µL PBS-T for imaging. Cells were imaged immediately on a Zeiss LSM 780 confocal microscope at X60 magnification (NA 1.2) under water immersion with sequential excitation of the multiple fluorophores. All imaging parameters were identical across all experimental repeats and were set as follows: scan speed: 25.21µs/pixel, line averaging: 1. During image acquisition, 2D scans were taken at positions where particle localisation on the cell membrane was observed.

2.10.4 Confocal Microscopy for CD45 Localisation – Analysis

To assess the relationship between CD45 and MNP intensity within given membrane regions of interest (ROIs), 2D scans were analysed in ZEN blue software v3.4 using the unmix and measure tools. Initially, each image was subjected to a background subtraction using a segment of black pixels from each image. Regions of interest were drawn on sections of the cell membrane where particle staining could be detected, and the unmix and measure tools provided a measurement of staining intensity for each of the CD45 and MNP channels. For

dynabead controls, ROIs were drawn on regions of the membrane in direct contact with the bead, whilst for unstimulated controls random sections of membrane were chosen across each cell in each field of view. Staining intensity measurements were normalised to ROI size, to provide a measurement of CD45 intensity per μm^2. These measurements were then used to assess the effect of magnetic force application of the distribution of CD45 within particle-bound membrane regions.

2.11 Production of a Halbach Array for Shear Force Application

2.11.1 Halbach Array Design

For assessment of the effect of shear force application on TCR signalling and $CD4^+$ T cell activation, we designed and built a Halbach array to act as a rotational magnetic field centred around a tissue culture petri dish of 30mm in diameter (henceforth referred to as sample dish).

Briefly, neodymium iron boron magnets (8mm cubes, N42 grade) were placed into the ring array as illustrated in figure 2.2. Arrows within each magnet in figure 2.2 display magnetic flux direction of north for each individual magnet. Arrangement of the magnets as shown produces a largely uniform magnetic field across the sample dish and permits the change of direction of the magnetic field with rotation as described elsewhere[260]. A gear profile along the edges of the array permitted programmable rotation of the array. In brief, a 2000Kv (2000rpm per 1V input) brushless motor was used to permit rotation of the array, which also incorporated a microcontroller to read out in real time the frequency of rotations per second. This was monitored within all experiments performed and kept consistently at a rotational frequency of 1Hz.

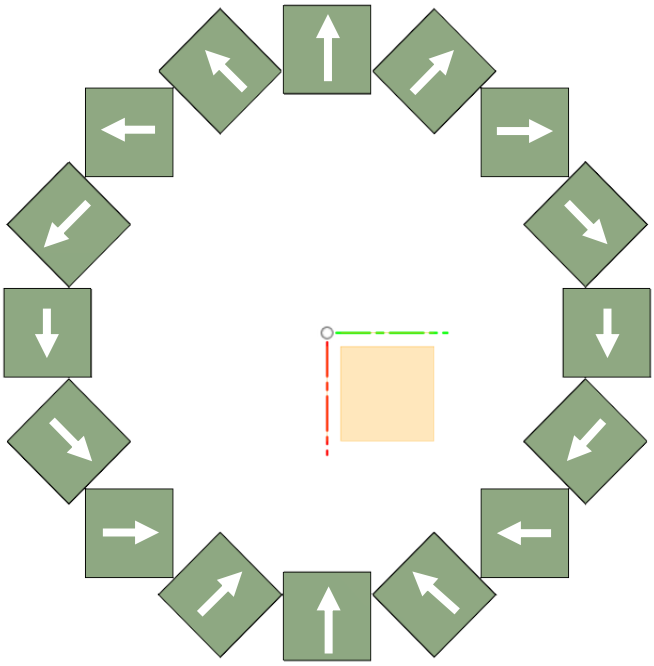


Figure 2.2– Birds eye view of the magnet arrangement within the Halbach array. Each green square represents the position of an individual 8mm cuboid neodymium iron boron magnet and the white arrows within each magnet position illustrates the direction of magnetic north for each individual magnet.

2.11.2 Halbach Array Magnetic Field Profiles and Force Calculations

The magnet arrangement displayed in figure 2.2 produced a largely uniform magnetic field of 0.146T ± 0.0001T across the main body of the sample dish. The field strength across the sample dish and how this moves throughout one complete rotation is shown in figure 2.3.

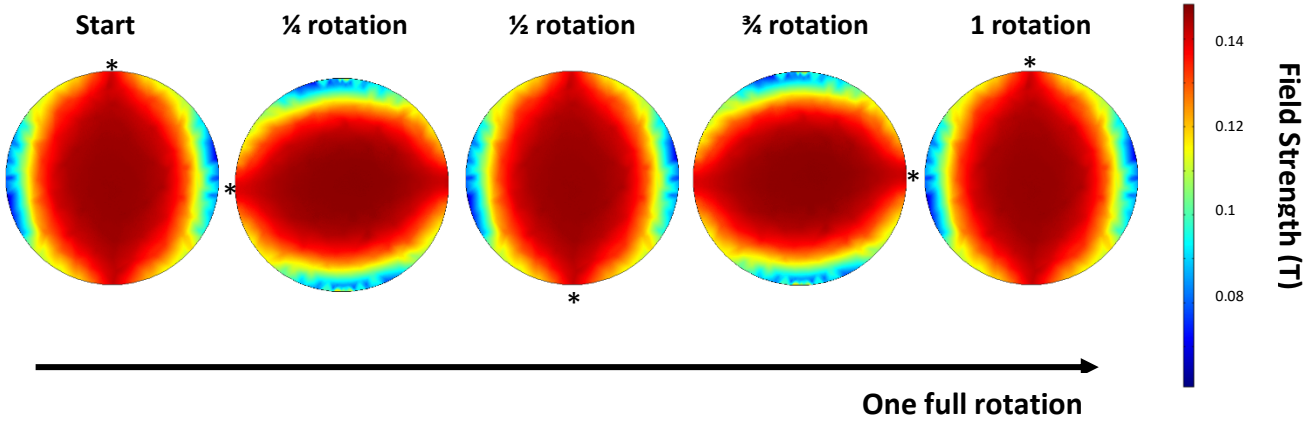


Figure 2.1 - Modelling of halbach array field profiles through one full rotation. Gradation of blue-red colour outlines the field profile across the same dish provided by the Halbach array, indicating a large degree of field strength (T) uniformity across the sample dish. Images from left to right track the field profile of the Halbach array through 1 full anti-clockwise rotation, with the asterisk functioning as a reference point throughout.

Figure 2.3 identifies how the rotating magnetic array will induce a shear motion of any particles tagged onto the cell surface of CD4+ T cells, as these particles align with their 'easy-axis' throughout the continual rotation of the array. Use of magnetic array allows for the comparison of force application with MICA instrument, with induction of shear motion of an MNP that ultimately 'resets' back to its starting position as the array completes one full rotation.

2.11.3 Calcium Signalling Experiments

All steps in calcium signalling experiments were performed in calcium assay buffer (phenol red free 1640-RPMI (Gibco, 11835063) + 2.5mM probenecid (AAT-Bioquest, 20060-AAT) and 3% FCS) unless otherwise stated. Purified $CD4^+$ T cells from the Tg4 mouse were loaded with Fura-2 AM ratiometric calcium indicator dye (Invitrogen, F-1221), by incubation of cells at $2x10^6$/mL with a final concentration of 5µM Fura-2 AM at 37°C for 1 hour. Cells were then washed three times by centrifugation at 1800rpm for 5 minutes at 4°C, before treatment with functionalised MNPs as described in 2.6. Cells were then washed three times in PBS and resuspended at $2x10^6$/mL in PBS prior to adhesion to poly-l-lysine (PLL, Sigma Aldrich, P4707) coated glass bottomed imaging petri dishes (Cellvis, D29-20-0-N). Glass bottomed petri dishes were coated with PLL by addition of 500µL PLL per dish and incubation at 37°C for at least 30 minutes, prior to 3 washes with 500µL PBS, after which petri dishes were allowed to dry at room temperature for at least 30 minutes. For adhesion of cells onto PLL coated petri dishes, 500µL cells at $2x10^6$/mL in PBS were plated into the petri dish and allowed to adhere for a minimum of 30 minutes on ice. Non-adherent cells were then removed by three washes with 250µL calcium assay buffer, before addition of a final imaging volume of 250µL calcium assay. Imaging was performed on a custom-built

Cairn FRET microscope for live calcium imaging (University of Birmingham, COMPARE suite), under X40 magnification with oil immersion. Samples were excited by wavelengths of 340nm and 380nm, each providing emission at 510nm. The Fura-2 AM ratiometric calcium indicator dye allows for an accurate determination of intracellular calcium as follows. Briefly, in the absence of intracellular calcium, the Fura-2 dye is excited by wavelengths of 380nm, which shifts to 340nm in the presence of intracellular calcium, allowing for the determination of intracellular calcium as a ratio of emission at 510nm when excited at 340 and 380nm.

Calcium imaging experiments with the Halbach array to induce a shear motion on the particles were performed as followed. Petri dishes were positioned in the Halbach array, and the instrument was secured in position on the microscope stage. For the first 30-60 seconds of the time course, images were taken with the array off to establish a calcium signalling baseline with no force application. After this baseline period, the array was turned on with a rotational frequency of 1Hz and images were collected for a further 10 minutes as a minimum. Images corresponding to excitation at 340 and 380nm were taken every two seconds across the entire time course.

To determine the calcium signalling response, the 340:380 ratio for each individual cell in the entire field of view was calculated across the time course. The baseline period was used to normalise the force induced calcium signalling response, by dividing the peak calcium signalling ratio post-magnetic field application by the baseline calcium signal (Fmax/F0, where F=calcium signalling fluorescence as determined by 340:380 ratio, Fmax=peak calcium signal post force application and F0=baseline calcium signal).

2.12 Single Molecule Localisation Microscopy

$CD4^+$ T cell purified from Tg4 mice as previously described were treated with 1µm MNPs functionalised with 1µg CD3 as per 2.5 ($1µm^{Mid}$ MNPs). Following treatment with particles, cells were treated with magnetic force in ibidi imaging chamber (ibidi, 80807) for time periods indicated in the body of the text before fixation by addition of PFA to a final concentration of 4%. Cells were fixed at 4°C for 20 minutes, before 3 washes by addition of 250µL PBS. Cells were then blocked in 250µL 5% BSA made in PBS for 1 hour at room temperature, before 3 further PBS washes and incubation with 250µL anti-TCRβ AF647 (H57-597, biolegend, 1:100 in PBS) at room temperature for 1 hour. Cells were then washed three times in PBS and stored in 250µL PBS overnight and imaged the following day. On the day of imaging, all conditions were put into 200µL 0.2M mercaptoethilamine (MEA, pH 7.5) prior to image acquisition.

Images were acquired on a Nikon dSTORM SMLM microscope (University of Birmingham, COMPARE suite) at x100 magnification under oil immersion. TIRF angles were optimised for each image acquisition. Image acquisition parameters were as follows; initial fluorophore activation was achieved exposure to the 405nm laser at 100% power for 100 frames, followed by collection of fluorophore locations for 5000 frames, with the 640nm laser at 20% power. This cycle was repeated for a total of 6 times for each sample, to produce an acquisition time period for fluorophore collection of 30,000 frames and approximately 10 minutes. Images were not collected whilst fluorophore reactivation phases were run (excitation with 405nm laser). Following acquisition, all images were analysed using the FIJI plug in 'THUNDERSTORM', to generate pixel maps of fluorophore detection. Fluorophore detections that appeared within 20nm of one another were merged to one detection in an

attempt to account for multiple-blinking. Within this merged image, molecules of an intensity less than 1000 were filtered out. A region of interest (ROI) was drawn on each cell, encapsulating the region in contact with the glass slide whilst excluding the outer membrane regions for the purposes of removing noise from these regions. Each ROI was then run through Rstudio to generate clusters using a dbScan clustering algorithm. The following parameters were utilised for this: minimum detections per cluster = 10, maximum detections per cluster = 10,000, dbScan radius = 20, dbScan threshold = 3. These dbScan parameters were chosen based on previously published work utilising single molecule localisation microscopy for the investigation of TCR clusters[261]. The dbScan algorithm produced parameters such as number of detections per cluster (i.e., number of TCRs per cluster), cluster area, cluster density and number of clusters identified. Finally, cluster maps were produced in MATLAB to visualise distribution of membrane TCRs.

2.13 $CD4^+$ T Cell Restimulation and Phenotype Assessment

$CD4^+$ T cells from Tg4 mice were stimulated with 250nm or 1µm functionalised particles, with and without magnetic force application as described in 2.7 and maintained in culture for 72 hours in the presence of 20U/mL IL-2. At day 3, live cells were purified by density gradient centrifugation, by layering 5mL cell suspension over 3mL room temperature ficoll-paque (Cytiva, 17544602), and centrifugation at 1800rpm for 20 minutes at room temperature with no brake. Live cells were then carefully removed from the ficoll interface and washed 3 times in complete RPMI + 10% FCS by centrifugation at 1800rpm for 5 minutes at 4°C. Cell number and viability were then determined. All post-ficoll viabilities were >90%.

For T cell restimulation, either the I-A^u expressing B cell lymphoma 'PL8', or bulk splenocytes from the B10.PL mouse were used as antigen presenting cells (APCs). Spleens harvested from the B10.PL mouse were processed as described in 2.1. Viable $CD4^+$ T cells isolated via ficoll purification were co-cultured with APCs in round bottomed 96 well plates, at a 1:2 ratio ($1x10^5$ T cells:$2x10^5$ APCs), in the presence of the Ac1-9 MBP peptide routinely used within the Wraith laboratory[262] (henceforth called the 4K peptide), at a range of concentrations as shown. Where indicated, cells were also re-stimulated in the presence of 20U/mL IL-2. Following restimulation for 24 hours, $CD4^+$ T cell phenotype was assessed by surface staining for activation markers and co-inhibitory receptors as per 2.9.1.

2.13.1 Co-Inhibitory Receptor Blockade

Where indicated, co-inhibitory receptor blockade was including in restimulation experiments to evaluate the role of CTLA-4 or PD-1 expression on $CD4^+$ T cell phenotype. Briefly, $CD4^+$ T cells were incubated with anti-CTLA-4 (Clone: UC10-4F10-11, BD Pharmigen, 553719) and/or anti-PD-1 (clone: 29F.1A12, BioXCell, BE0273) blocking antibodies for 2 hours at 37°C, at concentrations of 2µg/mL and 10µg/mL respectively. Following incubation with blocking antibody, APC, 4K peptide and IL-2 (if required) were added as per 2.13.

2.14 Enzyme Linked Immunosorbent Assays

For assessment of cytokine production, cell culture supernatants were collected at time points indicated and stored at -20°C for future assessment of cytokine content by enzyme linked immunosorbent assays (ELISA). Assessment of IL-10 secretion was performed using the ELISA-Max mouse IL-10 kit (Biolegend, 431414) as per manufacturers instructions. Assessment of IL-2 and IFNγ secretion were performed as follows. All supernatants were

freeze-thawed no more than twice. All supernatants were diluted appropriately (in 1% BSA for IL-2 and IFNγ, in assay diluent for IL-10) so that cytokine concentration values were determined in the linear range of the appropriate standard curve.

For assessment of IL-2 and IFNγ secretion, the following protocol was followed. All reagent dilutions for either cytokine are shown in table 2.11. Firstly, ELISA-max plates (Biolegend, 423501) were coated with 100µL capture antibody (diluted in 1X coating buffer, Biolegend, 79104) overnight at 4°C. The following day, plates were washed three times with PBS + 0.05% tween and blocked in 100µL 1% BSA in 1X PBS for 1 hour at room temperature under constant agitation. Plates were washed three times, before addition of 100µL diluted supernatants or 100µL standards across a serial dilution, of which the top standard was maintained at 1000pg/mL (IL-2: Biolegend, 79073, IFNγ: Biolegend, 575309, serial dilution for standards 1-7, standard 8: 1% BSA alone). Plates were incubated with supernatants and standards for 2 hours at room temperature under constant agitation. Plates were then washed three times, before addition of 100µL biotinylated detection antibody diluted in 1% BSA and incubation at room temperature for 1 hour under constant agitation. Plates were washed three times, and 100µL horseradish peroxidase (HRP) diluted in 1% BSA was added, followed by a 1 hour incubation as described. Plates were then washed five times before addition of 100µL of 3,3',5,5'-Tetramethylbenzidine (TMB) solution, before stopping of the reaction at an appropriate point by addition of 100µL of H_2SO_4. Absorbance was then measured at 450nm, and cytokine concentrations calculated relative to the standard curve.

Cytokine	Antibody / Reagent	Dilution Factor	Diluent	Supplier + Catalogue number
IL-2	Anti-mouse IL-2 capture	1:200	1% BSA in 1X PBS	Biolegend, 503702
IL-2	Anti-mouse IL-2 biotinylated detection	1:2000	1% BSA in 1X PBS	Biolegend, 503804
IFNγ	Anti-mouse IFNγ capture	1:1000	1% BSA in 1X PBS	Biolegend, 505802
IFNγ	Anti-mouse IFNγ detection	1:2000	1% BSA in 1X PBS	Biolegend, 505704
IL-2 and IFNγ	HRP	1:1000	1% BSA in 1X PBS	Biolegend, 405103
IL-2 and IFNγ	TMB	1:100	Phosphate citrate buffer (PCB, Sigma Aldrich, P4809) and 2µL H_2O_2 per 10mL PCB	Sigma Aldrich, T2885
IL-2 and IFNγ	2M H_2SO_4	N/A	N/A	Honeywell Research Chemicals, 35276

Table 2.11 – ELISA Reagents

2.15 Immune Suppression Assays

2.15.1 Inhibition of Naïve $CD4^+$ T cell Proliferation

Firstly, $CD4^+$ T cells were purified from Tg4 mice and treated with 1µm MNPs functionalised with 1µg or 10µg CD3 as per 2.6. Where indicated, cells stimulated with 10µg CD3 particles were also treated with 10nM of the PI3K inhibitor CAL-101 (Selleckchem, S2226). $CD4^+$ T cells treated with these particles were stimulated with magnetic force for 1 hour and maintained in culture for 3 or 7 days in the presence of 20U/mL IL-2. For 7-day cultures, IL-2 was replenished at both day 3 and 5. These cultures are hence force referred to as putative suppressors. At day 3 or day 7, immune suppression assays were set up as

follows. Viable cells from putative suppressor cultures were isolated via ficoll gradient purification as previously described in 2.13. Bulk splenocytes from B10.PL mice were utilised as source of APC, and naïve $CD4^+$ responders were sourced from Tg4 CD45.1 transgenic mice, to allow for distinction of the responder population from the putative suppressor population based on the expression of CD45.1. Bulk splenocyte cultures from spleens of either mouse were produced as per 2.1, whilst $CD4^+$ naïve responders were purified as per 2.3. Naïve $CD4^+$ responder populations were then labelled with CTV proliferation dye as per 2.8.2. Naïve $CD4^+$ responders and APC were then plated into round bottomed 96 well plates at concentrations of $1x10^5$/well and $2x10^5$/well respectively, before addition of putative suppressors at $1x10^5$/well, $5x10^4$/well and $2.5x10^4$/well for ratios of 1:1, 1:2 and 1:4 respectively with the naïve $CD4^+$ responding population. Cultures were then stimulated with 10µg/mL of 4K peptide to stimulate proliferation of the naïve responder population. Where indicated, exogenous IL-2 was included at a final concentration of 20U/mL to assess its effect on reversing observed suppression.

72 hours later, degree of immune suppression was assessed by measurement of proliferation from CTV labelled naïve $CD4^+$ Tg4 responder populations. Briefly, cultures were surface stained as described in 2.9.1 and proliferation of $CD4^+$ $V\beta8^+$ $CD45.1^+$ populations was assessed by means of CTV dilution.

For parallel assessment of cytokine production, cultures were restimulated with PIGS for 4 hours, surface stained, fixed, and intracellularly stained for cytokine production as described in 2.8.2 and 2.9.2. Briefly, IL-10 production was assessed in $CD4^+$ $V\beta8^+$ $CD45.1^+$ and $CD4^+$ $V\beta8^+$ $CD45.1^-$ populations.

2.15.2 DC – Putative Suppressor Co-Cultures

Putative suppressor cultures were stimulated as described in 2.15.1, covering the following conditions; 1µm^{Mid} CD3 MNPs, 1µm^{Hi} CD3 MNPs, 1µm^{Hi} CD3 MNPs + 10nM CAL101 (all 3 conditions ± 1 hour of magnetic force). Cultures were maintained in 20U/mL to day 7 as described in 2.15.1, at which point viable cells from each culture were purified via ficoll gradient centrifugation as per 2.13. CD11c^{+} dendritic cells (DCs) were purified from the spleens of B10.PL mice as per 2.3. Putative suppressors and purified CD11c^{+} cells were then co-cultured at 1x10^{5}/well of either cell type, in 200µL containing ± 10µg/mL 4K peptide for 24 hours at 37°C.

24 hours later, cell surface expression of CD80 and CD86 on CD11c^{+} MHC-II^{+} events was determined by standard cell surface staining as per 2.9.1, using the antibodies shown in table 2.12. Cells were immediately acquired on a LSR-X20-Fortessa as standard.

Target	**Fluorophore**	**Clone**	**Dilution**	**Supplier**
TCR Vβ8	PE	F23.1	1:400	BD Pharmigen
CD4	PerCP Cy5.5	RM4-5	1:200	Biolegend
MHC-II	AF700	M5/114.15.2	1:200	Biolegend
CD80	FITC	16-10A1	1:200	Biolegend
CD86	BV605	GL-1	1:400	Biolegend
CD11c	BV786	N418	1:200	Biolegend
Fixable viability dye	ef780 (APC)	N/A	1:1000	Thermo Fisher

Table 2.12 - Antibodies used for surface staining in DC – putative suppressor co-culture assays.

2.16 *In vitro* Th1 Polarisation

Single cell suspensions were produced from Tg4 mice as per 2.1, before naïve splenocytes were plated at $4x10^6$/mL in 24 well plates in a total volume of 500µL complete RPMI + 10% FCS. Cells were then immediately stimulated with 500µL of 20µg/mL of the Ac1-9 MBP peptide routinely used within the Wraith laboratory[262] (known as the 4K peptide) (GL Biochem) and 10ng/mL recombinant mouse IL-12 (rmIL-12, Peprotech, 210-12-10) in complete RPMI + 10% FCS, producing a final culture volume of 1mL with the following end concentrations; $2x10^6$/mL naïve splenocytes, 10µg/mL 4K and 5ng/mL rmIL-12. At 72 hours, cells were supplemented with a final concentration of 20U/mL IL-2 (R&D, 202-IL). If cultures were beginning to turn yellow due to acidification of the media as the cells proliferated, cultures were split 1:2 and fed with fresh media.

At day 7, live cells were recovered over a ficoll-paque density gradient, where 15mL cell suspension was layered over 10mL room temperature ficoll. The gradient was then centrifuged for 25 minutes at 1800rpm at room temperature with no brake, before live cells were removed off of the ficoll interface. Live cells were then washed three times in at least 10mL complete RPMI + 10% FCS by centrifugation at 1800rpm for 5 minutes, before cell number was then determined.

Live cells were then restimulated on plate bound anti-CD3 for a further 72 hours. Here, 48 well plates were incubated with 500µL of 1µg/ml anti-CD3 (145-2C11 clone) at 37°C for 2 hours before 3 PBS washes. Live cells were then plated at $1x10^6$/mL, 500µL/well and maintained at 37°C for 72 hours. Finally, polarised Th1 cells were then transferred into a fresh, non-anti-CD3 coated 48 well plate, fed with 20U/mL IL-2 and rested for a further 72 hours prior to use in assays.

2.17 Data Representation and Statistical Analysis

All data and graphs were produced in Prism v8-9 (GraphPad), and statistical analysis performed as per figure legends for each figure. Where appropriate, data was assessed for normality within the Prism software, prior to the application of the appropriate parametric or non-parametric test. All results from statistical tests are displayed in figure legends and in the text. Where blank, results are non-significant.

CHAPTER 3

3 External Force Application to the TCR to Influence TCR Triggering

3.1 Introduction

Whilst our knowledge of both ligand recognition by the TCR, and how activating (i.e., TCR-CD3 ligation and CD28 ligation) and inhibitory (i.e., checkpoint inhibitor ligation) signals influence T cell activation continues to grow, the precise mechanism of how ligation of TCR ligands translates across the membrane to internal biochemical signal is still lacking. Elucidating this mechanism would be of benefit to both our basic immunological understanding as well as potentially harnessing great therapeutic benefit to manipulate TCR signalling for clinical outcomes in both settings of autoimmunity and cancer.

As previously described, numerous mechanisms to answer this critical and age-old question have been proposed. Over the past 10-15 years, a growing amount of evidence supports a role for force application to the TCR complex in initiating a TCR trigger[47,167,183,188]. The earliest evidence for such an effect comes from Reinherz and colleagues, where Protein G coupled polystyrene particles of 1µm in diameter were functionalised with antibodies against CD3, or with peptide loaded MHC complexes (pMHC). In experiments utilising an optical trap, within which the bead is fixed in place, functionalised particles were presented to purified $CD8^+$ T cells from N15 transgenic mice on a RAG knockout background (N15TCRtgRag2$^{-/-}$). $CD8^+$ T cells from this transgenic line all express a clonotypic TCR specific for a vesicular stomatitis virus nuclear protein octapeptide, VSV8 (RGYVYQGL). Oscillatory force application to the TCR-particle interaction was achieved through movement of the focused particle relative to the poly-l-lysine immobilised T cell. Presentation of particles

functionalised with the 145-2C11 clone of anti-mouse CD3ε drove a TCR triggering calcium response in the absence of any external forces. However, force application of approximately 50pN to a typically non-activatory clone of anti-CD3εγ (17A2) was able to drive a calcium signalling response that was otherwise absent when force application was not applied. A similar force induced affect was observed when using particles functionalised with pMHC molecules using the VSV8 peptide. Importantly, this effect of force application on TCR triggering calcium flux was not observed when an unrelated Sendai virus derived peptide (SEV9) was used, which binds H2-Kb with a similar affinity to that of VSV8 but is not recognised by the N15 TCR[183,263].

These studies indicate that the TCR can indeed interpret external mechanical force and translate this into internal biochemical signalling. However, the current studies do not shed light on the mechanism by which this could process may take place and does not interrogate whether the TCR calcium signalling observed is of sufficient magnitude to trigger robust T cell activation, which must be the case if the TCR is to interpret external mechanical forces and input this information into activated T cell output and T cell fate.

To this end, we have utilised small superparamagnetic nanoparticles (henceforth called magnetic nanoparticles, MNPs) to apply dynamic force to the TCR-CD3 complex over extended time periods. When functionalised with TCR-CD3 ligands and exposed to external magnetic fields of a known magnitude, accurate force magnitudes can be imposed on the MNP-TCR/CD3 interaction. Whilst other studies have also utilised magnetic particles to study TCR signalling, authors here have only made use of static magnetic fields to apply forces to the TCR-CD3 complex[264–266]. Use of static magnetic fields will apply fixed field gradients to the MNPs, and therefore only apply a static force to the TCR-CD3 complex,

which fails to fully reproduce the physiological conditions under which antigen recognition takes place, where force application to the TCR-CD3 complex is likely to be dynamic and constantly modulated[183,267].

The 'MICA' bioreactor (magnetic ion channel activation) has been demonstrated to influence cell mechanotransduction through MNP tagged receptor activation[237,238,258]. The MICA instrument functions as a computer programmable oscillating magnet, which is a set of magnetic arrays that oscillates underneath a tissue culture plate with a frequency of 1Hz, cycling between an 'ON' and 'OFF' position every second. Programming the array to be positioned at a known distance from the tissue culture plate in the 'ON' position, together with the known strength of the magnetic field, allows for the precise calculation of the force magnitude transferred to the MNP every second as described in 2.7. The cyclical motion of the apparatus means that the force application achieved is constantly cycled between on and off, and hence achieves a dynamic pulling magnetic force on the MNP-TCR/CD3 interaction.

To test whether external force application to the TCR using our system could influence TCR signalling and T cell activation, we mainly utilised Nr4a3-FT reporter mice within which the Nr4a3 protein transcribed at the end of the calmodulin-calcineurin-NFAT pathway is linked to a fluorescent reporter in the form of a mutant mCherry protein (see 2.1)[257]. The mCherry mutant is initially fluorescent in a blue form with a half-life of approximately 4hours, after which the protein decays to a more stable and longer lived red fluorescent protein with a half-life of approximately 20hrs[257]. As well as Nr4a3-FT mice, we also utilised Tg4, RTO and B10.PL mice from the Wraith laboratory for these studies. The Nr4a3-tocky model is a fluorescent reporter line on a non-transgenic C57BL/6 background, and hence

will express a TCR repertoire that has been allowed to naturally progress through the process of thymic selection. In contrast to this, the Tg4 mouse from the Wraith laboratory is a transgenic mouse model on a $H2^{u}$ expressing B10.PL background, in which 95% of the $CD4^{+}$ T cells express a transgenic TCR specific for the Myelin Basic Protein (MBP) Ac1-9 peptide (Ac-ASQKRPSQR)[256]. The RTO mouse was produced by crossing the Tg4 line with a Rag2 deficient B10 line, thus producing a Tg4 Rag KO line (RTO). As a result, within the RTO mice VDJ rearrangement of T and B cell receptor genes is not possible given the lack of expression of Rag2. Therefore, studying the effect of external force on TCR signalling within these mouse models allows for this investigation to take place within the fluorescent reporter Nr4a3 line, as well as investigating this in a transgenic TCR model whilst still controlling for the TCR repertoire by monitoring responses in the non-transgenic background mouse and pure transgenic RagKO line. In other words, use of these mouse models allows us to test whether force application to the TCR can influence TCR signalling both in TCR transgenic mouse models, and non-transgenic mouse models expressing a normal TCR repertoire.

3.2 Optimisation of 250nm MNPs for External Force Application

3.2.1 Force application to 250nm MNPs upregulated Nr4a3 expression

$CD4^{+}$ T cells from the Nr4a3-tocky mouse were purified as described in 2.3 and bound to $250nm^{Mid}$ MNPs, functionalised with anti-CD3 antibodies (145-2C11 clonotype), on ice for 30 minutes before PBS washing to remove unbound particles. Figure 3.1 displays that incubation of $CD4^{+}$ cells with a final concentration of 50µg/mL of functionalised MNPs was sufficient to drive an upregulation of Nr4a3 expression when subjected to external magnetic force for 1 hour. In these experiments, force application was applied as described for 1 hour

and cells were then maintained in a 37°C 5% CO_2 incubator for a further 4 hours to allow for TCR signal progression, protein translation and transcription to take place before assessing Nr4a3 expression in the blue form (i.e., the active TCR signal) in $CD4^+$ T cells by flow cytometry. As a positive control to drive Nr4a3 expression cells were also stimulated with PMA-Ionomycin (PI, a potent chemical activator of TCR signalling pathways that bypasses the need for engagement of the TCR). It was found that with force application, $CD4^+$ Nr4a3 expression slightly increased from 7.8% to 14.0% when treated with final concentrations of 25µg/mL MNPs, which rose to an increase from 12.8% to 24.7% with 50µg/mL MNPs. The effect of external force application appeared to plateau when Nr4a3-Tocky CD4+ T cells were treated with 100µg/mL MNPs (no magnetic force: 16.5% Nr4a3+, with magnetic force: 20.7% Nr4a3+). As a result, pre-treatment with 50µg/mL of functionalised $250nm^{Mid}$ MNPs was carried forward.

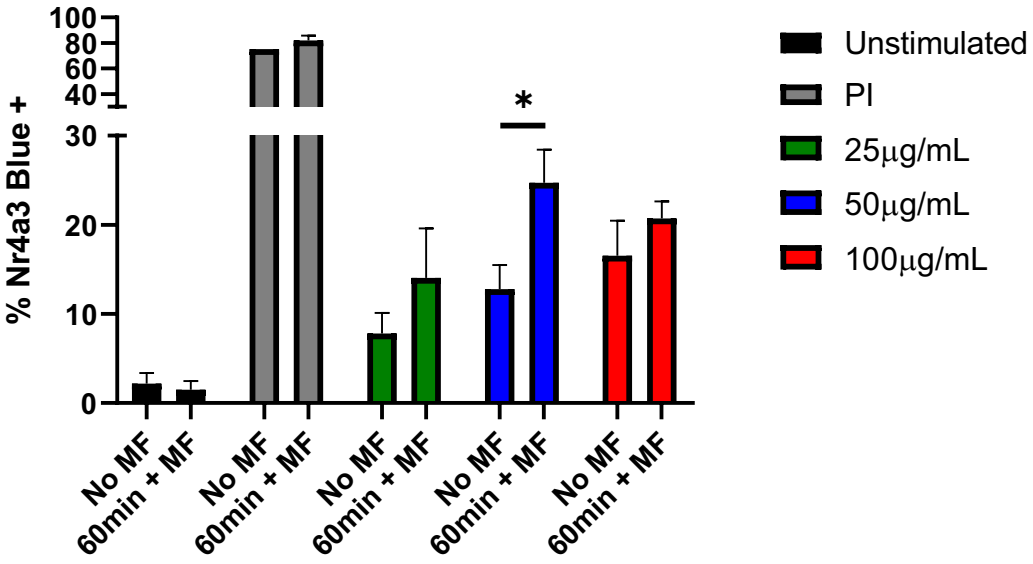


Figure 3.1 – Optimisation of $250nm^{Mid}$ MNP concentration for TCR signalling studies. In brief, 250nm MNPs were functionalised with 1µg of anti-CD3 (145-2C11) as described in 2.5 prior to addition of these particles to CD4+ T cells, at final particle concentrations as shown (25, 50 or 100µg/mL). Any non-bound particles were then removed by PBS washing. Treated $CD4^+$ T cells were then plated at $4x10^5$/well in 800µL total volume of complete RPMI + 10% FCS. External magnetic force was applied for 1 hour as described in 2.7 and cells were maintained in a 37°C 5% CO_2 incubator for a further 4 hours until Nr4a3 expression was assessed by flow cytometry. Unstimulated conditions were treated with medium alone (i.e., no particles) and PMA-Ionomycin (PI) stimulation served as a positive control. Data shown is mean ± SD from at least 2

independent experiments (3 for 100µg/mL and 50µg/mL conditions). Each independent experiment contains a minimum of 2 technical replicates. Statistical analysis assessed by 2-Way ANOVA with Sidak's post-tests, * p=0.0471.

3.2.2 Force application for 1hour is required to upregulate Nr4a3 expression

For mechanosensing through the MNPs protocol to be a true initiating mechanism behind the TCR trigger, force application on the time scale of seconds-minutes must be able to induce a TCR signalling response as previously shown elsewhere[183]. To assess this, purified CD4⁺ T cells from naive Nr4a3-Tocky mice were treated with 50µg/mL 250nm^{Mid} MNPs functionalised with anti-CD3 antibodies (145-2C11 clonotype) before being subjected to magnetic force for 15, 30 or 60 minutes as shown in figure 3.2.

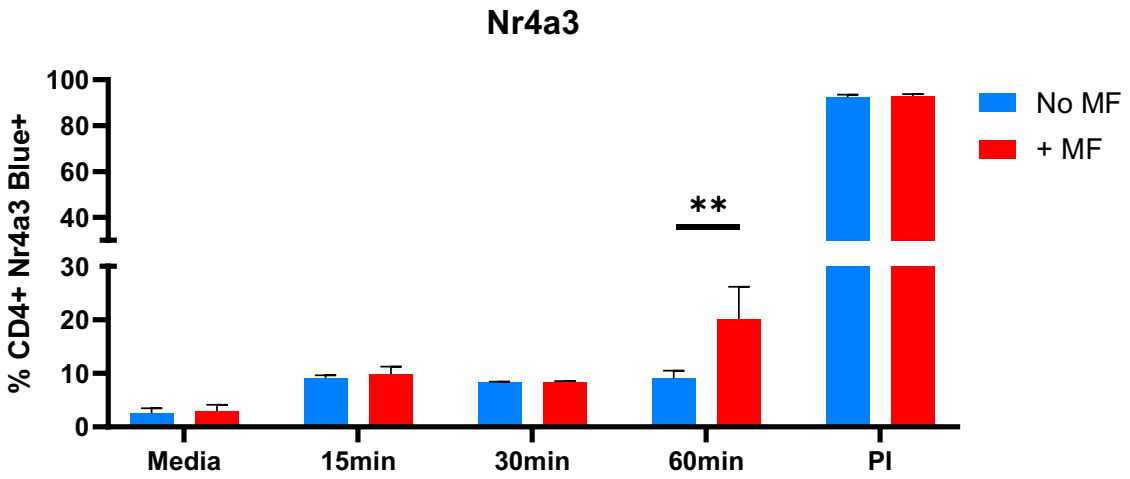


Figure 3.2 – Force application for 1 hour drives an upregulation of Nr4a3 expression. Splenic CD4⁺ T cells isolated from Nr4a3-FT mice were treated with anti-CD3 (145-2C11) functionalised 250nm^{Mid} MNPs as previously described. Magnetic force was applied for 15, 30 or 60 minutes, with Nr4a3 expression being measured 4 hours post force application. Force application for 1 hour drove a significant upregulation of Nr4a3 expression. Treatment with medium alone or PMA-Ionomycin (PI) served as negative and positive controls respectively. Bar graphs show mean ± SD of data from 3 independent experiments. Each independent experiment contains a minimum of 2 technical replicates. Statistical analysis assessed by 2-Way ANOVA with Sidak's post-tests, ** p=0.0023.

As per previous experiments shown in figure 3.1, force application for 1 hour upregulated the percentage of CD4⁺ T cells expressing Nr4a3 from an average of 9.1% to 20.2%. Shorter

time frames of force application for 30 minutes and 15 minutes had no effect on Nr4a3 expression (averages of 9.2% and 9.8% -/+ magnetic force, and 8.3% and 8.3% -/+ magnetic force for 15 minutes and 30 minutes respectively). In other experiments, magnetic force application for 5 minutes was compared alongside a 60 minute control, where 5 minutes of force application failed to induce an upregulation of Nr4a3 expression (data not shown).

3.2.3 Functionalisation with activating antibodies is required to drive TCR signalling

Previous work has shown that oscillatory force application to clonotypes of anti-CD3 antibody that are typically considered 'non-activating' is sufficient to drive a TCR calcium signal[183,268]. In this work, use of optical traps for force application coupled with simultaneous live microscopy to monitor internal calcium fluxes showed that use of particles functionalised with 'activating' clones of anti-CD3 (145-2C11) was sufficient to drive a calcium signal without the need for external force application, whilst force application to particles functionalised with 'non-activating' clones of anti-CD3 (17A2) allowed for observation of a calcium signalling response that was otherwise absent without force application.

To test this in our dynamic magnetic force protocol, we functionalised 250nm MNPs as per 2.5, again with the addition of 1µg of total antibody during the functionalisation process to produce 250nm^{Mid} MNPs. Here, we made use of either anti-CD3 (17A2), or anti-TCRβ (H57-597), which is also typically considered a non-activating antibody capable of binding to the TCR-CD3 complex. CD4^{+} T cell were then treated with 50µg/mL of functionalised MNPs as per 2.6, before force application for 1 hour. Force application to either of the functionalised particle groups was unable to drive an upregulation of Nr4a3 expression

(figure 3.3) as previously found when using the activating clone of anti-CD3 (145-2C11, figures 3.1-3.2).

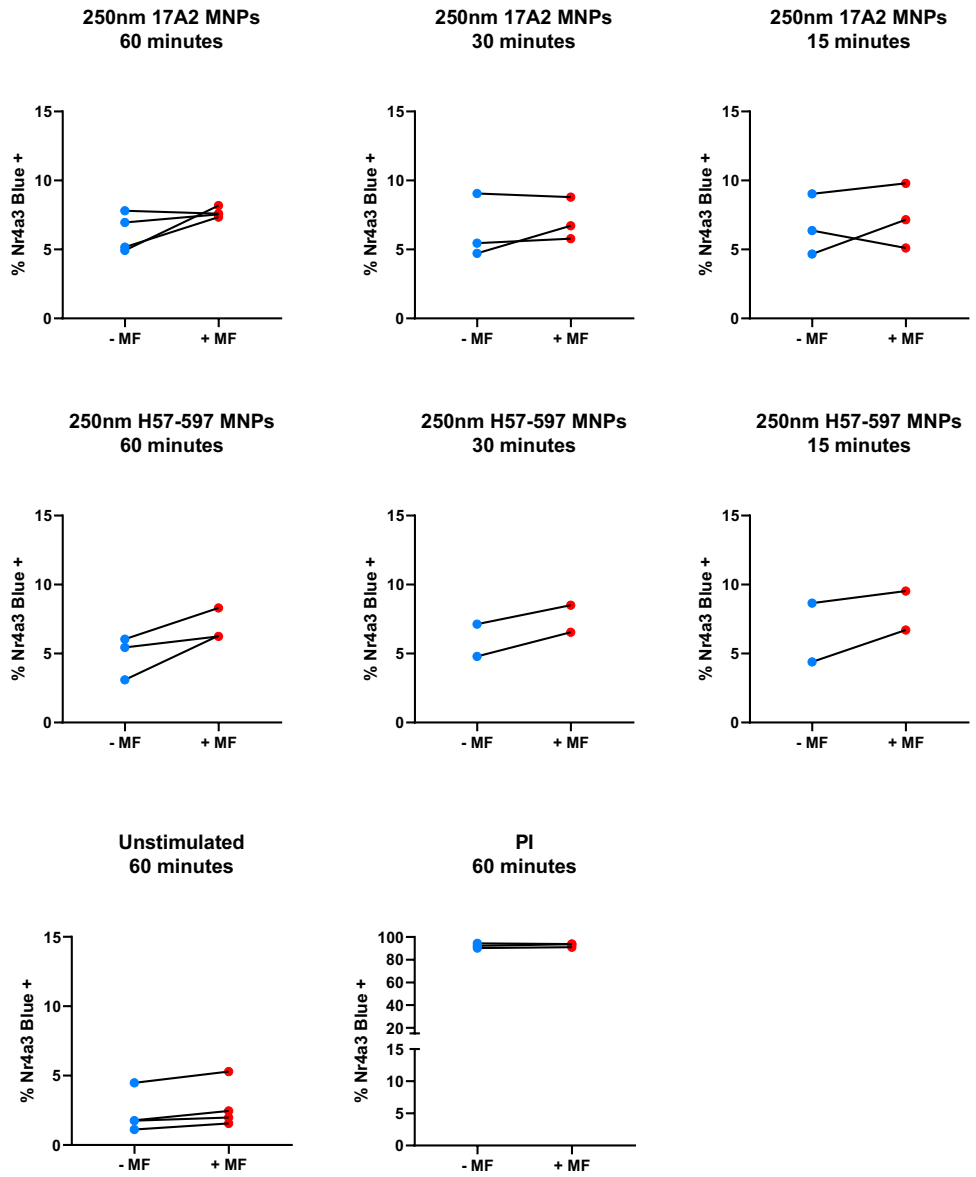


Figure 3.3 – Functionalisation of 250nm MNPs with non-activating antibodies fails to promote upregulation of Nr4a3 expression. 250nm MNPs were functionalised with either anti-CD3εγ (17A2) or anti-TCRβ (H57-597) antibodies as per 2.5 (to produce 250nm^{Mid} MNPs) and were bound to purified CD4^{+} Nr4a3-FT T cells at concentrations of 50µg/mL as described. Magnetic force (MF) was applied for times shown, and Nr4a3 expression was assessed 4 hours post force application. Unstimulated or PI stimulated cells were utilised at negative and positive controls respectively. Each line represents one individual experiment, connecting no MF and +MF conditions for one independent experiment. Data shown from at least 2 independent experiments (N=2 for H57-597 15min and 30min. N≥3 for all other conditions). Each independent experiment contains a minimum of 2 technical replicates. Upregulation of Nr4a3 in response to these particles was not observed.

In these experiments, media controls showed 2.28% of cells expressing Nr4a3 with no magnetic force application, and 2.82% with 1 hour of magnetic field application. Utilisation of 250nm^{Mid} MNPs functionalised with either 17A2 or H57-597 antibodies induced approximately 5% of cells to express Nr4a3 over the media control background without magnetic force (17A2; averages of 6.7%, 6.4% and 6.7% cells Nr4a3+ for 15/30/60min respectively. H57-597; averages, of 6.5%, 6.0% and 4.9% cells Nr4a3+ for 15/30/60min respectively). However, this was not significantly enhanced with any time of magnetic force treatment studied (17A2; averages of 7.4%, 7.1% and 7.7% for 15/30/60min respectively. H57-597; averages of 8.12%, 7.6% and 7.0% for 15/30/60min respectively).

3.2.4 Activation markers CD69 and CD25 are also upregulated with 1 hour magnetic force application to 250nm MNPs

Given the finding that 1 hour of magnetic field application upregulated the expression of Nr4a3 in Nr4a3-Tocky mice when analysed 4 hours post field application, we sought to investigate whether other cell surface T cell activation markers (CD69, CD25) behave in a similar manner in response to external magnetic force application. Experiments were set up as previously described, where purified CD4^{+} T cells from Nr4a3-Tocky mice were bound with anti-CD3ε (145-2C11) functionalised 250nm^{Mid} MNPs, before being subjected to 1 hour magnetic force application, and maintained in a 37°C incubator before flow cytometric analysis of cell surface activation marker expression 4 hours post magnetic force application. As displayed in figure 3.4, Nr4a3 expression was again increased with magnetic force application, from an average of 7.9% Nr4a3+ to 13.9% Nr4a3+. Cell surface T cell activation markers CD69 and CD25 also showed small upregulations with 1 hour force application, from averages of 10.4% to 13.3%, and 9.2% to 11.4% for percentage CD69+ and CD25+ respectively.

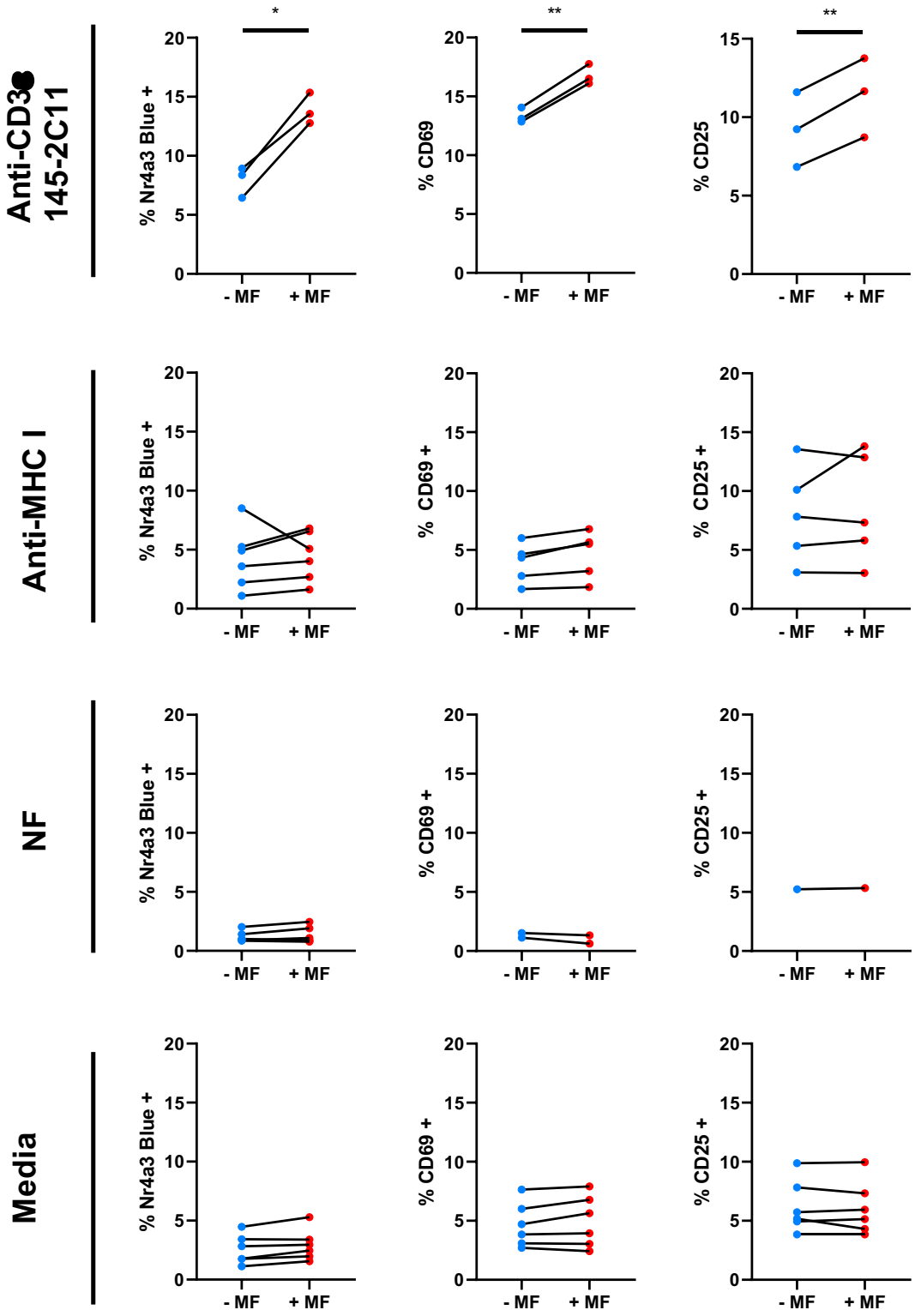


Figure 3.4 – CD69 and CD25 are also upregulated with 1 hour of Magnetic Force Application. Purified $CD4^+$ T cells from Nr4a3-FT mice were treated with 50µg/mL of 250nm^{Mid} MNPs functionalised with either anti-CD3ε (145-2C11), or anti-MHC-I or no antibody (non-functionalised, NF) as described in 2.5 and 2.6. Magnetic force (MF) was applied for 1 hour, before Nr4a3, CD25 and CD69 expression was assessed by flow cytometry 4 hours post force application. Data shown from at least 3 independent experiments, each line connects no MF and + MF from the same experiment. Statistical analysis performed via paired T-test, Nr4a3 * p=0.0135, CD69 ** p=0.0015, CD25 ** p=0.0048.

Alongside 250nm^{Mid} MNPs functionalised with anti-CD3ε, particles were also functionalised with an off target antibody control, that binds protein on the cell surface and transfers force to its specific receptor and thus the cell membrane but does not go through the TCR-CD3 complex. To this end, antibodies against MHC-I proteins were chosen, due to the high levels of expression of MHC-I on the cell surface. Anti-mouse MHC-I H-2K^{b} (clonotype AF6-88.5) was selected as this has been shown to successfully stain the H-2K^{b} class of MHC-I, expressed by C57BL/6 mice. The Nr4a3-FT reporter mouse is on a C57BL/6 background and thus this antibody was expected to successfully bind cell surface MHC-I proteins on CD4^{+} T cells isolated from the Nr4a3-FT mice. Staining with this antibody and counterstaining with a fluorescently labelled anti-mouse IgG2a secondary antibody confirmed successful binding of the AF6-88.5 antibody to H-2K^{b} (data not shown).

Utilisation of these MHC-I functionalised MNPs in a magnetic force assay showed that magnetic force application for 1 hour is unable to induce upregulations of either Nr4a3, CD69 or CD25 (figure 3.4). Without magnetic force, the percentage of cells positive for Nr4a3, CD69 or CD25 was 4.3%, 3.9% and 8.0% respectively. Magnetic force application for 1 hour failed to upregulate these expression patterns, with averages of 4.5%, 4.6% and 8.6% of cells positive for Nr4a3, CD69 and CD25 respectively. As an additional control, non-functionalised (NF) particles were also utilised (produced as per 2.5), which again failed to induce expression of any of the three T cell activation markers studied (figure 3.4).

3.3 Effect of Co-stimulation on Responses to 250nm MNPs

To this point, 250nm^{Mid} MNPs have only been functionalised with anti-CD3 antibodies, which has allowed for the mapping of the time of magnetic force required to drive an upregulation in TCR signalling, as well as determining which clone of anti-CD3/anti-TCR is

required to drive these responses. However, it has long since been known that robust activation of naïve T cells requires both stimulation through the TCR-CD3 complex and stimulation through the CD28 cell surface receptor, known as co-stimulation, achieved physiologically through ligation of (most commonly) CD80 and CD86 on the surface of APCs. To investigate how giving a co-stimulatory signal would influence our system of magnetic force application, we sought to functionalise 250nm^{Mid} MNPs with anti-CD3 alone, or an equivalent amount of anti-CD3 and anti-CD28 (i.e., a total quantity of 1µg of each antibody was added during the functionalisation process as per 2.5, whilst anti-CD3 only particles received only 1µg of anti-CD3 antibody). It should be noted that both anti-CD3 and anti-CD28 antibodies used were Hamster IgG antibodies (clones 145-2C11 and 37.51 respectively), thus allowing for the same capture antibody to be used in the functionalisation process as described in 2.5. Additionally, CD4^{+} T cells from the Nr4a3-FT reporter mouse were also treated with anti-CD3 only coated MNPs alongside soluble anti-CD28 antibody at 2µg/mL, to assess the effect of force application through the CD28 molecule through comparison of particle bound and soluble forms of anti-CD28 delivery (figure 3.5).

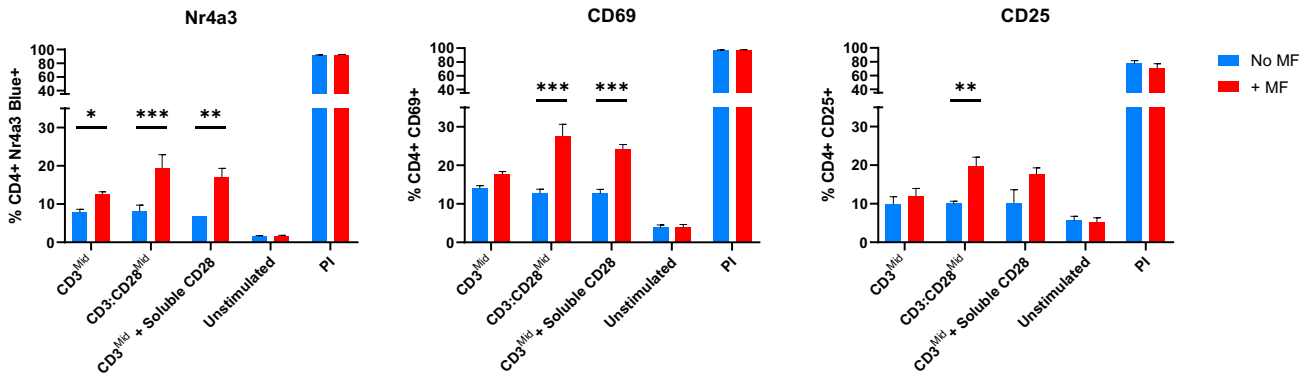


Figure 3.5 – Effect of Co-stimulation on Responses to 250nm^{Mid} MNPs. Purified CD4^{+} T cells from Nr4a3-FT mice were treated with 50µg/mL 250nm^{Mid} MNPs functionalised with either anti-CD3 alone, or equal amounts of anti-CD3 and anti-CD28. For CD3 + soluble CD28 treatments, cells were pre-treated with CD3 functionalised 250nm^{Mid} MNPs as described and were also stimulated with soluble CD28 at a final concentration of 2µg/mL. Magnetic force (MF) was provided for 1 hour, and T cell activation was assessed by flow cytometry 4 hours post MF application. Data shown from 3 independent experiments, each independent experiment contains a minimum of 2 technical replicates. Statistical analysis assessed via 2-way Anova with Sidak's post-tests. Nr4a3: * p= 0.0423, *** p< 0.0001, ** p= 0.0011. CD69: CD3:CD28 *** p<0.0001, CD3 + soluble CD28 *** p= 0.0002. CD25 ** p= 0.0041.

As shown in figure 3.5, providing anti-CD28 stimulation in these experiments greatly increased the percentage of cells positive for each marker of TCR signalling when subjected to 1 hour of magnetic force. Without magnetic force treatment, Nr4a3 expression was in the range of 6.9-8.1% for the three bead treatment strategies. However, with application of 1 hour magnetic force, this rose to 12.49%, 19.42% and 16.92% for anti-CD3 alone, anti-CD3:CD28 co-coated particles or anti-CD3 alone with soluble CD28 respectively. Similar trends were observed for CD69 and CD25 expression, with no magnetic force expression levels in the range of 12.6-14% for CD69 and 9.8-10.2% for CD25, which rose to 17.58%, 27.53% and 24.23% (CD69), and 11.99%, 19.75% and 17.58% (CD25) for CD3 alone, CD3:28 or CD3 alone with soluble CD28 stimulation strategies. These results demonstrate that as expected, provision of co-stimulatory signals to naïve CD4^{+} T cells increases the level of activation observed, yet importantly shows that magnetic force effects on T cell activation are driven through the TCR-CD3 complex.

3.4 Increased anti-CD3/CD28 Loading on 250nm MNPs Negates Effect of Magnetic Force

To investigate whether magnetic force effects still enhance T cell activation at higher background levels of signalling (that is, signalling levels in the absence of magnetic field application), the CD3 and CD3:CD28 loading on the surface of 250nm MNPs was increased 10-fold from absolute quantities of 1µg to 10µgof CD3 and CD28 antibodies, to produce 250nm^{Hi} MNPs as per methods section 2.5. A direct increase in fluorescent signal was observed when increasing the amount of antibody used in the functionalisation process, as measured by flow cytometry as per figure 3.6.

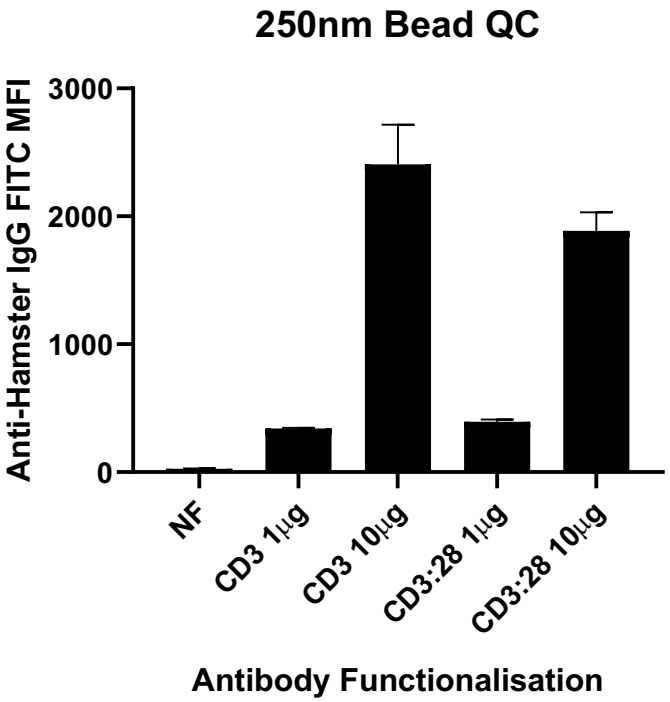


Figure 3.6 – Optimisation of Surface Antibody Concentration on 250nm MNPs. Quality control staining to assess how much antibody is loaded onto 250nm MNPs was performed as described in 2.9.4. Levels of particle-bound antibody was measured by determining the mean fluorescence intensity (MFI) of anti-Hamster IgG stained functionalised MNPs.

These differentially loaded 250nm MNPs were then used in a functional T cell activation assay, again assessing T cell activation by means of CD69 expression with and without 1

hour of magnetic force application. Whilst significant upregulations of CD69 were still observed with 1 hour of force application to 250nm^{Mid} MNPs, increasing the surface level of functionalised antibodies bypassed the effects of magnetic force on T cell activation. In these scenarios, CD69 expression in response to 250nm^{Hi} MNPs was already sufficiently high without force application (approx. 70-80% of cells CD69+) and magnetic force application had no effect on levels of CD69 expression.

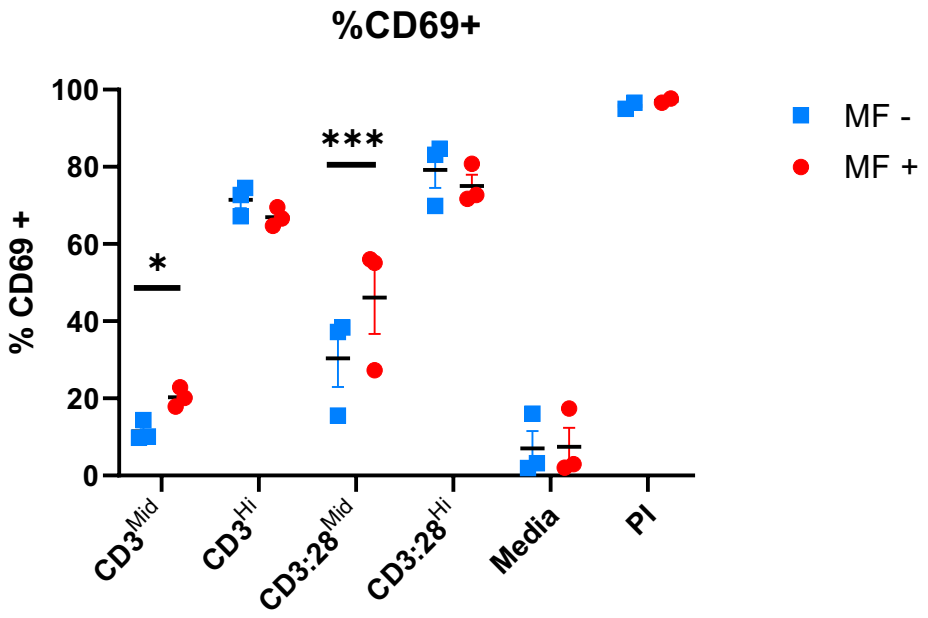


Figure 3.7 – Increasing Surface Antibody Concentration on 250nm MNPs Bypasses Magnetic Force Induced T Cell Activation. Purified CD4+ T cells from Tg4 transgenic mice were bound to 250nm^{Mid} or 250nm^{Hi} MNPs functionalised with either anti-CD3 or anti-CD3 and anti-CD28 antibodies as shown. Magnetic force (MF) was applied for 1 hour, and T cell activation was assessed by CD69 expression 4 hours post MF application. Data shown from 3 independent experiments, statistical analysis performed via 2-Way ANOVA, * $p = 0.0101$, *** $p < 0.0001$.

3.5 Optimisation of 1µm MNPs for External Magnetic Force Application

Whilst 250nm^{Mid} MNPs have shown that external force application can drive an upregulation in TCR signalling, the effects observed with these particles are somewhat small, with observed percentage of cells signalling in the approximate range of 10-30%. In an attempt to improve on this, we investigated the TCR signalling responses in Nr4a3-FT

reporter mice, in response to anti-CD3 functionalised 1µm MNPs. These particles have a diameter of 1µm, and an overall surface area approximately 16 times as large as the 250nm MNPs as outlined in equation 1 below. Previous work has identified that physical symmetry between T cell and APC is important for T cell activation, as this physical symmetry permits prolonged immune synapse stability[269]. Lack of symmetry at the synapse has been proposed to promote synapse imbalance[269], possibly through the loss of force balance at the contact site[270]. Therefore, utilisation of the larger 1µm MNPs may provide a more successful platform to achieve T cell activation. Additionally, 1µm MNPs will exert a larger force to the TCR-CD3 complex than the 250nm MNPs as outlined in 2.7.

$$Surface\ Area\ (A) = 4\pi r^2$$

$$1um\ MNPs: A = 4\pi 0.5^2 = 3.14um^2$$

$$250nm\ MNPs: A = 4\pi 0.125^2 = 0.2um^2$$

$$\frac{A(1um\ MNPs)}{A(250nm\ MNPs)} = \frac{3.14}{0.2} = 15.7$$

Equation 3.1 - Surface Area Calculations for 1µm and 250nm MNPs.

As before, purified $CD4^+$ T cells from Nr4a3-FT reporter mice were treated with 1µm MNPs at 10-fold concentration titration of 50, 5 or 0.5µg/mL. At the same time as titrating the concentration of particles used to treat the cells with, the total quantity of anti-CD3 used in the functionalisation process was also titrated 10-fold across a 100-fold range (figure 3.8: 10µg CD3 – red groups, 1µg CD3 – blue groups, and 0.1µg CD3 – green groups) thus investigating the level of bead-bound CD3 on the particle surface in the same experiments (as per table 2.3). These particles are henceforth denoted as $1\mu m^{Lo}$, $1\mu m^{Mid}$ and $1\mu m^{Hi}$. All

experimental groups were either given no magnetic force treatment or were treated with magnetic force for 1 hour in line with previous experiments, before T cell activation was assessed by flow cytometry at 4 hours post force treatment.

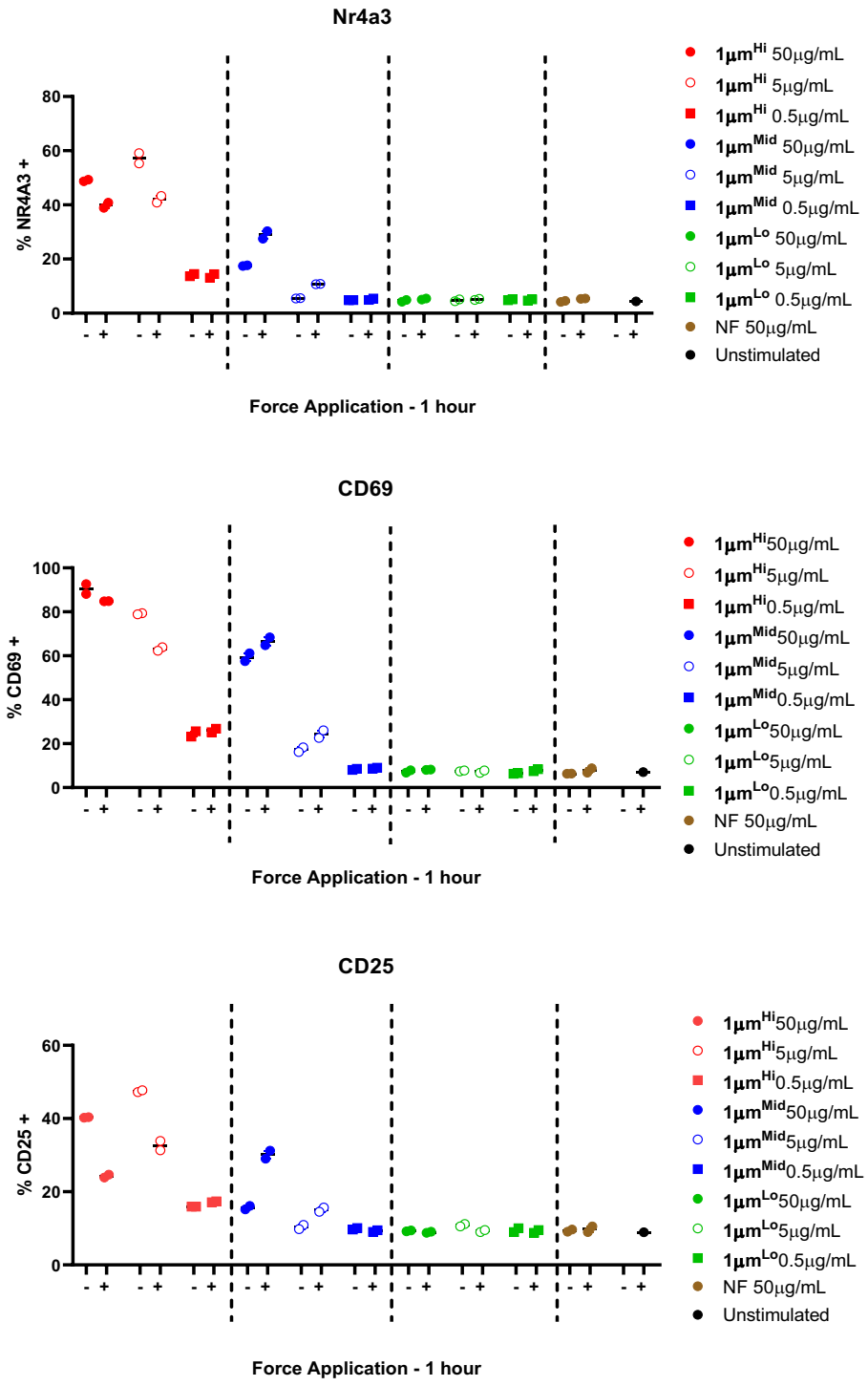


Figure 3.8 – Optimisation of particle concentration for 1µm MNPs. Purified CD4⁺ T cells from the spleen of Nr4a3-FT reporter mice were treated with 1µm^{Hi}, 1µm^{Mid} or 1µm^{Lo} MNPs (as shown in bold in the figure legend), across a concentration range of particle treatment as shown (50, 5 and 0.5µg/mL). Non-functionalised (NF) particles were included as a vehicle only control. Pre-treatment of CD4⁺ T cells with 50µg/mL of particles gave optimal responses to magnetic force. As a result, this concentration was taken forward for future experimentation. Data shown from 1 independent experiment, representative of 2 independent repeats. Each independent experiment contains a minimum of 2 technical replicates.

As shown in figure 3.8, 1µm^{Lo} MNPs were unable to induce Nr4a3, CD69 or CD25 expression at any particle treatment concentration used. However, 1µm^{Mid} MNPs induced expression of all 3 activation markers when cells were treated with 50µg/mL of MNPs, conditions under which expression of Nr4a3 and CD25 were also enhanced with magnetic force treatment. Finally, 1µm^{Hi} MNPs also induced significant expression of all 3 activation markers when cells were treated with 50µg/mL or 5µg/mL of MNPs. Interestingly, expression of Nr4a3 and CD25 were downregulated with magnetic force treatment under these conditions. Given the clean effects of the magnetic force treatment on Nr4a3 and CD25 at 50µg/mL for 1µm^{Hi} and 1µm^{Mid} particles, a treatment concentration of 50µg/mL was considered optimal and taken forward to future experiments.

These experiments were then repeated using the 50µg/mL concentration for treatment of Nr4a3-FT purified CD4^{+} T cells, to investigate the apparent change in magnetic force affect when increasing the surface level of anti-CD3. Figure 3.9 shows that as before, magnetic force treatment to 1µm^{Mid} MNPs significantly increased Nr4a3, CD69 and CD25 expression, whilst magnetic force treatment of 1µm^{Hi} MNPs induced a downregulation of Nr4a3 and CD25 expression. As an off-target control, 1µm MNPs were also functionalised with anti-MHC-I, using 10µg of total antibody during functionalisation as per 2.5, thus applying magnetic force to a cell surface receptor irrelevant for TCR signalling in our setting. Use of these MHC-I coated particles did not induce expression of Nr4a3, CD69 or CD25 under any setting.

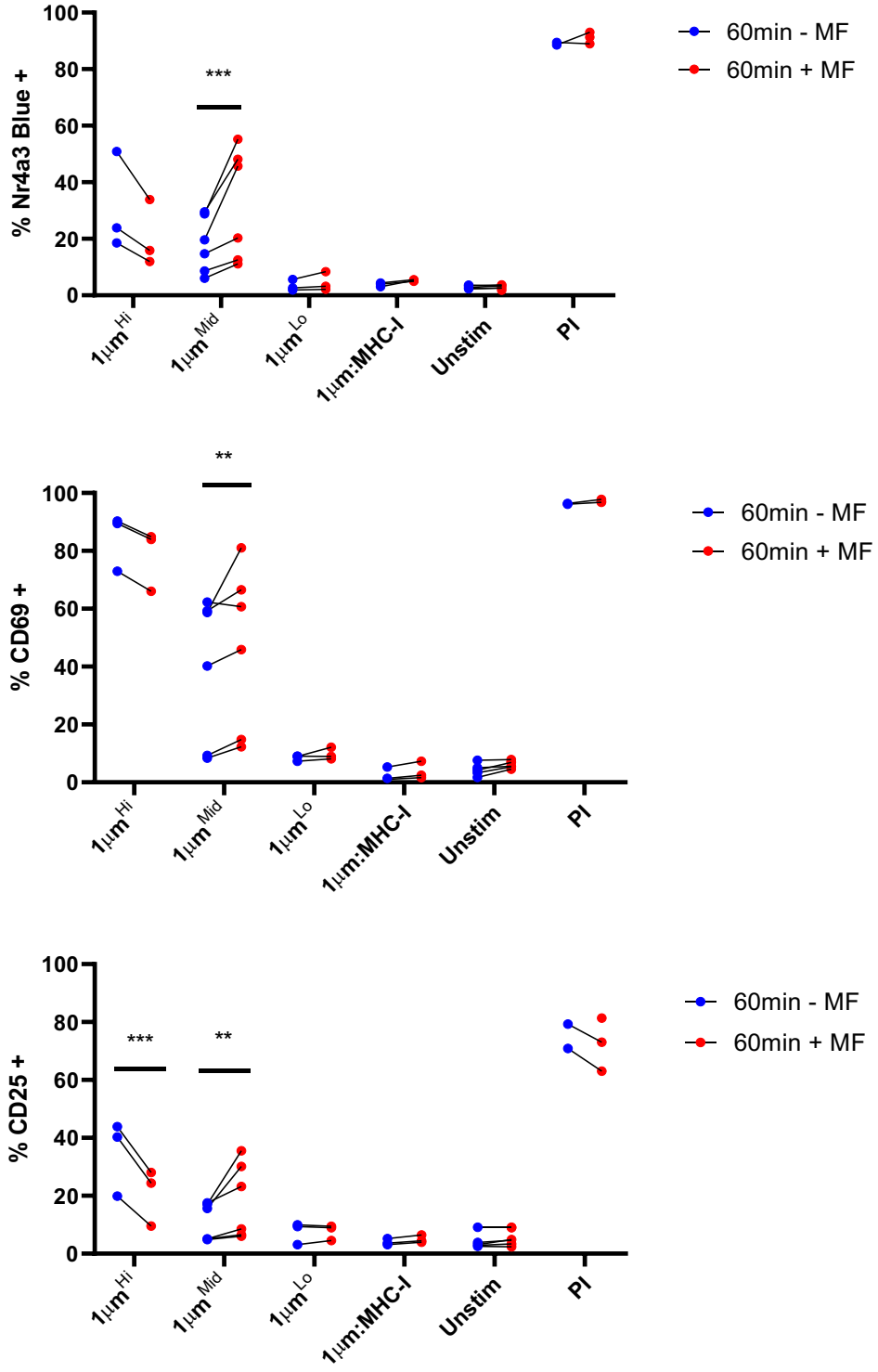


Figure 3.9 – Force application to 1µm^{Hi} or 1µm^{Mid} MNPs induces differential effects on TCR signalling. CD4^{+} T cells from Nr4a3-FT mice were treated with 50µg/mL 1µm^{Hi}, 1µm^{Mid} or 1µm^{Lo} MNPs as described. Magnetic force was applied for 1 hour with T cell activation assessed by flow cytometry 4 hours post force application. Each line connects no MF and + MF conditions from one indpendent experiment. Data shown represents atleast 3 independent experiments for each condition. Each independent experiment contains a minimum of 2 technical replicates. Statistical analysis assessed by 2-way ANOVA with Sidak's post-tests. Nr4a3: 1µm^{Hi}, p=0.065, 1µm^{Mid}, *** p=0.0003. CD69: 1µm^{Mid} ** p=0.0085. CD25: 1µm^{Hi} *** p=0.0002, 1µm^{Mid} ** p=0.0036.

To confirm that functionalised MNPs had infact bound increased levels of anti-CD3 antibody between the 1µm^{Mid} and 1µm^{Hi} CD3 groups, fluorescence was again measured by flow cytometry when staining these particles with an anti-Hamster IgG FITC antibody to determine levels of CD3 loading. A clear increase in fluorescence was observed when increasing the surface CD3 levels from 1µg to 10µg as shown in figure 3.10. Figure 3.10 also outlines how surface CD3 loading for the 1µm MNPs compares with the 250nm MNPs.

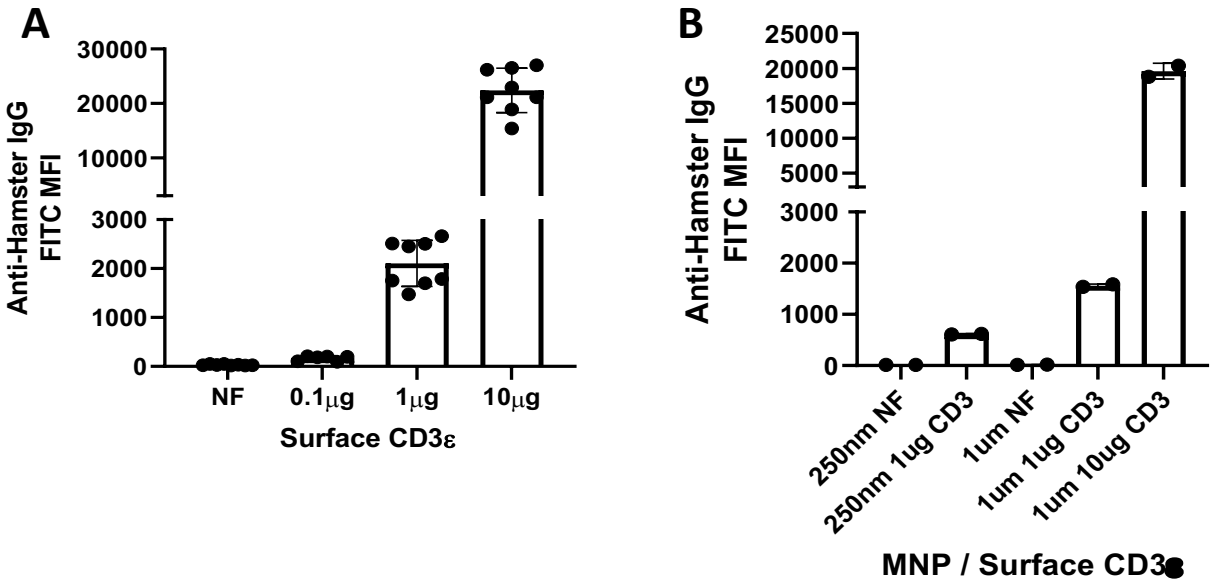


Figure 3.10 – Surface CD3 on functionalised 250nm and 1µm MNPs. A) 1µm MNPs were functionalised with 0.1, 1 or 10µg CD3 (145-2C11 clone, Isotype: Hamster IgG), or left non-functionalised (NF) as previously described in 2.5. Levels of particle bound antibody after functionalisation was assessed by staining with FITC conjugated anti-Hamster IgG before assessment of FITC MFI by flow cytometry as described in 2.9.4. A clear dose response was observed over the antibody functionalisation range tested. **B)** 250nm or 1µm MNPs were functionalised with levels of anti-CD3 as shown before assessment of particle-bound antibody by flow cytometry as previously described. Particles which induce upregulation of T cell activation when subjected to magnetic force (MF) were found to bind similar levels of surface anti-CD3, whilst particles which dampen T cell activation in the presence of MF were found to bind far higher levels of anti-CD3.

These results indicate that when signal 1 strength is originally low (250nm^{Mid} or 1µm^{Mid} anti-CD3 MNPs), force application serves to increase TCR signalling strength and positively influence T cell activation. However, when signal 1 strength is high (1µm^{Hi} MNPs) force application negatively impacts TCR signalling and serves to dampen T cell activation.

3.6 Effect of Magnetic Force on T Cell Activation in Transgenic Mouse Models

To this point, all mapping of the responses to anti-CD3 / anti-CD3 + CD28 functionalised MNPs has been done on purified CD4s from the Nr4a3-FT reporter mouse, used as a distal reporter of TCR signalling. This mouse model is a non-TCR transgenic, and therefore expresses a normal TCR repertoire successfully set during thymic selection. Therefore, to address the possibility of heterogeneity within this population affecting responses to stimulation with functionalised MNPs and force, we analysed signalling responses in TCR transgenic mouse models including a TCR transgenic on a Rag2 KO background. Here, we utilised the Tg4 transgenic mouse model from the Wraith lab[256], where approximately 95% of the $CD4^+$ T cells from this mouse express a transgenic Vα4+ Vβ8.2+ TCR specific for the Ac1-9 peptide from myelin basic protein (MBP) in complex with MHC-II $H\text{-}2^{u}$ [256]. Therefore, using purified $CD4^+$ T cells from this mouse, we were able to address the effect of external magnetic force application on a more homogenous $CD4^+$ population. However, as approximately 5% $CD4^+$ T cells from the Tg4 transgenic model can express endogenous TCRβ chains, we at the same time investigated the effect of magnetic force on T cell activation in the RTO mouse model. The RTO model is a Tg4 TCR transgenic model on a Rag2 KO background, and thus $CD4^+$ T cells from this mouse are unable to undergo TCR gene rearrangement and therefore exclusively express the Tg4 TCR. As an additional control in these experiments, we investigated responses to magnetic force application in the B10.PL mouse line, which forms the background of the Tg4 transgenic model.

3.6.1 Tg4 vs RTO vs B10.PL

In these experiments we aimed to assess whether the upregulation in TCR signalling in response to magnetic force treatment could be replicated in the transgenic models

described. However, it should be noted that typical spleen sizes from the RTO KO mouse were incredibly small and resulted in a far smaller single cell splenocyte suspension being obtained from these mice when compared to the Tg4 (approx. $10x10^6$ vs $80\text{-}100x10^6$ for RTO and Tg4 respectively). This is a result of the knockout meaning that not only can T cells not rearrange their TCR genes, but this is also true for B cells and their B cell receptor (BCR) genes which encode the BCR. For this reason, $CD4^+$ T cells were not purified from bulk splenocyte cultures in this set of experiments as losses of $CD4^+$ T cell numbers off the negative selection column would result in very low cell numbers to set up a functional experiment. Therefore, bulk splenocyte cultures were treated with 50µg/mL MNPs as shown and $CD4^+$ T cells were focussed on by gating on TCR $V\beta8^+$ $CD4^+$ events by flow cytometry.

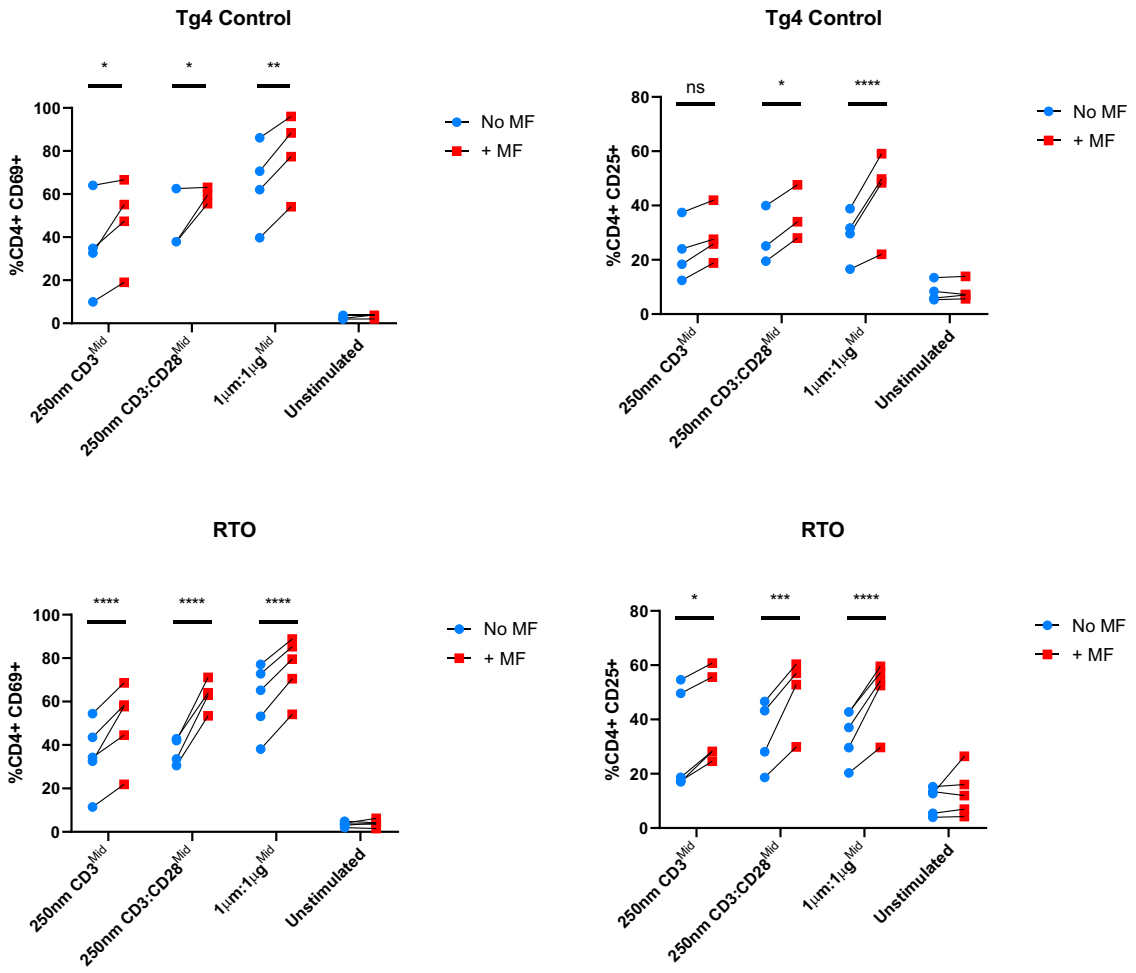


Figure 3.11 – Effects of Magnetic Force on TCR Signalling - Tg4 vs RTO Experiments. Single cell suspensions from spleens of Tg4 or RTO mice were pre-treated with functionalised 250nm^{Mid} or 1µm^{Mid} MNPs as shown. Magnetic force (MF) was applied for 1hour before CD69 and CD25 expression on Vβ8^{+} CD4^{+} T cells was assessed 4 hours post MF application. Each line connects no MF and + MF conditions from one individual experiments. Graphs shown at least 4 independent experiments. Each independent experiment contains a minimum of 2 technical replicates. Statistical significance assessed via 2 way-ANOVA with Sidak's post-tests. Tg4 CD69; * p=0.202, * p=0.0213, ** p=0.0051. Tg4 CD25; ns p=0.0537, * p=0.0101, **** p<0.0001. RTO CD69; **** p<0.0001. RTO CD25; * p=0.0104, *** p<0.0001, **** p<0.0001.

As outlined in figure 3.11, magnetic force was again shown to positively influence TCR signalling when applied to 250nm^{Mid} anti-CD3, 250nm^{Mid} anti-CD3:CD28 or 1µm^{Mid} anti-CD3 MNPs, in both Tg4 and RTO mice. Expression of both CD69 and CD25 was increased on average by approximately 10-20% across all particle groups with force application, in both Tg4 and RTO mice. No significant differences were observed when comparing the 2 strains of mice.

Similar results were obtained when performing TCR signalling experiments in B10.PL mice. As described for figure 3.11, bulk splenocyte cultures were used before gating on TCR^+ $CD4^+$ events to assess the effect of magnetic field application on TCR signalling and T cell activation. Force application for 1 hour induced significant upregulation of CD69 expression in all particle conditions tested, whilst robust CD25 upregulation was observed when using $1\mu m^{Mid}$ MNPs (figure 3.12).

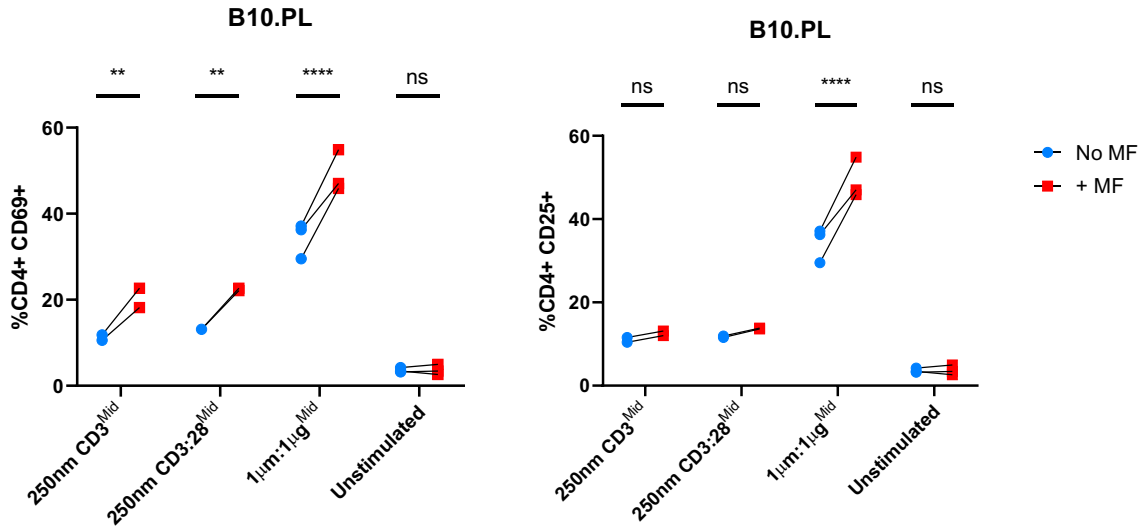


Figure 3.12 – Effect of Magnetic Force Application on TCR Signalling in B10.PL Mice. Single cell suspensions from B10.PL mice were treated with functionalised $250nm^{Mid}$ or $1\mu m^{Mid}$ MNPs as shown. Magnetic force (MF) was applied for 1 hour, and CD25 and CD69 expression on $TCR\beta^+$ $CD4^+$ T cells was measured 4 hours post field application. Each line connects no MF and + MF conditions from one individual experiment. Graphs displayed 3 biological replicates from 2 independent experiments for $1\mu m^{Mid}$ MNPs, and 2 biological replicates from 1 independent experiment for $250nm^{Mid}$ MNPs. 250nm MNP data is representative of 2 independent repeats. Each independent experiment contains a minimum of 2 technical replicates. Significance assessed by 2-way ANOVA with Sidak's post-tests. Left to right: CD69 ** p=0.0064, ** p=0.0063, *** p=0.0002. CD25 **** p<0.0001.

These results indicate that the effects of magnetic force application can be observed in a variety of mice with varied TCR specificities, including the Nr4a3-FT and B10.PL strains which express more of a typical 'wild type' TCR repertoire, and the RTO and Tg4 transgenic mice strains, which express the Tg4 TCR both with and without a RAG KO background.

3.7 T Cell Activation in Response to Functionalised MNPs are TCR Triggering Specific

Whilst use of off-target antibodies to functionalise MNPs provides evidence that T cell activation events observed must go through the TCR-CD3 complex, use of inhibitors to block TCR proximal signalling would provide robust evidence that effects of magnetic field induced signalling must go through the TCR and are not a result of target effects such as non-specific membrane stretch permitting calcium entry into the cell, triggering release of calcium ion stores from the endoplasmic reticulum and thus non-specifically triggering TCR signalling pathways. To this end we utilised PP2, a potent and selective inhibitor of Src family kinases (Lck, Fyn etc)[271] which will therefore inhibit the phosphorylation of CD3 chain ITAMs. The ability of 10µM PP2 treatment to inhibit responses to 250nm^{Mid} and 1µm^{Mid} MNPs with and without magnetic force was assessed in Tg4 mice as shown in figures 3.13 and 3.14 respectively.

$CD4^+$ T cells were purified from the spleen of Tg4 mice and treated with anti-CD3 functionalised 250nm^{Mid} or 1µm^{Mid} MNPs, hence utilising conditions where magnetic force has shown positive upregulation of TCR signalling as per figures 3.4 and 3.9 respectively. At the same time as particle treatment, cells were also treated with 10µM PP2 or an equivalent concentration of DMSO as a negative control. PP2 and DMSO concentrations were maintained throughout the particle washing steps. Inclusion of 10µM PP2 was sufficient to inhibit upregulation of CD69 in response to magnetic force treatment for both 250nm and 1µm MNPs (figures 3.13 and 3.14 respectively). Levels of CD69 expression observed in PP2 treated cultures were at equivalent levels of the unstimulated controls across all experiments (approximately 1-3%).

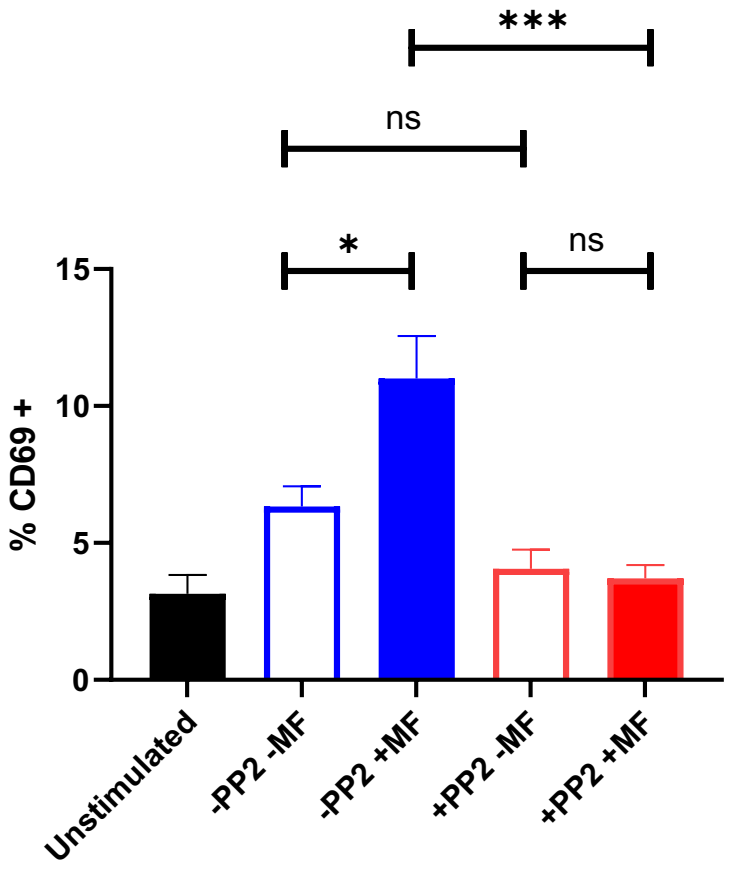


Figure 3.13 – PP2 Blockade Inhibits Magnetic Force Induced TCR Signalling to 250nm^{Mid} anti-CD3 MNPs. Purified CD4^{+} Tg4 T cells were stimulated with 250nm^{Mid} anti-CD3 MNPs, ± magnetic force (MF) for 1hour. To assess whether responses were TCR signalling specific, cells were also treated with final concentrations of 10µM PP2 (red bars). T cell activation was assessed by CD69 expression 4hours post MF application. Treatment with PP2 prevents CD69 expression in response to 250nm^{Mid} CD3 MNPs. Bar graphs show mean ± SD of 4 independent experiments. Significance assessed by One-way ANOVA with Tukey's post-tests. * p=0.0183, *** p=0.0004.

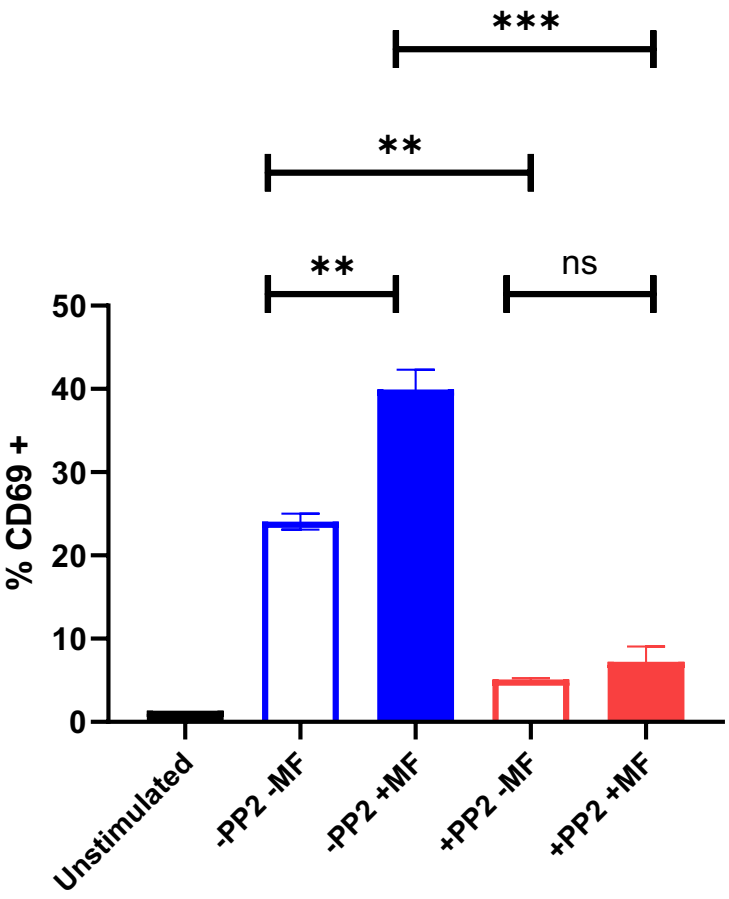


Figure 3.14 – PP2 Blockade Inhibits Magnetic Force Induced TCR Signalling to 1µm^{Mid} CD3 MNPs. CD4^{+} T cells purified from Tg4 mice were stimulated with 1µm^{Mid} CD3 MNPs ± 1hour magnetic force (MF) and ± 10µM PP2. T cell activation was analysed by flow cytometry 4 hours post MF application by means of CD69 expression. Treatment with 10µM PP2 prevents CD69 expression in response to 1µm:1ug CD3 MNPs ± MF. Bar graphs shown mean ± SD of duplicates from 1 experiment, representative of 2 independent experiments. Significance assessed by One-way ANOVA with Tukey's post-tests.

3.8 External Magnetic Force Drives Nuclear Accumulation of Transcription Factors

Given the observed TCR specific effects of magnetic force on CD4^{+} T cell activation, we hypothesised that force application in our system may be inducing TCR signalling, as others have previously shown in experiments measuring calcium flux as earlier described. As our magnetic force application protocol using the MICA bioreactor is not compatible with live calcium imaging, we chose to measure phosphorylation of extracellular signal-regulated

kinase (ERK) and lymphocyte specific protein tyrosine kinase (Lck), as proximal readouts of TCR signalling.

$CD4^+$ T cells from Tg4 mice were treated with $1\mu m^{Mid}$ or $1\mu m^{Hi}$ MNPs as previously described. External magnetic force was applied for 15, 30 or 60 minutes, after which cells were fixed and permeabilized, and intracellular expression of phosphorylated ERK, Lck or SHP-1 (pERK/pLck/pSHP-1) was assessed by flow cytometry.

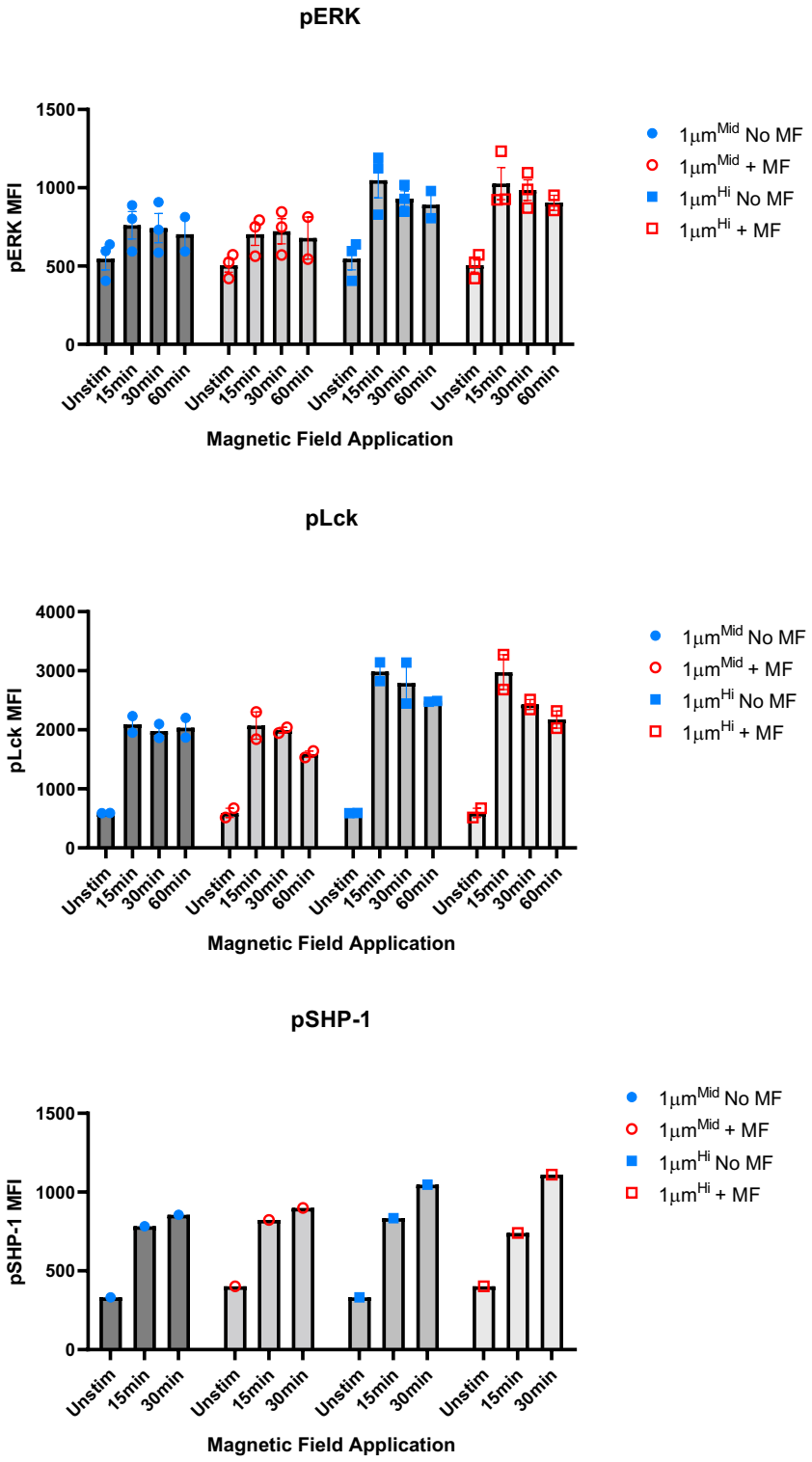


Figure 3.15 – Magnetic Force Application Does Not Specifically Influence TCR Signalling Pathways. CD4⁺ T cells purified from Tg4 mice were treated with 1μm^{Mid} or 1μm^{Hi} MNPs as per 2.6. Following stimulation with magnetic force (MF) for time frames shown, cells were fixed, surface stained and permeabilised before intracellular staining for phosphorylated signalling proteins as per 2.9.3. Whilst stimulation with CD3 coated MNPs was able to induce phosphorylation of ERK (top), Lck (middle) and SHP-1 (bottom), MF application showed no effect of ERK/Lck/SHP-1 phosphorylation. Top: pERK data from 3 independent experiments. Middle: pLck data from one experiment, representative of 3 independent repeats Bottom: pSHP-1 data from one experiment, representative of two independent repeats.

Whilst increase in anti-CD3 on 1µm MNPs gave rise to increased levels of pERK and pLck as expected, application of magnetic force was unable to induce an upregulation in phosphorylation of either protein (figure 3.15). SHP-1 phosphorylation was also observed as a result of anti-CD3 stimulation, but again showed no response to magnetic force application. This result may reflect low sensitivity within the phosflow methodology employed, and suggests that in order to mediate the observed effects on Nr4a3, CD69 and CD25 expression, external magnetic force may induce an accumulation of nuclear translocation of transcription factors and that this accumulation of signalling events may permit cells to reach the threshold required for T cell activation[116,272,273]. To test this, we hypothesised that 4 pulses of 15 minutes of magnetic force treatment should induce the same level of Nr4a3 expression as 1 full 60 minute pulse, as outlined in figure 3.16. $CD4^+$ T cells isolated from Nr4a3-FT mice were treated with $1µm^{Mid}$ CD3 MNPs are previously described (2.6) and were subjected to either a single 15 minute pulse of magnetic force, a single 60 minute pulse, or 4 rounds of 15 minute pulses each separated by 15 minutes of no magnetic field treatment, so that the total 'on' time equalled 60minutes (figure 3.16).

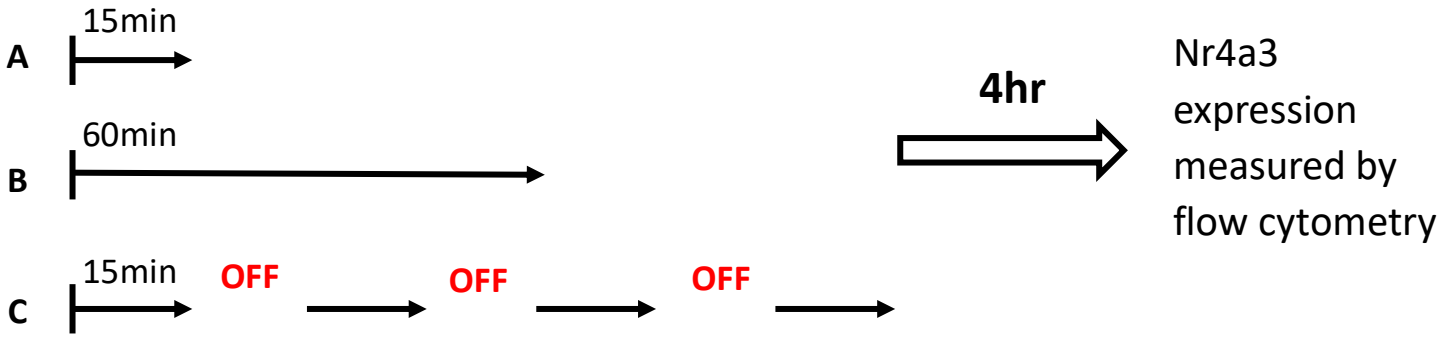


Figure 3.16 – Schematic of Force Induced Signal Accumulation Experimental Protocol. A+B) Force application is provided for 15mins (A) or 60mins (B) in one continuous pulse with Nr4a3 expression measured 4 hours after force application. C) Four rounds of 15min pulses of force application were provided, with each pulse separated by a 15min period of no force application (represented by OFF). Nr4a3 expression was measured 4hours after application of the pulsatile force application strategy to determine the effect of force on signal accumulation.

As per previous experiments, 1 hour of magnetic force application was able to drive a significant upregulation in Nr4a3 expression (figure 3.17, 15.43% cells Nr4a3+ with no magnetic force, 25.08% with 1 hour) whilst 15 minute alone gave rise to a much smaller upregulation (18.8% Nr4a3+). Interestingly, 4 rounds of 15 minute magnetic force treatment, each separated by a 1 5minute period of no force treatment (C, figure 3.16) also drove a significant upregulation of Nr4a3 to a slightly greater extent than 1 hour treatment alone (figure 3.17, 32.23% Nr4a3+).

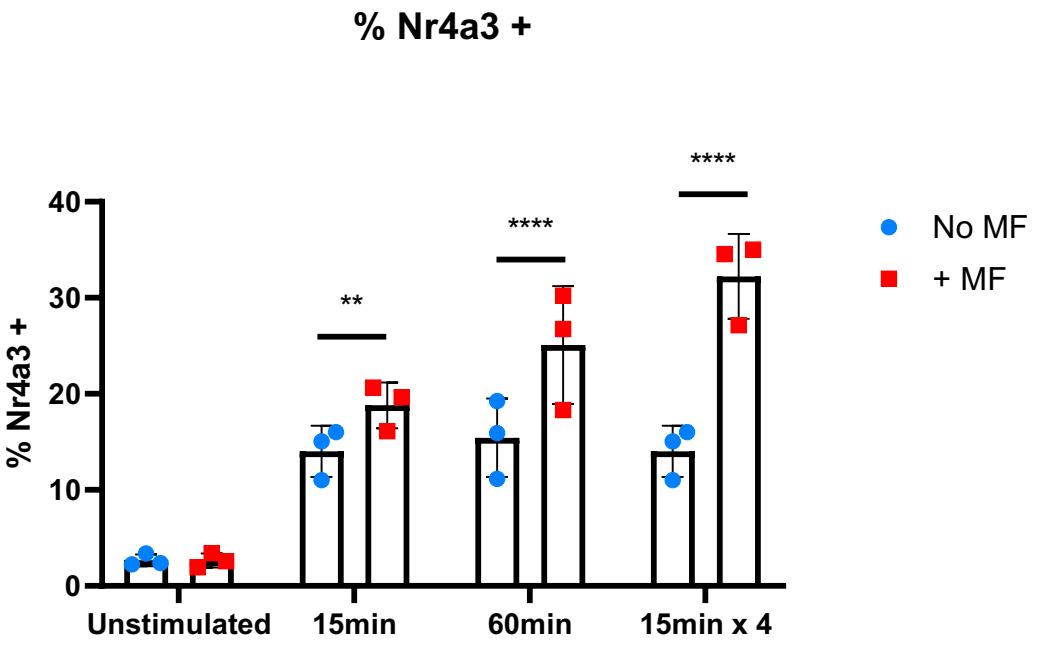


Figure 3.17 – Pulsatile Magnetic Force Treatment Leads to an Accumulation of Nr4a3 Expression. Pulsatile magnetic force strategies as described in figure 3.16 were applied to $CD4^{+}$ Nr4a3-FT T cells pre-treated with $1\mu m^{Mid}$ MNPs. Assessment of Nr4a3 expression 4 hours post MF application showed a large upregulation of Nr4a3 expression when 15min MF was provided as 4 pulses, indicating an accumulation of TCR signalling. Bar graphs represent 3 independent experiments, statistical analysis assess via 2-way ANOVA with Sidak's post-tests. 15min ** p= 0.0023, 60min **** p<0.0001 , 15min x 4 **** p<0.0001.

Nr4a3 expression has been previously shown to be dependent on signalling through the calcineurin-calmodulin pathway downstream of TCR triggering[274], where NFAT dephosphorylation ultimately permits NFAT nuclear entry and subsequent Nr4a3 transcription. To demonstrate that magnetic force application results in accumulation of nuclear NFAT over the period of 1 hour, we adapted the protocol of the pulsatile magnet experiment to specifically target the calcineurin-calmodulin pathway between each 15 minute pulse. Cyclosporin A (CsA) is a fungal derived immunosuppressive agent, known to mediate its effects through inhibition of the TCR signalling cascade[275,276]. CsA is known to form a complex with cyclophilin, which in turn blocks phosphatase activity of calcineurin and thus can be used to probe nuclear accumulation of NFAT (A, figure 3.18)[277,278]. In our adapted pulsatile magnet protocol, CsA was added to a final concentration of 1μM sequentially between each 15min magnetic force pulse (C-F, figure 3.19).

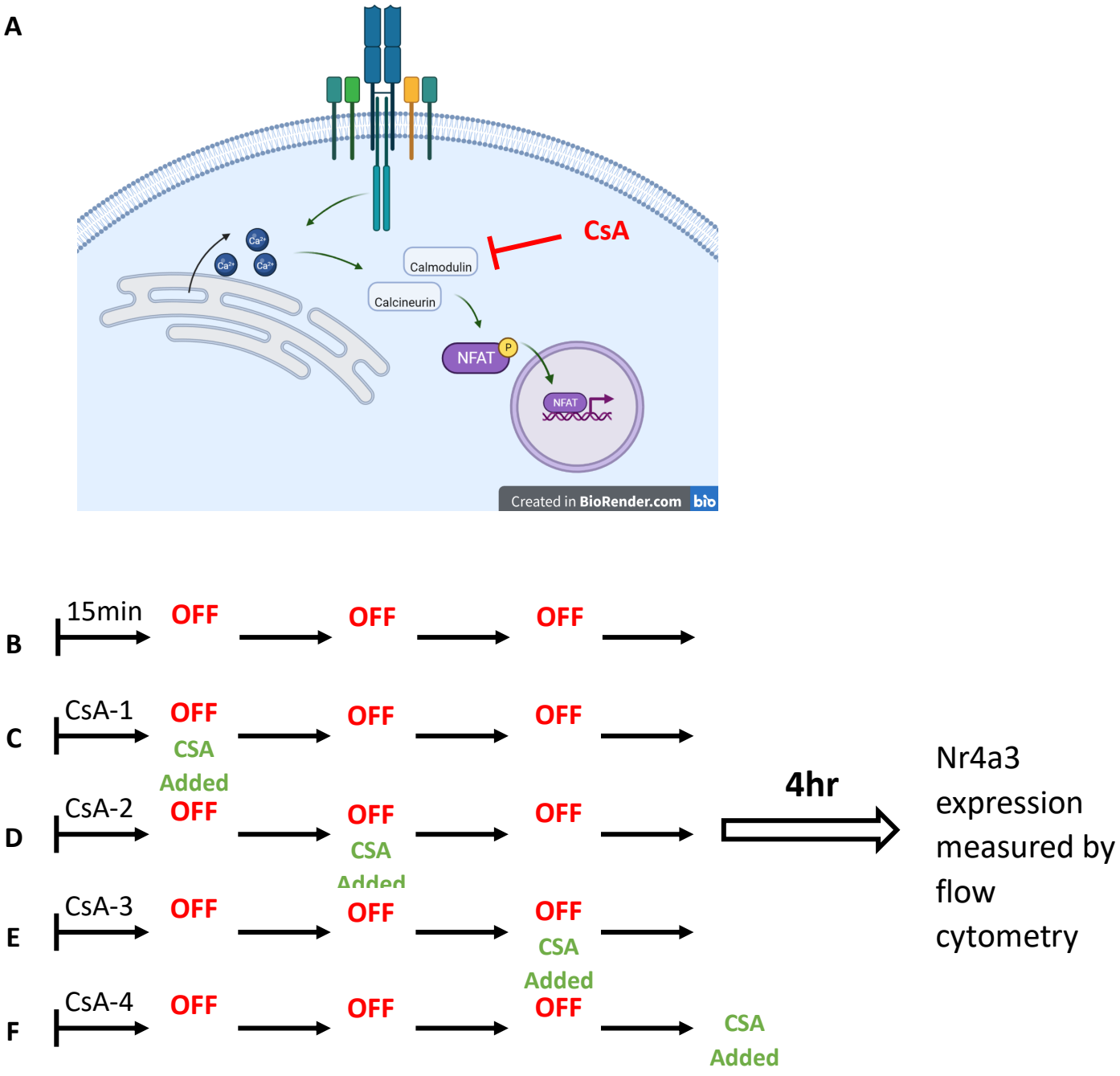


Figure 3.18 – Cyclosporin A (CsA) Addition to Probe Nuclear Accumulation of NFAT. A: CsA inhibits phosphatase activity of calmodulin, preventing NFAT dephosphorylation and nuclear translocation. B-F: Addition of CsA between each of four individual 15 minute magnetic force pulses prevent further NFAT nuclear translocation. B: Four 15 minute pulses are provided, each separated by a 15 minute gap in force application. C-F: CsA is added to the culture to a final concentration of 1µM in a sequential manner (added after the first, second, third or fourth pulse in C-F respectively). Magnetic force is still applied for the remaining pulses as indicated after CsA is added. Nr4a3 expression is measured 4 hours post force application.

Four pulses of 15 minutes of magnetic force gave rise to a significant increase in Nr4a3 expression over no magnetic force controls, which was blocked when CsA was added in a sequential manner out to the third pulse. Of conditions where CsA was added to block the NFAT pathway, we only detected significant upregulation of Nr4a3 when all four magnetic forces were completed prior to any CsA addition (CsA-4, figure 3.18-F and figure 3.19). Addition of CsA at all pulse stages prior to this (CsA 1-3, figure 3.18-C-E) prevented significant upregulation of Nr4a3 in response to magnetic force treatment (figure 3.19).

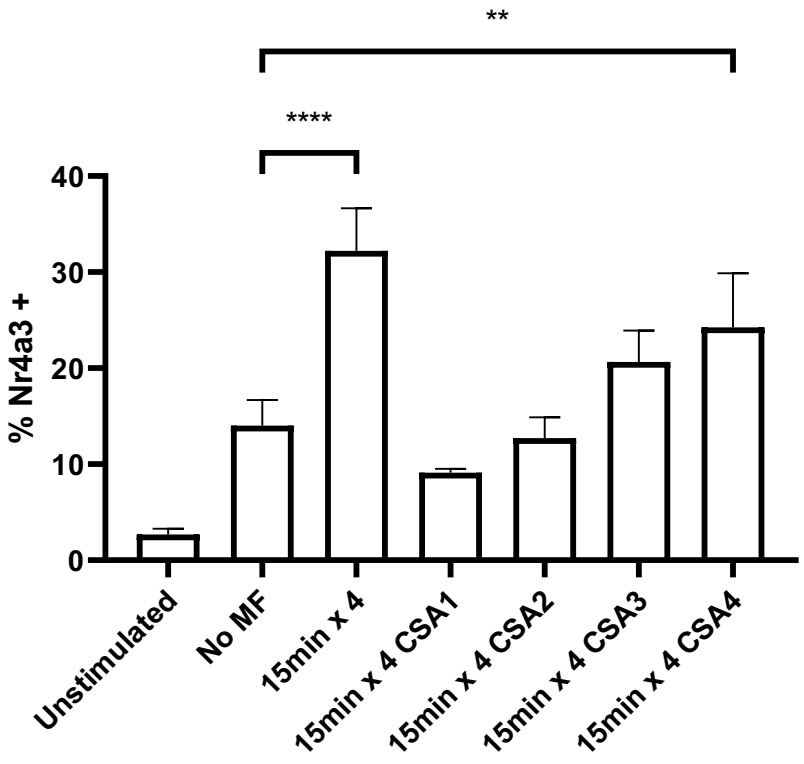


Figure 3.19 – Pulsatile Magnetic Force Treatment Drives Nuclear NFAT Accumulation. Nr4a3-FT $CD4^+$ T cells were treated with $1\mu m^{Mid}$ CD3 MNPs and were given four rounds of 15 minute magnetic force pulses with or without sequential CsA addition (1µM) as described in figure 3.18. Significant upregulation of Nr4a3 expression is only observed when all four rounds of force application are completed prior to CsA addition. Data from 3 independent experiments, significance assessed by one-way ANOVA with Dunnett's multiple comparisons comparing all conditions to no magnetic force (MF) control. ****, $p<0.0001$, **, $p=0.0085$. Not shown: Unstimulated vs No MF, **, $p=0.0038$.

Taken together, these results indicate that force application in our system acts to promote accumulation of signalling intermediates, such as nuclear translocation of

transcription factors (fig 3.17-3.19), thus influencing T cell activation. Our findings indicate that this process occurs over the period of 1 hour, a time frame consistent with other studies[265], indicating that nuclear localisation of NFAT is required to reach thresholds required for T cell activation.

3.9 Effect of Magnetic Force Application on $CD4^+$ T Cell Proliferation and Cytokine Production

Finally, to assess whether force application influences functional $CD4^+$ T cell responses, we measured T cell proliferation and cytokine production 72 hours post 1 hour magnetic force application. As previously described when measuring Nr4a3, CD69 and CD25, we have found that force application to sub-optimal signal 1 strength MNPs ($250nm^{Mid}$ MNPs, $1\mu m^{Mid}$ CD3 MNPs) serves to upregulate T cell activation, whilst force application to high signal 1 strength ($1\mu m^{Hi}$) MNPs serves to dampen T cell activation. To determine whether this pattern translates through to proliferative responses, we isolated $CD4^+$ T cells from Tg4 mice and labelled these cells with cell trace violet (CTV) as described (2.8.2). These CTV^+ cells were then treated with all groups of MNPs tested to this point ($250nm^{Mid}$ MNPs: CD3 alone, CD3:CD28, CD3 alone + soluble CD28. 1µm MNPs: 1µm:1µg or $1\mu m^{Hi}$), where force application was then applied for 1 hour. Cells were maintained in a 37°C 5% CO_2 incubator for 3 days, at which point cell proliferation was assessed by measuring CTV dilution. At the same time, cytokine production was assessed by intracellular cytokine staining (ICCS, as described in 2.9.2) following restimulation with phorbol 12-myristate 13-acetate (PMA) and ionomycin (PI) for 3 hours in the presence of GolgiStop. PMA activates protein kinase C (PKC), and together with the calcium ionophore ionomycin can bypass the TCR itself but

switch on TCR signalling pathways[279,280]. Therefore, restimulation with PI in this setting recalls expression of all open gene loci at that point in time, that are controlled by the TCR.

3.9.1 250nm MNPs

Force application to all strategies of TCR stimulation with 250nm^{Mid} MNPs showed that force application for 1 hour upregulates the observed CD4^{+} T cell proliferation observed at day 3 (figure 3.20, 3.21), as evidenced by a significant decrease in the percentage of cells that remained undivided (i.e., in generation 0) for each condition with field application (figure 3.21). Unsurprisingly, strongest levels of proliferation were observed when co-stimulation was provided, either by bead bound or soluble CD28 stimulation, as shown in the representative CTV traces in figure (figure 3.20).

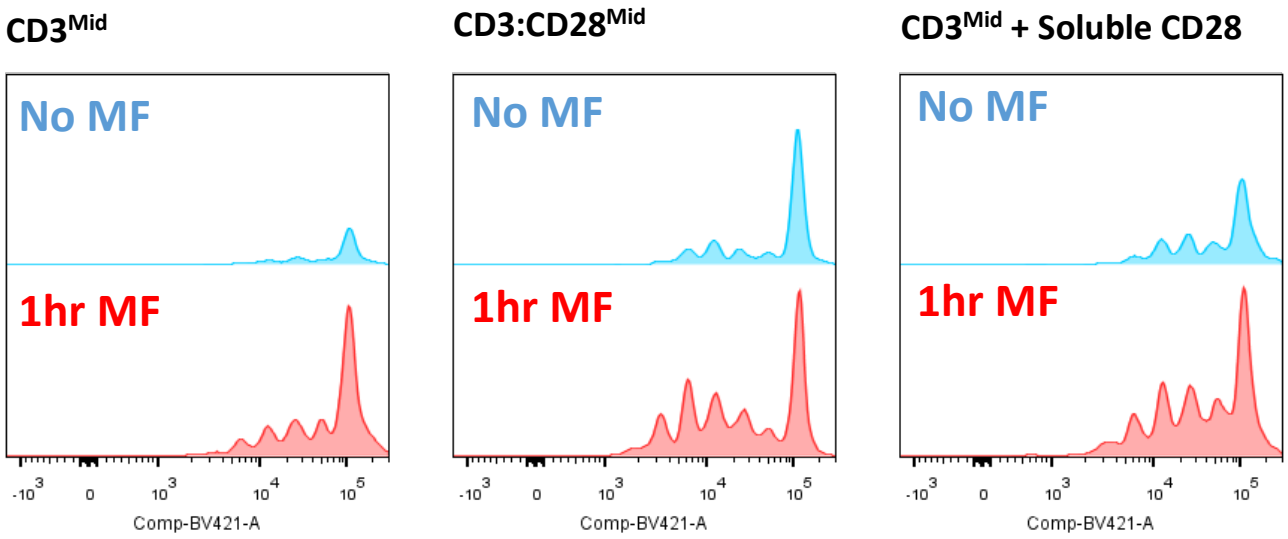


Figure 3.20 – Representative CTV traces for 250nm MNP stimulated CD4^{+} Tg4 T cells. Purified CD4^{+} T cells from Tg4 mice were stained with cell trace violet (CTV) proliferation dye as described in 2.8.2. Cells were treated with functionalised 250nm MNPs as previously described and magnetic force (MF) was applied for 1hour. Cell proliferation was assessed at day 3 by means of CTV dilution. Traces representative of 3 independent experiments.

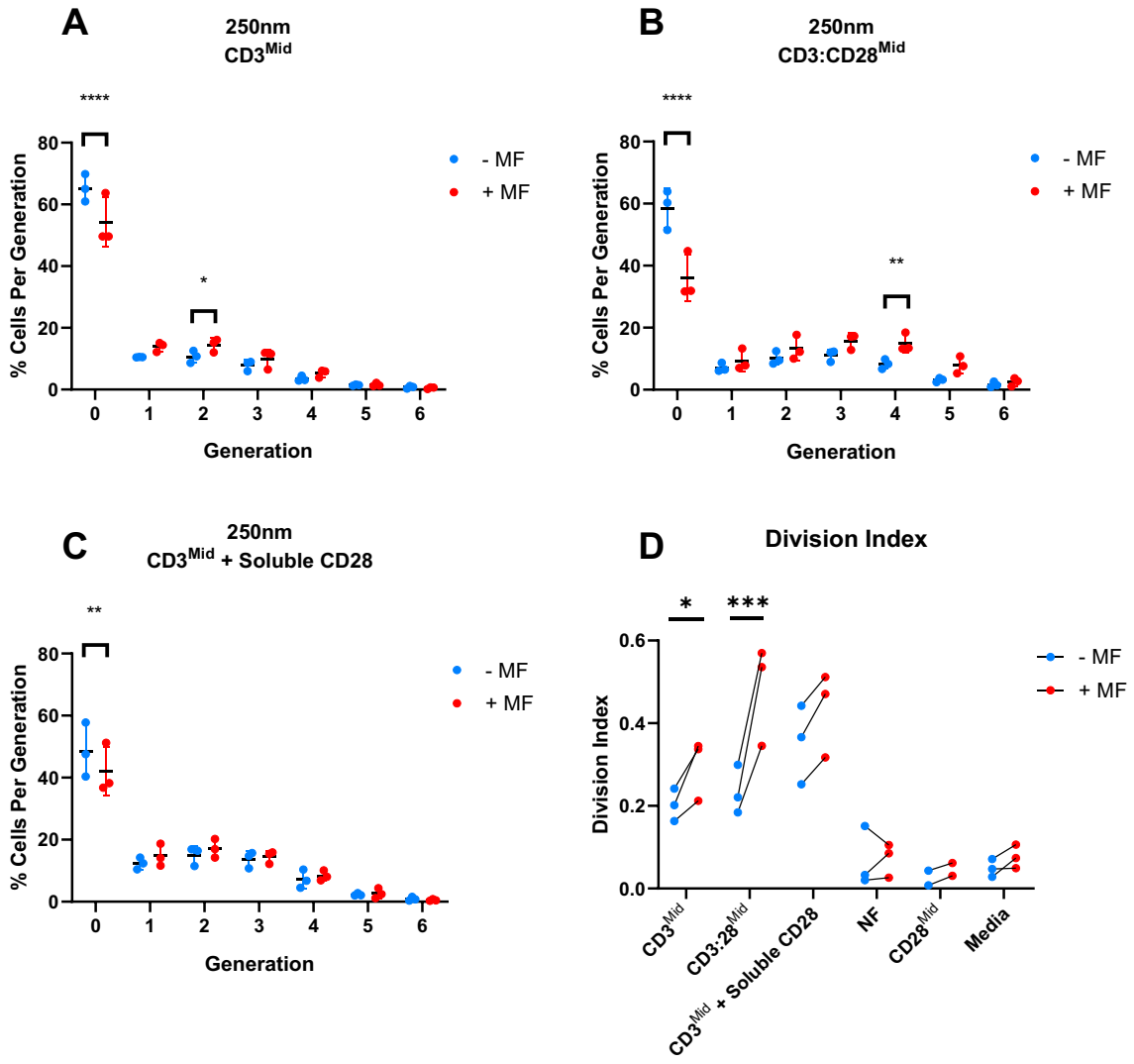


Figure 3.21 – CTV Analysis from 250nm MNP proliferation experiments. A-C: Percentage of cells per division peak in the CTV traces (figure 3.20) was analysed for 250nm^{Mid} anti-CD3 alone, 250nm^{Mid} anti-CD3:CD28 and 250nm^{Mid} anti-CD3 alone + soluble CD28 (2µg/mL) conditions. Magnetic force (MF) application to all 3 conditions was found to induce a significant decrease in percentage of cells remaining undivided (generation 0), indicative of MF induced cell proliferation. Generation 0, CD3 alone $p<0.0001$, CD3:CD28 $p<0.0001$, CD3 + soluble CD28 $p=0.0048$. **D:** MF induces significant upregulation of division index for 250nm^{Mid} anti-CD3 (* $p=0.0262$) and 250nm^{Mid} anti-CD3:CD28 MNPs (*** $p<0.001$). MF induced upregulation of the division index for 250nm^{Mid} anti-CD3 + soluble CD28 conditions was also observed, although this did not reach significance ($p=0.0746$). Proliferation was not observed for particle controls (non-functionalised (NF) or functionalised with CD28 alone) or an unstimulated media control. **A-D:** All statistical analysis assessed by 2-way ANOVA with Sidak's post-tests.

These results indicate that force application to 250nm MNPs not only increases expression of T cell associated activation markers, but that these effects translate through to an effect on T cell functionality evidenced by an increase in T cell proliferation. When

measuring Interferon gamma (IFNγ) and Interleukin-2 (IL-2) production by ICCS at the same time as measuring cell proliferation, we found a clear reliance on CD28 stimulation for IL-2 production, and no effect of magnetic force application on IL-2 production in any incidence (figure 3.22). However, magnetic force application to 250nm MNPs functionalised with both CD3 and CD28 induced a large upregulation in IFNγ expression, which was not found upon stimulation with CD3 alone, or when soluble CD28 was provided in the culture medium.

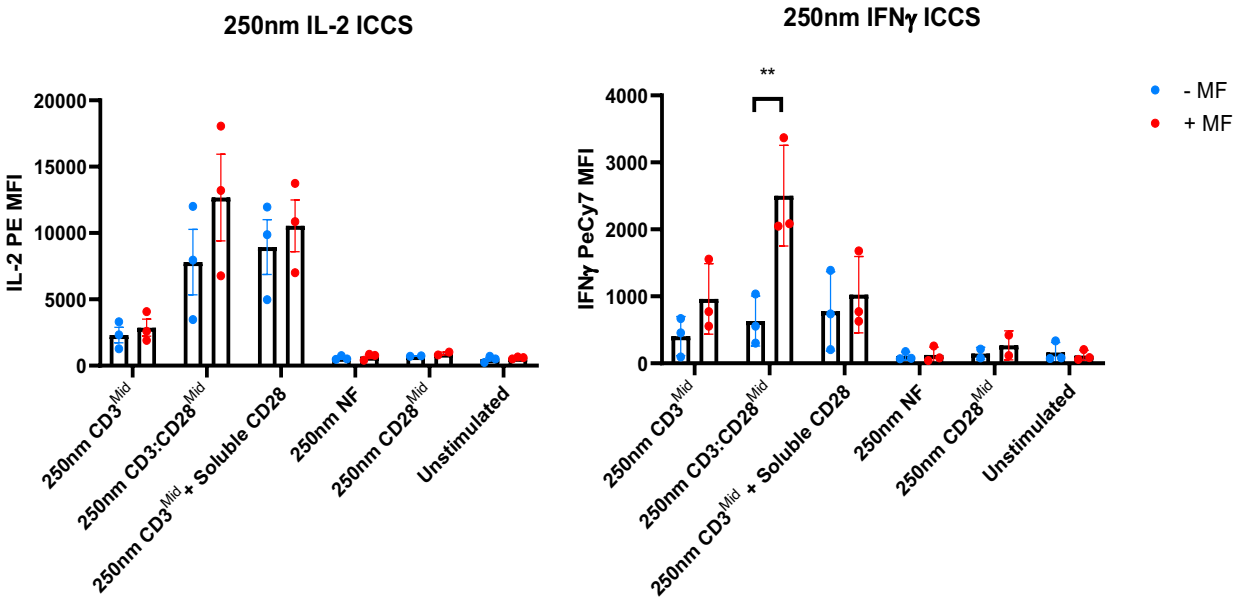


Figure 3.22 – ICCS analysis of IFNγ and IL-2 production in response to 250nm MNPs and magnetic force. CD4+ T cell from Tg4 transgenic mice were stimulated with 250nm^{Mid} MNPs as shown for 72 hours after being subjected to +/- 1hour magnetic force (MF). Cytokine production was assessed by intracellular cytokine staining (ICCS) as described in 2.8.2. Bar graphs show data from 3 independent experiments. Force application to 250nm MNPs functionalised with anti-CD3:CD28 induced an upregulation in IFNγ production (**, p= 00032). Statistical analysis performed via 2-way ANOVA with Sidak's post tests.

Importantly, neither cell proliferation or cytokine production was observed when 250nm particles were functionalised with CD28 antibodies alone or were left non-functionalised (NF).

3.9.2 1µm MNPs

Force application to 1µm MNPs functionalised with differential CD3 loadings reproduced

the findings observed when analysing Nr4a3, CD69 and CD25. Force application to 1µm^{Mid} MNPs induced a robust upregulation in cell proliferation, an effect which reversed when CD3 loading on the particle surface was increased to 10ug CD3 (figure 3.23).

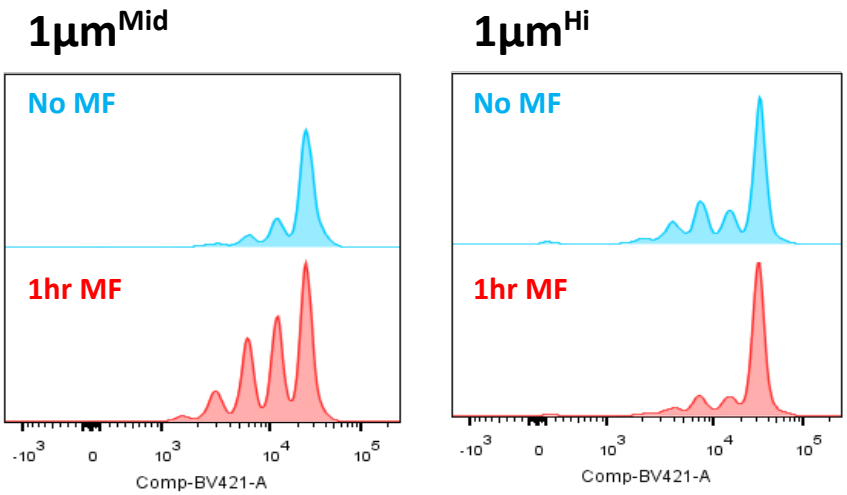


Figure 3.23 – Representative CTV traces from 1µm MNP proliferation assays. Purified CD4$^+$ T cells from Tg4 mice were stained with cell trace violet (CTV) proliferation dye as described in 2.8.2. Cells were treated with functionalised 1µm^{Mid} (left) or 1µm^{Hi} (right) MNPs as previously described and magnetic force (MF) was applied for 1hour. Cell proliferation was assessed at day 3 by means of CTV dilution. Traces representative of 3 independent experiments.

Force modulation of proliferative responses reached significance when analysing the percentage of cells found in each cell division peak, where less cells remain undivided when treated with 1µm^{Mid} MNPs and magnetic force, whilst the reverse was found to be the case for 1µm^{Hi} MNPs (figure 3.24).

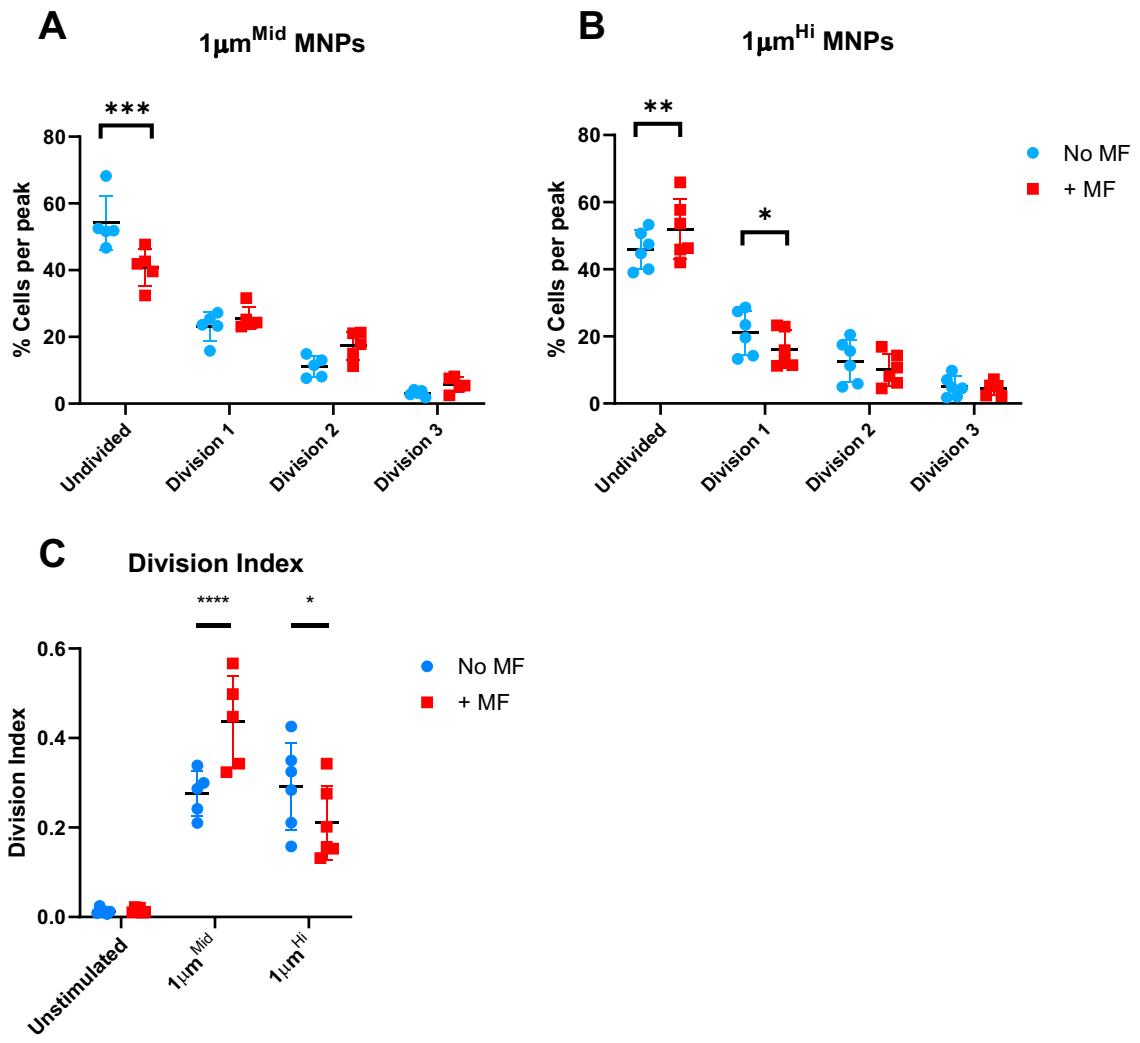


Figure 3.24 – CTV analysis from 1µm MNP proliferation experiments. A-B: Percentage of cells per division peak in the CTV traces (figure 3.23) was analysed for cells treated with 1µm^{Mid} (A) or 1µm^{Hi} (B) MNPs. Magnetic force (MF) application induced an upregulation in cell proliferation when applied to 1µm^{Mid} MNPs (A, *** p<0.0001) as shown by a decreased number of cells remaining undivided. MF application to 1µm^{Hi} MNPs induced a blockade in cell proliferation, evidence by an increase in the undivided population (B, ** p= 0.0015). C: MF application positively and negatively impacts the division index for CD4s stimulated with 1µm^{Mid} or 1µm^{Hi} MNPs respectively (**** p<0.0001 , * p= 0.0108). Statistical analysis performed via 2-way ANOVA with Sidak's post-tests. Data shown from at least 4 independent experiments.

However, for both CD3 loadings of 1µm MNP, we were unable to observe robust expression of either IL-2 or IFNγ when analysed by ICCS (figure 3.25).

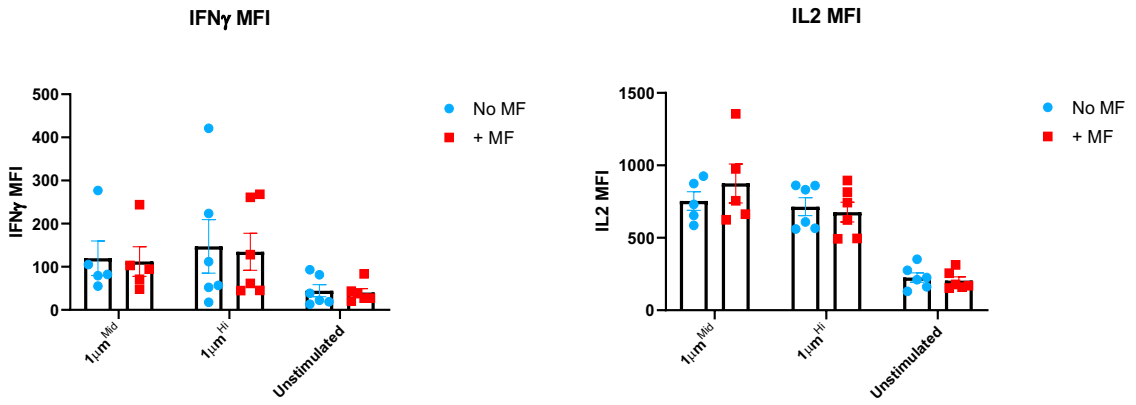


Figure 3.25 – ICCS analysis of IFNγ and IL-2 production in response to 1µm functionalised MNPs and magnetic force. Purified CD4+ T cells from Tg4 transgenic mice were stimulated with 1µm^{Mid} or 1µm^{Hi} MNPs, for 72hrs after being subjected to +/- 1hour magnetic force (MF). Cytokine production was assessed by intracellular cytokine staining (ICCS) as described in 2.8.2. Application of 1hour MF showed no effect on production of either IFNγ or IL-2. Bar graphs show mean ± SD from at least 4 independent experiments.

3.10 Discussion

3.10.1 Force Application for T Cell Activation

Previous work investigating mechanosensory behaviour by the TCR has focussed on specialised single cell experimental systems, applying force to TCRs on a single cell basis most commonly making use of optical traps and biomembrane force probes (BFP) whilst monitoring calcium signalling as an output. While mechanistically revealing, this work has failed to address whether force application to the TCR influences functional TCR signalling beyond calcium influxes. Calcium influx is one of the very first biochemical events to take place inside a T cell whose TCR has ligated a pMHC molecule. It has been shown previously that calcium influxes in naïve T cells are inherently heterogenous, but broadly can exist in three main states: transient, where calcium signals are initiated but return to baseline within a period of a few minutes, sustained, where signals remain elevated for a long period of time, or oscillatory, where calcium signalling is still observed for a long period of time but oscillates over this time period[281,282]. Given that sustained calcium signalling is known to be

required for robust T cell activation and that TCR stimulation strength can control the rate of these calcium oscillations[283], it is conceivable that non-productive TCR interactions between TCR and pMHC may induce transient calcium influxes that do not reach the threshold required for T cell activation (fig 3.26). Of course, this may be a product of the lifetime of these TCR-pMHC interactions, which may itself be controlled by force dynamics as proposed by the catch-bond vs slip-bond model from Evavold and colleagues[196,197,199,284]. However, whether force induced TCR triggering as observed in optical trap experiments[183,188] reaches the threshold required for T cell activation remains to be investigated.

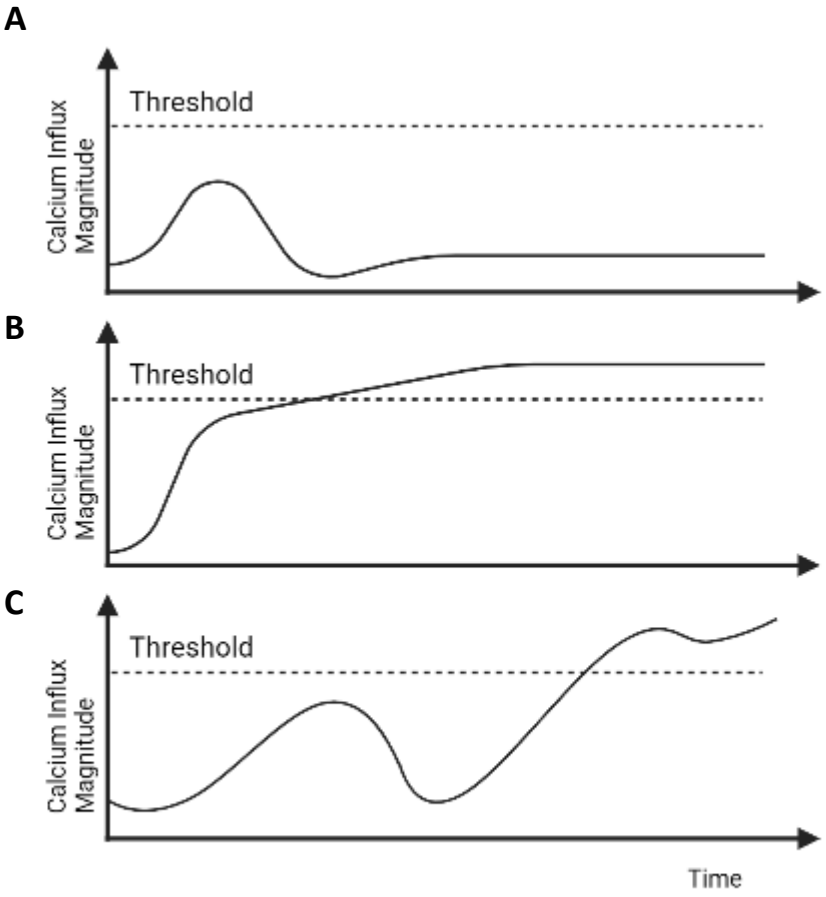


Figure 3.26 – Calcium Signals Induced Downstream of the TCR. TCR specific calcium signals have been shown to exist in transient (A), sustained (B) or oscillatory (C) states. These variations in TCR biochemical signalling imply that initial TCR triggers must reach a given threshold for signalling cascade progression and subsequent T cell activation. Image created in BioRender.

Here, we present evidence that force application to the TCR using antibody coated MNPs specifically induces TCR signalling, evidenced by the lack of response to particles functionalised with off-target antibodies targeting cell surface receptors not involved in propagating a $CD4^+$ TCR signal (MHC-I, figures 3.4 and 3.9 for 250nm and 1µm MNPs respectively). Blockade of signalling responses with the Src kinase inhibitor PP2 further proves that signalling responses induced by anti-CD3 or anti-CD3:CD28 coated particles are the consequence of TCR triggering (fig 3.27).

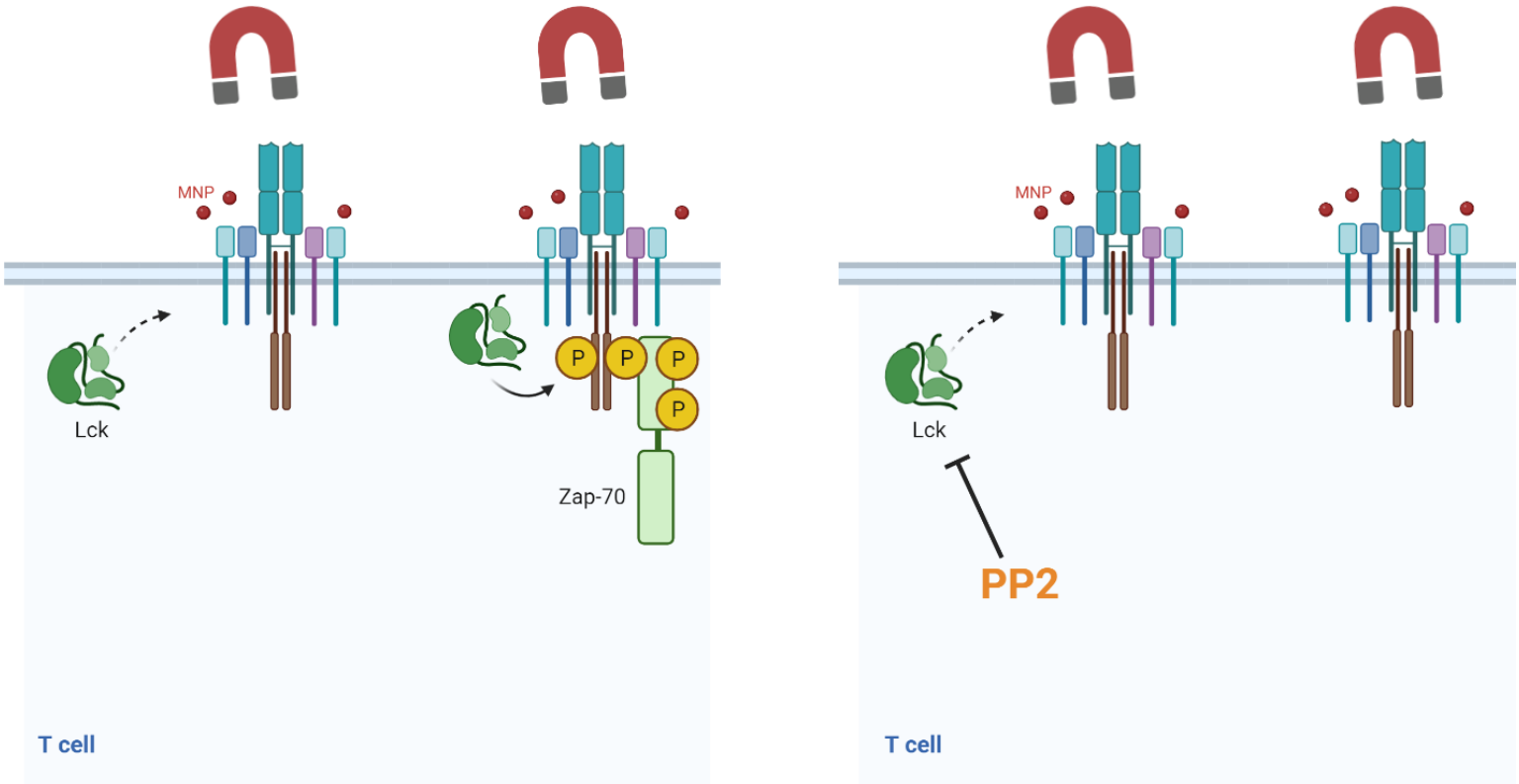


Figure 3.27 – Src kinase inhibition proves TCR signalling responses to functionalised MNPs are TCR specific. As shown in 3.7, effects of magnetic force (MF) on T cell activation are driven through TCR signalling. Use of PP2 to block Src kinases such as Lck thus inhibiting TCR-CD3 phosphorylation prevents MF induced $CD4^+$ T cell activation. Image created in BioRender.

Force application with our MNP protocol, achieved using the MICA instrument described in section 2.7, allows for force application to MNP-labelled TCRs potentially in multiple different modes. For instance, as described in figure 2.1, it is possible that labelled TCRs on any given CD4+ T cells may be pushed into, pulled perpendicular to, or pulled along the cell membrane.Given the dynamic nature of the T cell – APC interaction, whereby the TCR is constantly pushing and pulling against pMHC molecules[252], and given that these cells are crawling along one another subjecting proteins and receptors at the engaged membranes to shear forces[267], it is conceivable that force application with the MICA instrument represents force applications in modes that closely represent those that can occur naturally.

Importantly, we find that magnetic force application is able to influence distal TCR signalling pathway events (Nr4a3, CD69 and CD25 expression) and can also impact $CD4^+$ T cell functionality as measured by cell proliferation and cytokine production. In our approach we have mainly focussed on anti-CD3 coated magnetic particles and have achieved varied signal 1 strengths by titrating the level of CD3 on the surface of these particles. However, given its importance in achieving robust T cell activation we have also assessed the impact of force application through the costimulatory CD28 molecule. It has previously been shown that interpretation of mechanical cues in T cells is more associated with the CD3 molecule rather than CD28[193]. In these studies, $CD4^+$ T cells cultured on polyacrylamide gels tagged with anti-CD3 and anti-CD28 antibodies showed that variation of the rigidity of the gel over a range of 0-200kPa affected IL-2 secretion, where increased secretion correlated with an increase in gel rigidity, peaking at 100kPa after which point secretion began to marginally reduce. Repeating these experiments with gels tagged only with anti-CD3 (where anti-CD28 stimulation was provided by anti-CD28 antibodies tethered to 4µm polystyrene beads) reproduced the rigidity dependent effects on IL-2 secretion. However, when applying the

same logic but reversing this strategy (gel tagged anti-CD28, polystyrene bead tagged anti-CD3) no effect of IL-2 secretion was observed. Therefore, the authors concluded that interpretation of mechanical cues by $CD4^+$ T cells is associated more closely with CD3 signalling than that of CD28[193].

In order to validate this in our protocol, we utilised 250nm MNPs and functionalised these with either CD3 alone, or equal amounts of anti-CD3 and anti-CD28 (CD3:CD28). This allowed us to ask if CD28 signalling is involved in interpretation of mechanical stimuli in our system, where CD3:CD28 co-coated MNPs produced highly similar magnitudes of Nr4a3, CD69 and CD25 expression in response to 1 hour magnetic force than CD3 alone MNPs where the culture medium was supplemented with soluble CD28 (i.e., conditions where CD28 stimulation was provided in a force independent manner). These results are in line with the previous findings[193] and suggest that CD28 signalling is not involved in force sensing by $CD4^+$ T cells. This conclusion is also affirmed when measuring cell proliferation, as force application achieves similar levels of upregulation of cell proliferation in both CD3:CD28 and CD3 + soluble CD28 conditions.

However, we did observe a disparity between these two conditions when measuring IFNγ production, where force application to CD3:CD28 co-coated particles induces a large upregulation in IFNγ production, an effect which is not observed in CD3 MNPs + soluble CD28. The reason for this disparity is somewhat unclear but may arise from a number of factors. Firstly, this may be a concentration dependent effect. Whilst it is known how much anti-CD28 antibody is given to the 250nm MNPs during functionalisation, and whilst the concentration of particles delivered to the $CD4^+$ T cells is also known, several difficult to measure variables still exist in this protocol that may affect the resultant strength of co-

stimulatory signal in these conditions. These include the functionalisation efficiency of antibody onto particle, and the number of particles any given cell may bind. Therefore, there may be a difference in co-stimulatory signal strength between the CD3:CD28 and CD3 + soluble CD28 conditions that may give rise to this discrepancy. Further experimentation would be required to test this, where CD28 levels (both bead bound and soluble) should be titrated to assess this.

Additionally, antibody binding kinetics such as dissociation rates for various receptors are known to be different when measured in 2D and 3D systems. This is unsurprising when considering that in a cell-cell interaction, protein-protein interactions within this will be governed in 2D due to limitations imposed by the cell membranes themselves, and thus are effected by factors including protein density, force on the bond and membrane fluctuations, whilst interactions between cell surface receptors and soluble molecules are free from these factors and are thus governed in 3D[285]. Indeed, 2D dissociation rates between adhesion proteins CD2 and CD58 have been estimated to be approximately 100-fold slower than 3D rates[286]. Other studies are in agreement with this, where lifetimes of the CD2-CD58 bond have been estimated to be two-orders of magnitude longer than the lifetime of the same interaction when measured in 3D[287,288]. Additionally, since this data suggest that CD28 signalling is required for IFNγ production and given that sustained signalling is known to be required to drive cytokine production, it is conceivable that an advantage of the solid support provided by being particle bound may promote more sustained CD28 signalling when compared with soluble CD28 stimulation, thus affecting IFNγ production. With this in mind, it is highly likely that binding of the CD28 antibody to the solid MNP structure will alter these kinetics when compared to delivering CD28 as a soluble antibody and may give rise to the difference between the two groups when measuring IFNγ production. However,

the wealth of evidence when measuring activation marker expression and cell proliferation strongly supports the claim that interpretation of force by T cells occurs through the TCR-CD3 complex, and not the CD28 molecule.

3.10.2 Correlation between TCR engagement and T cell activation

Within this chapter, we have utilised MNPs functionalised with a titrated level of anti-CD3 antibodies. Use of these particles identified a correlation between TCR engagement and T cell activation, summarised in table 3.1. Use of particles functionalised with low levels of antibodies induced low levels of T cell activation, which was then enhanced the presence of force application (figures 3.7 and 3.8 for 250nm and 1µm particles respectively). Interestingly, when levels of antibody functionalisation were increased from approximately 500-1000/µm^2 to approximately 5000/ µm^2, magnetic force application failed to induce an upregulation in observed T cell activation. This data identifies the link between TCR engagement and T cell activation and suggests that force manipulation of the TCR promotes activation when levels of engagement are below the required threshold for T cell activation.

Particle	Antibodies per surface area unit	T cell activation observed in absence of MF	Effect of MF application
1µm^{Hi}	7103/µm^2	↑↑↑↑	↓
250nm^{Hi}	4095/µm^2	↑↑↑	-
1µm^{Mid}	710.3/µm^2	↑↑	↑
250nm^{Mid}	409.5/µm^2	↑	↑
1µm^{Lo}	71.03/µm^2	-	-

Table 4.1 – Correlation between antibodies per surface area unit on the particle surface and T cell activation with magnetic force application. MNPs were functionalised with a titration of anti-CD3, producing levels of antibodies per surface area shown as described in 2.5. Observed T cell activation in response to these MNPs identifies that force application to MNPs functionalised with 500-1000 antibodies per surface area unit induces an upregulation in T cell activation, whilst increased levels of antibody per surface area unit (to approx. 4000 antibodies/µm^2) results in robust T cell activation regardless of force application. Further increase in antibody per surface area unit levels, to approx. 7000 antibodies/µm^2, resulted in an inhibition in T cell activation with force application.

It is estimated that any given T cell can express approximately 10^5 TCRs on its cell surface[289]. Early data has suggested that T cell activation can be achieved through the

recognition of as little as one pMHC molecule on the surface of an APC[290]. However, it is known that any given pMHC molecule is able to engage and trigger multiple TCRs, with some estimates suggesting that as little as 100 pMHC molecules is able to induce the triggering of up to 20,000 TCRs and induce T cell activation[291,292]. Our data reaffirms the correlation between the number of engaged TCRs and subsequent TCR signalling strength and the functional activation response from these interactions, but also proposes that force manipulation of TCRs can contribute to the output of these interactions. Putting this into context with the current models of TCR triggering, this may suggest that force application to the TCR induces a degree of TCR clustering that may contribute to the functional response to force application. This idea is explored in more detail in chapter 4.

3.10.3 TCR Signalling Thresholds for T Cell Activation

Whilst force application shows a clear effect on T cell activation, it is important to establish how this mechanical input is manipulating TCR signalling pathways to modulate T cell activation. Substantial percentages of cells are observed to be expressing Nr4a3, CD69 and CD25 when stimulated with functionalised MNPs alone and no magnet field. However, when subjected to external magnetic force, cells that were not expressing markers of T cell activation are now capable of doing so. Interestingly, we were unable to detect an increase in signalling protein phosphorylation when analysed by flow cytometry. However, both the lack of signalling in response to MNPs functionalised with off target antibodies and the fact that blockade of Src family kinases through use of PP2 prevents observed signalling responses, we can be confident that effects of force application is indeed acting via the TCR signalling pathways. Therefore, the lack of increase in signalling protein phosphorylation detected may reflect low sensitivity within the protocol employed. In addition, we find that force application induces an accumulation of signalling events along the NFAT pathway to

promote robust Nr4a3 expression, suggestive of force induced triggering of T cell activation thresholds across the period of 1 hour, in agreement with other reports[265].

The idea of fixed thresholds for functional T cell responses is not necessarily a new concept. Previously published work has shown that whilst on a population level, stronger TCR signalling correlates with more robust T cell activation in an analogue manner, on a single cell level this behaviour is much more digital and follows more of a switch like trend upon the reaching of a given threshold for T cell activation[273,293,294]. In previous *in vitro* studies utilising fetal thymic organ cultures, inhibition of ZAP-70 activity correlated with a decrease in the number of cells completing positive selection, in a graded analogue manner. However, when using a Nur77-eGFP reporter to assess the levels of integrated TCR signalling in those cells that complete positive selection, cells that had completed positive selection expressed an invariant amount of eGFP irrespective of inhibitor dose. These results indicate that ZAP70 inhibition alters the number of cells reaching a given signalling threshold to complete positive selection but does not alter the threshold itself[273,293]. Additionally, similar threshold related behaviour has been suggested to exist for commitment to T cell proliferation. In these experiments, when assessing T cell proliferation on a population level, the level of proliferation observed correlates well with the titration of both anti-CD3ε stimulation and ZAP-70 inhibition. However, when assessing the level of TCR signalling again utilising a Nur77-eGFP reporter on cells that had committed to cell proliferation, these cells again express a uniformly high level of GFP independent of the level of anti-CD3ε stimulation or ZAP-70 inhibition utilised within the experiment[294].

Therefore, we hypothesize that magnetic force application serves to permit the reaching of this threshold in a population of $CD4^+$ T cells that otherwise do not reach it. To prove this,

experiments blocking accumulation of signalling through the NFAT pathway were performed, where Nr4a3 expression was then monitored as a read out of TCR signalling successfully reaching the nucleus. In these experiments, CsA was added periodically in a pulsatile magnet application protocol to prove that A) over the period of 1 hour accumulation of signalling through the NFAT pathways exists and permits cells to reach the required threshold for Nr4a3 expression and that B) blockade of the NFAT pathway across this hour period prevents further signal accumulation and thus blocks this threshold from being reached. Our experiments conclusively indicate that force application indeed allows for signal accumulation to occur in this manner, and that this accumulation reaches thresholds required for commitment to Nr4a3 expression and cell proliferation.

One remaining question from this chapter is why force application appears to switch effects from positively to negatively impacting T cell activation when signal 1 strength on the surface of the particle is increased? In order to address this question, we hypothesized that perhaps inhibitory signalling pathways downstream of the TCR may play a role in these conditions as a negative feedback mechanism on TCR signalling to prevent over stimulation. We monitored phosphorylation of SHP-1, a tyrosine phosphatase that has been shown to be phosphorylated and activated downstream of TCR ligation and is known to dephosphorylate Lck in a negative feedback mechanism of TCR signalling inhibition[59,62,295]. However, we also observed no differences in SHP-1 phosphorylation when $CD4^+$ T cells were stimulated with $1\mu m^{Mid}$ or $1\mu m^{Hi}$ MNPs both with and without magnetic force treatment. Therefore, this effect cannot be attributed to signal modulation by SHP-1 activity. However, it may be possible that not only do certain thresholds exist for a cell to commit to productive activation, but thresholds beyond this may also exist that once reached, negative signalling pathways/proteins (in this case, other than SHP-1, such as Cbl-b recruitment[70,71] or

activation of other protein phosphatases such as DUSP proteins[48,296,297]) begin to play a role to dampen and control T cell responses. This has previously been shown in the case of the MAPK/ERK pathway, where strong persistent signalling induced via epidermal growth factor (EGF) stimulation in HeLa cells was shown to trigger expression of delayed early genes which in turn repress expression of immediate early genes[298]. Further experimentation would be required to test this in $CD4^+$ T cells, where a similar CsA-inhibition experiment across the pulsatile magnet system may be potentially revealing. If with early CsA mediated pathway inhibition, the negative impacts of magnetic field application to the $1\mu m^{Hi}$ MNPs is blocked, this may suggest that over the period of 1 hour of force application accumulation of TCR signalling is reaching such thresholds that inhibitory mediators begin to play a role to control the TCR signalling response.

3.10.4 Concluding Remarks

This chapter illustrates a robust body of research that demonstrates that force application can modulate T cell activation. We illustrate that force application permits accumulation of TCR signalling to reach set thresholds for T cell activation, evidenced via accumulation of NFAT pathway signalling events required for robust Nr4a3 expression (as illustrated in figure 3.28). Additionally, we have shown that when TCR signal strength is originally low, force application positively influences T cell activation evidenced by upregulation of T cell activation markers, cell proliferation and cytokine production. However, when TCR strength is originally high, force application serves to downregulate activation marker expression and cell proliferation. This illustrates an intriguing platform for

force interpretation by the TCR, where force application through the TCR-CD3 complex can modulate T cell response.

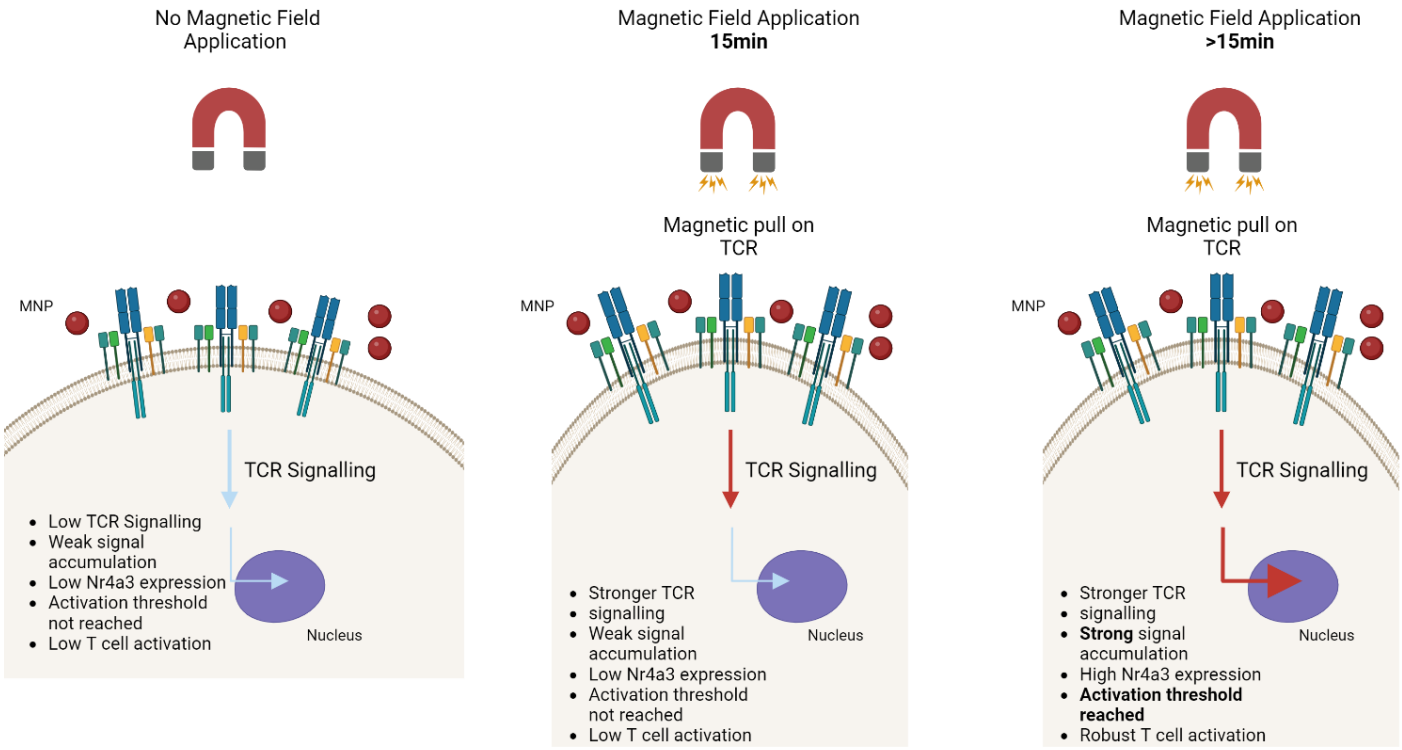


Figure 3.28 – Summary illustration of magnetic force (MF) induced accumulation of signalling intermediates along the TCR-NFAT pathway, which promotes robust T cell activation. In the absence of force application, low levels of TCR signalling is observed resulting in T cell activation thresholds not being triggering. In the event of force application for small time frames (such as 15 minutes), TCR signalling is increased but fails to reach the threshold required for robust T cell activation. When this time frame of force application in increased (for example, up to 1 hour total), signal accumulation along the TCR-NFAT pathway is observed, resulting in the triggering of thresholds required for robust T cell activation.

CHAPTER 4

4 TCR Mobilisation and Clustering – A Potential Mechanism of Action for Magnetic Force Induced TCR Triggering

4.1 Introduction

Previous studies have shown that the TCR protein complex remains relatively mobile throughout the processes of pMHC ligation, initiation of TCR signalling and T cell activation[104,106,109,111]. Indeed, this is implied in the aggregation and serial triggering models of TCR triggering which propose that TCR motility with respect to other TCRs and activating kinases influences TCR signalling[125,130]. The reorganisation of the TCR itself, associated signalling molecules and other cell surface receptors including co-stimulatory (e.g., CD28) and inhibitory (e.g., CTLA-4, PD-1, Tigit) molecules within the developing immune synapse is known to control TCR signalling. As described in 1.6, upon pMHC ligation the TCR moves within the plasma membrane towards the cSMAC controlled by cytoskeletal dynamics which propel the TCR along a flow of actin polymerisation. Signalling molecules are found to be enriched within the pSMAC, which has been suggested to be the site of active TCR signalling, whilst larger inhibitory phosphatases such as CD45 are excluded to the dSMAC on account of their large rigid ectodomains being incompatible with the close approximation of the cell membranes of T cell and APC, mediated by the physical distance over which the TCR-pMHC bond exists (estimated to be 14-15nm[44]).

Whilst originally thought to be the site of active TCR signalling, our understanding of the cSMAC has since evolved to a point where it is now suggested that TCR signalling has already occurred for receptors found in the cSMAC[104,111]. Instead, this region is proposed to serve as a site to mediate TCR-CD3 complex downregulation mediated by molecules such as

Cbl-b, which also localises at the cSMAC and has been shown to ubiquitinylate CD3ζ molecules[69,299,300].

Given its importance in controlling TCR signalling, we set out to monitor TCR dynamics in our magnetic force application system aiming to reveal how magnetic force is influencing TCR signalling. Here, we identify that TCR downregulation occurs in response to force application, and that this occurs concurrently with activation marker expression, where force application induces a clear population of $CD4^+$ T cells that are TCRlo $Nr4a3^+$. Importantly, not only is this response mediated by the actin cytoskeleton, as evidenced by use of the actin polymerisation inhibitor Latrunculin A, but blockade of active TCR signalling using the Src kinase inhibitor PP2 indicates that TCR downregulation is phosphorylation dependent and thus inherently linked to active TCR signalling. These results indicate that force application in our system serves to modulate membrane TCR organisation and promote pseudo-synapse formation, hereby promoting TCR signalling and T cell activation. In line with this, we also show that CD45 exclusion from areas of the membrane where bound particles are found also occurs in settings where T cell activation is readily observed in response to magnetic field. This chapter hence reveals that external magnetic force application to the TCR induces TCR membrane reorganisation and promotes $CD4^+$ T cell activation.

4.2 Force Application Induces TCR Downregulation

4.2.1 TCR Downregulation occurs under the same conditions as force induced TCR triggering

To assess how magnetic force influences TCR dynamics, we first sought to investigate whether force application could induce TCR downregulation, given that this can be

considered the end point of the TCR journey through a developing immune synapse. To this end, 250nm^{Mid} MNPs were functionalised with 2C11, 17A2 or H57-597 antibodies as described (section 2.5) and magnetic force was applied for 15, 30 or 60 minutes as per previous experiments. TCR expression was monitored 4 hours after force application by flow cytometry. Interestingly, figure 4.1 shows that TCR downregulation only occurs under conditions in which T cell activation was readily observed in chapter 3. Force application to 250nm^{Mid} MNPs functionalised with 17A2, or H57-597 antibodies did not induce observable TCR downregulation. However, force application to 250nm^{Mid} MNPs functionalised with 2C11 antibodies induced significant TCR downregulation as early as 30 minutes (no magnetic force MFI: 12000, + magnetic force MFI: 9600), but the largest levels of TCR downregulation was observed after force application for 1 hour (no magnetic force MFI: 11400, + magnetic force MFI: 7600).

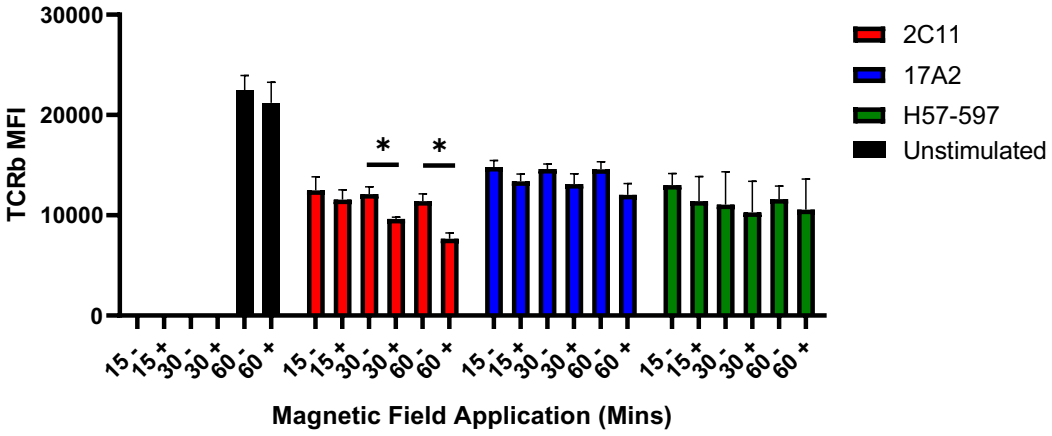


Figure 4.1 – Force induced TCR downregulation occurs under the same conditions with which force induces T cell activation. Force application to 250nm^{Mid} MNPs functionalised with anti-CD3ε clone 145-2C11 induced signficant TCR downregulation at 30 and 60 minutes. Bar graphs show mean ± SD from 2 independent experiments. Statistical analysis assessed by one-way ANOVA with Tukey's post tests. 2C11 30 minutes, * p=0.0196. 2C11 60 minutes, * p=0.0291.

4.2.2 Magnetic force induced TCR downregulation acts through manipulation of the TCR-CD3 complex

Given the force induced effects on TCR expression, we again assessed whether co-stimulatory signalling in this system was able to modulate TCR expression. To investigate this, we treated $CD4^+$ T cells with the same $250nm^{Mid}$ MNP protocol, i.e., particles functionalised with either anti-CD3 alone, both anti-CD3 and CD28 (CD3:CD28) or particles functionalised with CD3 alone alongside stimulation with soluble anti-CD28 (figure 4.2).

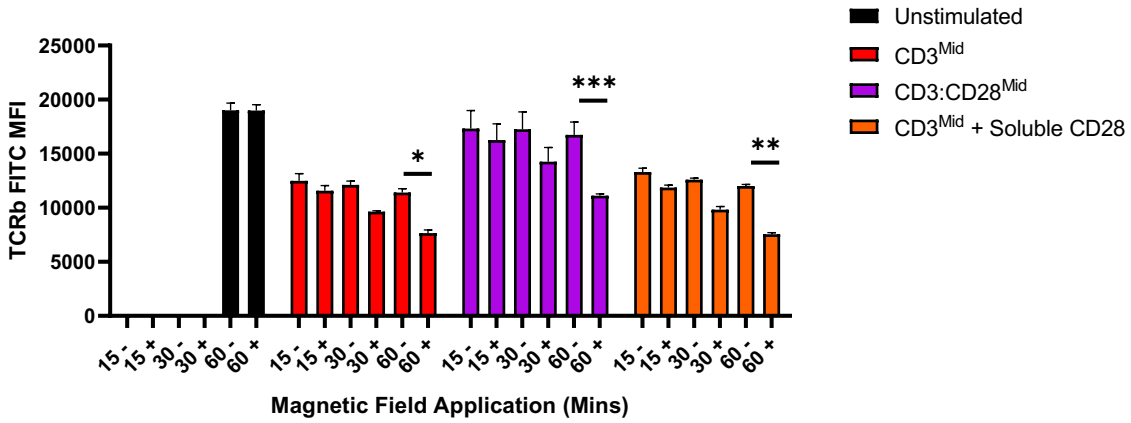


Figure 4.2 – Influence of co-stimulation on TCR downregulation kinetics. Significant TCR downregulation is observed with 60 minutes of force application to $250nm^{Mid}$ MNPs regardless of stimulation with particle bound or soluble CD28. Bar graphs shown mean ± SD from at least 2 independent experiments. Statistical analysis assessed by two-way ANOVA with Tukey's post-tests. 60-minute time points; CD3 alone * p=0.0256, CD3:CD28 *** p=0.0002, CD3 + soluble CD28 ** p=0.0042. Unstimulated controls not tested with 15 or 30 minutes of force application.

These experiments identified that force application for 60 minutes was again able to induce significant TCR downregulation across all 250nm MNPs treatments tested. Importantly, and as was the case for force induced activation marker expression, TCR-CD3 stimulation was found to be the driving factor behind force induced TCR downregulation. When comparing MFIs for the 60 minute time points for CD3 alone or CD3 + soluble CD28, very little difference was observed (no magnetic force MFI: 11400, 12000, + magnetic force MFI: 7600, 7500 for CD3 alone and CD3 + soluble CD28 respectively), indicating that

stimulation with soluble CD28 had no effect on TCR expression. However, whilst still downregulated with 60 minutes force application, CD3:28 particles had a higher level of TCR expression (no magnetic force MFI: 16000, + magnetic force MFI: 11000). This result can likely be attributed to competition of binding by the capture antibody from CD28 antibodies in the functionalisation process since both the CD3 and CD28 antibodies utilised are Hamster IgG clones. Therefore, co-coating particles with CD28 at the same time as CD3 antibodies may result in less CD3 binding, giving rise to the discrepancy in TCR expression. This of course was not the case when measuring activation events in chapter 3. However, this is perhaps unsurprising given the potent effects of co-stimulation on amplifying TCR stimulation pathways.

Interestingly, whilst not statistically significant when analysing TCR downregulation by MFI, it was observed that TCR downregulation appears to precede the onset of detectable magnetic force induced Nr4a3 expression. Figures 4.1 and 4.2 show that in conditions where magnetic force induces T cell activation at 1hour (2C11 CD3 alone in figure 4.1, and all 60 minute timepoints in figure 4.2), force application not only induces significant TCR downregulation at the 60 minute time point, but also appears to induce a downregulation as early as 30 minutes which does not reach significance. To address this further, the same experiments were analysed for TCR expression on a single cell level, looking for percentages of cells that become TCRlo in response to magnetic force application, 4 hours after force application. This analysis shows that TCR downregulation appears to accumulate across the time course, reaching a maximum with 60 minutes of force application (figure 4.3).

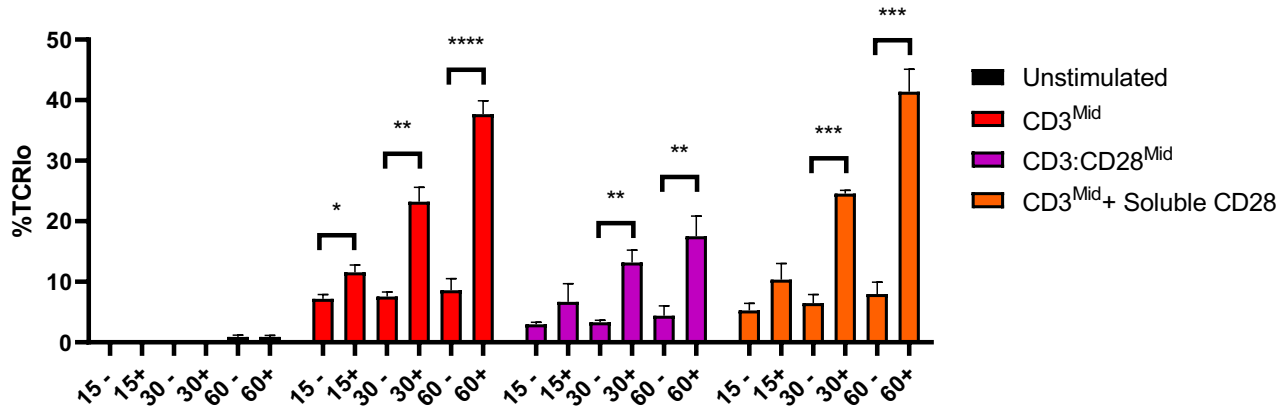
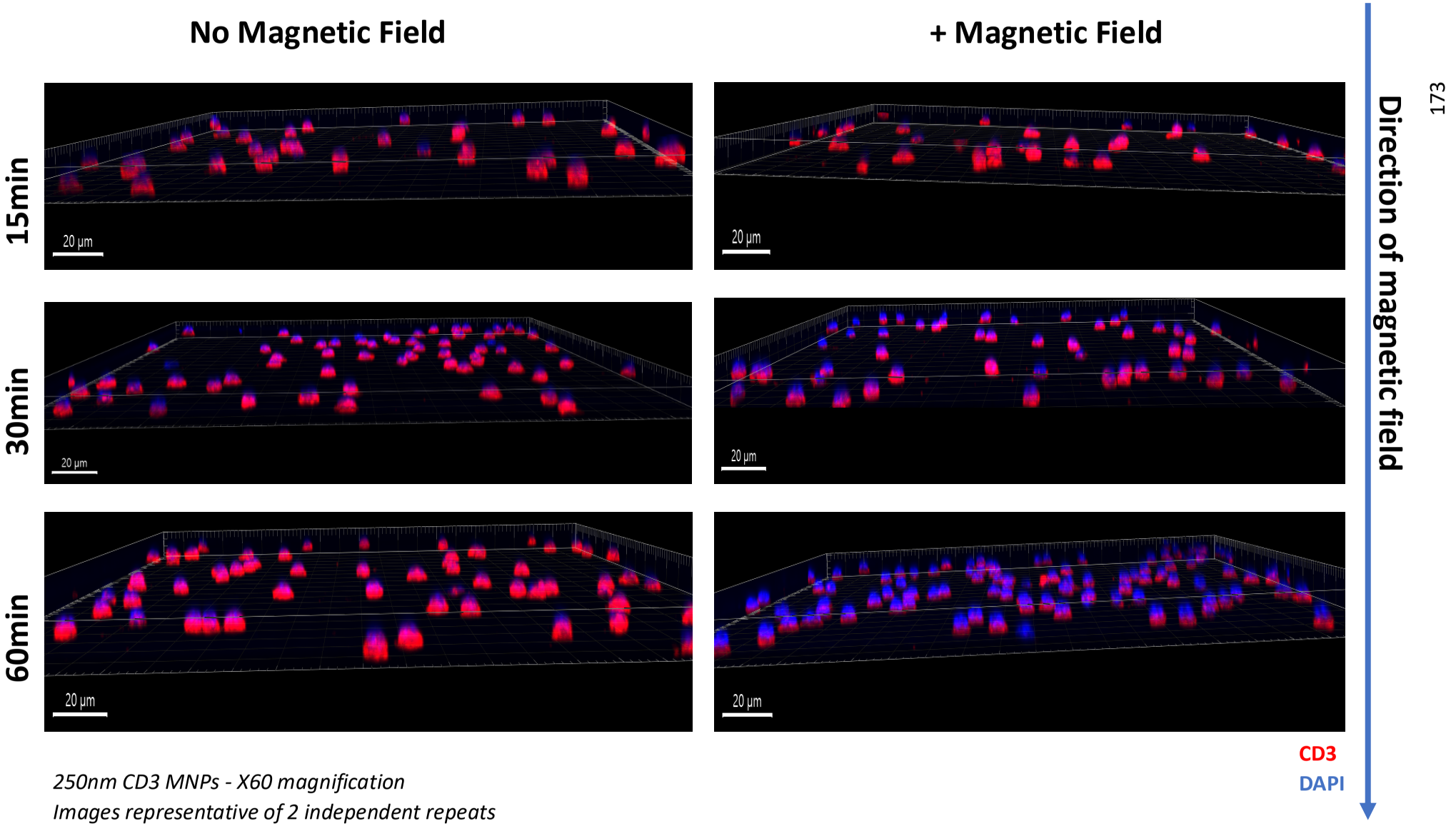


Figure 4.3 - TCR downregulation accumulates over the time course of magnetic force application reaching a maximum at 1 hour of force application. $CD4^+$ T cells from Nr4a3-FT mice were stimulated with functionalised $250nm^{Mid}$ MNPs as shown, and subjected to magnetic force for 15, 30 or 60 minutes. Unstimulated controls were subjected to magnetic force for 60 minutes only. Bar graphs display mean ± SD from at least 2 independent experiments. Statistical analysis assessed by two-way ANOVA with Tukey's post-tests. CD3: * p=0.0116, ** p=0.0024, **** p<0.0001. CD3:28: 30 minutes ** p=0.0096, 60 minutes ** p=0.0098. CD3 + soluble CD28: 30 minutes *** p=0.0002, 60 minutes *** p=0.0002.

4.2.3 TCR downregulation occurs in a magnetic force directional manner

Given that robust, reproducible TCR downregulation was readily observed with 1 hour of magnetic force application, it became apparent that perhaps over the course of this 1 hour time period, the dynamics of the TCR membrane organisation may be controlling T cell activation in response to magnetic force treatment. To this end, we aimed to investigate the membrane distribution of the TCR-CD3 complex over time with magnetic force application. $CD4^+$ T cells isolated from Tg4 mice were treated with $250nm^{Mid}$ anti-CD3 functionalised MNPs, as previously described, and magnetic force was applied for 15 or 60 minutes. After magnetic force treatment, cells were immediately fixed and stained for surface CD3 together with counterstaining for DAPI (see section 2.10.1), before analysing TCR-CD3 distribution by confocal microscopy (see section 2.10.2). Representative images from these experiments are shown in figure 4.4.



250nm CD3 MNPs - X60 magnification
Images representative of 2 independent repeats

Figure 4.4 - Membrane distribution of TCR-CD3 complex with magnetic force treatment. Purified $CD4^+$ T cells from Tg4 mice were treated with $250nm^{Mid}$ anti-CD3 functionalised MNPs as previously described and subjected to 15 or 60 minutes of magnetic force treatment, before immediate fixation and staining for surface CD3. Dramatic decreases in CD3 fluorescence were observed, which appeared to occur in a manner toward the direction of magnetic force application. Images representative of 2 independent experimental repeats.

It should be noted that in the representative z-stacks shown in figure 4.4, magnetic force application in these images is applied directionally as indicated. This is achieved through the use of the MICA system described earlier (see section 2.7), which acts as an oscillating magnet underneath the tissue culture plate. Therefore, magnetic force application by MICA is unidirectional, and TCR-CD3 downregulation occurs towards the direction of magnetic force application. This is evidenced by an accumulation of CD3 (red fluorescence, figure 4.4) at the base of the cell, consistent with the direction of force application.

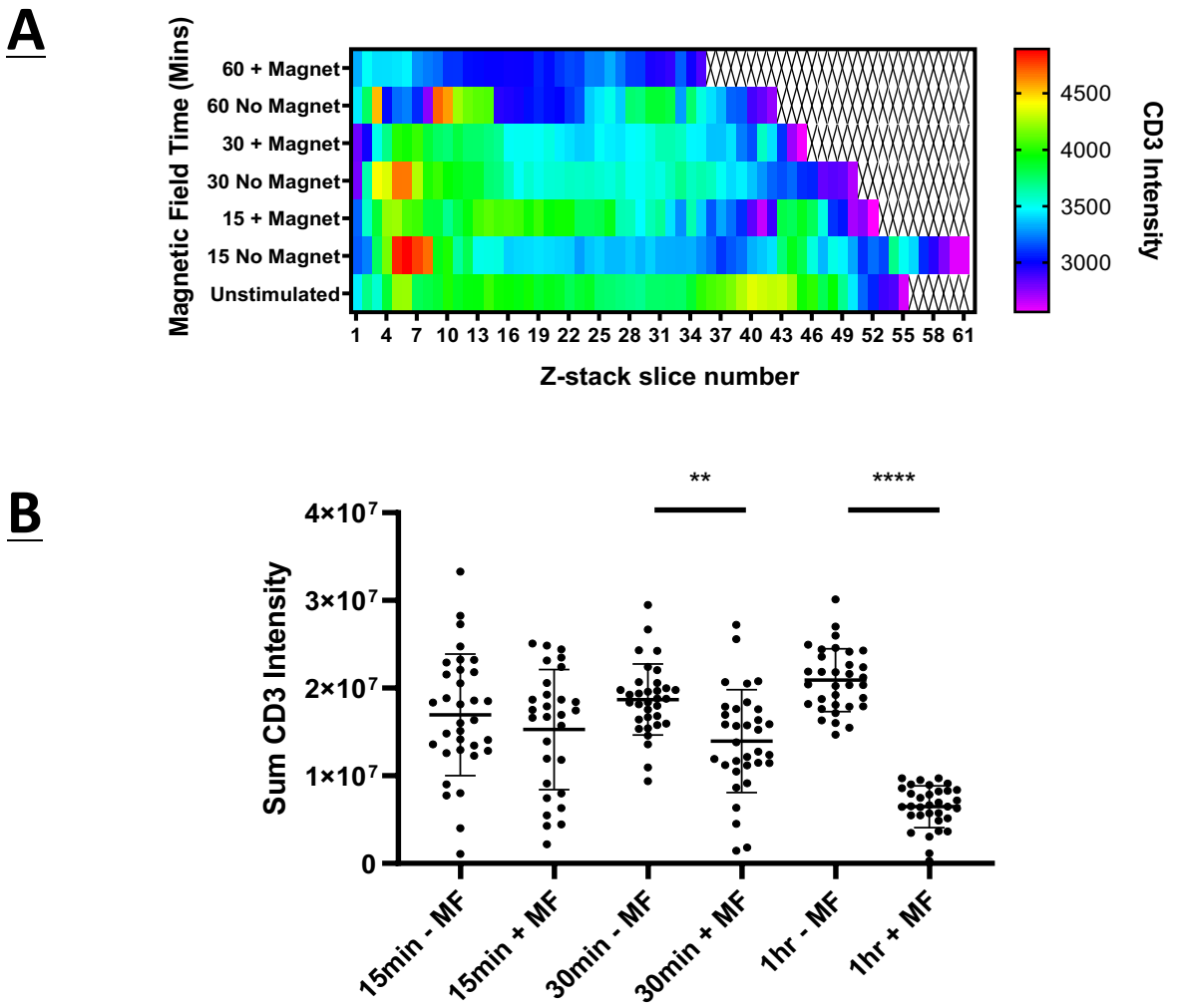


Figure 4.5 – TCR-CD3 downregulation occurs in a magnetic field dependent directional manner (A) and accumulates across the time course of force application (B). Surface CD3 expression as determined by confocal microscopy shown in 4.4 was analysed for intensity per z stack slice (A) and accumulative CD3 intensity (B) to determine both dimensional and global CD3 expression patterns as described in 2.10.2. B) Normalcy of the data was first assessed in Prism v9 before significance was assessed via One-Way ANOVA with Tukey's post-tests. ** p=0.0037, **** p<0.0001.

Clearly, TCR-CD3 downregulation with 1 hour of force application was readily detected by confocal microscopy, as indicated by the striking decrease in red fluorescence in figure 4.4 and the quantification of this in figure 4.5. This observation was not found with 15 minutes of magnetic force application yet began to become apparent at the 30 minute time point (figure 4.5B), in line with the MFI flow cytometry data displayed earlier (figures 4.1, 4.2). Figure 4.5A indicates that TCR-CD3 downregulation is occurring in a magnetic field directional manner by tracking CD3 fluorescence throughout the entire z stack. Lower z stack slice numbers indicate CD3 fluorescence picked up at the base of cell, with increasing z stack numbers indicating the stack moving further up the cell body toward to the top of the cell. Therefore, this data portrays the profile of directional TCR-CD3 migration over the time course of magnetic force application. Additionally, figure 4.5B displays the accumulative sum of CD3 intensity throughout the entire z stack for each condition and, therefore is a similar method of determining global TCR-CD3 expression as measuring TCR MFI by flow cytometry. In this analysis, surface CD3 stained on non-permeabilized cells was found to be significantly downregulated with magnetic force application as early as 30 minutes, reaching a maximum with 60 minutes of force application, in line with the findings reported in figures 4.1 and 4.2.

It should be noted that, given that force application was applied from underneath the cells in figure 4.4, it may be possible that force application for 60 minutes is sufficiently long enough to ‘squash’ the cells tightly against the coverslip given that the cells are loaded with particles in suspension meaning particles on top of the cell volume will be pushing towards the cell under force application. This could conceivably alter the cellular morphology and provide the basis for the loss of CD3 detection in higher z-stack slices as displayed in figure 4.5A. However, if this were the case and alteration of the cellular morphology under force

resulted in a perceived downregulation of the TCR, we would expect to find a loss of CD3 detection in higher z-stack slices, but no effect of force application on overall CD3 intensity on these cells. As shown in figure 4.5B, when measuring the accumulative CD3 intensity throughout the entire z-stack, we find that force application induces a clear loss of surface CD3 staining. Since these findings are also in agreement with independent experiments analysed by flow cytometry (figures 4.1-4.3), we conclude that force application to the TCR induces TCR-CD3 downregulation.

4.2.4 Alteration of signal 1 strength on 1µm MNPs correlates with the degree of TCR downregulation

To this point we have shown that TCR expression is downregulated in response to external magnetic force application with 250nm MNPs in the same conditions by which force application induces TCR signalling and T cell activation. We next sought to address whether this was still true for 1µm MNPs, which provided a differential response to magnetic force application based on levels of CD3 on the particle surface (figure 3.9). Therefore, we treated purified Nr4a3-FT $CD4^+$ T cells with $1\mu m^{Lo}$, $1\mu m^{Mid}$ or $1\mu m^{Hi}$ MNPs and applied magnetic force for 60 minutes before assessing TCR expression levels 4 hours post force application (figure 4.6).

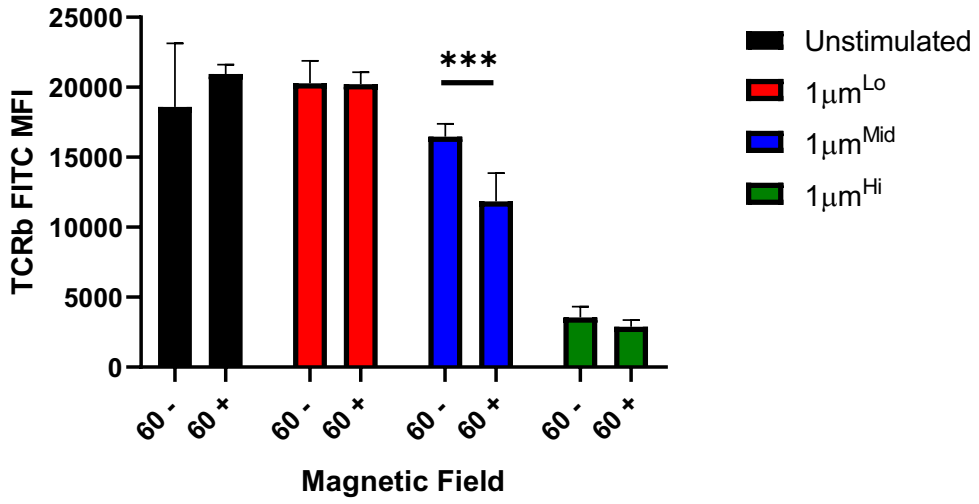


Figure 4.6 - TCR expression in response to force application to anti-CD3 functionalised 1µm MNPs. Force application induced robust TCR downregulation in response to 1µm^{Mid} MNPs, whilst substantial force independent TCR downregulation was observed with 1µm^{Hi} MNPs. Bar graphs show mean ± SD from at least 2 independent experiments. Statistical analysis assessed by two-way ANOVA with Sidak's post-tests, *** p=0.0005.

In line with findings from the 250nm MNP, force application for 60 minutes induced robust TCR-CD3 downregulation in response to 1µm^{Mid} MNPs (figure 4.6, blue bars, no magnetic force MFI: 16000, + magnetic force MFI: 11000). Additionally, we saw a striking downregulation of the TCR in response to 1µm^{Hi} MNPs, independent of magnetic force application (figure 4.6: green bars, figure 4.7). These data indicate a correlation between TCR downregulation and anti-CD3 coated MNP signal 1 strength.

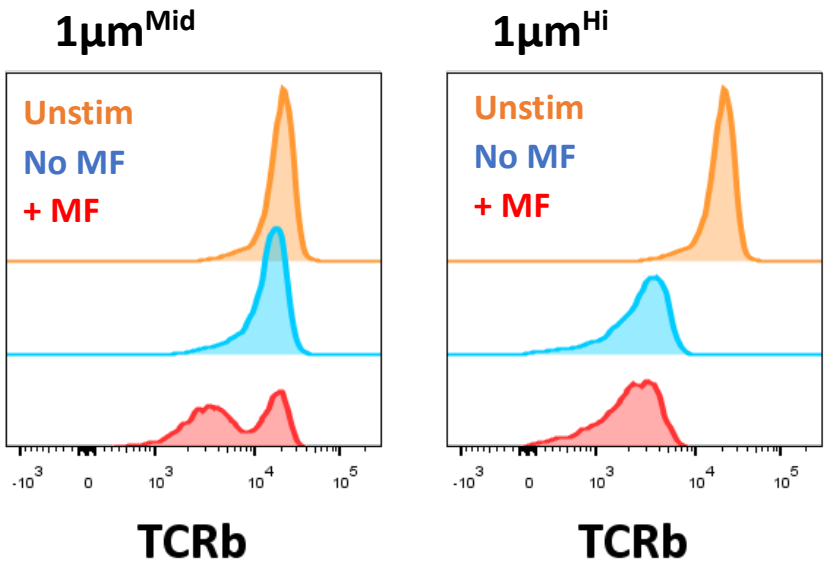


Figure 4.7 - Representative TCR histograms from 1µm MNP experiments. CD4+ T cells purified from Nr4a3-Ft mice were treated with 1µm MNPs functionalised with 1µg or 10µg anti-CD3 antibodies (i.e., $1µm^{Mid}$ or $1µm^{Hi}$ MNPs), prior to force application for 1 hour. TCR expression was assessed 4 hours post force application by flow cytometry. Robust TCR downregulation occurs in response to force application for $1µm^{Mid}$ MNPs functionalised with 1µg CD3 yet is force independent $1µm^{Hi}$ MNPs. Histograms representative of at least 3 independent experimental repeats.

Finally, we investigated if the kinetics of magnetic force induced TCR downregulation in response to $1µm^{Mid}$ MNPs was the same as that for $250nm^{Mid}$ MNPs (figure 4.3). In these experiments, purified $CD4^+$ T cells from Nr4a3-FT mice were treated with $1µm^{Mid}$ MNPs and subjected to magnetic force for 15, 30 or 60 minutes before TCR expression was assessed 4 hours post force application (figure 4.8). Similar results were observed for 1µm MNPs as for 250nm MNPs (figure 4.3), where TCR downregulation appears to accumulate across the time course of force application, reaching a maximum at 60 minutes of force application. Additionally, we also investigated the kinetics of TCR downregulation at additional staining time points (1 hours, 2 hours and 4 hours post force application) on $CD4^+$ T cells stimulated with $1µm^{Mid}$ MNPs stimulated with magnetic force for 15 or 60 minutes. Importantly, we found highest levels of TCR downregulation on $CD4^+$ T cells that were stimulated with 1 hour of magnetic force at the 4 hour staining time point (appendix figure 8.1).

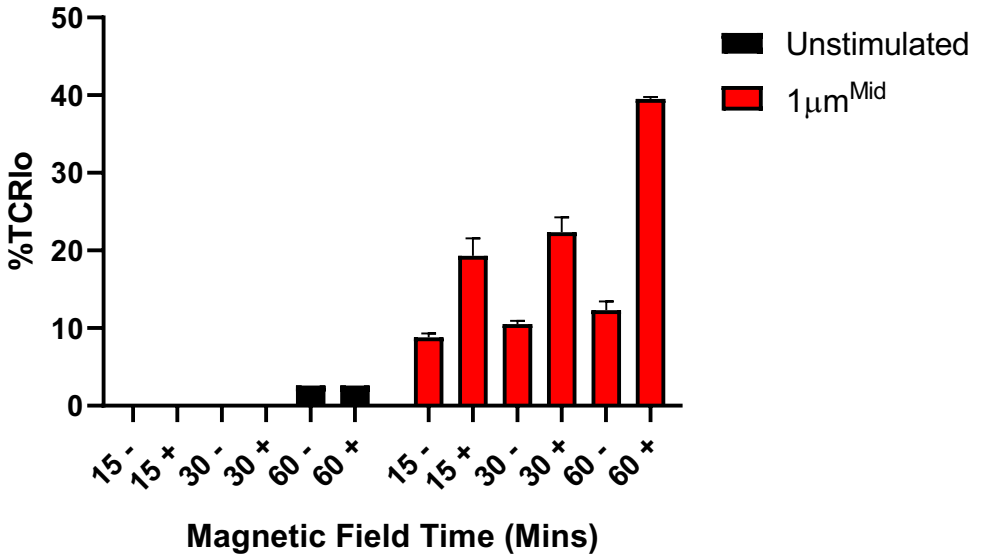


Figure 4.8 – TCR downregulation kinetics in response to 1μm^{Mid} MNPs and force application show that TCR downregulation accumulates across the time course. Bar graphs show mean ± SD from one experiment, representative of 3 independent repeats.

4.3 Cycling TCR Staining Protocols Catch TCR Downregulation in the act

To confirm that these effects on TCR expression were indeed a result of TCR internalisation and downregulation and not a result of particle mediated steric hinderance, a surface vs cycling vs total TCR staining protocol was employed as described in 2.9.5. In brief, cells were stimulated with 250nm^{Mid} or 1μm^{Mid} anti-CD3 MNPs and subjected to +/- magnetic force for 1 hour. To assess levels of cycling TCR, cells were immediately stained with anti-TCRβ antibodies for 2 hours. This allows for the assessment of any surface TCR whilst also staining TCRs that are actively internalised during this 2 hour period. In contrast, surface TCR levels were measured by standard surface staining for 25 minutes after this 2 hour period. Finally, total TCR levels were detected by first surface staining as described, before cell fixation, permeabilization and subsequent intracellular TCR staining to stain for

all TCRs. Gating strategies for this analysis are shown in figures 4.9 and 4.10, for 250nm^{Mid} and 1µm^{Mid} anti-CD3 MNPs respectively.

Cycling TCR staining protocols showed an increase in percentage of cells found in the TCRhi gate for both 250nm^{Mid} and 1µm^{Mid} MNPs (figures 4.9 and 4.10 respectively). This indicates that stained but internalised TCRs in the cycling staining protocol are still detected, and those cells that are internalising their TCRs subsequently show increased stained-TCR fluorescence, providing evidence of directly internalised TCRs. Finally, staining for total TCR expression following cell permeabilization showed that almost all TCRs could then be stained as only 0-5% of cells for 250nm^{Mid} MNP conditions and 0-2% of cells for 1µm^{Mid} MNP conditions remained in the TCRlo gate (250nm: figures 4.9 + 4.11, 1µm: figures 4.10 + 4.12). This analysis, together with the TCR downregulation data shown above provides a solid basis for magnetic force induced TCR downregulation under the same force conditions that induces CD4^{+} T cell activation.

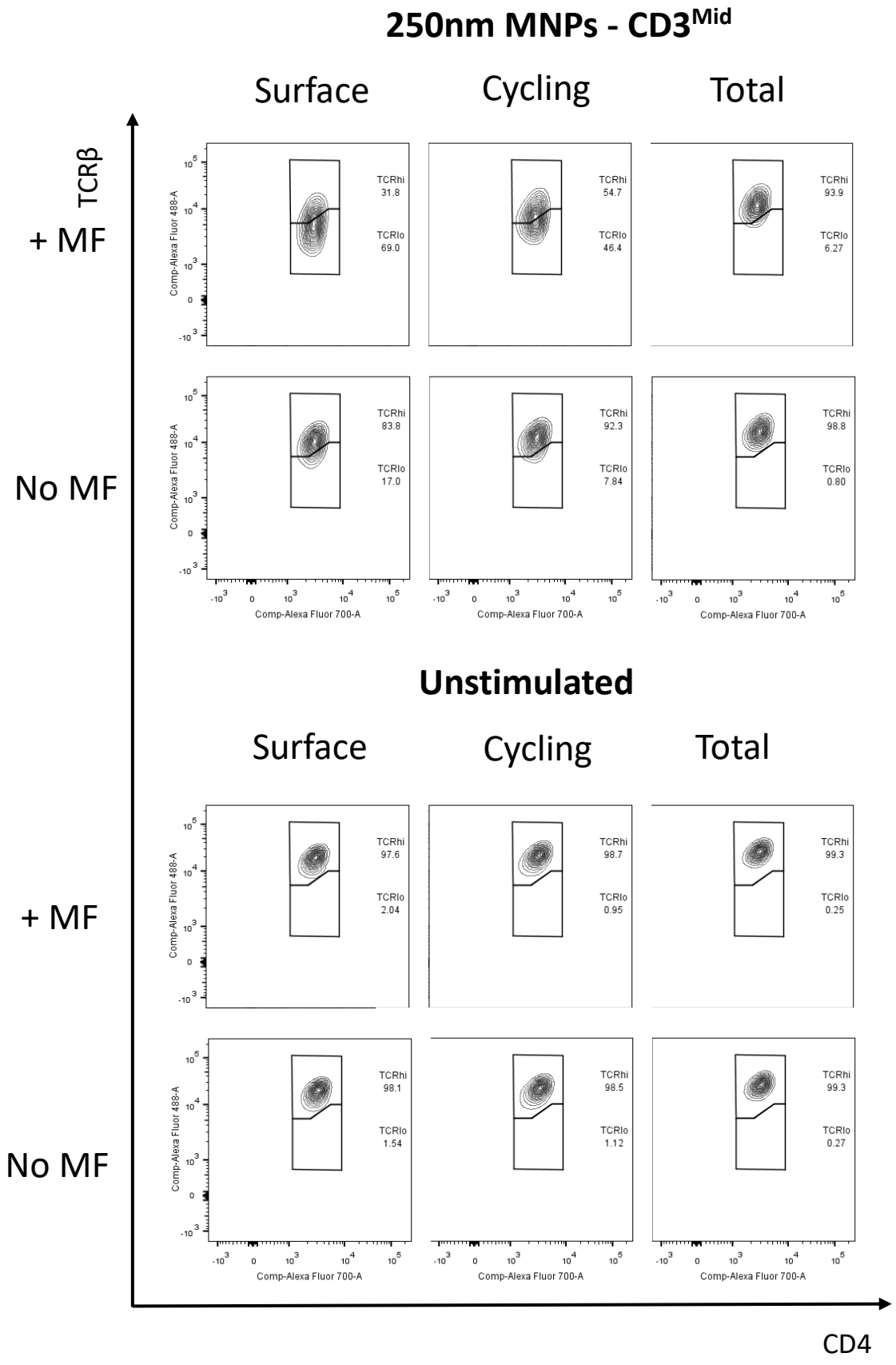


Figure 4.9 - Surface vs Cycling vs Total TCR staining protocols for 250nm MNPs Reveals TCR Internalisation. $CD4^+$ T cells were stimulated with $250nm^{Mid}$ anti-CD3 MNPs and subjected to 60 minutes of magnetic force, before assessment of surface vs cycling vs total TCR expression as per 2.9.5. Cycling TCR staining protocols enable the visualisation of actively internalised TCRs.

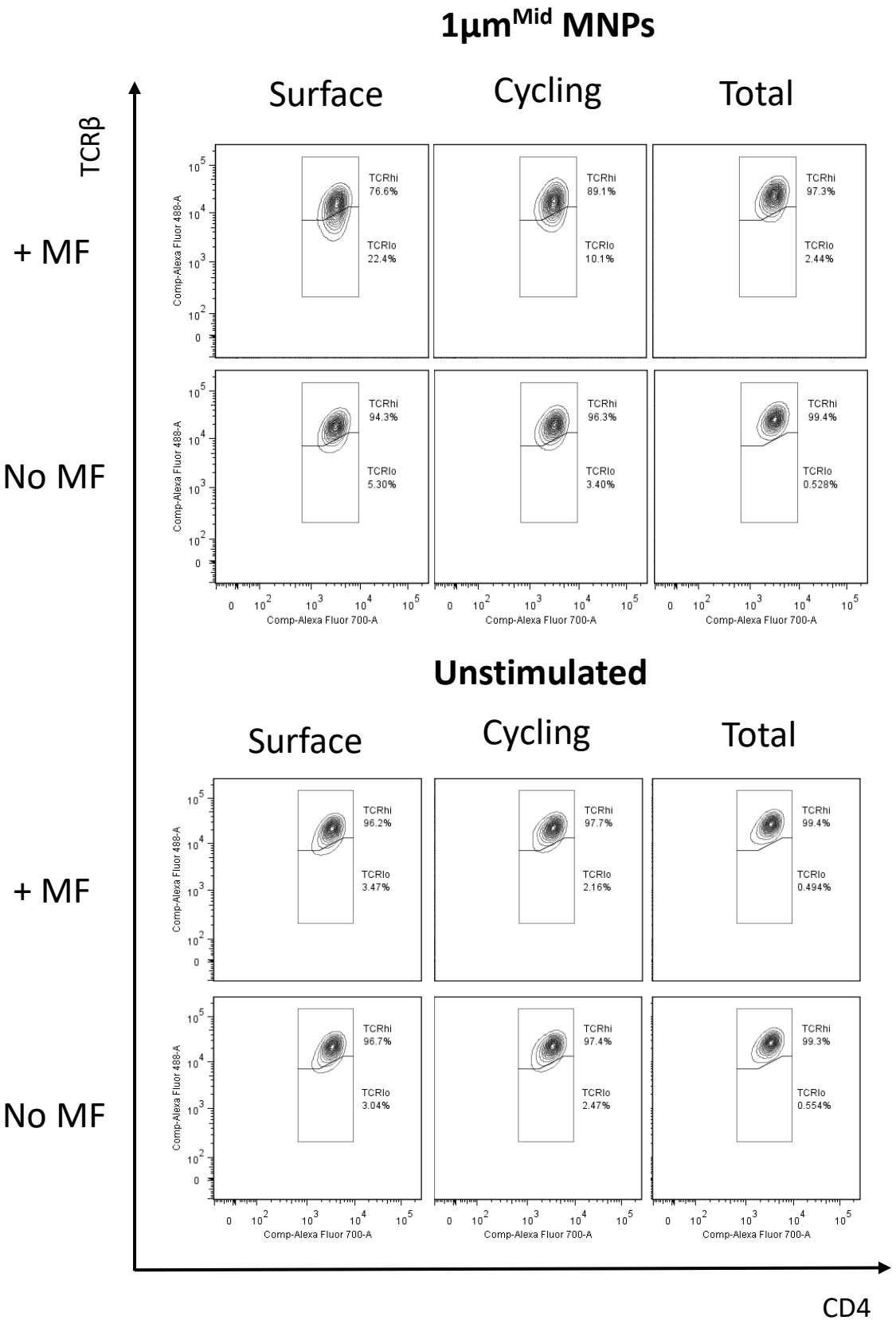


Figure 4.10 – Surface vs Cycling vs Total TCR Expression for 1µm^{Mid} MNP stimulated CD4^{+} T cells. Nr4a3-FT CD4^{+} T cells were stimulated with 1µm^{Mid} MNPs and subjected to +/- 60 minutes magnetic force before assessment of surface vs cycling vs total TCR expression as described in 2.9.5. Cycling TCR staining protocols identify a population of actively internalised TCRs.

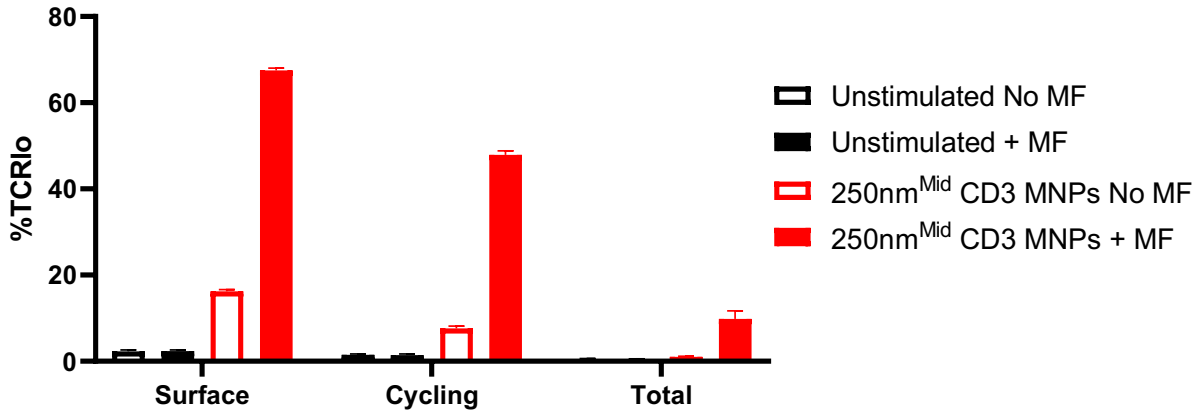


Figure 4.11 - Surface vs Cycling vs Total TCR Analysis for 250nm^{Mid} anti-CD3 MNPs. Force application for 60 minutes induces robust TCR downregulation, which cycling TCR staining protocols identify a population of actively internalised TCRs. TCR staining following cell permeabilization allows for staining of the majority of TCR molecules. Bar graphs show mean ± SD from one experiment, representative of at least 3 independent repeats.

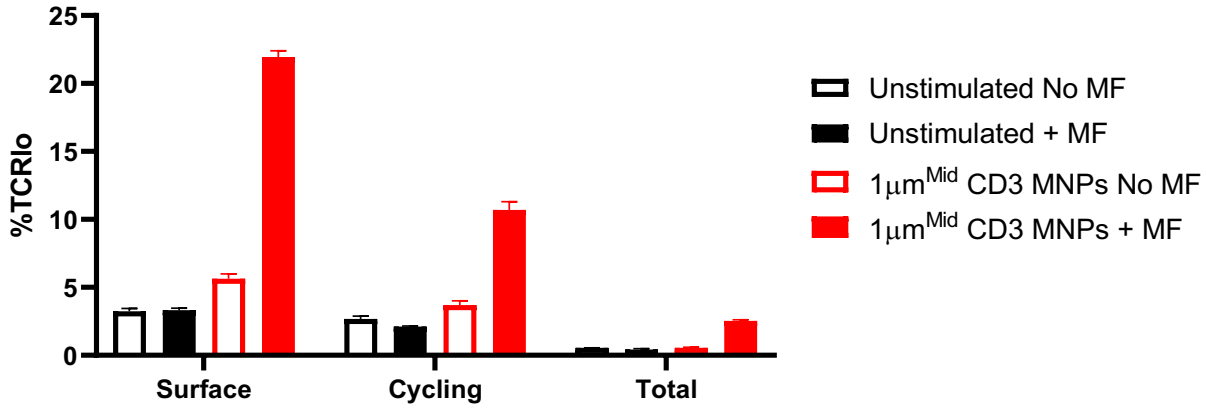


Figure 4.12 - Surface vs Cycling vs Total TCR Analysis for 1μm^{Mid} MNPs. Force application for 60 minutes induces substantial TCR downregulation with cycling TCR staining protocols identifying a population of actively internalised TCRs. Intracellular TCR staining following cell permeabilization allows for staining of the majority of TCR molecules. Bar graphs show mean ± SD from one experiment, representative of at least 3 independent repeats.

4.4 TCR Downregulation Occurs Concurrently with TCR Triggering

4.4.1 TCRhi/TCRlo analyses and expression of TCR signalling markers

To assess whether force induced TCR downregulation and T cell activation are linked, and not mutually exclusive events, we sought to determine whether those cells that downregulate their TCR are those that show evidence of TCR signalling and T cell activation, as measured by Nr4a3 expression. For this analysis, Nr4a3-FT purified $CD4^+$ T cells were treated with $250nm^{Mid}$ MNPs functionalised with anti-CD3 alone, anti-CD3 and CD28, or anti-CD3 particles and soluble CD28 as previously described. Magnetic force was applied for 1 hour, with T cell activation being analysed 4 hours post force application. Cells were stratified based on their TCR expression in TCRhi or TCRlo gates as shown in figures 4.9 and 4.10, before assessing T cell activation based on expression of Nr4a3, CD69 and CD25 by cells within each gate (figure 4.13). Force application induces a clear population of $CD4^+$ T cells that are TCRlo but also express activation markers Nr4a3, CD69 and CD25 (figure 4.13-A). However, force application had no effect on activation marker expression on cells that remain TCRhi (figure 4.13-B), indicating that force application induces TCR downregulation and it is those cells that become TCRlo that display evidence of T cell activation in response to force application.

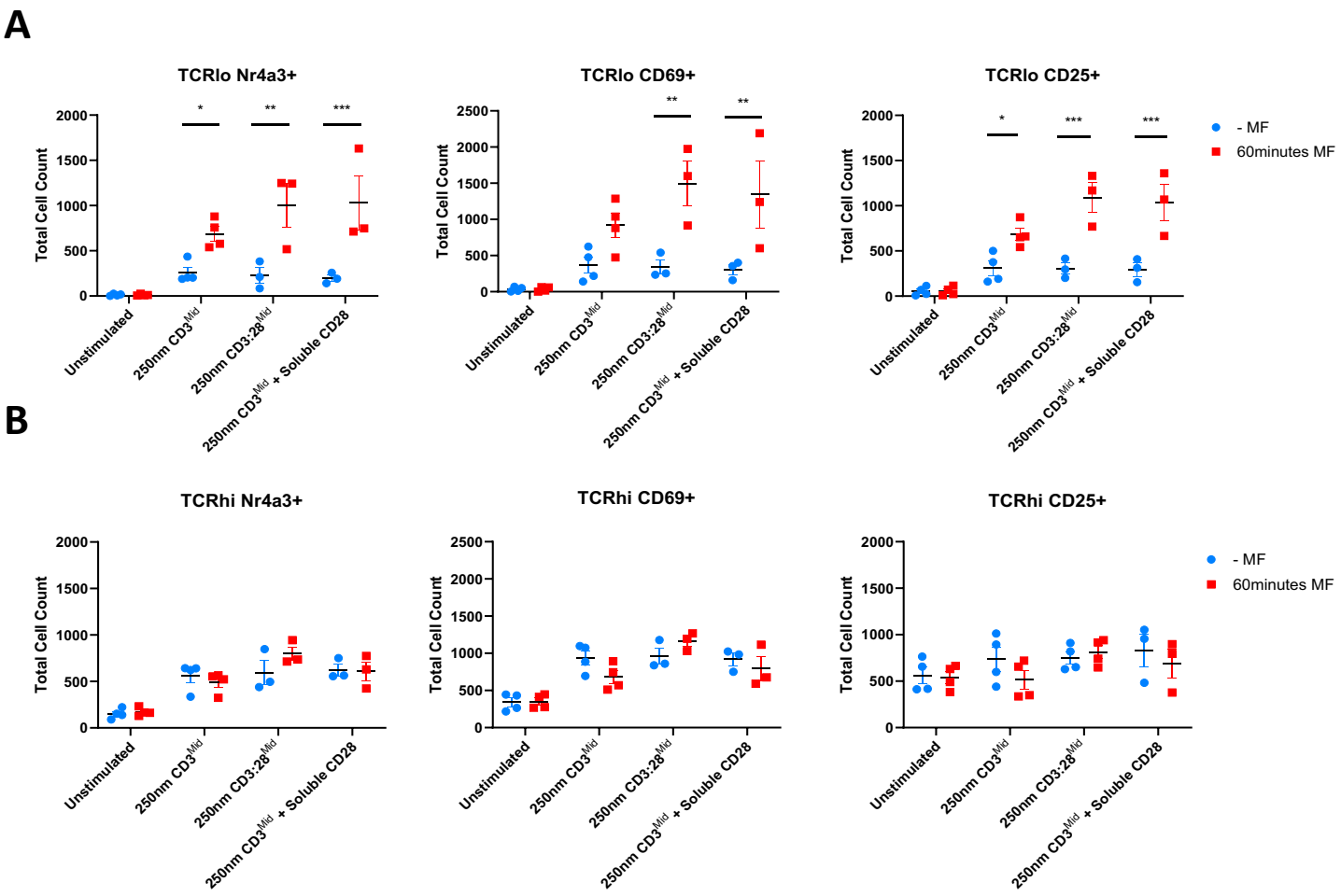


Figure 4.13 - Magnetic Force Induces TCR Downregulation and Activation Marker Expression Concurrently in Response to 250nm MNPs. $CD4^+$ T cells purified from Nr4a3-FT mice were treated with 250nm MNPs functionalised as shown and subjected to 1 hour of force before assessment of TCR downregulation and activation marker expression 4 hours post force application by flow cytometry. Force application induced activation marker expression in TCRlo populations (A) but not in TCRhi population (B). Statistical analysis assessed by two-way ANOVA with Sidak's post-tests. TCRlo panel (A): CD3, Nr4a3 * p=0.0283, CD25 * p=0.0138. CD3:CD28, Nr4a3 ** p=0.0015, CD69 ** p=0.0012, CD25 *** p=0.0002. CD3 + soluble CD28, Nr4a3 *** p=0.0009, CD69 ** p=0.0025, CD25 *** p=0.0003.

Importantly, the relationship between TCR internalisation and activation marker expression existed for both 250nm ^{Mid} MNPs (figure 4.13) and 1µm^{Mid} MNPs. Figure 4.14 indicates that as is the case for 250nm MNPs, force application to 1µm^{Mid} MNPs induces a TCRlo population, which are expressing activation markers Nr4a3, CD69 and CD25 (figure 4.14-A), whilst very little effect of force application is found on activation marker expression within the TCRhi population (figure 4.14-B).

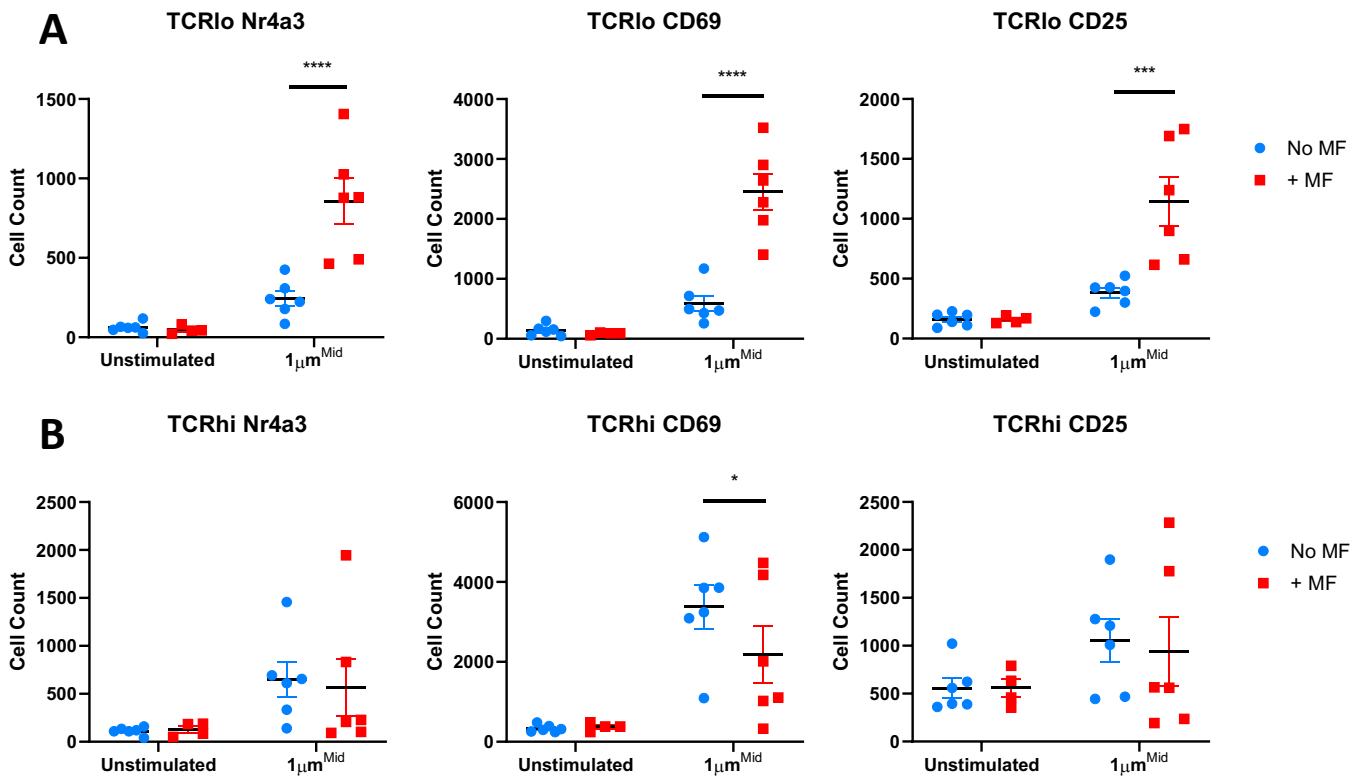


Figure 4.14 - Magnetic force Application Induces TCRlo Nr4a3+, CD69+ and CD25+ cells in Response to 1μm^{Mid} MNPs. CD4^{+} T cells purified from the Nr4a3-FT mouse were treated with 1μm^{Mid} MNPs and subjected to 60 minutes magnetic force as previously described. Analysis of activation marker expression within TCRlo (A) and TCRhi (B) gates revealed that force application induces activation marker preferentially in TCRlo cells. Data shown from 6 independent experiments. Statistical analysis assessed by two-way ANOVA with Sidak's post-tests. TCRlo gating (A): Nr4a3 **** p<0.0001, CD69 **** p<0.0001, CD25 *** p=0.0009. TCRhi gating (B): CD69 * p=0.0109.

This relationship between TCR downregulation and activation marker expression sheds light on how magnetic force application to the TCR can influence CD4^{+} T cell activation, whereby force application may induce TCR membrane re-organisation and permit sustained TCR signalling, with TCR downregulation being an endpoint readout of this response. Previous work on mechanosensory activity by the TCR has provided evidence that the TCR may function as an anisotropic mechanosensor, where it is able to interpret the directionality of the force it encounters and modulate its biochemical response accordingly[188].

Force application using MICA as described in section 2.7 serves to apply force unidirectionally (normal force, i.e., perpendicular to the tissue culture plate) and we have shown that use of this mode of force application induces TCR-CD3 mobilisation towards the direction of magnetic field (figure 4.4). These TCRs are ultimately downregulated, resulting in a population of TCRlo activation marker positive $CD4^+$ T cells (figures 4.13-4.14). To assess whether shear motion induction of the particle in our magnetic nanoparticle protocol was able to induce the same effect on T cell activation, we designed and built a Halbach array for inducing a shear motion on the particle. Design of the Halbach array including magnetic field profiles is detailed in section 2.11.

In brief, the Halbach array functions as a continually rotating array of fixed magnets, where the rotating magnetic field applies a shear motion to MNPs bound to the cell surface within the array. Design of the Halbach array also permitted the assessment of calcium signalling downstream of the TCR in response to shear force application. It should be noted, however, that this mode of force application is entirely distinct from force application with MICA and that live calcium imaging signalling is not compatible with the MICA instrument. Calcium signalling experiments with the Halbach array are described in appendix section 8.3.

To compare force application with MICA (normal force) and the Halbach array (shear motion), side by side experiments using purified $CD4^+$ T cells from the Nr4a3-FT mouse were utilised to directly compare the effect of 60 minutes of either mode of force application on TCR and Nr4a3 expression as per 2.7 and 2.11 for normal and shear motion respectively. As previously described, force application with MICA to either $250nm^{Mid}$ CD3:CD28 or $1\mu m^{Mid}$ MNPs again induced concurrent TCR downregulation and Nr4a3 expression, resulting in the induction of a TCRlo $Nr4a3^+$ population. However, magnetic field application to these

particles with the Halbach array failed to induce any detectable force induced TCR downregulation or Nr4a3 expression. Therefore, in our protocol, the data suggests that normal force application is able to induce TCR mobilisation and re-organisation to permit TCR signalling yet shear motions of the particle are not. We propose that the continual changing of magnetic field direction in the rotating Halbach array is insufficient to induce TCR mobilisation and re-organisation that is otherwise found when applying constant unidirectional normal force with MICA and as a result does not permit TCR signalling to take place.

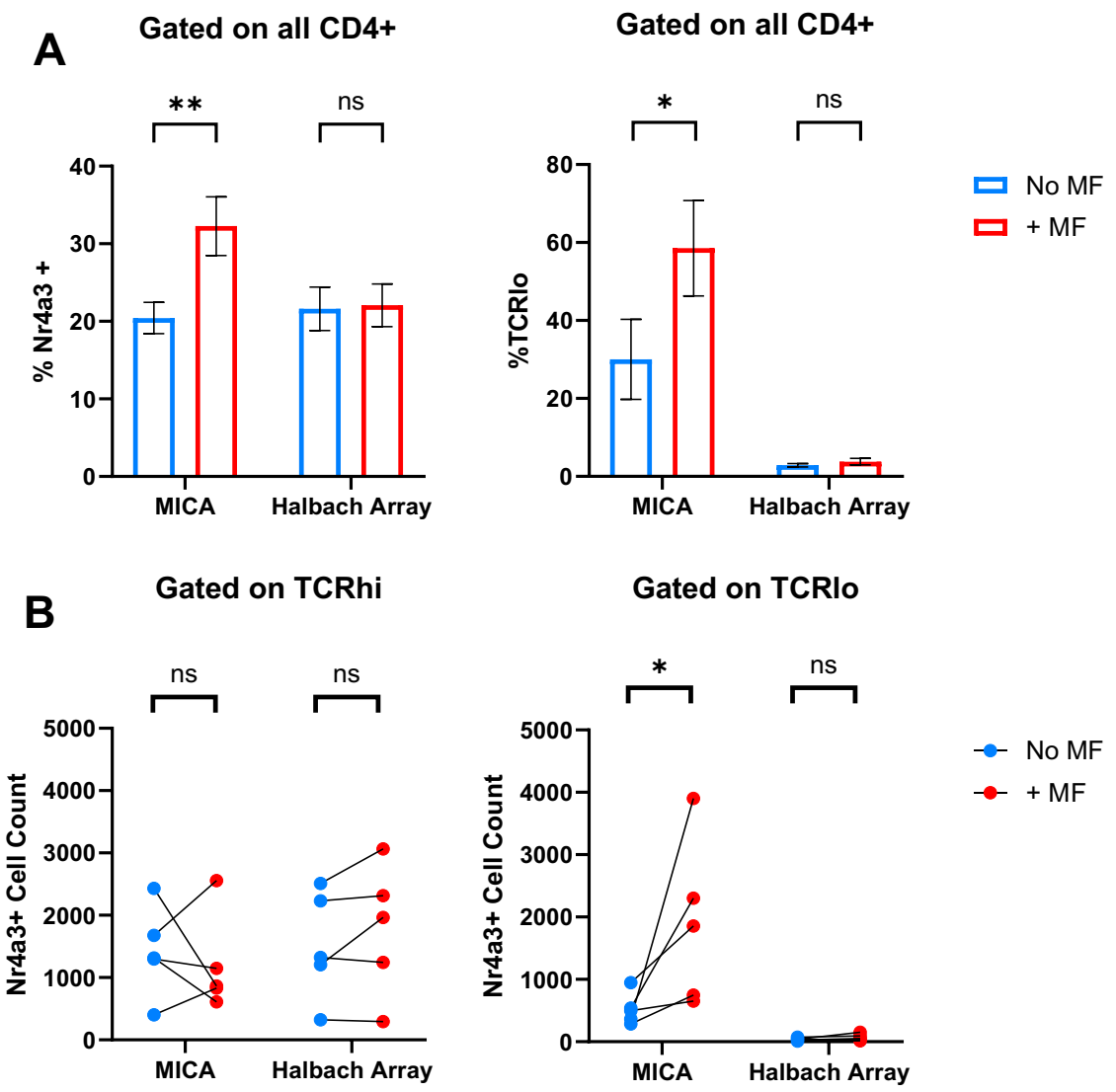


Figure 4.15 – Normal Force Application Induces TCRlo Nr4a3⁺ CD4⁺ Phenotypes – 250nm^{Mid} MNPs. Nr4a3-FT CD4⁺ T cells were treated with 250nm^{Mid} anti-CD3:CD28 MNPs and subjected to 60 minutes of either normal force (MICA, 2.7) or shear force (Halbach array, 2.11), with assessment of TCR and Nr4a3 expression 4 hours post force application by flow cytometry. Only normal force application induces Nr4a3 expression within the TCRlo population. Data shown from 5 independent experiments. Bar graphs in A show mean ± SD from 5 independent experiments, whilst line plots in B connect no MF and + MF conditions from each independent experiment. Statistical analysis assessed via two-way ANVOA with Sidak's post-tests. Panel A: ** p=0.0078, * p=0.0393. Panel B: * p=0.0259.

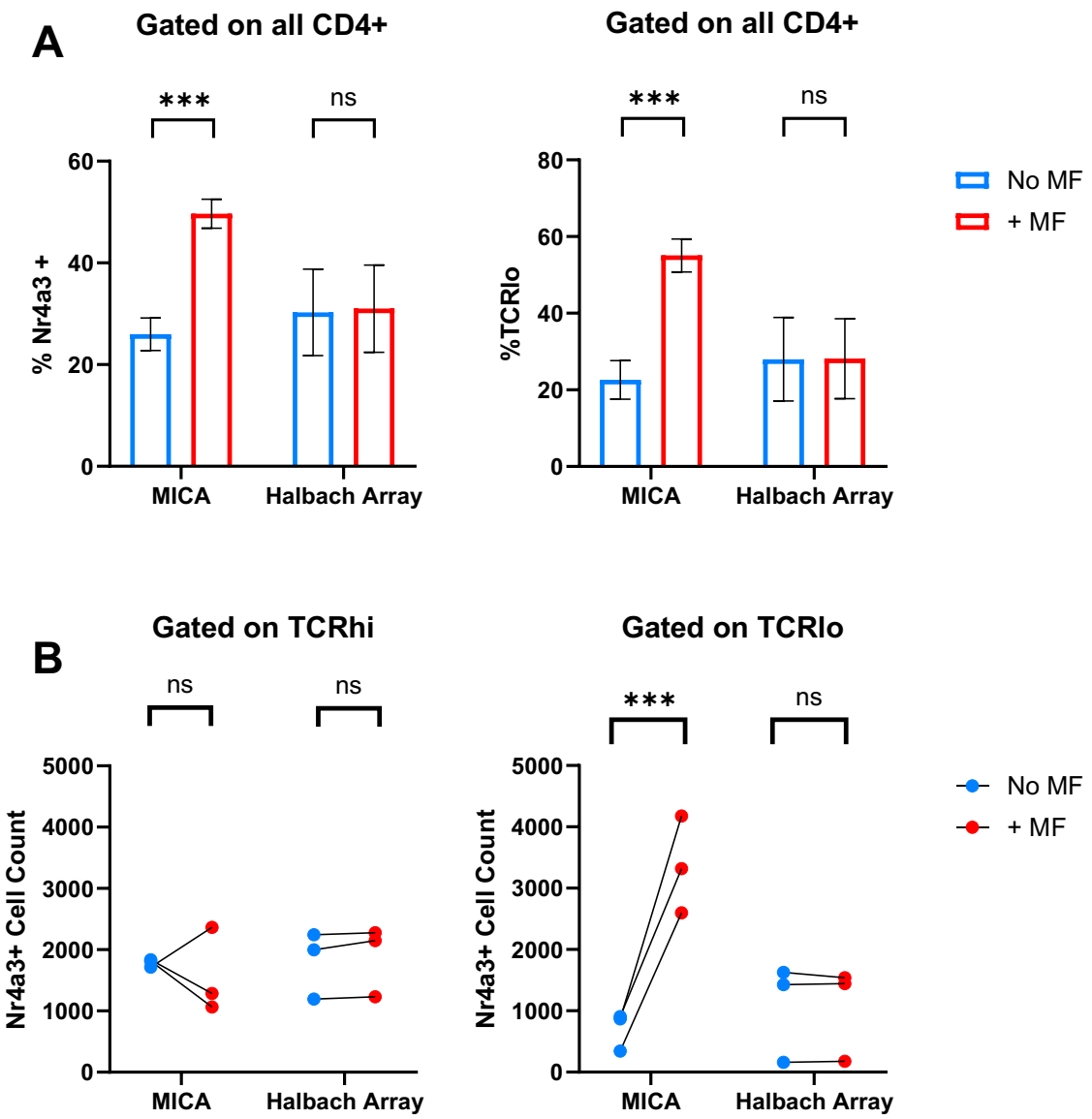
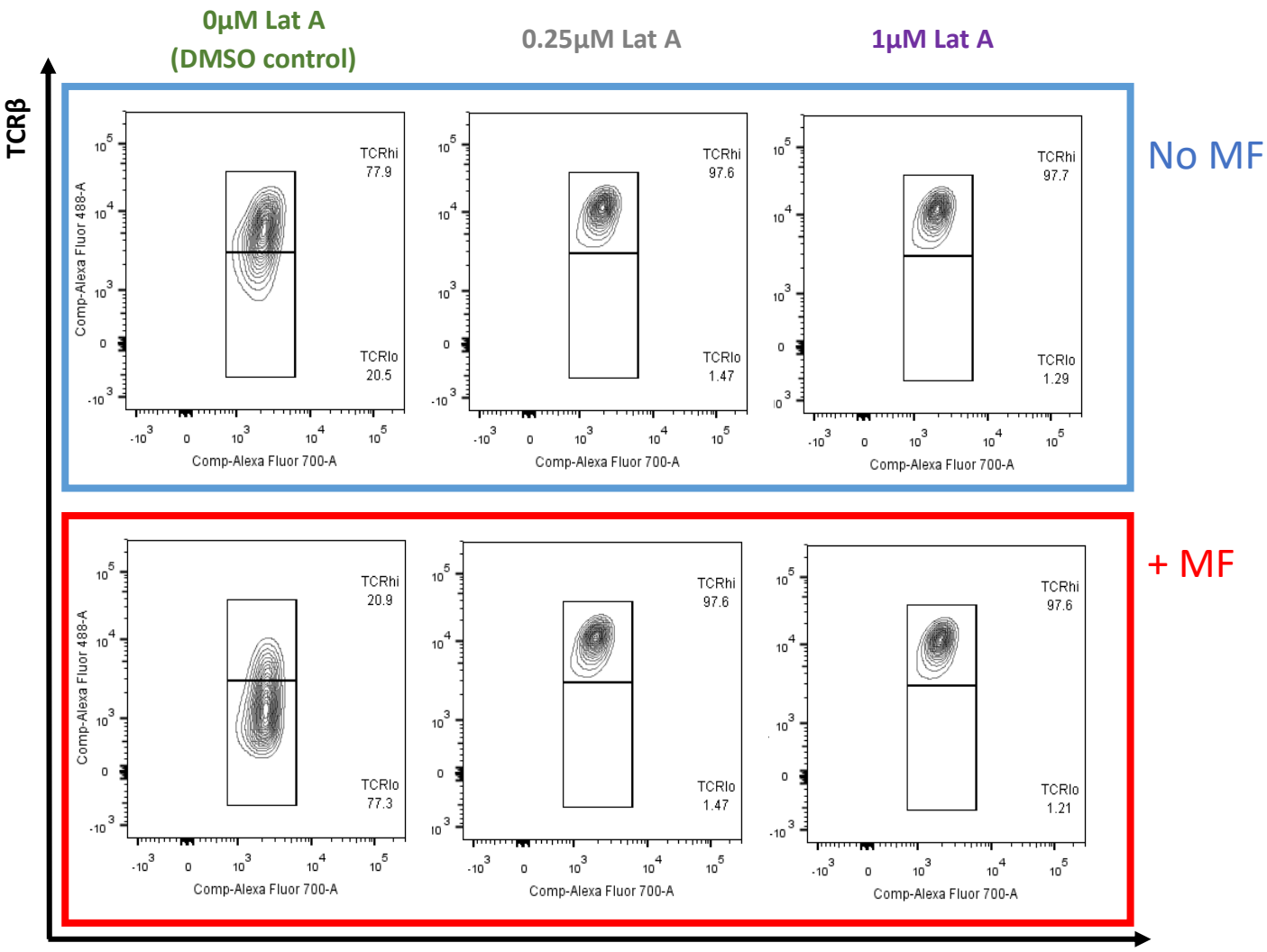


Figure 4.16 – Normal Force Application to 1µm^{Mid} MNPs induces TCRlo Nr4a3^{+} CD4^{+} Phenotypes. Purified CD4^{+} T cells from Nr4a3-FT mice were treated with 1µm^{Mid} MNPs and subjected to 1 hour of normal (MICA, 2.7) or shear (Halbach array, 2.11) force prior to phenotypic assessment by flow cytometry 4 hours later. Force application with MICA induced Nr4a3 expression in the TCRlo population. Data shown from 3 independent experiments. Bar graphs in A represent mean ± SD, whilst line plots in B connect no magnetic force (MF) and + MF from each independent experiment. Statistical significance assessed by two-way ANOVA with Sidak's post-tests. Panel A, %Nr4a3 *** p=0.0004, %TCRlo *** p<0.0001. Panel B *** p=0.0007.

4.5 Cytoskeletal Dynamics Control TCR Downregulation

Data to this point indicate that force application to magnetic nanoparticles functionalised to target the TCR-CD3 is able to modulate membrane organisation of TCRs ultimately resulting in their downregulation, and that those cells that undergo this process are those that express T cell activation markers in response to force application. Given the cytoskeletal dependent physiological process of TCR migration through the membrane and ultimate downregulation in formation and function of the IS, as described earlier (see section 1.6), we aimed to investigate whether perturbation of the cytoskeleton would prevent force induced TCR downregulation and whether these cells were then unable to respond to stimulation with anti-CD3 MNPs and magnetic force.

To investigate this, we utilised the actin polymerisation inhibitor Latrunculin A (Lat A), which binds and sequesters globular actin and hence prevents its inclusion into a growing actin filament during the process of actin polymerisation[111,252,301,302]. Treatment with 0.25µM Lat A was enough to induce a blockade in TCR downregulation in response to anti-CD3 MNP treatment regardless of magnetic force treatment (figure 4.17). Figure 4.17 displays representative FACS plots for 1µm^{Mid} MNPs, yet it should be noted that this was observed for all particles tested (250nm^{Mid} anti-CD3 only and 250nm^{Mid} anti-CD3:CD28 MNPs).



Plots from 1µm^{Mid} MNPs
Representative of at least 3 independent repeats

Figure 4.17 - Blockade of the actin cytoskeleton with Latrunculin A blocks TCR downregulation. Force application to Nr4a3-FT CD4^{+} T cells when treated with MNPs targeting the TCR-CD3 complex fails to induce TCR downregulation when cells are pre-treated with Latrunculin A (Lat A). Cells were subjected to 60 minutes of force in the presence of increasing concentrations of Lat A. Concentrations of Lat A were maintained throughout the entire experiment. Plots representative of at least 3 independent experiments, for 1µm^{Mid} CD3 MNPs, 250nm^{Mid} anti-CD3 and anti-CD3:CD28 MNPs.

Importantly, blockade of TCR downregulation also prevented expression of Nr4a3 in response to magnetic force application, in the context of cells stimulated with 250nm^{Mid} anti-CD3 MNPs, 250nm^{Mid} anti-CD3:CD28, and 1µm^{Mid} MNPs (figure 4.18). Here, gating on TCRhi and TCRlo populations indicates that in the absence of Lat A, force application induces a population of TCRlo Nr4a3^{+} cells as previously described. However, use of Lat A to block TCR downregulation also prevents the expression of Nr4a3 as these are not then simply

found in the TCRhi gate, indicating the importance of force induced TCR membrane re-organisation on T cell activation.

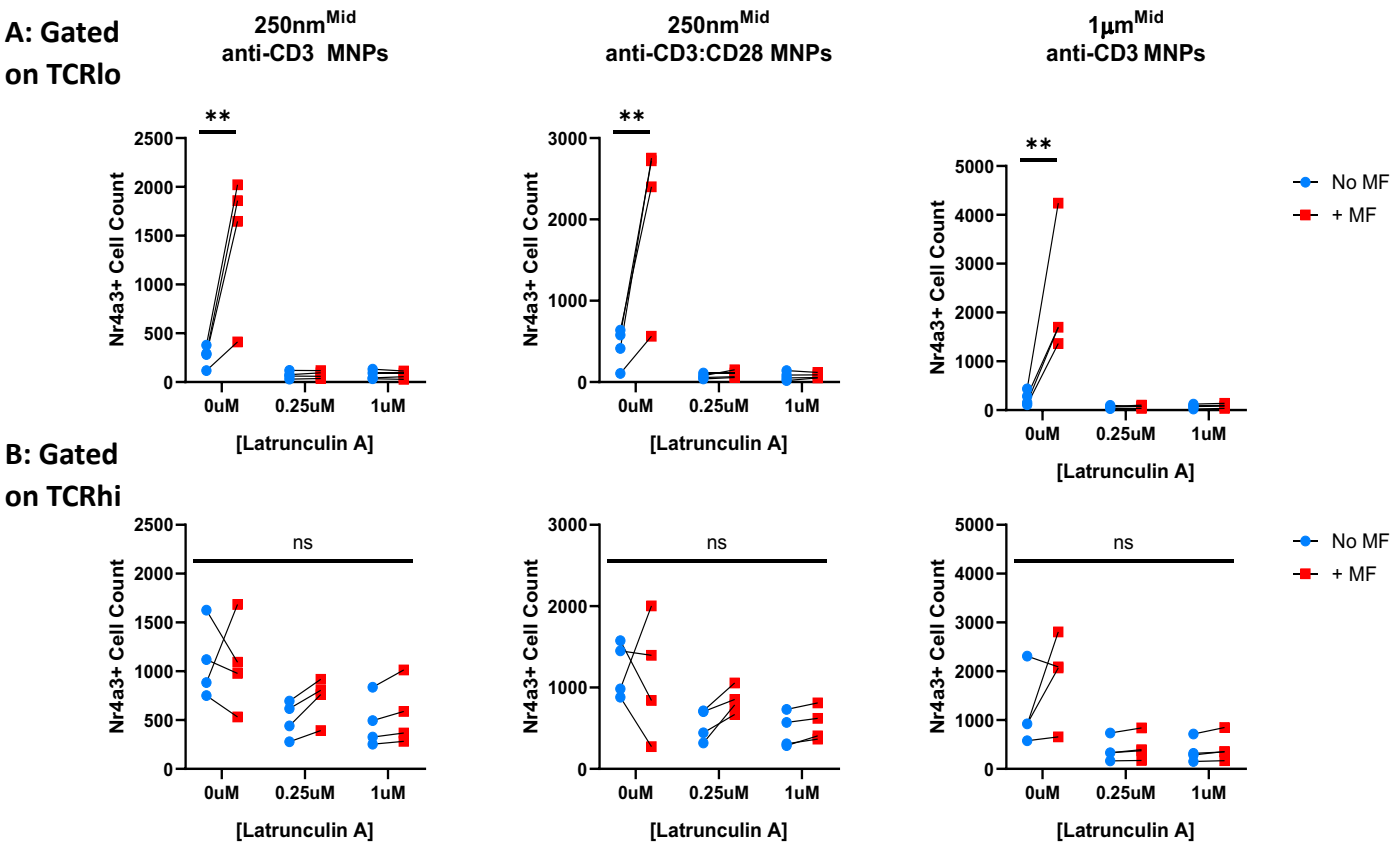


Figure 4.18 - Inhibition of TCR downregulation with Latrunculin A Prevents Nr4a3 Expression. Purified CD4+ T cells from Nr4a3-Ft mice were treated with functionalised MNPs and increasing concentrations of Lat A as shown. Force was applied for 60 minutes, and TCR and Nr4a3 expression was assessed by flow cytometry 4 hours post force application, to investigate Nr4a3 expression in TCRlo (A) and TCRhi (B) populations. Treatment with Lat A prevents the induction of a TCRlo Nr4a3+ phenotype in response to force application. Graphs show 4 independent experiments, with each line connecting no MF and + MF conditions from each independent repeat. Statistical analysis assessed by two-way ANOVA with Sidak's post-tests. 250nm^{Mid} CD3 MNPs: ** p=0.0003, 250nm^{Mid} CD3:CD28 MNPs: ** p=0.0002, 1µm^{Mid} CD3 MNPs: **p=0.0008.

4.6 Blockade of Active TCR Signalling Prevents TCR Downregulation

Given the importance of the actin cytoskeleton in IS formation, it is somewhat unsurprising that force induced TCR downregulation displayed such heavy reliance on the actin cytoskeleton. However, we have previously shown that TCR downregulation occurs only in response to 250nm MNPs functionalised with the 145-2C11 anti-CD3 antibodies, and not when 250nm MNPs were functionalised with antibodies targeted to the TCR-CD3

complex that are largely considered non-activating clones (anti-CD3εγ clone 17A2and anti-TCRβ clone H57-597, figure 4.1). This result implies a reliance not only on an intact actin cytoskeleton, but also on active signalling, given that TCR downregulation was not observed when 250nm particles were functionalised with TCR-CD3 targeting clones that did not induce robust TCR signalling. To test this further, we assessed the dynamics of TCR downregulation in response to $250nm^{Mid}$ anti-CD3 MNPs and $1\mu m^{Mid}$ anti-CD3 MNPs, in the presence or absence of 10μM PP2 to block the TCR trigger (figure 4.19-4.20).

These results indicate that TCR downregulation relies on the action of Src family kinases, as downregulation of the TCR in response to magnetic force application was blocked by pre-treatment with 10μM PP2. Therefore, TCR downregulation in response to external magnetic force application is an active, signalling dependent process, during which force application induces TCR membrane reorganisation ultimately resulting in TCR downregulation. This is in agreement with other reports, which have shown that simultaneous knockdown of Lck or Fyn marginally inhibits TCR downregulation upon activation, yet either use of broader acting tyrosine phosphatases such as PP2 prevents ligand induced TCR downregulation[303].

Finally, we observed a difference in TCR downregulation dependent on stage of pathway inhibition. Here, we clearly show that use of the Src kinase inhibitor PP2 prevents force induced TCR downregulation. However, this was not the case in the experiments described earlier when the NFAT pathway was blocked through use of CsA. In these experiments, treatment of $CD4^+$ T cells with 1μM CsA (sufficient to inhibit further Nr4a3 expression) failed to effect force induced TCR downregulation (appendix figure 8.2). We therefore conclude that TCR downregulation is controlled by non-calmodulin dependent TCR signalling pathways initiated by Src kinases.

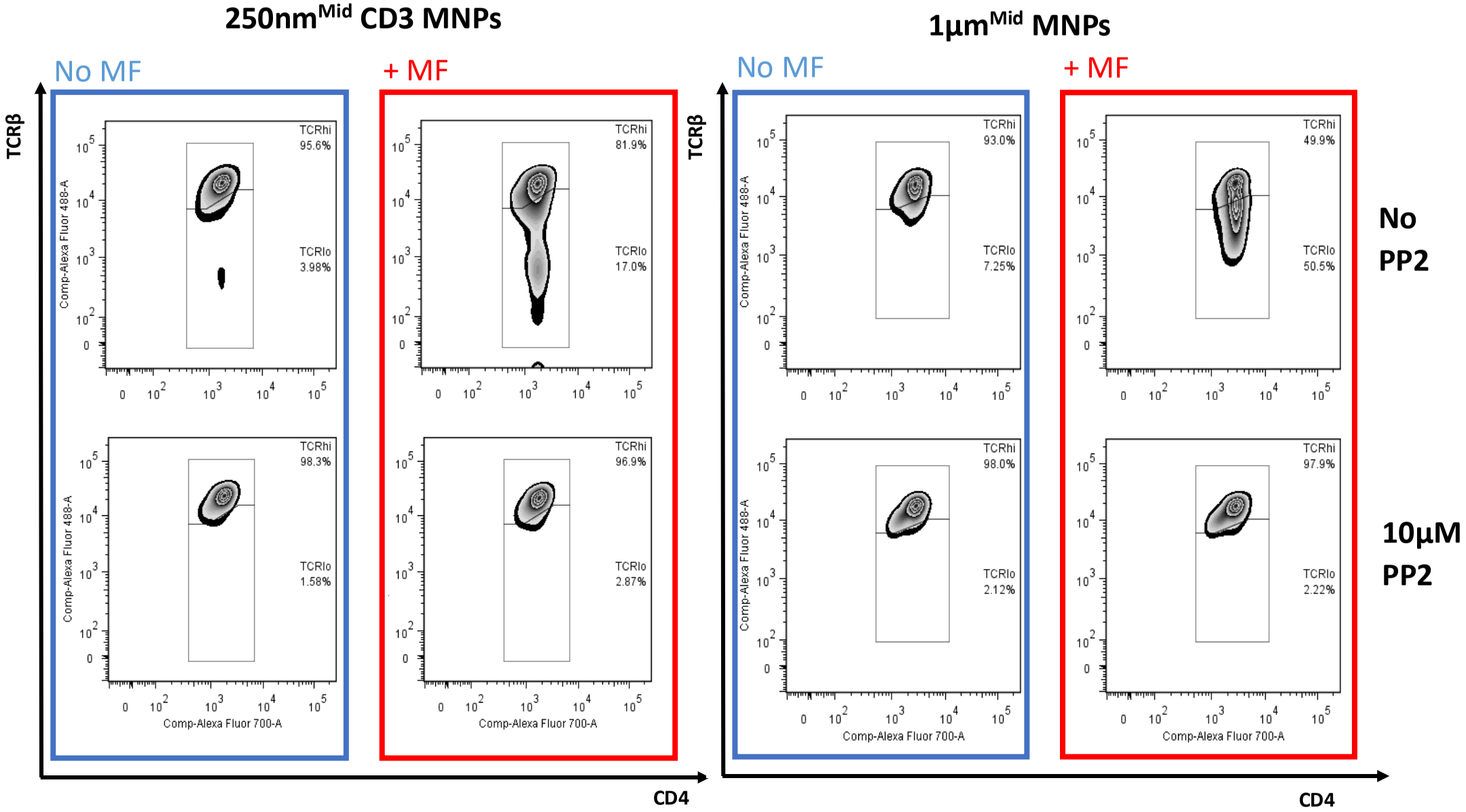


Figure 4.19 - Blockade of active TCR signalling by treatment with 10µM PP2 prevents force induced TCR downregulation.
Representative FACS plots displayed here show that treatment with PP2 prevents force induced TCR downregulation in the context of both 250nm and 1µm anti-CD3 MNPs. FACS plots representative of at least 3 independent experiments.

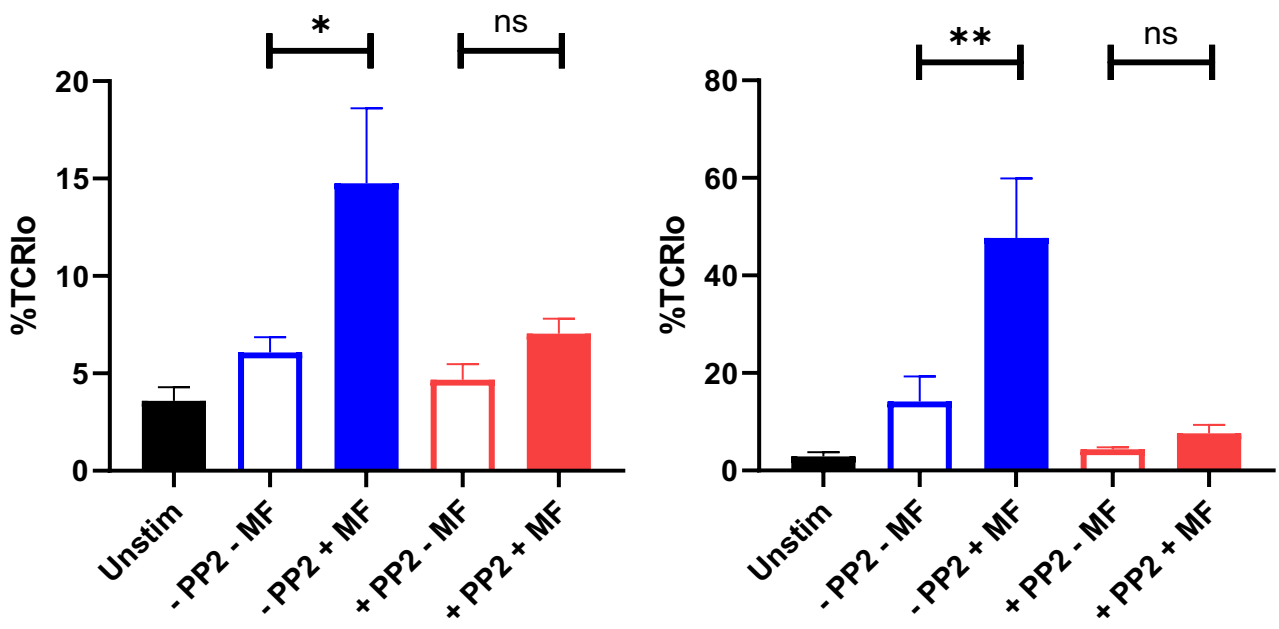


Figure 4.20 - PP2 Treatment Prevents Force Induced TCR Downregulation. Purified CD4+ T cells from the Tg4 mouse were treated with either 250nm^{Mid} anti-CD3 MNPs (left) or 1µm^{Mid} MNPs (right) in the presence (red bars) or absence (blue bars) of 10µM PP2. Force was applied for 60 minutes, before assessment of TCR expression 4 hours post force application. Concentrations of PP2 were maintained throughout the experiment. Data shown from at least 3 independent experiments. Bar graphs show mean ± SD. Statistical analysis assessed by one-way ANOVA with Tukey's post-tests, 250nm MNPs * p=00483, 1µm MNPs ** p=0.0084.

4.7 Force Application Induces CD45 Segregation from Particle-Membrane Contact Zones

Force induced TCR downregulation can be considered a hallmark of force induced IS formation, whereby data suggests that force application induces membrane reorganisation of the TCR and subsequent TCR downregulation, and that these processes are governed by both active TCR-CD3 phosphorylation and cytoskeletal dynamics. To further probe whether hallmarks of the IS facilitate TCR signalling in response to magnetic force, we investigated the distribution of the trans-membrane phosphatase CD45 with respect to membrane bound MNPs in response to force application. As discussed previously, phosphatase activity by CD45 is a negative regulator of TCR signalling and is excluded from TCR-pMHC contact

regions within a physiological IS owing to its large extracellular domain, hereby facilitating TCR signalling[145,146].

Here, purified $CD4^+$ T cells from the Tg4 mouse were treated with $250nm^{Mid}$ anti-CD3 MNPs and $1\mu m^{Mid}$ anti-CD3 MNPs as previously described (see section 2.6). Cells were then subjected to 60 minutes of magnetic force before immediate fixation and assessment of membrane CD45 expression together with the localisation of membrane bound MNPs as described in 2.10.3 and 2.10.4. As a positive control, cells were allowed to interact with anti-mouse CD3/CD28 dynabeads for 15 minutes to induce dynabead-$CD4^+$ T cell binding and subsequent CD45 reorganisation, before immediate fixation and assessment of membrane CD45 expression. Representative images from these experiments are displayed in figure 4.21.

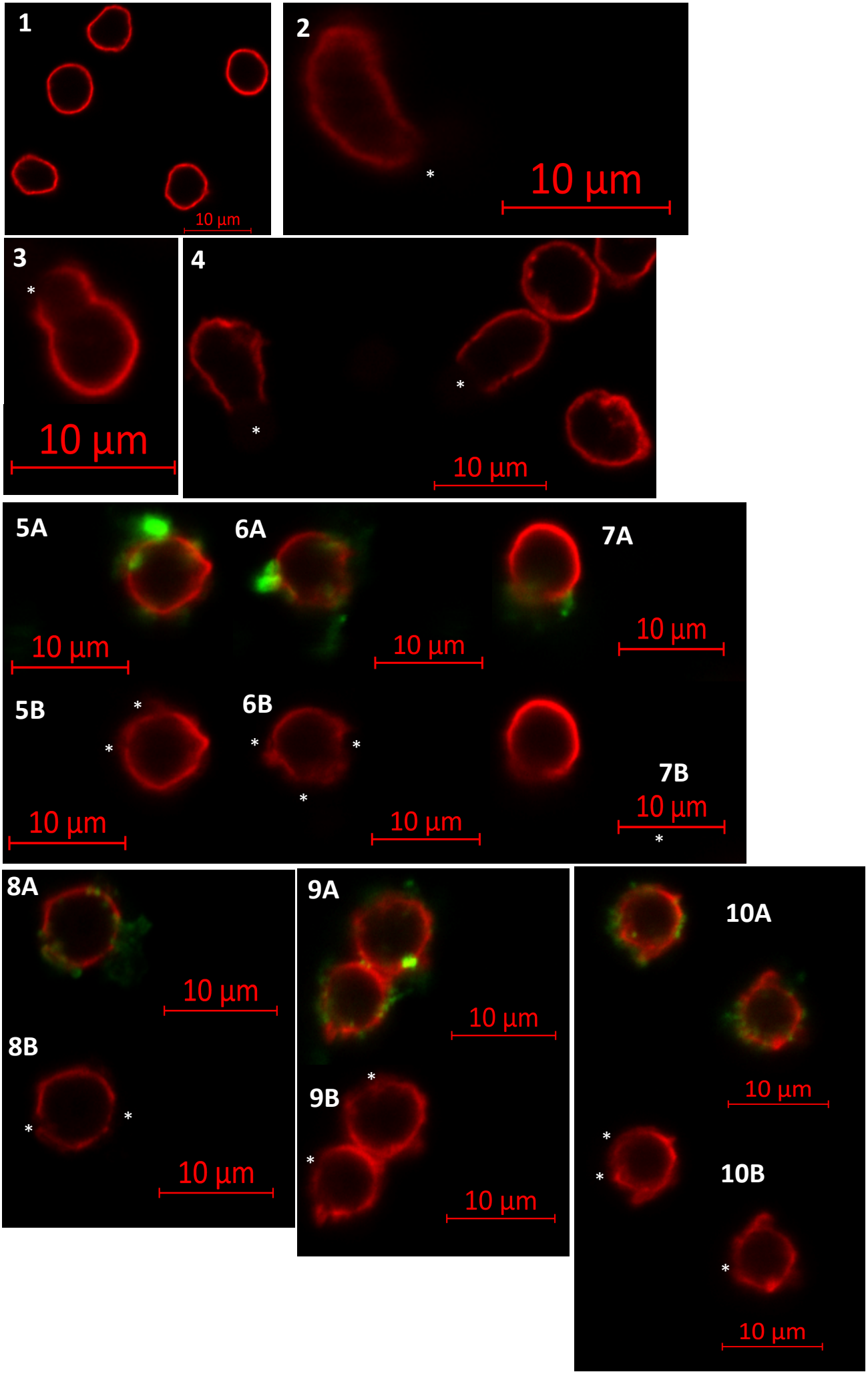


Figure 4.21 - Representative Images from CD45 Confocal Microscopy Experiments. Representative images (x60 magnification) indicating membrane localisation of CD45 (red) and functionalised MNPs (green) from unstimulated (1) or dynabead (2-4) controls, and 1µm^{Mid} MNPs (5-8) or 250nm^{Mid} anti-CD3 MNPs (9-10). For particle conditions (5-10), A and B images correspond to the same cell, with the MNP channel excluded in the B images to indicate regions of CD45 membrane remodelling. * marks regions of membrane where loss of CD45 intensity is apparent. Scale bars are shown on each image.

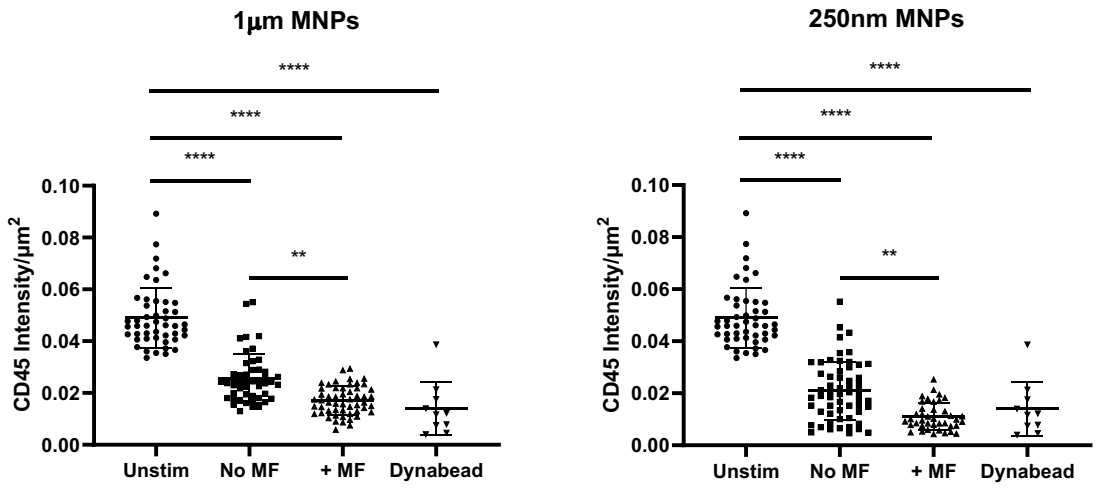


Figure 4.22 - Force application to 250nm^{Mid} and 1µm^{Mid} anti-CD3 MNPs induce CD45 exclusion from particle-membrane contact zones. CD4^{+} T cells from Tg4 mice were treated with 1µm^{Mid} (left) or 250nm^{Mid} anti-CD3 MNPs (right) and subjected to 60 minutes magnetic force as previously described. Membrane CD45 expression was assessed as per 2.10.3 and 2.10.4. Force application to both particles tested induced exclusion of CD45 from areas of membrane that were bound to functionalised MNPs. Data represenative of 3 independent repeats. Normalcy was first assessed in Prism v9, before statistical significance was assessed by Kruksal-Wallis with Dunn's post-tests. 1µm^{Mid} CD3 MNPs, all **** p<0.0001, ** p=0.001. 250nm MNPs, all **** p<0.0001, ** p=0.005.

Force application to either 250nm^{Mid} or 1µm^{Mid} anti-CD3 MNPs was found to induce exclusion of CD45 from areas of the membrane directly in contact with MNPs (figure 4.22). Given that CD45 exclusion can be considered a further hallmark of pseudo-IS formation in response to force, we investigated the reliance of CD45 exclusion on the actin cytoskeleton and active TCR phosphorylation, using 1µM Lat A and 10µM PP2 respectively, as previously displayed for TCR downregulation (figures 4.17-4.20). As was the case for TCR downregulation, CD45 exclusion was found to be prevented through inhibition of both actin polymerisation and active TCR signalling when tested in the context of force application to 1µm^{Mid} MNPs (figure 4.23).

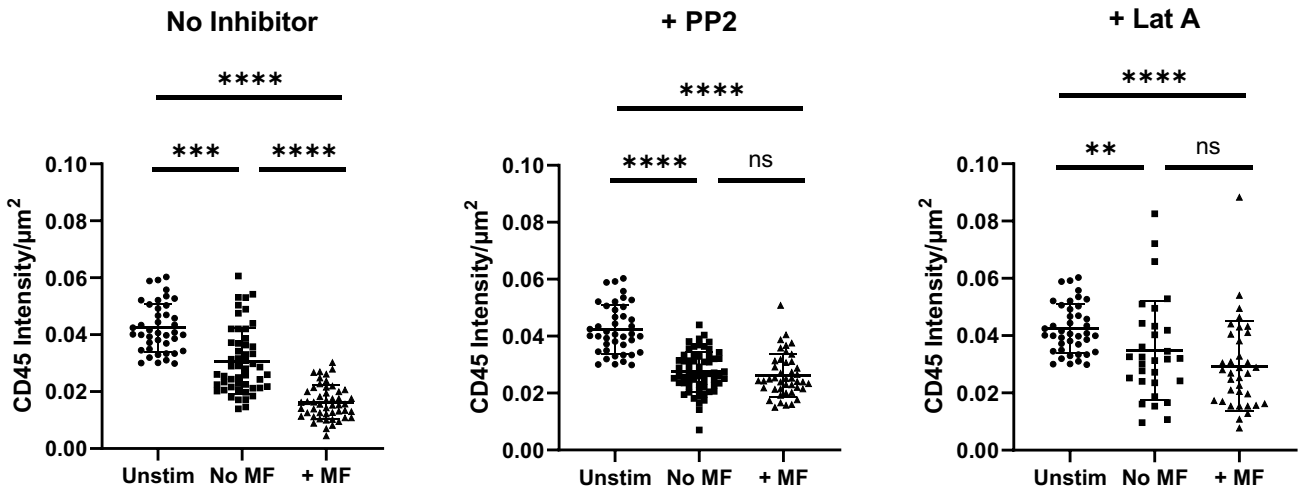


Figure 4.23 - Force induced CD45 exclusion relies on actin polymerisation and active TCR-CD3 phosphorylation. $CD4^+$ T cells from Tg4 mice were treated with $1\mu m^{Mid}$ MNPs and either 10µM PP2 (middle) or 1µM Lat A (right), before force application for 60 minutes and assessment of membrane CD45 expression as described in 2.10.3 and 2.10.4. Treatment with both PP2 and Latrunculin A prevents force induced CD45 exclusion from regions of membrane-particle contact. Data representative of 2 independent repeats. Normalcy was first assessed in Prism v9, before statistical significance was assessed by Kruskal-Wallis with Dunn's post-tests. No inhibitor, **** p<0.0001, *** p=0.0003, +PP2 **** p<0.0001, +Lat A **** p<0.0001, ** p=0.0098.

Figure 4.23 shows that in the absence of any inhibitor, CD45 intensity within areas of membrane-particle contact was depleted in response to stimulation with $1\mu m^{Mid}$ CD3 MNPs in the absence of force application (Unstimulated control CD45 intensity: $0.042/\mu m^2$, $1\mu m^{Mid}$ MNP no MF CD45 intensity: $0.031/\mu m^2$). However, force application induced a further decrease in CD45 intensity in these areas of membrane-particle contact ($1\mu m^{Mid}$ CD3 + MF CD45 intensity: $0.016/\mu m^2$). CD45 exclusion in response to particles in the absence of force application was not reversed by treatment with PP2 or Lat A (unstim control CD45 intensity: $0.042/\mu m^2$ vs $0.027/\mu m^2$ and $0.035/\mu m^2$ for +PP2 no MF and +Lat A no MF respectively), yet further exclusion of CD45 in response to force application was prevented by use of either inhibitor (+PP2 CD45 intensity: $0.027/\mu m^2$ no MF vs $0.026/\mu m^2$ + MF; +Lat A CD45 intensity: $0.035/\mu m^2$ no MF vs $0.029/\mu m^2$ + MF). These data indicate that binding of $1\mu m^{Mid}$ MNPs to membrane TCR-CD3 complexes is enough to induce localised CD45 re-organisation independent of downstream signalling, yet enhanced CD45 exclusion in response to

magnetic force application, known to be required for robust TCR signalling[145,148,304], is dependent on both TCR-CD3 phosphorylation and actin cytoskeletal dynamics.

4.8 Single Molecule Microscopy Reveals the Presence of Force Induced TCR Clustering

The data discussed thus far form part of a growing body of evidence supporting force induced TCR-CD3 membrane re-organisation as a mechanism for force induced TCR signalling and T cell activation. Not only may enhanced aggregation of TCR-CD3 complexes in response to force alter TCR signalling, but depletion of negative phosphatases from these regions will further shift the kinase-phosphatase balance in the favour of TCR signalling. To address this, and to attempt to visualise formation of these TCR clusters in response to magnetic forces, single molecule localisation microscopy (SMLM) via stochastic optical reconstruction microscopy (STORM) was employed as a method to visualise formation of TCR clusters as described in section 2.12.

Briefly, purified Tg4 $CD4^+$ T cells were treated with $1\mu m^{Mid}$ MNPs as previously described, before force application for 5, 15 or 30 minutes. An additional time point of 60 minutes of force application followed by a 2-hour incubation at 37°C was also performed. These conditions replicate the cycling TCR stain shown earlier (figures 4.9-4.12, described in 2.9.5), serve as a time point within which significant TCR downregulation will have taken place, and therefore allow for a full kinetic assessment of TCR cluster formation. Stimulation of cells on immobilised anti-CD3/CD28 for 15 minutes served as a positive control. Representative cells from these experiments are shown in figure 4.24, whilst images in the form of MATLAB cluster maps from these experiments are shown in figure 4.25.

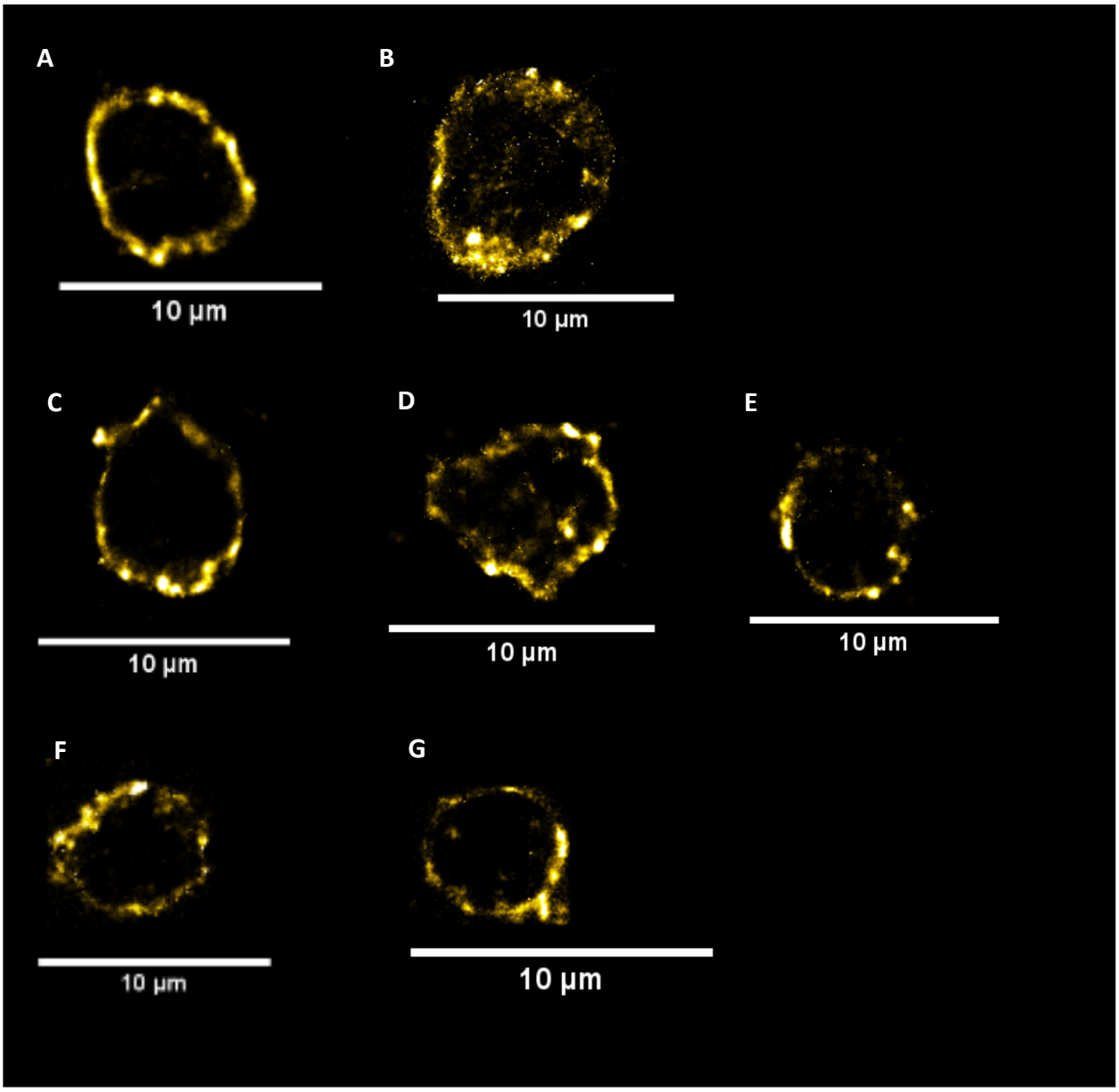
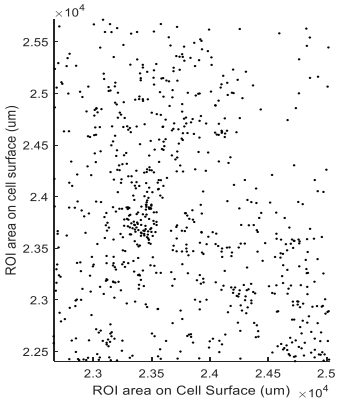
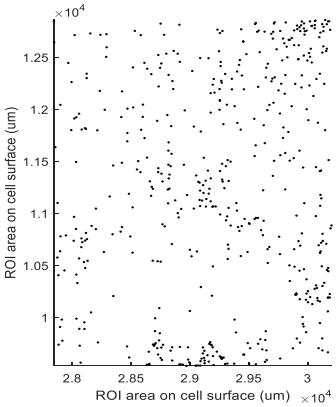


Figure 4.24 – Representative images from STORM experiments mapping surface TCR organisation with magnetic field stimulation. $CD4^+$ T cells from the Tg4 mouse were stimulated with $1\mu m^{Mid}$ MNPs as described, before being subjected to MF for 5min (D), 15min (E), or 30min (F), or 60min followed by a 2hr (G) wait as described. Cells were also either left unstimulated (A), stimulated on glass immobilised anti-CD3/CD28 (B), or were treated with $1\mu m^{Mid}$ MNPs but were not subjected to MF (C) as controls. Images show TCR staining from SMLM STORM imaging as per methods section 2.12. Images representative of at least 2 independent experiments per condition.

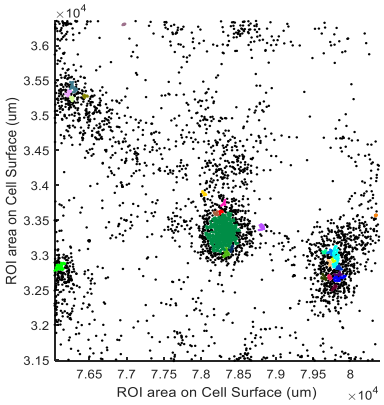
1A



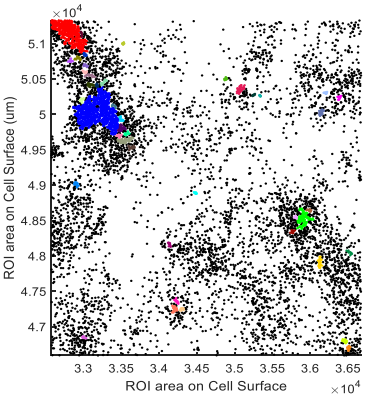
1B



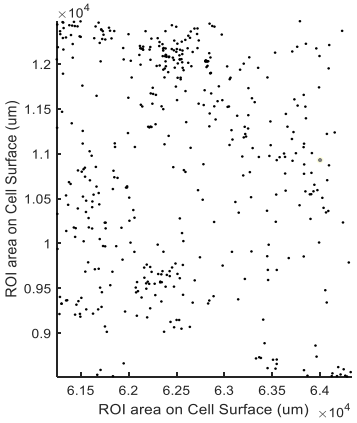
2A



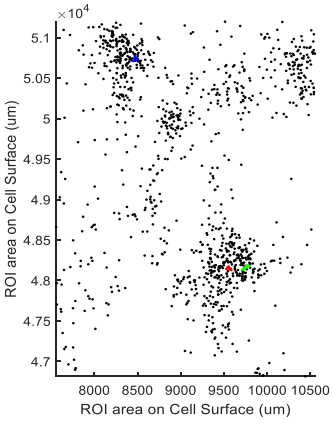
2B



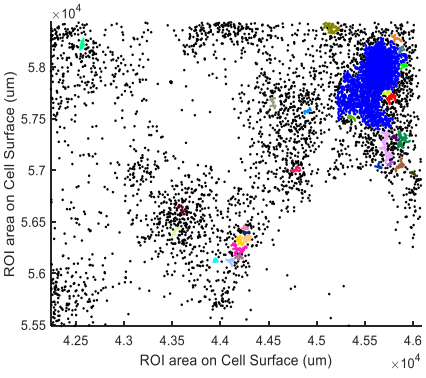
3A



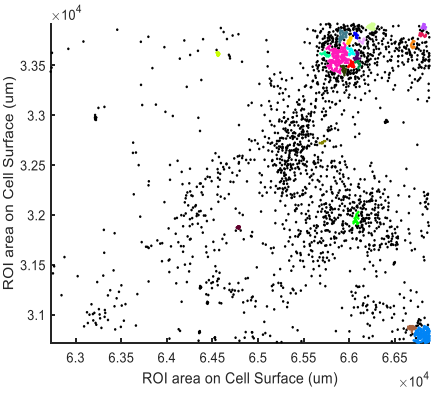
3B



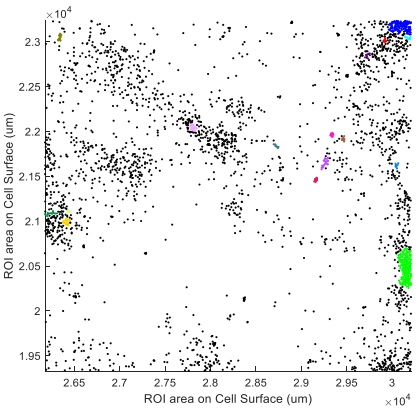
4A



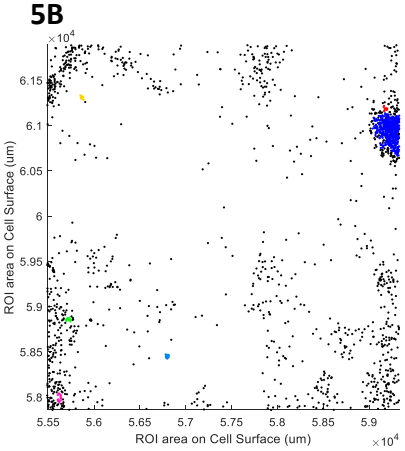
4B



5A



5B



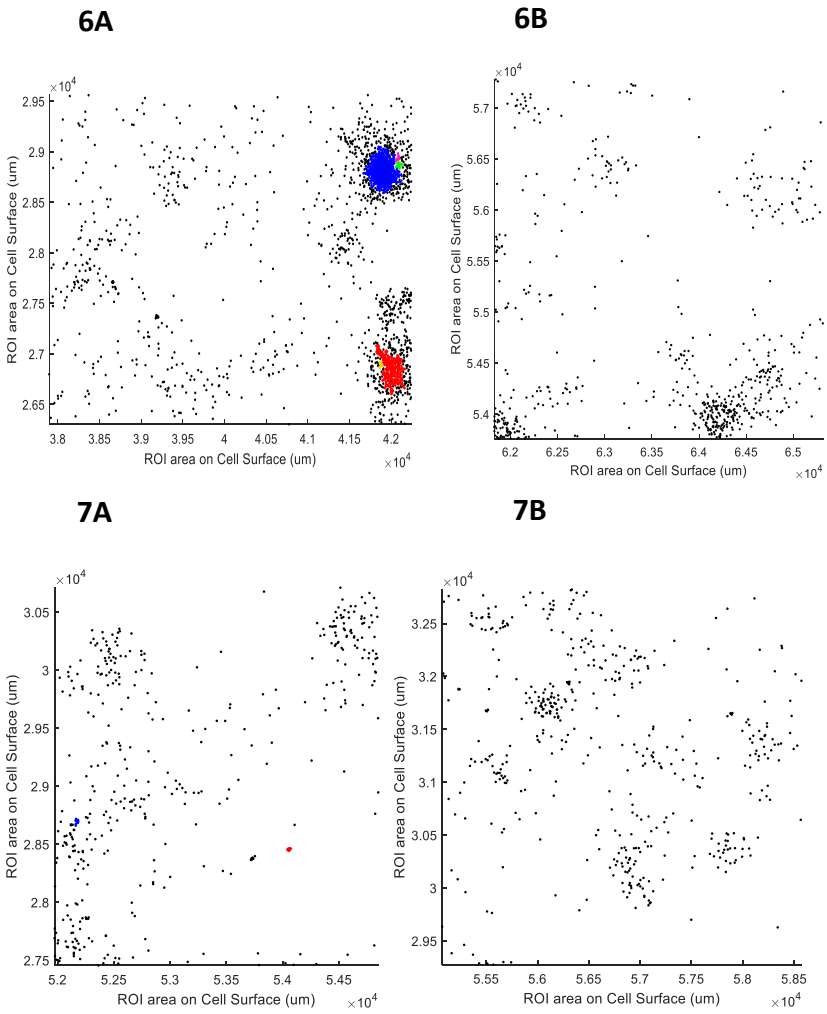


Figure 4.245 - Single molecule cluster maps from STORM Image Analysis. Surface TCR clusters were measured as per 2.12, with TCR cluster maps being produced in MATLAB post image acquisition. Images show duplicate cluster maps from 2 regions of interest (A and B) per conditions. Conditions shown: 1) Unstimulated 2) Immobilised CD3/CD28 control 3) No MF 4) 5min MF 5) 15min MF 6) 30min MF 7) 60min MF + 2hr wait. Images representative from 2 independent experiments. Colours shown on cluster maps indicate the positions of clusters identified by the dbScan software. Black points in the cluster maps indicate positions of TCR molecules not allocated into a cluster. Cluster maps show formation of clusters in response to magnetic force application at 5 and 15 minutes, which then returns to baseline at 30 minutes and beyond.

Across all TCR stimulated experimental conditions, very little change in cluster properties was observed. Here, there appeared to be no difference in number of TCR molecules per cluster (figure 4.26A), cluster area (figure 4.26C) or density (figure 4.26D) across all conditions. It should be noted that when analysing these parameters, a large spread in the data was observed indicating wide heterogeneity in the TCR clusters detected upon stimulation. However, we found a striking upregulation in the number of individual clusters

detected in response to the CD3/CD28 positive control (figure 4.26B). This upregulation was also observed in response to force application to the 1µm^{Mid} CD3 MNPs for 5 minutes and was sustained out to 15 minutes of force application. TCR cluster detection appeared to return to baseline beyond these early time points.

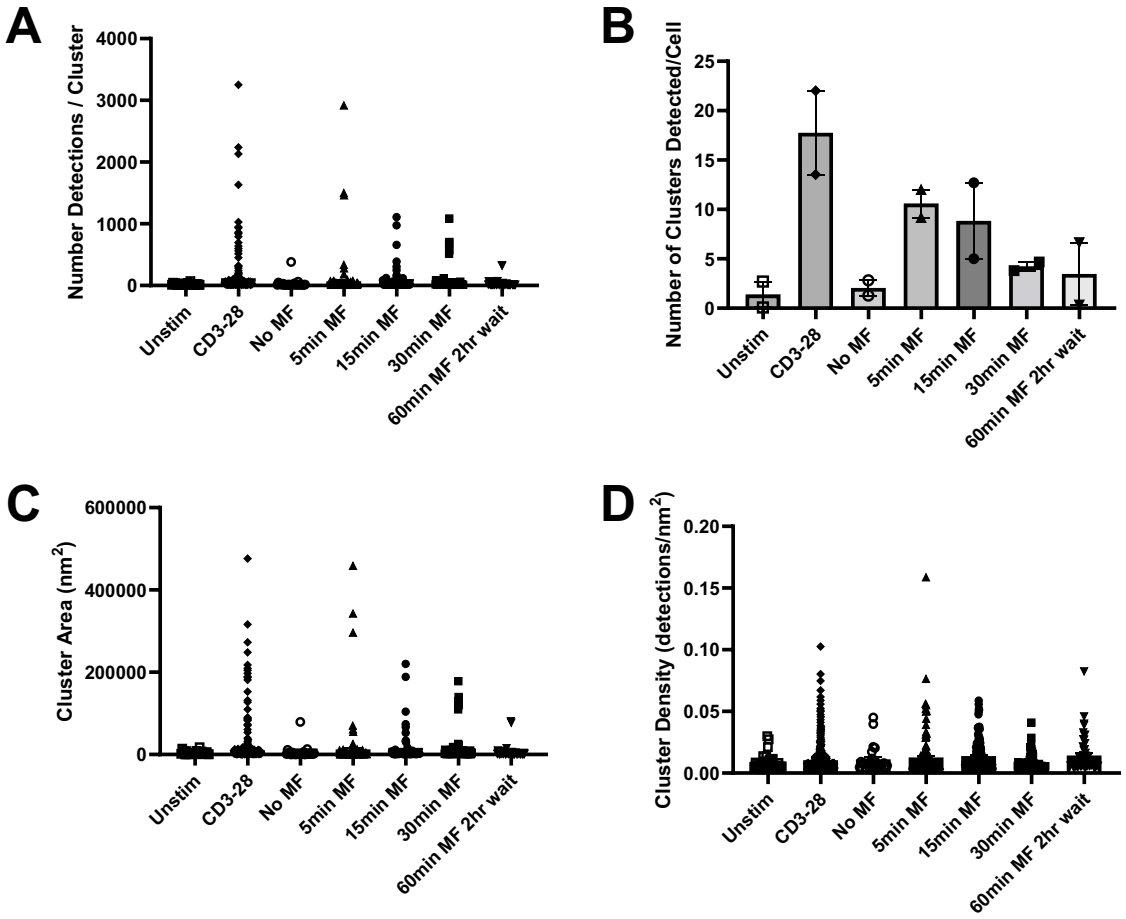


Figure 4.256 – Force application induces TCR cluster formation with 5 and 15 minutes. CD4$^+$ T cells from Tg4 mice were treated with 1µm^{Mid} CD3 MNPs and subjected to magnetic force for time periods shown. At each time point, cells were fixed and stained for surface TCR for cluster analysis as per 2.12. Very little effect of magnetic force was observed on number of TCRs per cluster (A), cluster area (C) or cluster density (D). However, both force application for 5 and 15 minutes, and stimulation with the positive control (CD3-28) induced a detectable increase in number of TCR clusters formed. At time points beyond 15 minutes, TCR cluster formation appeared to return to baseline levels. Data from 2 independent experiments. A/C/D – graphs show all data points, with mean ± SD. B – bar graphs show mean ± SD.

These findings raise an important question concerning the relationship between TCR triggering and TCR cluster formation. It is conceivable that formation of these clusters serves

as the initiating mechanism of TCR triggering by increasing proximity of multiple TCRs for activating kinases as proposed in aggregation models of TCR triggering. On the other hand, previous work on IS formation has identified monomeric TCRs as capable of identifying antigenic pMHC molecules and driving intracellular signalling[137], whereby TCR microcluster formation then serves as a mechanism to promote sustained TCR signalling to drive robust T cell activation[111,305,306]. We therefore simply asked what comes first in our protocol: does TCR cluster formation drive TCR phosphorylation, or is TCR phosphorylation required to promote cluster formation?

To address this question, we repeated these 5- and 15-minute time point experiments with the addition of 10μM PP2, known to block the TCR signalling response to functionalised 1μm MNPs as previously shown (figures 3.13-3.14). An increase in number of clusters detected was again found with 5 minutes of force application, which appeared to be largely blocked by PP2 addition. We also observed a striking blockade of TCR clustering by PP2 in response to the immobilised CD3/CD28 positive control (figure 4.27B). Together, these data suggest that TCR cluster formation requires active TCR phosphorylation and therefore may serve as a mechanism to promote increased TCR signalling in response to force application.

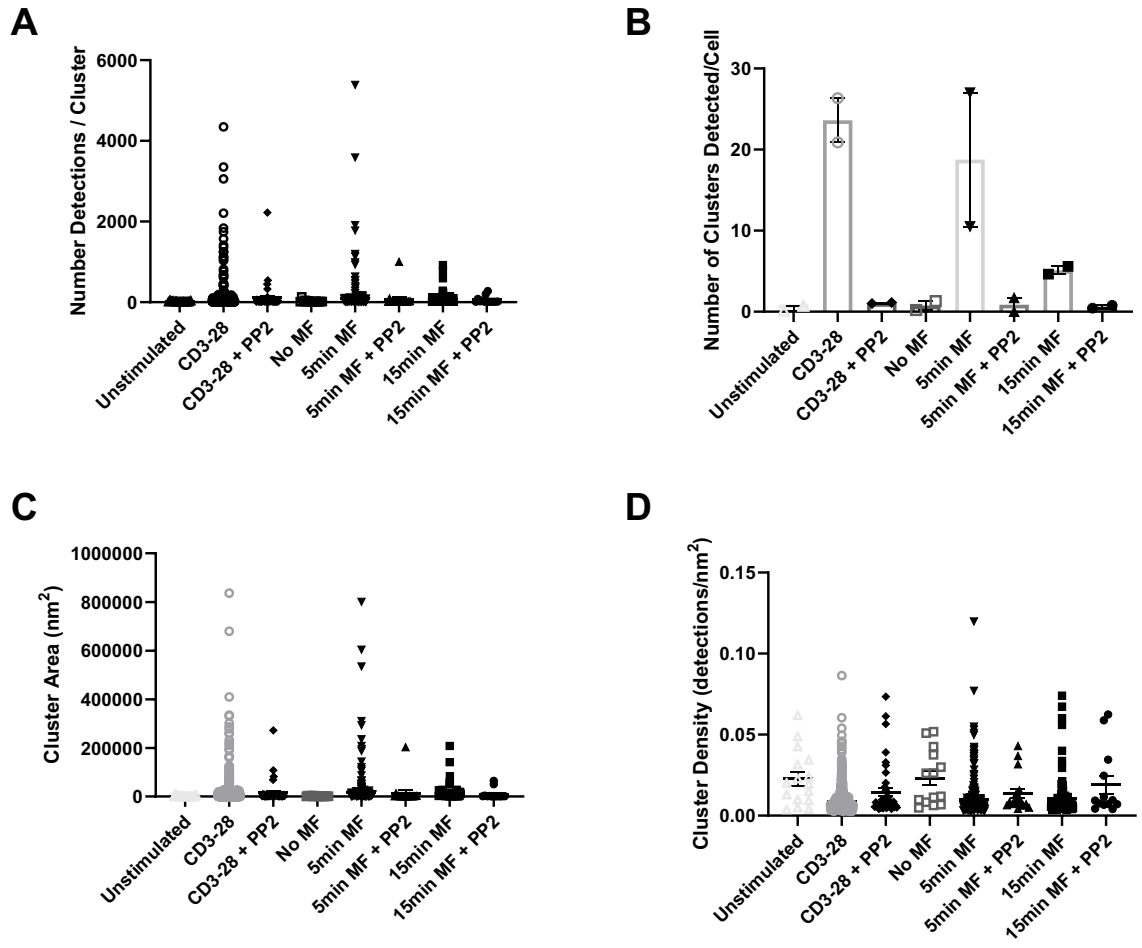


Figure 4.267 – TCR cluster formation is dependent on TCR phosphorylation. $CD4^+$ T cells from Tg4 mice were treated with $1\mu m^{Mid}$ CD3 MNPs and subjected to magnetic force for time periods shown. Where indicated, cells were pre-treated with 10μM PP2, which was maintained throughout the time course. At each time point, cells were assessed for surface TCR cluster formation as per 2.12. Treatment with PP2 inhibited TCR cluster formation (B) yet did not affect number of TCRs per cluster (A), cluster area (C) or cluster density (D). Data shown from 2 independent experiments. A/C/D – graphs show all data points, with mean ± SD. B – bar graphs show mean ± SD.

4.9 Discussion

In the context of T cell activation, the TCR itself is not a stationary receptor. During the forming immune synapse (IS) between T cell and APC, the TCR is rapidly re-organised into signalling active microclusters, which ultimately migrate to the cSMAC for cessation of signalling and TCR internalisation[104,115]. Here, we show that force application to the TCR is sufficient to permit TCR microcluster (TCR-MC) formation, TCR signalling and subsequent

TCR downregulation. The finding that force application induces a $CD4^+$ TCRlo $Nr4a3^+$ population proposes a striking scenario whereby force induced TCR re-organisation promotes signalling, and these TCRs are ultimately downregulated, producing a population of cells that have experienced a TCR signal and express less cell surface TCR as a result. It should be noted that the staining antibody in these TCR downregulation studies was an intact antibody, which may contribute to TCR downregulation through either basal activation of the receptor or by patching and capping phenomena. However, the staining antibody is a H57-597 anti-TCRβ clone, which when tested for activation capacity in chapter 3, showed very little effect on T cell activation (see figure 3.3). Therefore, we can be confident that TCR downregulation observed is not influenced through our staining protocols themselves, which were also performed at 4 degrees to minimise non-specific effects induced from the protocol itself. To address this by further experimentation, staining protocols can be repeated making use of Fab fragments to remove the possibility of staining antibody induced TCR downregulation.

However, substantial TCR downregulation was observed as a direct consequence of magnetic force application, which further strengthens the claim that the staining procedure does not influence this measurement. Therefore, we can propose with confidence that force application to the TCR induces TCR membrane reorganisation, in a process dependent on active TCR signalling and an intact actin cytoskeleton, subsequently promoting TCR signalling events and T cell activation. Indeed, the observations of force induced TCR-MC formation by single molecule localisation microscopy provides further evidence for force induced TCR re-organisation.

In support of the notion that force application induces TCR-MC formation driving TCR signalling and naive T cell activation is the fact that when performing T cell activation assays

on *in vitro* polarised Th1 Tg4 T cells, we find that force application here fails to induce an upregulation of CD69 expression (appendix figure 8.5). Previous reports have shown that in naive T cells, TCRs can exist on the membrane in pre-formed nanocluster, which can concatenate to form TCR-MCs upon TCR ligation as described in 1.6[104–107,109]. However, it has been reported that in memory $CD4^+$ T cells, TCR organisation on the membrane is altered whereby more TCRs are contained within pre-formed clusters, reducing the time taken to initiate a TCR signal upon TCR ligation and increasing sensitivity to antigen[307,308]. Therefore, we propose that force application to TCRs on naïve CD4+ T cells drives the formation of TCR-MCs required for signalling, yet this is not required in the context of antigen experienced Th1 cells.

4.9.1 Force Induced TCR Re-Organisation as a Mechanism of Promoting T Cell Activation

Force induced TCR downregulation was found to be dependent on an intact cytoskeleton, as induction of TCRlo $Nr4a3^+$ populations was prevented by treatment with the actin polymerisation inhibitor Latrunculin A. Given the importance of the actin cytoskeleton in the remodelling and reorganisation of surface proteins during a developing IS, this result is important yet perhaps somewhat unsurprising. However, strikingly the establishment of these force induced phenotypes was also found to be entirely dependent on active TCR-CD3 phosphorylation, evidence by the blockade of both TCR downregulation and TCR-MC formation by the Src kinase inhibitor PP2, and the lack of induction of TCRlo populations when particles were functionalised with non-activatory, yet TCR-CD3 targeting antibodies. These findings indicate that establishment of these phenotypes is a signalling dependent, active process, and therefore whilst force application clearly aids re-organisation of the TCR to permit signalling, this can perhaps be considered as a mechanism of promoting sustained

signalling required for T cell activation as opposed to a true TCR trigger initiating mechanism in itself.

Interestingly, the fact that TCR-MC formation was blocked by PP2 treatment (figure 4.27) supports previous reports that formation of TCR-CD3 clusters is in itself signalling dependent. Previous work has shown that formation of clusters of GFP-tagged CD3ζ molecules in cell-cell contacts requires calcium signalling and is prevented when treatment with calcium chelators (BAPTA/Ni^{2+}) blocks this calcium signalling[105]. However, other reports have proposed the opposite scenario where treatment of T cells with PP2 prior to their engagement with cognate antigen expressing planar lipid bilayers does not prevent the formation of TCR microclusters (TCR-MCs)[118]. These conflicting reports may arise from the different experimental systems used (live imaging of cell-cell contacts, vs use of planar lipid bilayers) and may reflect how well either experimental set up represents physiological settings. However, the results displayed here evidencing blockade of force induced TCR cluster formation, and indeed the unequivocal blockade of TCR clusters on immobilised antibody controls (figure 4.27), by treatment with PP2 agrees with the cell-cell contact imaging experiments.

Finally, we also provide evidence that force application not only induces re-organisation of the TCR itself, but also promotes enhanced segregation from negative phosphatases such as CD45. Importantly, and in line with TCR downregulation phenotypes, CD45 exclusion phenotypes also showed reliance on the actin cytoskeleton and active TCR phosphorylation, evidenced by the use of Latrunculin A and PP2 respectively (figure 4.23).

4.9.2 Mechanical Activation of the TCR to promote TCR-MC formation

As discussed, data presented in this chapter identifies an axis whereby force application to the TCR can induce TCR-MC formation, identified by others as the site of signalling active TCRs[106], which may subsequently promote TCR signalling to the threshold level required to trigger T cell activation. Indeed, others have reported similar observations with magnetic force application to the FcεRI receptor on mast cells, whereby force induced FcεRI clustering achieved via anti-IgE coated MNPs and pulsed field application with an electromagnetic needle induced robust calcium signalling[309].

However, whilst this axis of force induced clustering is a promising proposal, it does not directly comment on the ability of the TCR to function as a mechanosensor. It is possible that it is the upstream mechanical manipulation of the TCR that permits TCR-MC formation. In this scenario, force application to the TCR may induce localised conformational changes in the receptor that may permit or enhance receptor phosphorylation leading to the TCR-MC formation. In support of this hypothesis is the finding that TCR-MC formation was prevented by pre-treatment with the Src kinase inhibitor PP2, indicating dependence on TCR phosphorylation for TCR-MC formation.

As discussed in 1.7.4, the question of whether conformational changes in the TCR-CD3 complex induce TCR signalling remains a hotly debated topic. Multiple groups have proposed that conformational changes in CD3 docking sites in the TCR-CD3 complex may play a role in translating conformational change through the complex to initiate signalling[41,160,161,163], whilst other groups have reported the absence of conformational changes in a ligated TCR-CD3 complex[310]. However, it has also been reported that when using pMHC coated lipid beads, ligation of the TCR induces localised changes in membrane

lipid composition to release otherwise membrane bound ITAM residues[179], which is thought to shield these regions from spontaneous phosphorylation[176]. These findings provide a plausible mechanism for how TCR-CD3 ligation may induce release of ITAMs from the membrane, to permit receptor phosphorylation and induce TCR triggering. With this in mind, it is conceivable that dynamic force application to the TCR-CD3 complex may induce localised conformational changes that reveal ITAM residues and make them accessible for phosphorylation. These phosphorylation events may then permit or enhance TCR reorganisation into signalling active TCR-MCs. Importantly, in the aforementioned reports, whilst calcium signalling was blocked by PP2 treatment, TCR ligation induced changes in lipid compositions to initiate ITAM release were still found to occur in the presence of the Src kinase inhibitor[179]. This is important as it suggests that ITAM release from the membrane is independent of TCR phosphorylation and suggests that this event is upstream of both TCR phosphorylation and TCR-MC formation, where the latter is shown to be TCR phosphorylation dependent in our hands.

Finally, to probe the question as to whether upstream mechanical changes in the TCR-CD3 complex govern TCR-MC formation, it will be important to compare dynamic force application as achieved with MICA, with static force application using stationary magnets and fixed magnetic fields of the same field strength (i.e., comparing the same oscillatory magnetic set up as described with MICA, with an identical field profile in a non-oscillatory mode to achieve a 'static' magnetic field). In this scenario, dynamic force application via MICA may induce TCR-CD3 conformational changes that govern TCR-MC formation as proposed, whereas static magnetic fields may not induce the same magnetic pull on the receptor and therefore may not induce mechanical stresses on the receptor in the same manner, but may still induce TCR clustering by dragging receptors through the lipid

membrane[292,311]. Therefore, comparison of the ability of $CD4^+$ T cells to express Nr4a3 in response to functionalised MNPs and either dynamic MICA force application or static magnetic fields will reveal whether dynamic force application is required to induce T cell activation. If differences are observed, where static magnetic fields may be expected to induce lower levels of T cell activation, it would be important to follow this up by comparing TCR-MC formation with both modes of magnetic force application to investigate whether dynamic force application does control TCR-MC formation. Finally, if this was again found to be the case, this would provide direct evidence for mechanical manipulation of the TCR-CD3 complex to permit TCR-CD3 phosphorylation and TCR-MC formation. The exact conformational mechanism involved in this could then be investigated, where Förster resonance energy transfer (FRET) experiments between ITAM residues and the membrane, as described by others[179], would be a sensible starting point to investigate whether dynamic force application can induce ITAM release from the membrane.

4.9.3 Comparisons of Normal and Shear Motion Applications

The data within this chapter also suggest that whilst normal force application with MICA induces concurrent TCR downregulation and T cell activation, application of shear motions on the particle with the Halbach array fails to induce either event (figures 4.15-4.16). We hypothesize that this is a direct consequence of the different mode of magnetic field applications between the two methods. Force application with MICA can be considered dynamic and unidirectional, as the magnetic field oscillates beneath a tissue culture plate and hence provides a normal force, perpendicular to the tissue culture plate. We provide evidence that force application by MICA induces TCR mobilisation toward the direction of the magnetic field, and concurrently induces T cell activation. This mode of magnetic field

application is in contrast to the Halbach array, which exists as a continually rotating magnetic field, where the direction of the magnetic field is constantly changing as described in 2.11. Therefore, we hypothesize that reorganisation of the TCR is not induced via the Halbach array to the same degree as it is with force application via MICA, and therefore does not permit TCR signalling. Certainly, TCR downregulation comparisons between the two modes of force application would support this hypothesis. This hypothesis is summarised in figure 4.28.

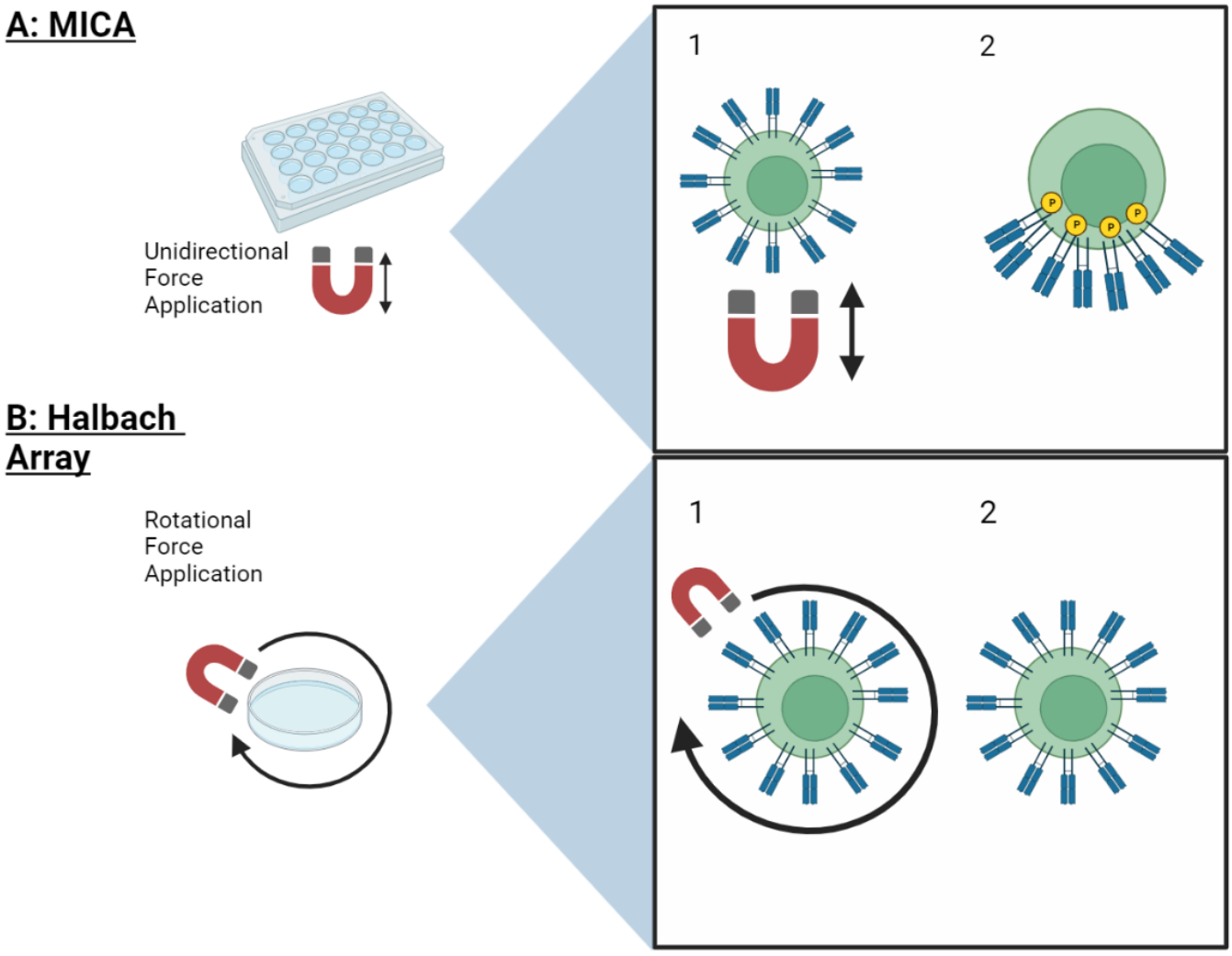


Figure 4.278 - Hypothesis for differential signalling responses with normal and shear force application. Normal force application was found to induce substantial TCR remodelling and TCR downregulation, hereby inducing a population of TCRlo activation marker+ $CD4^+$ T cells. Shear motion of the MNPs via application of the Halbach array however failed to induce TCR downregulation, suggestive of a lack of signalling permitting TCR re-organisation. Arrows indicate directional movements of magnetic fields. Image created in BioRender.

4.9.4 Concluding Remarks and Future Experimentation

This chapter presents a body of data where force manipulation of the TCR is able to induce membrane TCR reorganisation and initiate TCR signalling. We provide evidence for a number of hallmarks of immune synapse formation in our force application protocol, namely TCR-MC formation, TCR downregulation and CD45 exclusion. Therefore, it may be considered that pseudo-synapse formation through force manipulation of the TCR may promote force induced TCR signalling and T cell activation.

Interestingly, the kinetics of TCR cluster formation identify that force induced cluster formation occurs as early as with 5 minutes of force application (figure 4.26), whilst TCR downregulation kinetics highlight that internalisation of the TCR accumulates over the course of time course (figures 4.3 and 4.8). Therefore, it will be important to investigate the kinetics of CD45 exclusion, to identify its impact on either initiating or sustaining TCR signalling. For instance, whilst we show that CD45 exclusion occurs with 60 minutes of force application, if this is also found to occur at earlier time points then it may be possible that re-organisation of the TCR with respect to negative phosphatases such as CD45 is the trigger for force induced TCR signalling. The fact that cluster formation is abolished with the addition of PP2 may support this hypothesis, as it suggests a role for the kinase-phosphatase balance in the formation of signalling active TCR clusters. These hypotheses may be interrogated with in depth imaging, utilising techniques such as multi-colour SMLM to track the kinetics of TCR and CD45 membrane localisation with respect to one another.

Finally, investigation as to whether accumulation of TCR downregulation along the course of 60 minutes of force application (figures 4.3 and 4.8) contributes to the build-up of NFAT pathway signalling events that permit Nr4a3 expression will be of importance to fully

understand TCR triggering mechanisms in response to force. Previous evidence has suggested that following internalisation, endosomal TCR molecules may still be signalling active through the passive internalisation and subsequent co-localisation with membrane tethered Src family kinases such as Lck[116,312]. Therefore, it may be plausible that continual internalisation of signalling active TCR molecules in response to force application causes a build-up of intracellular signalling events, which also may act via segregation of these molecules from negative phosphatases, eventually reaching thresholds required for NFAT nuclear localisation and Nr4a3 expression.

CHAPTER 5

5 Force Modulated Signal 1 Strength – Effect on CD4$^+$ T Cell Phenotype and Function

5.1 Introduction

Data shown thus far outlines a platform whereby force application to the TCR can influence CD4$^+$ T cell signalling and activation, by promoting membrane TCR reorganisation and signalling events leading to T cell activation. We have shown that force application to anti-CD3 functionalised MNPs can increase the observed TCR signalling strength, as measured by Nr4a3, CD69 and CD25 upregulation and subsequent CD4$^+$ T cell proliferation (as discussed in chapter 3). The role of TCR signal strength in controlling phenotype and effector function of peripheral CD4$^+$ and CD8$^+$ is becoming increasingly well studied. Broadly, weak TCR signals have been suggested to promote functionally inert anergic phenotypes[313] whilst persistent strong TCR signals can promoted the emergence of exhausted or altered T cell phenotypes, often characterised by a loss of T cell effector function[313–315]. This role for TCR signal strength in controlling effector function has recently been well characterised for CD8$^+$ T cells in murine cancer models, whereby use of a SV40 large T antigen epitope 1 (TAG) mouse tumour model showed that neither high or low signal strength TCR interactions promoted *in vivo* tumour control, whereby low TCR signal strength promoted a state of functional inertia whilst high signal strengths resulted in co-inhibitory receptor upregulation and promoted tumour immune escape[313]. Interestingly, CRISPR-Cas9 based approaches to fine tune *in vivo* TCR signal strength, achieved by the authors through modulation of the CD8 co-receptor, permitted improved anti-tumoral activity and hence suggests the

preference for an intermediate TCR signalling strength for robust effector function in this model[313].

This role for TCR signal strength in controlling effector function has also been established for $CD4^+$ T cells. Trefzer and colleagues utilised a mouse model in which expression of the moth cytochrome c (MCC) peptide MCC_{93-103} can be regulated in DCs for presentation by H-$2E^k$, achieved through treatment with doxycycline (DOX). In this model, titration of the levels of DOX treatment hence regulates MCC_{93-103} presentation, allowing for control of *in vivo* signal strength to adoptively transferred AND TCR transgenic T $CD4^+$ T cells (AND T cells). Here, authors show that exposure to increasing antigen over a period of 10 days correlated with a loss of effector function measured by IL2, TNFα and IFNγ production, whilst these same cells also began to upregulate co-inhibitory receptors PD-1, Lag3 and CD200[315]. Highest levels of antigen exposure in this model (achieved using mice that constitutively express high levels of MCC in DCs) also correlated with a loss of surface TCR expression, which could be detected as early as 2.5 days post transfer. Modulation of TCR expression has also been proposed elsewhere as a mechanism for the emergence of altered T cell phenotypes[314]. C24 and C7 mouse models express transgenic TCRs which recognise the mycobacterial antigen $ESAT6_{1-20}$ with differing avidities[316,317] (C24 $CD4^+$ T cells have a high avidity for ESAT6, whilst C7 $CD4^+$ T cells have a low avidity for ESAT6). C24 and C7 T cells were polarised *in vitro* into Th1 T cells and transferred into host mice infected with *Mycobacterium tuberculosis* (*M. tuberculosis*). Interestingly, C24 Th1 T cells controlled the infection to a much poorer degree than C7 Th1 T cells, which the authors associated with persistent TCR downregulation of the high avidity C24 TCR[314]. Loss of effector function in C24 Th1 T cells correlated closely with loss of TCR expression yet was largely recovered through bypassing the TCR with PI treatment.

Given the wealth of evidence for TCR signal strength in governing effector function, we aimed to determine the effect of force modulated TCR signal strength on $CD4^+$ T cell phenotype in our magnetic force application protocol. Interestingly, where signal 1 strength is originally sub-optimal (in the context of stimulation with $250nm^{Mid}$ or $1\mu m^{Mid}$ MNPs), $CD4^+$ T cells are able to respond to rechallenge with peptide and APC as expected, and express low levels of co-inhibitory receptor in response to force manipulation of the original TCR stimuli. Conversely, use of $1\mu m^{Hi}$ MNPs to provide higher signal 1 strengths promotes an anergic response when rechallenged with APC and peptide, and $CD4^+$ T cells stimulated with $1\mu m^{Hi}$ MNPs and magnetic force upregulated numerous co-inhibitory receptors including CTLA-4 and Tigit.

We also observed that in line with previous studies, FoxP3 expression negatively correlated with TCR signal strength, whereby stimulation of $CD4^+$ T cells with $1\mu m^{Hi}$ MNPs induced a loss of FoxP3 expression, whilst use of $1\mu m^{Mid}$ MNPs promoted an outgrowth of $CD4^+$ $FoxP3^+$ T cells, which were partially lost through upregulation of signalling strength with force application. Finally, we attempted to address whether either phenotype induced here ($CD4^+$ $FoxP3^+$ co-inhibitory receptor low T cells produced through stimulation with $1\mu m^{Mid}$ MNPs, or $CD4^+$ $FoxP3^-$ co-inhibitory receptor high T cells produced through stimulation with $1\mu m^{Hi}$ MNPs) could induce immune suppression of the naïve Tg4 $CD45.1^+$ $CD4^+$ T cell response in co-culture assays. These experiments reveal the complex mechanisms involved in immune suppression; whereby low levels of suppression are observed from either induced $CD4^+$ phenotype albeit through potentially distinct suppressive pathways. This chapter therefore aims to investigate the effect of TCR signal strength on $CD4^+$ T cell phenotype and probe the therapeutic potential of the resulting induced phenotypes.

5.2 Force Modulation of Activation Marker and Co-Inhibitory Receptor Expression

To assess the effect of magnetic force application on $CD4^+$ T cell phenotype, $CD4^+$ T cells purified from Tg4 mice were treated with $250nm^{Mid}$ anti-CD3 MNPs, or $1\mu m^{Mid}$ or $1\mu m^{Hi}$ MNPs in the presence or absence of 1 hour external magnetic force as per methods section 2.7. Cells were then maintained in exogenous IL-2 until day 3 and restimulated with APC and 4K peptide for 24 hours as described in 2.13. $CD4^+$ T cell phenotype was then assessed via surface expression of CD69 (figure 5.1) together with various co-inhibitory inhibitors including CTLA-4, Tigit and PD-1 (figures 5.3-5.5).

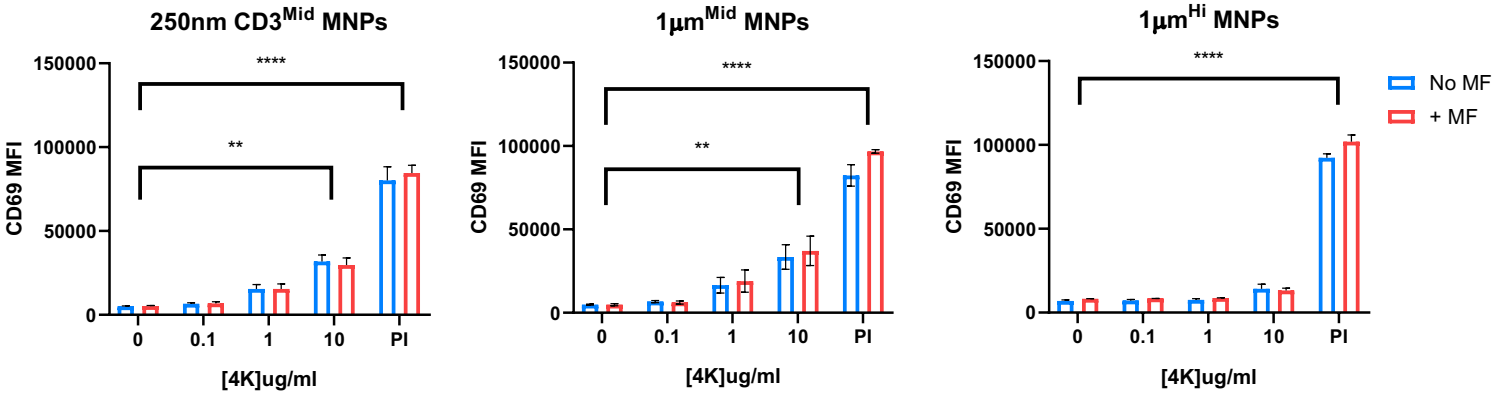


Figure 5.1 - High signal 1 strength MNPs induce an anergic phenotype upon restimulation through the TCR. $CD4^+$ Tg4 T cells were stimulated with anti-CD3 functionalised MNPs as shown and subjected to +/- 1 hour of magnetic force (MF). Cells were maintained in the presence of 20U/mL IL-2 for 72 hours, before restimulation with B10.PL splenocytes and 4K peptide at concentration shown as per 2.13. T cell reactivation was assessed 24 hours post restimulation by surface CD69 expression. Data shown from at least 3 independent experiments for each MNP. Significance assessed via two-way ANOVA with Tukey's post-test comparisons.

When analysing expression of CD69 upon restimulation with APC and peptide, we found a clear anergic phenotype correlating with the original signal 1 strength during the first round of stimulation (i.e., correlating with the level of anti-CD3 antibody coated onto the particle surface). When $CD4^+$ T cells were originally stimulated with lower signal 1 strength MNPs ($250nm^{Mid}$ anti-CD3 MNPs and $1\mu m^{Mid}$ MNPs), we found that these cells were able to

respond to peptide rechallenge 72 hours later (figure 5.1). It should be noted that these particles are termed 'low signal 1 strength' MNPs due to the fact that without magnetic force application, they induce generally low levels of T cell activation (as measured by Nr4a3, CD69, CD25 expression and cell proliferation in chapter 3), and because we have directly observed low levels of CD3 bound to the particle surface when measuring this by flow cytometry (chapter 3, figure 3.10A-B). However, when $CD4^+$ T cells were stimulated with $1\mu m^{Hi}$ MNPs, we found that this increase in signal 1 strength by increasing the level of particle bound anti-CD3 antibody promoted an anergic phenotype at day 3 when cells were stimulated through their TCR by re-challenge with 4K peptide and APC (figure 5.1). However, bypassing of the TCR at the point of re-stimulation through the use of PI recovered the ability of these cells to express the T cell activation marker CD69.

Assessment of cytokine production 24 hours post restimulation with APC and peptide also showed that upon stimulation with 1µm high dose CD3 MNPs, $CD4^+$ T cells were then entirely blocked in their ability to secrete IL-2 in response to peptide rechallenge (figure 5.2). Secretion of IFNγ also followed a similar trend albeit to a lesser extent, as cells appeared to secrete low levels of IFNγ in response to peptide rechallenge. However, antigen sensitivity by means of measuring IFNγ secretion lower for $1\mu m^{Hi}$ MNP stimulated cultures when compared with $1\mu m^{Mid}$ MNPs. This is largely a result of the increased levels of IFNγ secretion in the absence of peptide for these $CD4^+$ T cells, indicating that IFNγ production as measured by ELISA in these restimulation experiments is still being driven by the initial MNP mediated stimulation (i.e., round 1 stimulation). However, the lack of IL-2 production in response to peptide in high dose CD3 stimulated $CD4^+$ T cells when compared with low dose CD3 stimulated groups is unequivocal.

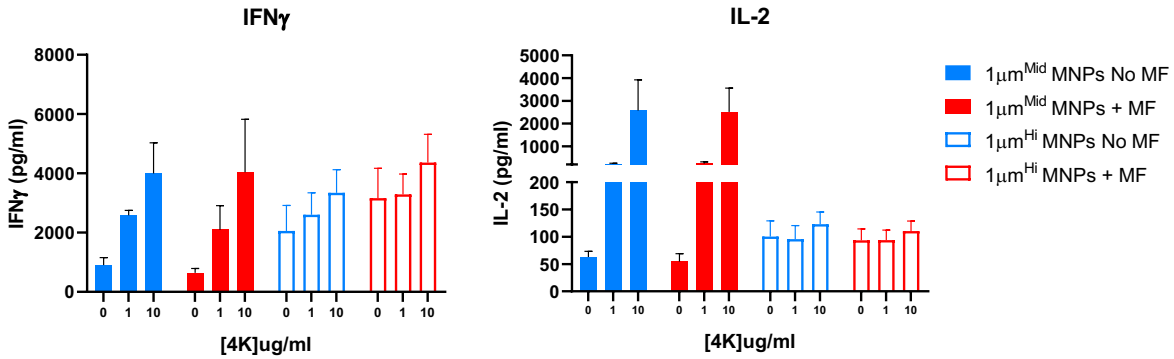


Figure 5.2 – Stimulation with 1μm^{Hi} MNPs alters IL-2 and IFNγ secretion upon rechallenge with APC and peptide. Following stimulation with 1μm MNPs and magnetic force for 1 hour as shown, CD4$^+$ Tg4 T cells were maintained in culture in 20U/mL IL-2 for 72 hours. CD4$^+$ T cells were then restimulated with APC and 4K peptide as per 2.13 for 24 hours prior to supernatant harvesting. Secretion of IFNγ and IL-2 was assessed by ELISA as per 2.14. Stimulation of CD4$^+$ T cells with 1μm^{Hi} MNPs blocks IL-2 and IFNγ secretion in response to peptide restimulation.

Expression of co-inhibitory receptors also showed an intriguing correlation with signal 1 strength. We again found that when CD4$^+$ T cells were initially stimulated with lower signal 1 strength MNPs (250nm^{Mid} anti-CD3 MNPs and 1μm^{Mid} MNPs), expression of co-inhibitory receptors Tigit, CTLA-4, PD-1 and Lag 3 was relatively low when analysed in the same peptide rechallenge experiments as per figures 5.3 and 5.4. Where expression of Tigit and PD-1 was observed in these experiments, this was solely dependent on rechallenge with peptide and was expressed in a dose dependent manner. Therefore, expression of Tigit and PD-1 in low signal 1 strength MNP conditions relies on antigenic strength at the point of restimulation and is not influenced by the antigenic strength during the initial stimulation with MNPs and force.

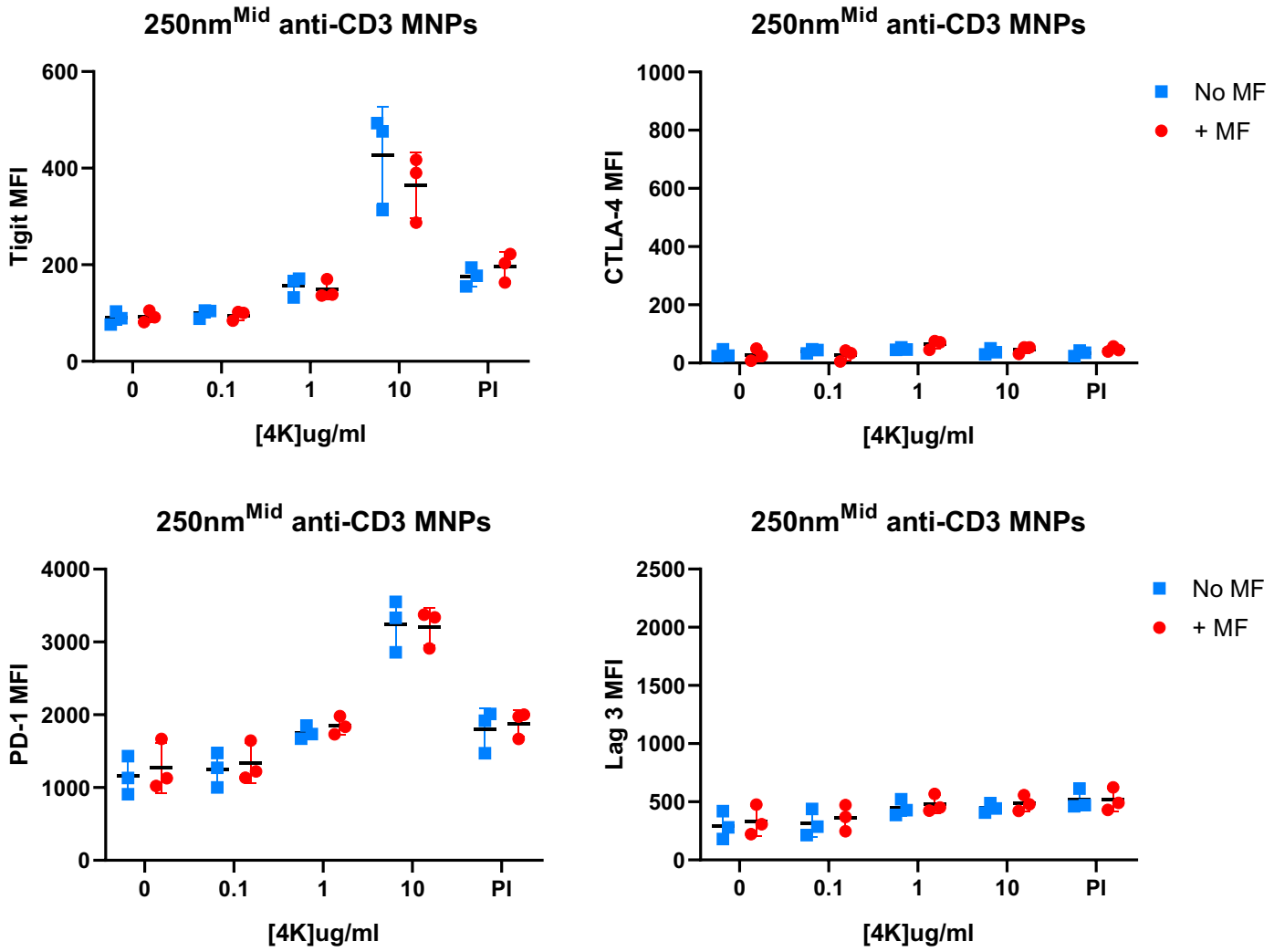


Figure 5.3 – Co-inhibitory receptor expression on CD4⁺ T cells stimulated with 250nm^{Mid} anti-CD3 MNPs is dependent on peptide concentration at the point of restimulation. CD4⁺ T cells stimulated with 250nm^{Mid} anti-CD3 MNPs +/- 1 hour magnetic force (MF) were restimulated after 72 hours with APC and 4K peptide as per 2.13. Surface CD4⁺ T cell phenotype was assessed 24 hours post restimulation by flow cytometry. Where co-inhibitory receptor expression was observed, this was driven by presence of antigen at restimulation. Data from 3 independent experiments.

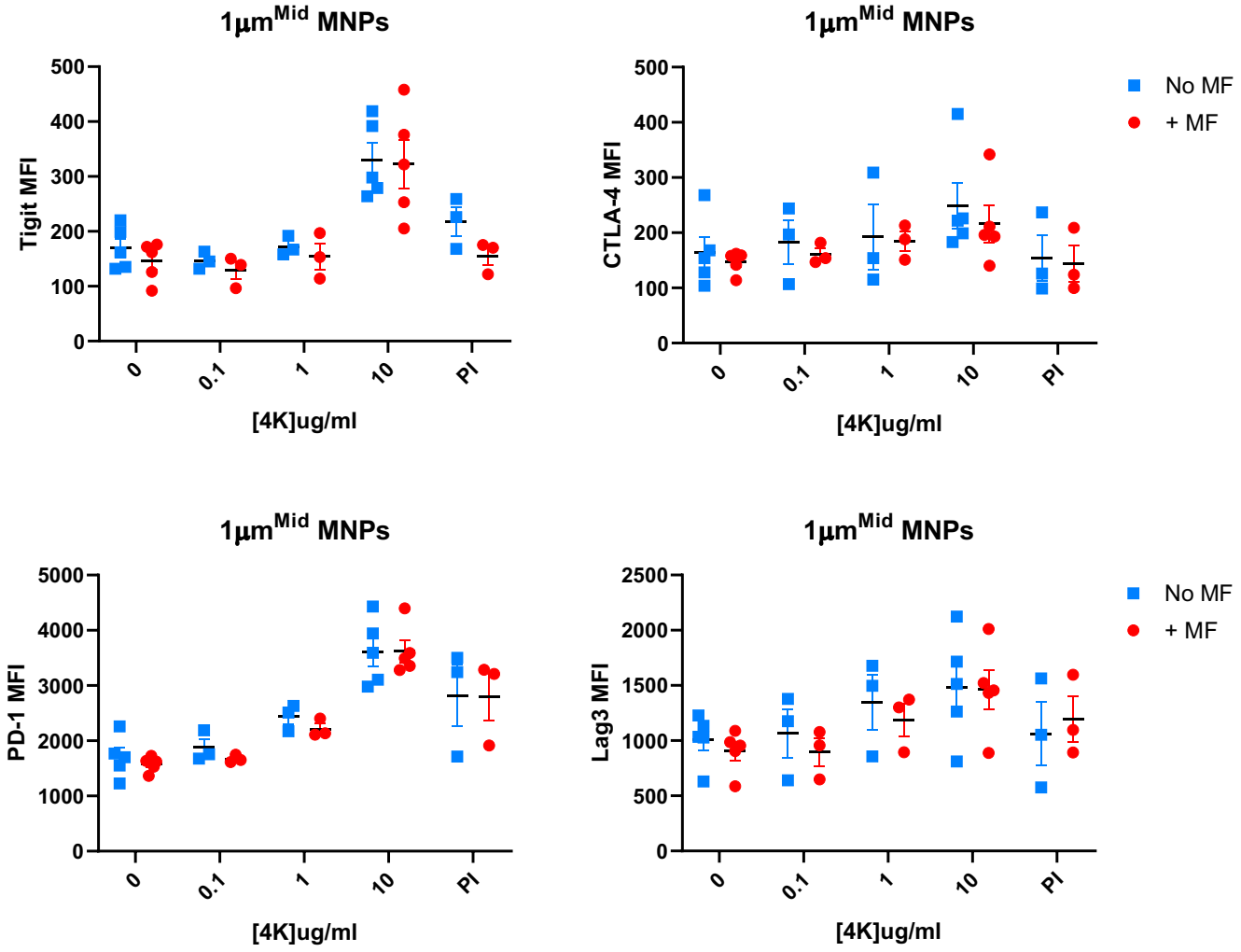


Figure 5.4 – Stimulation of CD4⁺ T cells with 1µm^{Mid} MNPs fails to induce robust co-inhibitory receptor expression. CD4⁺ T cells stimulated with 1µm^{Mid} MNPs +/- 1 hour magnetic force (MF) were restimulated after 72 hours with APC and 4K peptide as per 2.13. Surface CD4⁺ T cell phenotype was assessed 24 hours post restimulation by flow cytometry. Co-inhibitory receptor expression was driven in a peptide-dependent manner upon restimulation. Data shown from at least 3 independent experiments.

However, expression of co-inhibitory receptors in conditions stimulated with high signal 1 strength (1µm^{Hi}) MNPs promoted clear peptide independent expression of these co-inhibitory receptors (figure 5.5), evidenced by the lack of a dose dependent increase in expression and by substantially increased expression detected in the 0µg/mL 4K conditions when compared with the low signal 1 strength MNPs (0µg/mL conditions, figures 5.4 vs 5.5). Finally, we also saw a striking upregulation of Tigit, CTLA-4 and PD-1 upon 1 hour of force application to CD4⁺ T cells treated with 1µm^{Hi} MNPs (figure 5.5). These observations strike a

seemingly intriguing parallel with the T cell activation profiles displayed in chapter 3 and 4, where force application to these particles induced a significant downregulation in activation marker expression and proliferation (figures 3.9 and 3.23-3.24 respectively), whilst stimulation with the particles alone was sufficient to induce a rapid loss of TCR expression (figures 4.6-4.7). Therefore, there is mounting evidence for use of these 1µm MNPs functionalised with a high dose of CD3 antibodies to promote the induction of anergic $CD4^+$ phenotypes, and evidence clearly suggests that further increase of this signal 1 strength by applying external magnetic forces can modulate expression of co-inhibitory receptors.

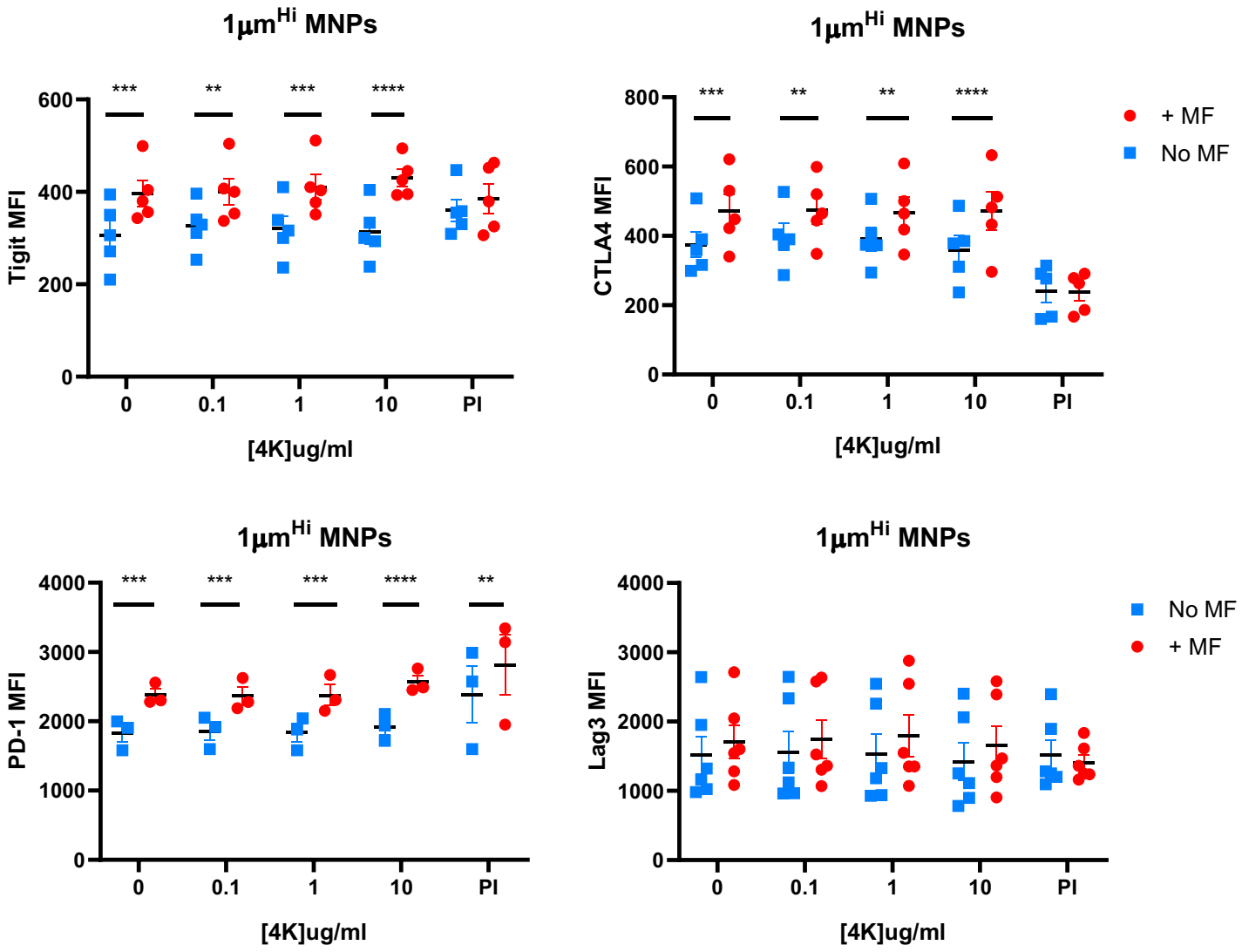


Figure 5.5 – Stimulation of CD4⁺ T cells with 1µm^{Hi} MNPs induces robust co-inhibitory receptor expression which is further upregulated by force application. CD4⁺ T cells were stimulated with 1µm^{Hi} MNPs +/- 1 hour of magnetic force (MF) and maintained in the presence of 20U/mL IL-2 for 72 hours before restimulation with APC and peptide for 24 hours and assessment of CD4⁺ T cell phenotype as per 2.13. Data shown from at least 3 independent experiments. Significance assessed via two-way ANOVA with Sidak's post-tests. Tigit, left to right: *** p=0.0005, ** p=0.0034, *** p=0.0005, **** p<0.0001. CTLA-4 left to right: *** p=0.0003, ** p=0.0032, ** p=0.0038, p<0.0001. PD-1, left to right: *** p=0.0001, *** p=0.0003, *** p=0.0002, **** p<0.00001, ** p=0.0012.

Whilst we found clear evidence for force induced upregulation of co-inhibitory receptors in the context of 1µm^{Hi} MNPs when measured by MFI (figure 5.5), we next assessed whether these co-inhibitory receptors are expressed by the same population of CD4⁺ T cells by measuring the percentage of CD4⁺ T cells double positive for Tigit and CTLA-4, and then investigated PD-1 expression within this double positive population. Figure 5.6 provides

clear evidence for an upregulation in CD4^{+} CTLA-4^{+} Tigit^{+} cells with force application to 1µm^{Hi} MNPs, whilst induction of a double positive population arising from stimulation with 1µm^{Mid} MNPs was not significant.

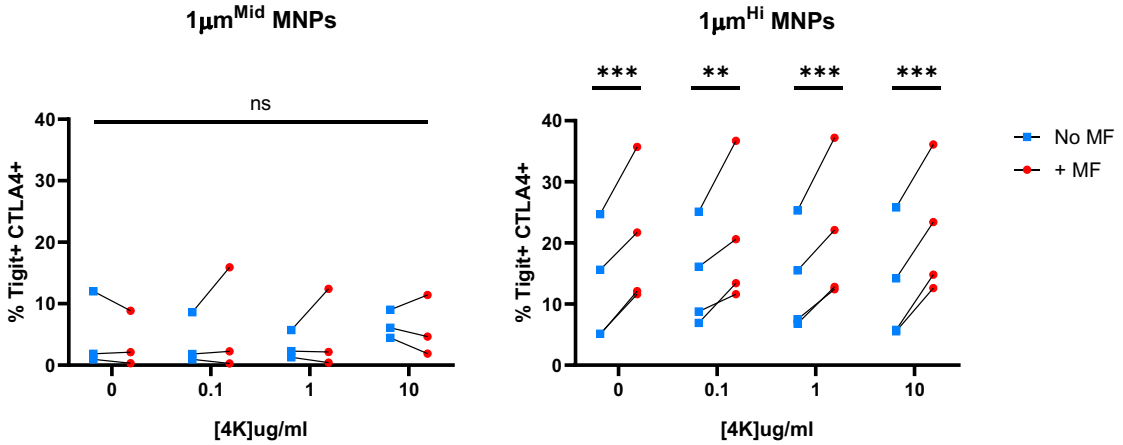


Figure 5.6 – Force application to 1µm^{Hi} MNPs increases co-expression of CTLA-4 and Tigit. CD4^{+} T cells were treated with 1µm^{Mid} MNPs (left) or 1µm^{Hi} MNPs (right) before force application for 60 minutes. Cells were maintained in the presence of 20U/mL IL-2 for 3 days, before restimulation for 24 hours as described in 2.13. Cells were then analysed for co-expression of surface Tigit and CTLA-4 by flow cytometry. Data shown from three (low dose CD3) or four (high dose CD3) independent experiments. Significance assessed by two-way ANOVA with Sidak's post-tests. 1µm^{Hi}, left to right: *** p=0.0006, ** p=0.0026, *** p=0.0008, *** p=0.0001.

Interestingly, whilst approximately 90% of CD4^{+} Tigit^{+} CTLA-4^{+} T cells were found to be PD-1 positive across all conditions (figure 5.7), we found that PD-1 expression was upregulated with increasing peptide dose when cells had been stimulated with 1µm^{Mid} MNPs only. A similar peptide dose dependent increase in PD-1 expression was not found in CD4^{+} T cells that were stimulated with 1µm^{Hi} MNPs (figure 5.7). This result may reflect the suggestion that PD-1 expression follows an activatory marker-like pattern, influenced by strength of TCR signal[318]. Therefore, the inability of CTLA-4^{+} Tigit^{+} CD4^{+} T cells from the 1µm high dose CD3 conditions to upregulate PD-1 in response to peptide antigen strikes an intriguing parallel with the CD69 data upon restimulation, and hence suggests a defect in

TCR signalling upon restimulation among CD4^{+} T cells previously stimulated with 1µm^{Hi} MNPs.

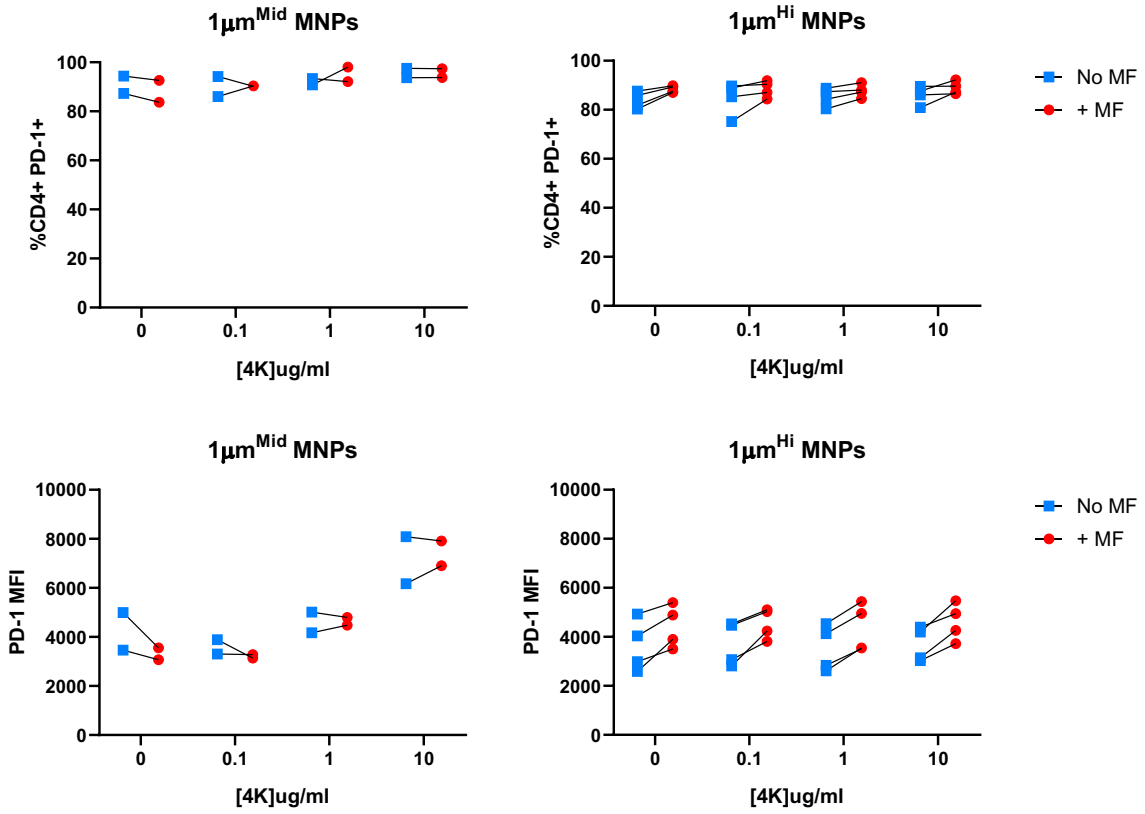


Figure 5.7 – PD-1 expression gated on CTLA-4^{+} Tigit^{+} CD4^{+} T cells identifies that PD-1 expression correlates with T cell activation. CD4^{+} T cells were stimulated with 1µm^{Mid} or 1µm^{Hi} MNPs +/- magnetic force (MF) and restimulated at day 3 with APC and peptide as per 2.13. PD-1 expression was determined on CD4^{+} CTLA-4^{+} Tigit^{+} cells, revealing that >80% of CTLA-4^{+} Tigit^{+} CD4^{+} T cells also co-expressed PD-1. PD-1 expression increased in a peptide dose dependent manner in 1µm^{Mid} MNP stimulated cultures, whilst this response was blocked in 1µm^{Hi} MNP stimulated cultures. Data shown from 2 (1µm^{Mid}) or 4 (1µm^{Hi}) independent experiments.

5.3 Exogenous IL-2 Fails to Reverse the High Signal 1 Strength Induced Anergic Phenotype

Previous studies have suggested that in its simplest form, establishment of an anergic phenotype is linked to an inability of T cells to produce IL-2 and is hence reversed by the presence of other IL-2 producing cells or through provision of exogenous IL-2[76,77,82]. We therefore investigated whether provision of exogenous IL-2 could reverse the anergic

phenotype observed when $CD4^+$ T cells were stimulated with $1\mu m^{Hi}$ MNPs (figures 5.1-5.2). Figure 5.8 indicates that despite provision of 20U/mL exogenous IL-2 during the 24 hour restimulation with APC and peptide, $CD4^+$ T cells stimulated with these high signal 1 strength MNPs still displayed a non-responsive, anergic phenotype upon restimulation when assessed by both CD69 and CD25 expression. We found that as previously shown (figure 5.1), CD69 expression in response to peptide appeared to be completely blocked when compared to cells stimulated with $1\mu m^{Mid}$ MNPs, whilst low levels of CD25 expression were observed in response to 10µg/mL 4K. However, when comparing CD25 expression profiles between the two signal 1 strength MNPs upon restimulation with peptide, it is clear that an anergic phenotype is still apparent at concentrations of 1µg/mL 4K. Unsurprisingly, we also found large upregulations of CD25 expression in both low and high signal 1 strength MNP stimulated cultures driven by the provision of exogenous IL-2.

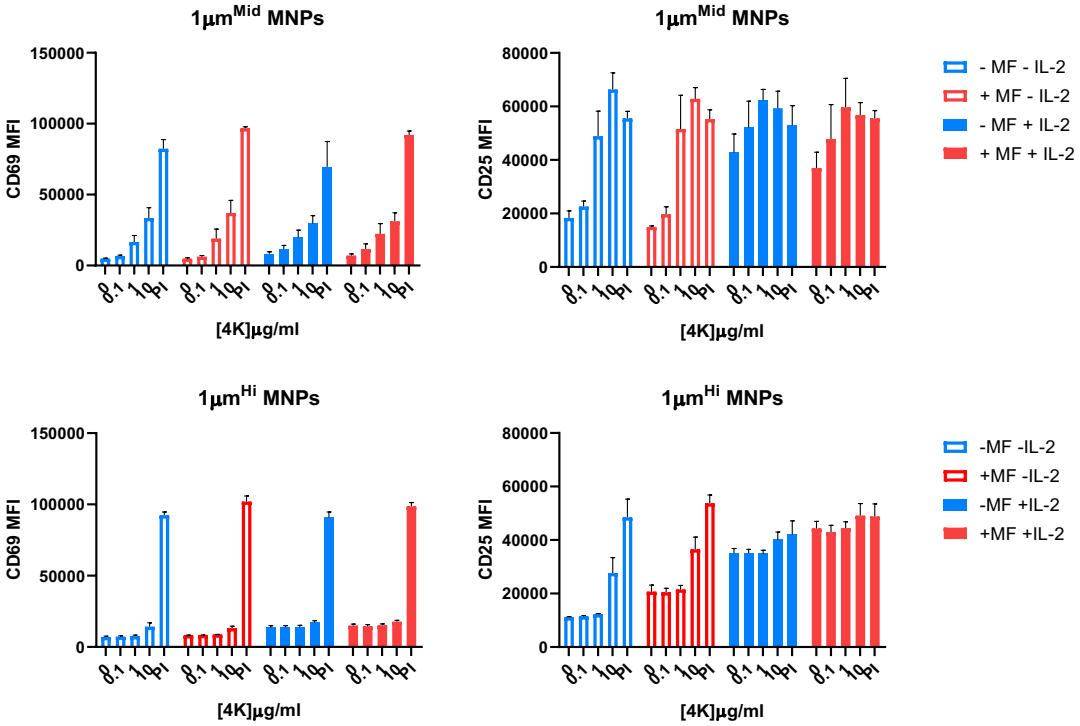


Figure 5.8 - Provision of exogenous IL-2 does not reverse the high signal 1 strength induced anergic phenotype. $CD4^+$ Tg4 T cells were stimulated with $1\mu m^{Mid}$ or $1\mu m^{Hi}$ MNPs +/- 1 hour magnetic force, and maintained out to 72 hours prior to restimulation as previously described. At the point of restimulation, 20U/mL exogenous IL-2 was also added as per 2.13. Assessment of $CD4^+$ T cell phenotype was determined 24 hours post restimulation. Data shown from at least 3 independent experiments.

5.4 Co-Inhibitory Blockade Fails to Reverse the High Signal 1 Strength Induced Anergic Phenotype

Given the striking force mediated increase in co-inhibitory receptor expression found through the use of $1\mu m^{Hi}$ MNPs, we sought to investigate whether expression of these co-inhibitory molecules at this time point modulates signalling through the TCR and gives rise to the anergic phenotype observed when these $CD4^+$ T cells were restimulated with the 4K peptide. To this end, we investigated the use of CTLA-4 blocking antibodies on the ability of the cells to respond to peptide. As previously described (see section 1.5), CTLA-4 is a co-inhibitory receptor that exerts its negative effects on TCR signalling and T cell activation through competition for binding of CD80 and CD86 on the APC cell surface[86,87,91]. Surface

expression of CD80 and CD86 on the surface of the PL8 cell line (a H-2^u expressing B cell lymphoma, and is the APC used in these restimulation experiments) is shown in appendix figure 8.6. $CD4^+$ T cells, treated with functionalised MNPs with or without magnetic force as previously, were treated with 2µg/mL anti-CTLA-4 blocking antibody for 2 hours at 37°C prior to the restimulation of these cells with APC and 4K. Figure 5.9 shows that as per previous experiments, the expression of both CTLA-4 and Tigit was upregulated in response to force application during initial T cell stimulation, and that CTLA-4 blockade was successful, evidenced by the decreased MFI upon surface staining with the same clonotype antibody (i.e., both the blocking antibody and staining antibody are the UC10 clone). However, despite successful CTLA-4 blockade, CD69 expression in response to peptide was not restored at any 4K concentration tested (figure 5.9).

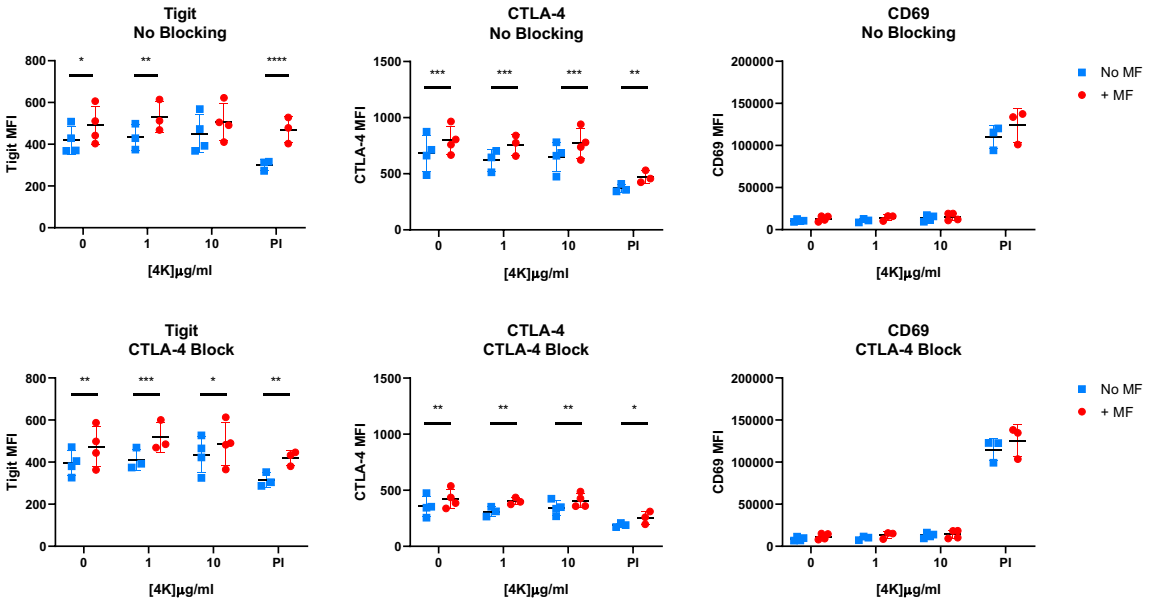


Figure 5.9 - CTLA-4 blockade does not restore ability to respond to restimulation through the TCR. $CD4^+$ T cells were stimulated with $1\mu m^{Hi}$ MNPs +/- magnetic force for 1 hour as previously described and maintained in culture for 72 hours in the presence of 20U/mL IL-2 before restimulation as per 2.13. At the point of restimulation, the effect of CTLA-4 blocking antibodies were assessed as described in 2.13.1. Data shown from 3 independent experiments. Statistical analysis assessed via two-way ANOVA with Sidak's post-tests. Tigit no blocking, left to right: * p=0.0161, ** p=0.0055, **** p<0.0001. CTLA-4 no blocking, left to right: *** p=0.0003, *** p=0.0002, *** p=0.0002, ** p=0.0023. Tigit with CTLA-4 block, left to right: ** p=0.0035, *** p=0.0009, * p=0.0374, ** p=0.001. CTLA-4 with CTLA-4 block, left to right: ** p=0.0044, ** p=0.0013, ** p=0.0063, * p=0.0139.

In line with a lack of CD69 re-expression in response to peptide stimulation, we also found that treatment of $CD4^+$ T cells with CTLA-4 blocking antibodies failed to restore IFNγ or IL-2 production when measured by ELISA in the supernatant 24 hours post restimulation (figure 5.10).

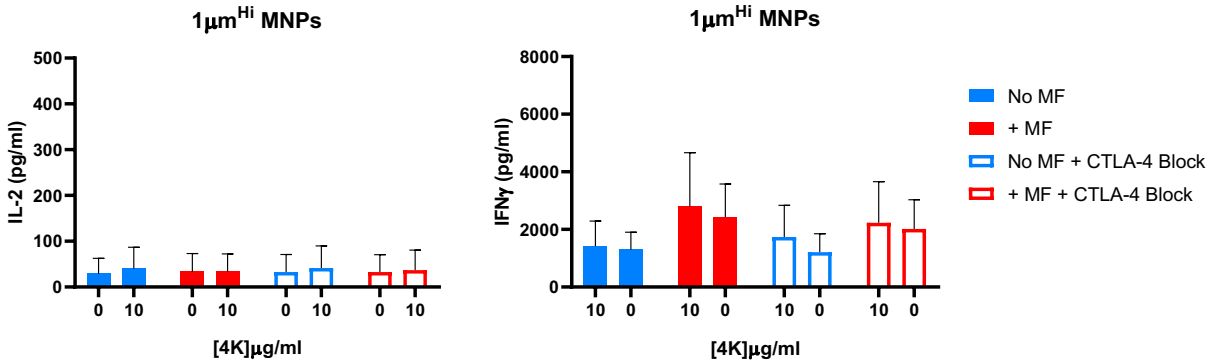


Figure 5.10 - CTLA-4 blockade does not restore IFNg or IL-2 production in response to TCR stimulation. Supernatants harvested at 24 hours post restimulation in CTLA-4 blockade experiments described in figure 5.9 were assessed for IL-2 (left) and IFNγ (right) secretion by ELISA as described in 2.14. Use of CTLA-4 blocking antibodies failed to restore IL-2 or IFNγ secretion that has been previously shown to be shut off in high dose CD3 1μm MNP stimulated $CD4^+$ T cells. Data shown from at least 2 independent repeats.

To assess the synergistic effect of expression of multiple co-inhibitory receptors on $CD4^+$ T cell activation, we investigated the ability of cells to respond to peptide with dual blockade of PD-1 and CTLA-4. These blocking antibody experiments were set up as previously described (see section 2.13.1), where cells were again treated with blocking antibodies for 2 hours before restimulation with APC and the 4K peptide. Surface staining with a fluorophore-conjugated antibody of the same clonotype as the blocking antibody again showed successful blockade of either co-inhibitory receptor. However, in line with results from CTLA-4 blockade experiments, blockade of PD-1 alone or both CTLA-4 and PD-1 failed to restore CD69 expression in response to TCR stimulation (appendix figure 8.7). Therefore, it is apparent that whilst expression of co-inhibitory receptors is modulated by force application, the inability of $CD4^+$ T cells to respond to restimulation with peptide is independent of expression of these co-inhibitory receptors.

5.5 Increased Antigenic Dose Reveals High Signal 1 Strength Induced Antigenic Insensitivity Upon Restimulation

To this point, data has revealed that stimulation of $CD4^+$ T cells with $1\mu m^{Hi}$ MNPs, which provide a high signal 1 strength during the first round of stimulation, promotes an anergic phenotype when restimulated with up to 10µg/mL 4K peptide 72 hours post initial stimulation, and that this phenotype is independent of IL-2 availability (figure 5.8) or co-inhibitory receptor expression (figure 5.9). Finally, we addressed whether further increase of the TCR signal strength at the point of restimulation would rescue CD69 expression (figure 5.11), and secretion of IL-2 and IFNγ (figure 5.12) in $CD4^+$ T cells that were initially stimulated with $1\mu m^{Hi}$ MNPs.

Interestingly, we find that as per previous experiments, 4K concentrations up to 10µg/mL failed to induce robust CD69 expression or IL-2 and IFNγ secretion in $CD4^+$ T cells stimulated with $1\mu m^{Hi}$ MNPs. Use of $1\mu m^{Mid}$ MNPs again showed a typical 4K-dose dependent titration curve when measuring CD69 expression post-restimulation (figure 5.11). Finally, a further 10-fold increase in 4K concentration rescued CD69 expression (figure 5.11), IFNγ secretion and small amounts of IL-2 secretion (figure 5.12) in $CD4^+$ T cells stimulated with $1\mu m^{Hi}$ MNPs. Interestingly, we found that despite requiring an increased 4K concentration at the point of restimulation to induce IFNγ secretion, once triggered, levels of IFNγ production in $CD4^+$ T cells stimulated with $1\mu m^{Hi}$ MNPs was approaching 2-fold higher than that of $CD4^+$ T cells stimulated with $1\mu m^{Mid}$ MNPs. Interestingly, this was not the case when measuring CD69 expression. These data indicate an increased signal 1 strength priming effect of $CD4^+$ T cells for IFNg production but not CD69 expression, which may reflect different threshold levels required for various T cell effector functions. However, all data to this point build a case for an anergic $CD4^+$ T cell phenotype induced by stimulation with high signal 1 strength

1μm^{Hi} MNPs, which is overcome by increasing antigenic strength upon restimulation, suggestive of a peptide insensitivity phenotype upon restimulation modulated by signal 1 strength during initial CD4^{+} T cell stimulation.

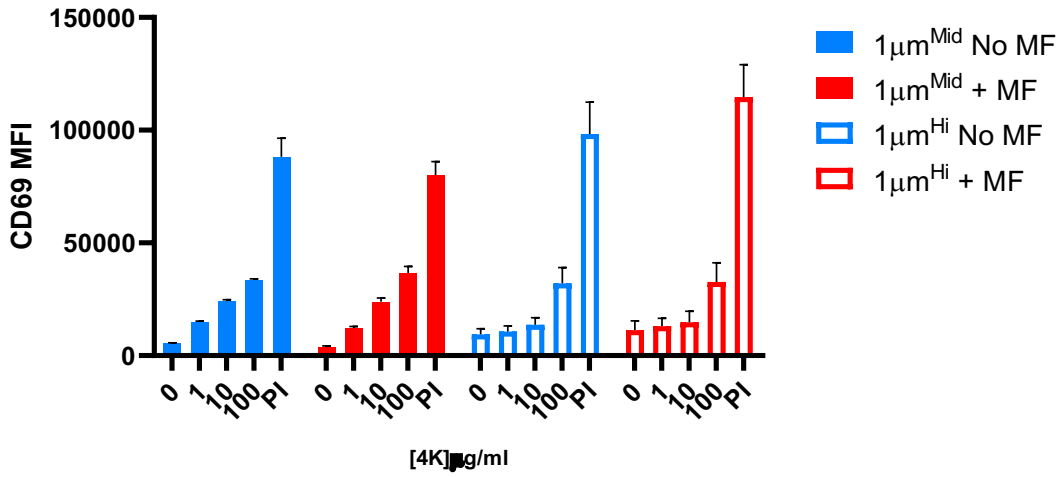


Figure 5.11 - CD69 expression via TCR stimulation is recovered by increased antigenic strength at restimulation in CD4^{+} T cells stimulated with 1μm^{Hi} MNPs. Following stimulation with 1μm^{Mid} or 1μm^{Hi} MNPs +/- magnetic force for 1 hour and maintenance of the culture in 20U/mL IL-2 for 72 hours, CD4^{+} T cells were restimulated with APC and 4K peptide at concentrations shown for 24 hours as per 2.13, before assessment of CD69 expression by flow cytometry. Data shown from 3 independent experiments. Increasing 4K concentration at the point of restimulation appeared to recover CD69 expression in response to peptide at the point of restimulation for 1μm^{Hi} stimulated cultures.

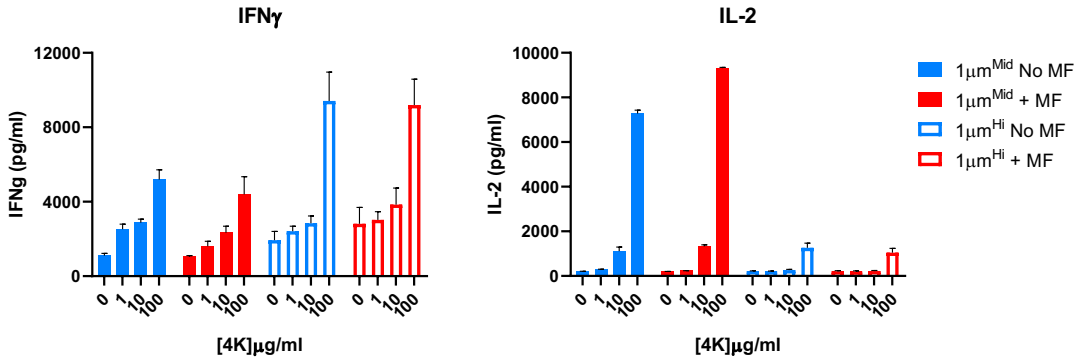


Figure 5.12 – Increased peptide concentration recovers IFNγ and IL-2 secretion in 1μm^{Hi} MNP stimulated CD4^{+} T cells. Supernatants harvested at 24 hours in restimulation experiments described in figure 5.11 were analysed for IFNγ (left) and IL-2 (right) secretion by ELISA as per 2.14. Data shown from 2 independent experiments. Increasing 4K concentration at the point of restimulation appeared to recover both IFNγ and IL-2 secretion in response to peptide at the point of restimulation for 1μm^{Hi} stimulated cultures.

5.5.1 Persistent TCR Downregulation Mediates the Antigen Insensitivity Phenotype

When taken together, the robust, magnetic force independent TCR downregulation observed in response to 1µm^{Hi} MNPs (figures 4.6-4.7, chapter 4) and the peptide insensitivity driven anergic phenotype found upon restimulation of these CD4^{+} T cells suggest that differential TCR expression between low- and high signal 1 strength stimulated cultures at the point of restimulation may drive the divergence of these phenotypes. Therefore, we hypothesised that TCR downregulation may persist *in vitro* and thus provide the basis for differential antigen sensitivity upon restimulation.

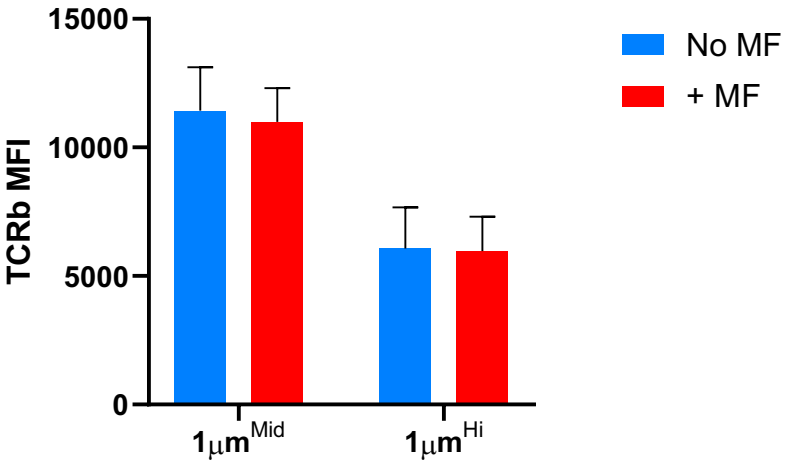


Figure 5.13 – TCR downregulation persists out to 72 hours in CD4^{+} T cells stimulated with 1µm^{Hi} MNPs. CD4^{+} T cells were stimulated with anti-CD3 1µm MNPs as shown, +/- 1 hour of magnetic force, before cell surface TCR expression was determined by flow cytometry as per 2.9.1 at 72 hours. Data shown from 3 independent experiments.

Figure 5.13 illustrates TCRβ MFI for CD4^{+} T cells 72 hours after treatment with 1µm^{Mid} or 1µm^{Hi} MNPs, ± 1 hour magnetic force application, which indicates that CD4^{+} T cells stimulated with 1µm^{Hi} MNPs express approximately 2-fold less TCR than their 1µm^{Mid} counterparts. This result suggests that given the early TCR downregulation data displayed in chapter 4 (figures 4.6-4.7, TCRβ expression analysed 4 hours post stimulation), re-expression of the TCR in CD4^{+} T cells stimulated with high signal 1 strength 1µm^{Hi} MNPs lags

behind that of those $CD4^+$ T cells stimulated with $1\mu m^{Mid}$ MNPs, and thus may mediate the altered peptide sensitivity of the anergic phenotype described in figures 5.8-5.12.

5.6 Immune Suppression Studies

5.6.1 Co-inhibitory receptor high $CD4^+$ T cells stimulated with $1\mu m^{Hi}$ MNPs fail to induce immune suppression at day 3

Given that data shown thus far indicates that force application to $1\mu m^{Hi}$ MNP stimulated $CD4^+$ T cells increases expression of multiple co-inhibitory receptors, we hypothesised that these cells may mediate the suppression of the immune response of other naïve Tg4 $CD4^+$ T cells. To assess this, co-culture experiments were set up as described in 2.15.1. In brief, $CD4^+$ T cells purified from the Tg4 mouse were first stimulated with $1\mu m^{Mid}$ or $1\mu m^{Hi}$ MNPs, in the presence or absence of magnetic force application for 1 hour at the start of the culture as per previous experiments. These cells, herein termed putative suppressors, were maintained in culture for 72 hours, before co-culture of viable cells from each condition with CTV labelled naïve $CD45.1^+$ Tg4 responders, APC and peptide. The number of putative suppressors was titrated across ratios of 1:1, 1:2 and 1:4 putative suppressors to naïve $CD45.1^+$ responders. Proliferation of the $CD45.1^+$ population was assessed 72 hours later by CTV dilution.

Figure 5.14 shows that despite the increased expression of co-inhibitory receptors on $1\mu m^{Hi}$ MNP stimulated putative suppressors, better immune suppression was observed when putative suppressors were produced with $1\mu m^{Mid}$ MNPs, as indicated by the decreased division index of the naïve $CD45.1^+$ responder population when co-cultured with the $1\mu m^{Mid}$ stimulated putative suppressors.

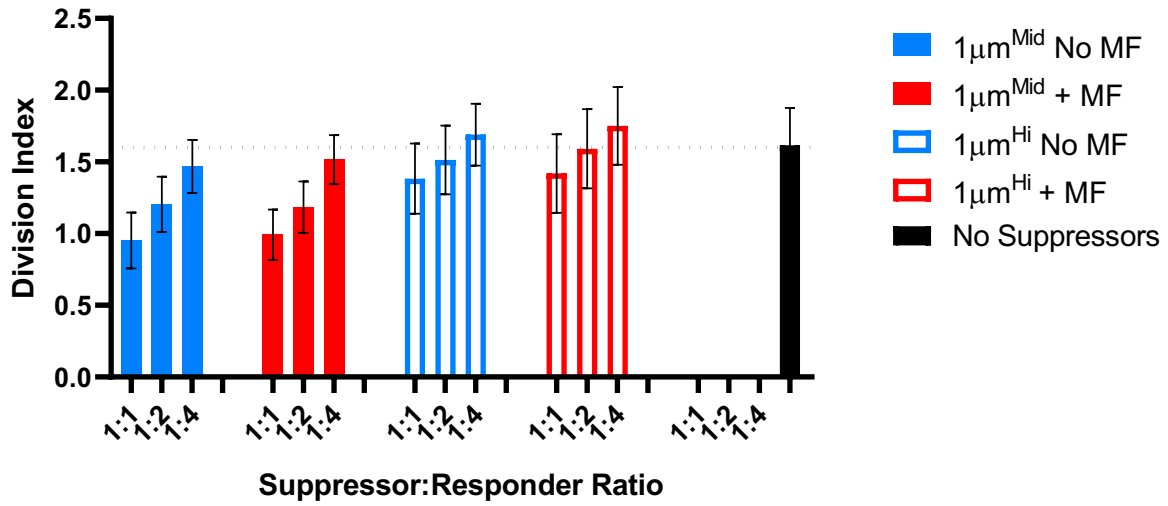


Figure 5.14 – Co-culture with 1μm:1μg stimulated putative suppressors mediates moderate immune suppression of naïve Tg4 CD45.1$^+$ CD4$^+$ T cells. Suppression assays using putative suppressors produced via stimualtion with 1μm^{Mid} or 1μm^{Hi} MNPs were performed as described in 2.15.1. Experiments shown here were performed after putative suppressors had been in culture for 72 hours. Co-culture of naïve Tg4 CD45.1$^+$ CD4$^+$ T cells with low signal 1 strength (1μm^{Mid} MNPs) stimulated putative suppressors induced the most robust immune suppression observed, evidenced by a decreased division index when gating on the naïve CD45.1$^+$ population. Data shown from at least 4 independent experiments.

To investigate this paradoxical result, we phenotyped the putative suppressor cultures used in these assays in more depth. Here, we again looked for expression of multiple co-inhibitory receptors together with the expression of the master transcription factor for Treg cells, FoxP3. This data indicates that despite an increased co-inhibitory receptor expression profile in the context of 1μm^{Hi} MNPs, where interestingly CTLA-4 was again upregulated with force application on both FoxP3$^+$ and FoxP3$^-$ populations (FoxP3$^+$ co-inhibitory receptor expression: figure 5.15. FoxP3$^-$ co-inhibitory receptor expression: appendix figure 8.8), we found a lack of FoxP3 expression when putative suppressor cultures were stimulated with 1μm^{Hi} MNPs (figure 5.15). Interestingly, we also found that force application to 1μm^{Mid} MNPs induces a partial loss of FoxP3 expression, outlining the relationship between TCR signalling strength and FoxP3 expression as reported elsewhere[319,320].

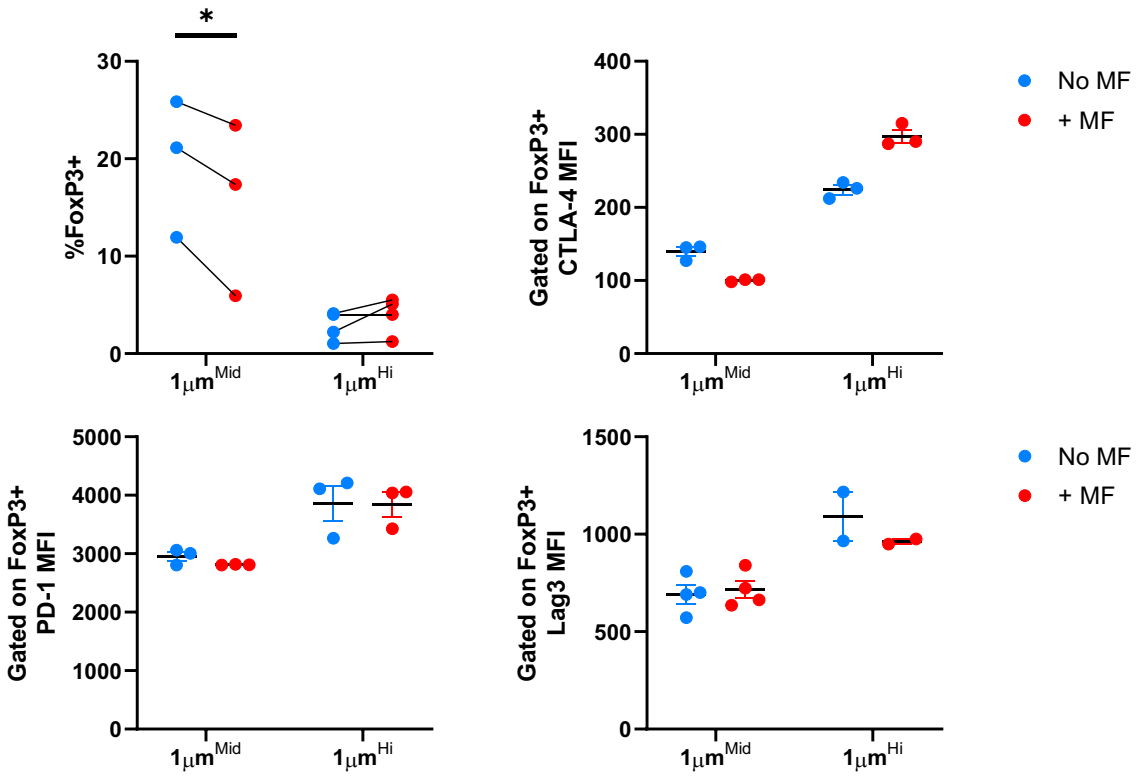


Figure 5.15 – FoxP3⁺ expression, and surface phenotype of FoxP3⁺ CD4⁺ T cells at day 3 upon stimulation with 1μm^{Mid} or 1μm^{Hi} MNPs. CD4⁺ T cells stimulated with 1μm^{Mid} or 1μm^{Hi} MNPs +/- 1 hour of magnetic force were stained for FoxP3⁺ expression at 72 hours as per 2.9.6, together with surface staining for various co-inhibitory receptors as per 2.9.1. All graphs show data representative of at least 3 independent repeats, except for %FoxP3⁺ expression which shows data from 3 independent repeats. Statistical analysis performed via two-way ANOVA with Sidak's post-tests. %FoxP3⁺, * p=0.0124.

Therefore, we hypothesised that the suppression observed from putative suppressor cultures stimulated with 1μm^{Mid} MNPs was related to an outgrowth of the FoxP3⁺ population in these cultures and may be mediated by a mechanism non-related to co-inhibitory receptor expression, such as competition for IL-2 consumption within the culture. To address this, we repeated these experiments and gave back exogenous IL-2 to a concentration of 20U/mL as per 2.15.1. This data indicates that at 1:1 ratios of putative suppressor to naïve responder, addition of exogenous IL-2 appears to partially reverse the observed immune suppression (figure 5.16) an effect that is lost by titrating away the number of suppressors used in the culture (i.e., at 1:2 and 1:4 ratios).

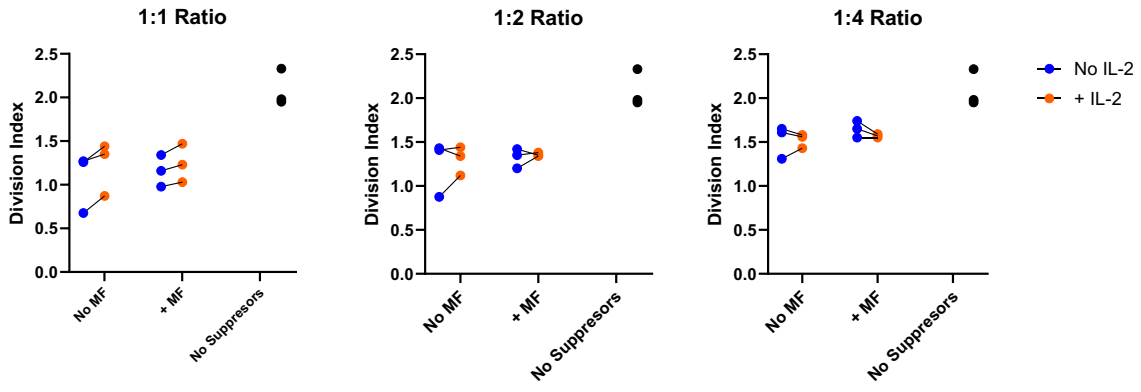


Figure 5.16 - Addition of exogenous IL-2 appears to partially reverse the observed immune suppression. Immune suppression co-culture experiments were performed as described in 2.15.1, utilising putative suppressors at day 3 following stimulation with 1µm^{Mid} MNPs +/- 1 hour of magnetic force. At the point of performing the co-culture, 20U/mL IL-2 was added as indicated. Addition of exogenous IL-2 induced a trend of reversing the observed immune suppression at the 1:1 ratio. Data shown from 2 independent repeats.

In an attempt to restore FoxP3 expression in 1µm^{Hi} MNP stimulated CD4$^+$ T cells, we treated CD4$^+$ T cells with the PI3K inhibitor CAL-101. Previous work by the Wraith lab has shown that expression of FoxP3 *in vitro* is lost when cells were stimulated with high doses of peptide antigen in the presence of IL-2 and TGFβ, yet use of CAL101 permitted sustained FoxP3 expression (unpublished observations). Additionally, other groups have also shown that inhibition of PI3K promotes FoxP3 expression in newly activated CD4$^+$ T cells[321], and therefore we treated CD4$^+$ T cells stimulated with 1µm^{Hi} MNPs with 10nM CAL-101 as per 2.15.1, and again assessed FoxP3 expression and suppressive capabilities whilst also measuring IL-10 secretion via ELISA.

Figure 5.17 illustrates that treatment with CAL101 fails to restore the loss of FoxP3 expression in 1µm^{Hi} MNP stimulated CD4$^+$ T cells. Given the previous findings from the Wraith laboratory, this result could perhaps be considered somewhat surprising. However, the effects of CAL101 on *in vitro* FoxP3 expression in this previous work utilised cells stimulated with APC and peptide, in the presence of TGFβ and IL-2. Therefore, in this

scenario CAL101 will target the PI3K pathway which will be active due to co-stimulatory molecule ligation on the CD4$^+$ T cell by CD80/CD86 on the APC surface. However, in the experiments displayed here, low- and high signal 1 strength 1µm MNPs are functionalised with anti-CD3 alone, and therefore the costimulatory pathway (with which PI3K is most closely associated to be downstream of[322,323]) is largely redundant in this protocol and therefore may give rise to this lack of effect for CAL101.

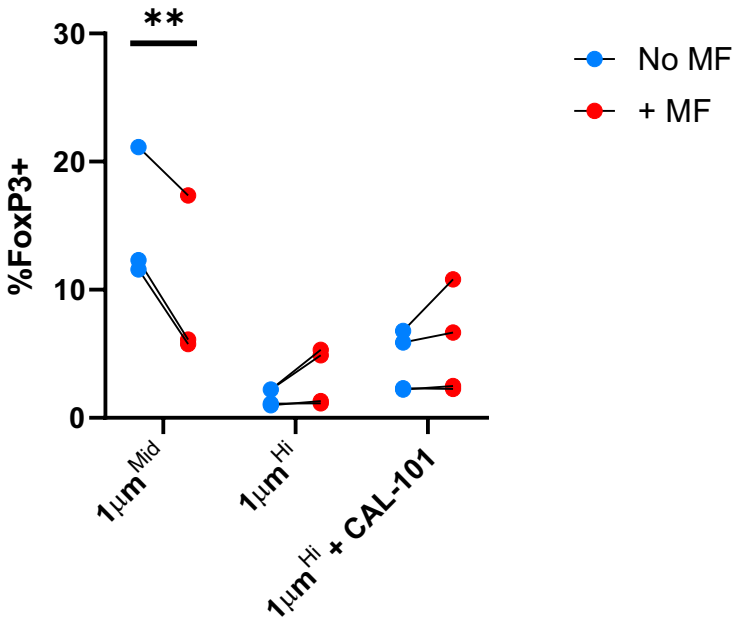


Figure 5.17 - Treatment with CAL101 fails to restore FoxP3 expression in 1µm^{Hi} stimulated CD4$^+$ T cells. CD4$^+$ T cells were stimulated with 1µm MNPs as shown +/- magnetic force (MF) for 1 hour. The effect of 10nM CAL101 treatment on FoxP3 expression in the context of stimulation with 1µm^{Hi} MNPs was assessed as described in 2.15.1. FoxP3 expression was determined at 72 hours post force treatment by flow cytometry as described in 2.9.6. Data shown from 2 independent experiments. Statistical significance assessed via two-way ANOVA with Sidak's post-tests, ** p=0.0016.

In line with the inability of CAL101 treated CD4$^+$ T cells to restore FoxP3 expression, we found that use of these putative suppressors in our immune suppression protocol failed to induce any observable suppression of the naïve CTV labelled CD45.1$^+$ Tg4 CD4$^+$ T cell response to APC and peptide (figure 5.18). Finally, we also found that when using putative suppressors stimulated with either 1µm^{Mid} MNPs, 1µm^{Hi} MNPs, or 1µm^{Hi} MNPs in the

presence of CAL101, all three protocols failed to induce robust IL-10 secretion when measured by ELISA (figure 5.18).

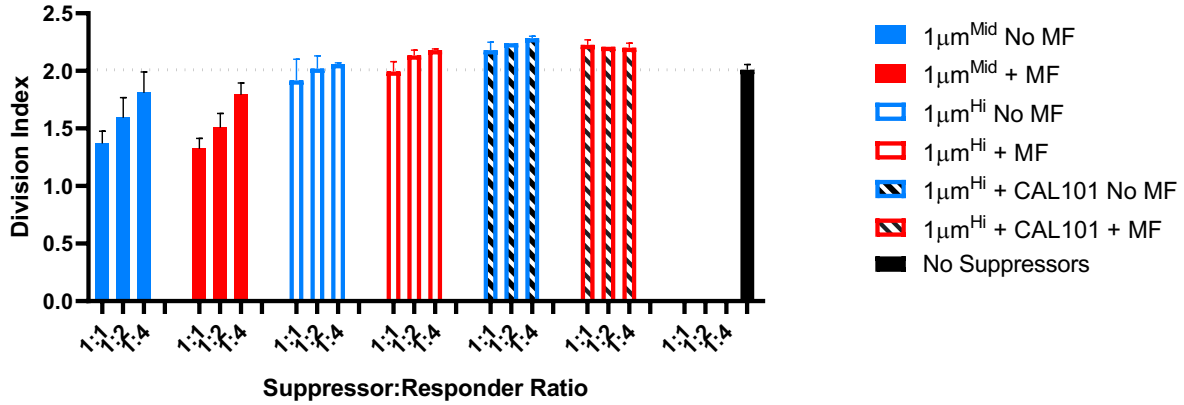


Figure 5.18 - CAL101 treatment fails to enhance immune suppression when putative suppressors are used at 72 hours. CD4⁺ T cells were stimulated with 1μm^{Mid} or 1μm^{Hi} MNPs +/- 1 hour of magnetic force, where 1μm^{Hi} CD3 groups were also treated with 10nM of CAL101 as per 2.15.1. At 72 hours, immune suppression co-culture assays were performed as per 2.15. As per figure 5.14, co-culture with putative suppressors stimulated via 1μm^{Mid} MNPs only induces suppression of the naïve Tg4 CD45.1⁺ CD4⁺ T cell response. Data shown from at least 2 independent experiments.

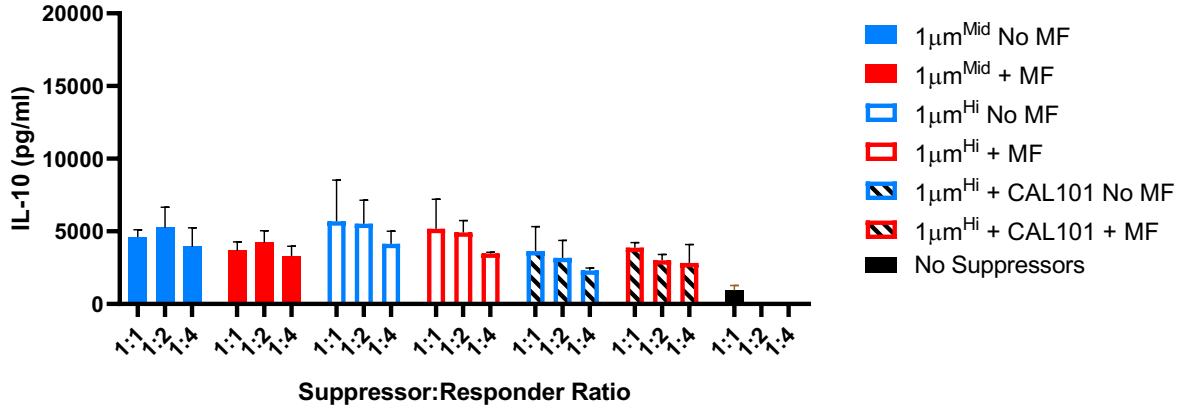


Figure 5.19 - 1μm anti-CD3 MNP stimulated putative suppressors secrete low levels of IL-10 when used at 72 hours. CD4⁺ T cells were stimulated with 1μm^{Mid} or 1μm^{Hi} MNPs +/- 1 hour of magnetic force, where 1μm^{Hi} CD3 groups were also treated with 10nM of CAL101. At 72 hours, immune suppression co-culture assays were performed as per 2.15, and supernatants were harvested 72 hours later. IL-10 secretion was determined by ELISA as per 2.14. Data shown from at least 2 independent experiments.

5.6.2 Treatment of CD4⁺ T cells with CAL101 induces a FoxP3⁻ IL-10⁺ suppressive population by day 7

To address whether the apparent outgrowth in FoxP3⁺ CD4⁺ T cells in response to stimulation with 1μm^{Mid} MNPs was stable in culture, we repeated these experiments but

instead chose to analyse CD4$^+$ T cell phenotype and suppressive capacity at a day 7 time point, as opposed to day 3 as displayed thus far. Figure 5.19 indicates that FoxP3 expression induced in the 1µm^{Mid} stimulated cultures is stable *in vitro* out to day 7, and again that force application to these MNPs is able to reduce FoxP3 expression as shown at 72 hours (figure 5.15).

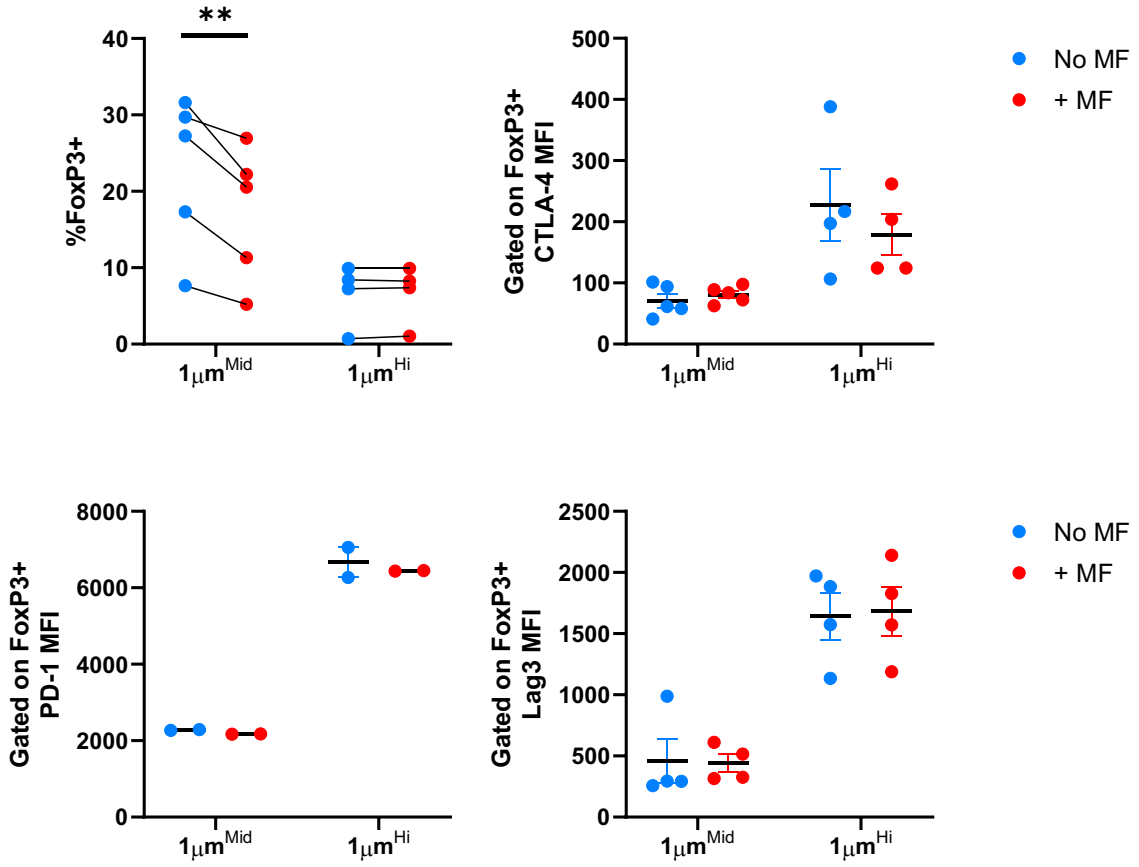


Figure 5.20 – Day 7 FoxP3 expression and surface phenotype of FoxP3$^+$ CD4$^+$ T cells in response to 1µm anti-CD3 MNP stimulation. CD4$^+$ T cells were stimulated with 1µm^{Mid} or 1µm^{Hi} MNPs, +/- 1 hour of magnetic force before assessment of FoxP3 expression as per 2.9.6 together with surface expression of co-inhibitory receptors as per 2.9.1 after a period of 7 days in culture. All graphs show data from at least 4 independent repeats, except PD-1 MFI which shows data representative of 2 independent repeats. Statistical analysis performed via two-way ANOVA with Sidak's post-tests, ** p=0.0017.

Additionally, co-inhibitory receptor expression again correlated with signal 1 strength, where expression of CTLA-4, PD-1 and Lag 3 was highest on CD4$^+$ FoxP3$^+$ T cells that had

been stimulated with 1µm^{Hi} MNPs. Co-inhibitory receptor expression profiles on CD4^{+} FoxP3^{-} T cells at this time point are shown in appendix figure 8.9. We again addressed whether CAL101 treatment could restore FoxP3 expression by day 7, and again found that treatment of CD4^{+} T cells with CAL101 was unable to reverse the loss of FoxP3 expression induced by stimulation with 1µm^{Hi} MNPs (figure 5.21). It should be noted that we also did not observe an effect on levels of co-inhibitory receptor expression in CAL101 treated cultures (data not shown).

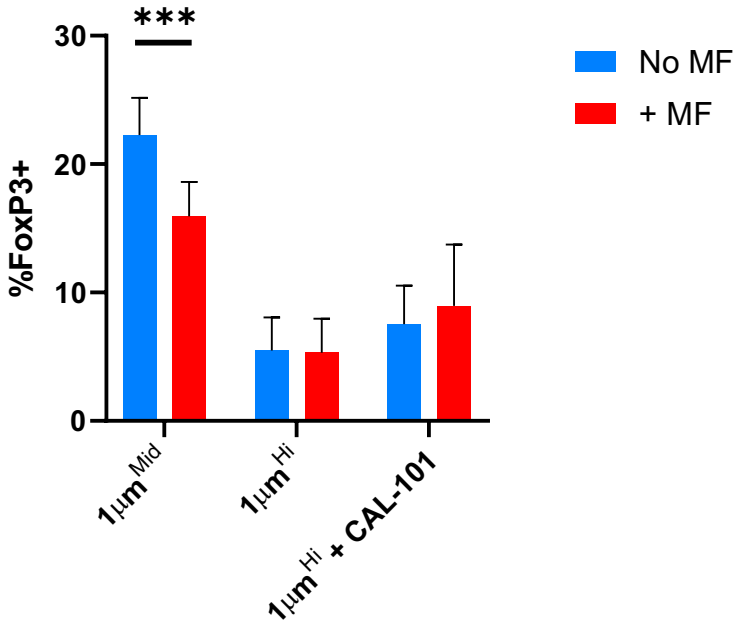


Figure 5.21 - Treatment of CD4^{+} T cells with CAL-101 fails to restore FoxP3 expression by day 7. CD4^{+} T cells were stimulated with 1µm^{Mid} or 1µm^{Hi} MNPs +/- 1 hour magnetic force, where 1µm^{Hi} stimulated cultures were also treated with 10nM CAL101 as shown. FoxP3 expression was determined at day 7 as per 2.9.6, where CAL101 treatment failed to recover FoxP3 expression in 1µm^{Hi} stimulated CD4^{+} T cells. Data shown from two independent repeats. Significance assessed via two-way ANOVA with Sidak's post-tests, *** p=0.0006.

When using these putative suppressors in Tg4 CD45.1^{+} CD4^{+} T cell suppression assays, we again observed low levels of suppression in response to co-culture with 1µm^{Mid} stimulated putative suppressors (figure 5.22, solid blue and red bars. Average division indices at 1:1, 1:2 and 1:4 ratios respectively: 1.76, 1.82 and 2.08 no MF, 1.84, 1.98 and 2.20 + MF). However,

we also observed similarly low levels of suppression of the naïve CD45.1^{+} response through co-culture with putative suppressors that had been stimulated with 1µm^{Hi} MNPs (figure 5.22, hollow blue and red bars. Average division indices at 1:1, 1:2 and 1:4 ratios respectively: 1.98, 2.04 and 2.18 no MF, 1.79, 1.89 and 2.05 + MF), which was not observed at day 3 (figures 5.14 and 5.18). The most robust levels of immune suppression were observed through co-culture with putative suppressors stimulated with 1µm^{Hi} MNPs and treated with CAL101. Interestingly, we also observed a moderate effect of force application within this condition, where force application to 1µm^{Hi} MNP and CAL101 treated conditions appeared to produce a slightly more potent suppressor (figure 5.22 hatched blue and red bars. Average division indices at 1:1, 1:2 and 1:4 ratios respectively: 1.63, 1.77 and 1.94 no MF, 1.25, 1.35 and 1.58 + MF).

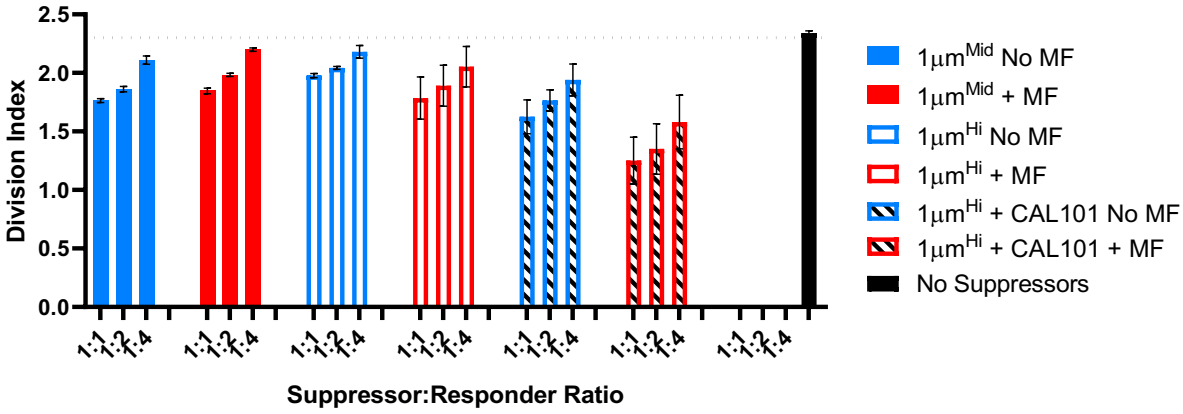


Figure 5.22 – 1µm^{Hi} and CAL101 treated putative suppressors induce robust immune suppression when used at day 7. Putative suppressors were stimulated with 1µm anti-CD3 MNPs as shown, +/- 1 hour magnetic force and +/- 10nM CAL101, and were maintained in culture in the presence of 20U/mL IL-2 for 7 days. Immune suppression assays were set up at day 7 as per 2.15.1. Proliferation analysis of naïve Tg4 CD45.1^{+} CD4^{+} T cells 3 days later revealed that use of 1µm^{Hi} and CAL101 treated putative suppressors induced the most robust levels immune suppression observed. Data shown from 2 independent experiments.

Interestingly, when analysing IL-10 secretion by ELISA from each putative suppressor population we again found low levels of IL-10 secretion from 1µm^{Mid} stimulated putative

suppressors (figure 5.23, solid blue and red bars), in line with the observations made at day 3 (figure 5.19). However, despite a lack of IL-10 secretion at day 3 from putative suppressors stimulated with 1μm^{Hi} MNPs, we found that these cultures secreted moderate levels of IL-10 by day 7 (figure 5.23, hollow blue and red bars), and that treatment with CAL101 seemed to increase the levels of IL-10 secretion observed (figure 5.23, hatched blue and red bars).

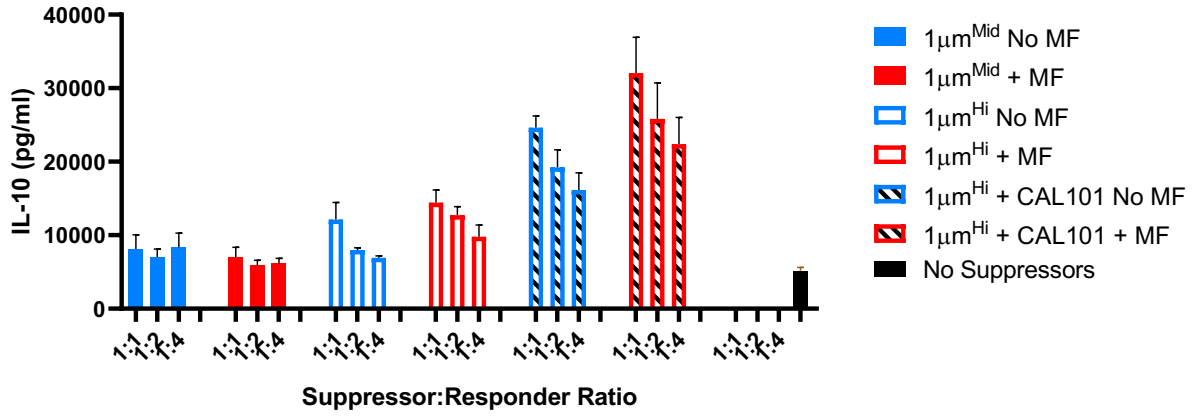


Figure 5.23 – 1μm^{Hi} and CAL101 treated putative suppressors secrete the highest levels of IL-10. Supernatants from immune suppression assays performed at day 7 as described in figure 5.22 were analysed for IL-10 secretion as per 2.14. Putative suppressors stimulated with 1μm^{Hi} MNPs together with 10nM CAL101 treatment promoted the highest levels of IL-10 secretion. Data shown from 4 independent experimental repeats.

The no suppressor controls shown in figure 5.23 suggest that the secreted IL-10 detected is being produced by these putative suppressor cultures; however, to confirm this we chose to perform intracellular cytokine staining (ICCS) by flow cytometry as per 2.9.2, to allow for the assessment of IL-10 expression from Vβ8$^+$ CD4$^+$ CD45.1$^-$ T cells (i.e., gating on Tg4 CD4$^+$ T cells and distinguishing between the suppressor (CD45.1$^-$) and naïve responder (CD45.1$^+$) population). This analysis agrees with the IL-10 secretion data, whereby moderate levels of IL-10 production was observed from 1μm^{Hi} MNP stimulated suppressors, which was again upregulated by CAL101 treatment (figure 5.24, hollow blue and red bars: no CAL101, hatched blue and red bars: + CAL101).

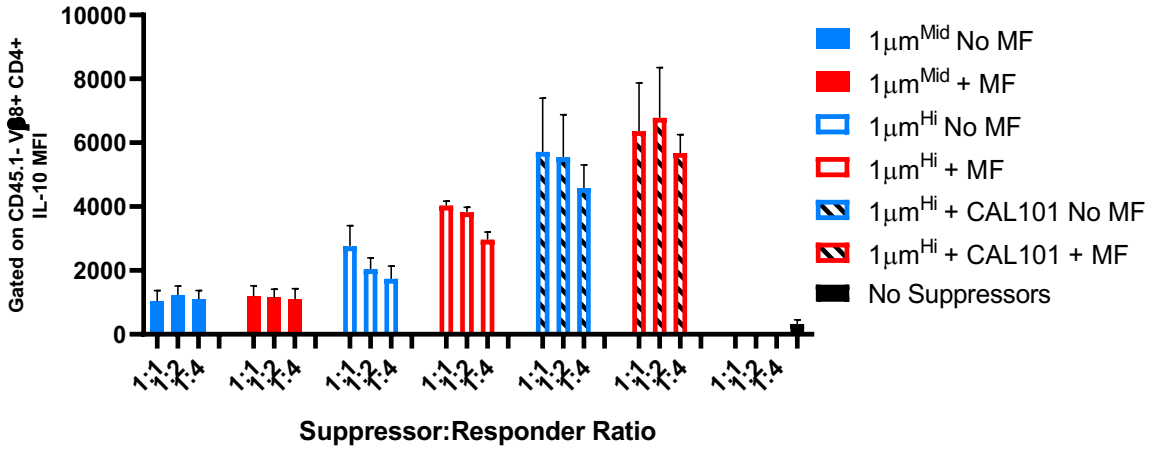


Figure 5.24 – ICCS analysis reveals the Vβ8$^+$ CD45.1$^-$ CD4$^+$ putative suppressor population as the producers of IL-10 in immune suppression co-culture assays. Immune suppression assays were performed as per 2.15, with intracellular cytokine staining (ICCS) being performed on day 7 as per 2.9.2 to determine which populations are producing IL-10. Gating on the putative suppressor population (Vβ8$^+$ CD45.1$^-$ CD4$^+$) reveals this population as the source of IL-10 detected in the supernatant (figure 5.23). Data shown from two independent experiments.

This data suggests 2 separate mechanisms of immune suppression dependent on signal 1 strength to the suppressor population. We have outlined that stimulation of CD4$^+$ T cells with low signal 1 strength 1μm MNPs (i.e., 1μm^{Mid} MNPs) induces an outgrowth of a CD4$^+$ FoxP3$^+$ population that can mediate low levels of immune suppression, potentially through competition for IL-2 (figures 5.14 and 5.16 respectively). However, these FoxP3$^+$ cells appear to make low amounts of IL-10 and therefore it is perhaps unsurprising that levels of suppression observed with this culture are relatively low. However, stimulation with high signal 1 strength 1μm MNPs (i.e., 1μm^{Hi} MNPs) appears to prevent FoxP3 expression, inducing a population of CD4$^+$ T cells that are FoxP3$^-$ (figures 5.15 and 5.20) but can begin to secrete IL-10 by day 7 (figures 5.23 – 5.24). Treatment of these cultures with CAL101 had no detectable effect on FoxP3 expression (figures 5.17 and 5.21) but promoted increased IL-10 expression at day 7 (figures 5.23-5.24). Therefore, these high signal 1 strength stimulated suppressors may mediate immune suppression via IL-10 secretion from CD4$^+$ FoxP3$^-$ T cells.

To confirm that IL-10 expressing CD4$^+$ T cells from 1µm^{Hi} MNP stimulated suppressors were indeed FoxP3$^-$, we co-stained for both IL-10 and FoxP3 at day 7 as per 2.9.6, to phenotype these suppressors before they entered the suppression assay protocol. As shown in figure 5.25 and the representative FACS plots in figure 5.26, we again observed an outgrowth of FoxP3$^+$ IL-10$^-$ CD4$^+$ T cells in suppressor conditions that were stimulated with 1µm^{Mid} MNPs. Again, force application to this condition induced a partial loss of FoxP3 expression. However, stimulation of CD4$^+$ T cells with 1µm^{Hi} MNPs resulted in a loss of FoxP3 expression yet promoted IL-10 expression from FoxP3$^-$ CD4$^+$ T cells. In line with IL-10 expression and secretion data shown in figure 5.23-5.24, force application to 1µm^{Hi} MNPs appeared to induce a small upregulation in IL-10 expression, whilst CAL101 treatment promoted the most robust IL-10 expression consistent with the suppressive capacity of these different suppressor populations (figure 5.22).

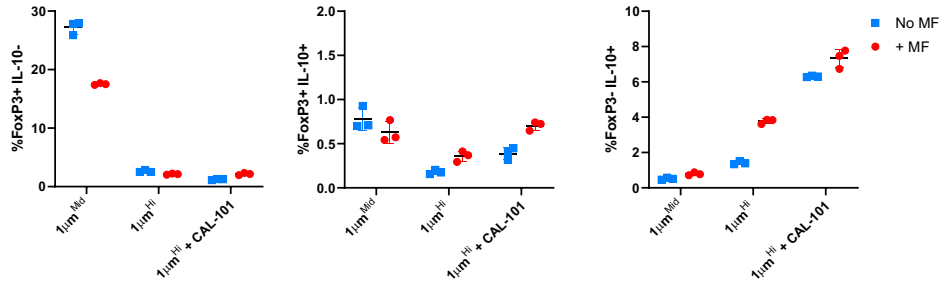


Figure 5.25 – Emergence of a FoxP3$^-$ IL-10$^+$ population correlates with TCR signal 1 strength and is increased by CAL101 treatment to 1µm^{Hi} stimulated CD4$^+$ T cells. CD4$^+$ T cells were stimulated with 1µm^{Mid} or 1µm^{Hi} MNPs +/- 1 hour of magnetic force as shown, where 1µm^{Hi} stimulated cells were also treated with 10nM CAL101. Cultures were maintained in 20U/mL IL-2 before co-staining for FoxP3 and IL-10 at day 7 as per 2.9.6. Data shown from 1 individual experiment, representative of at least 2 independent repeats.

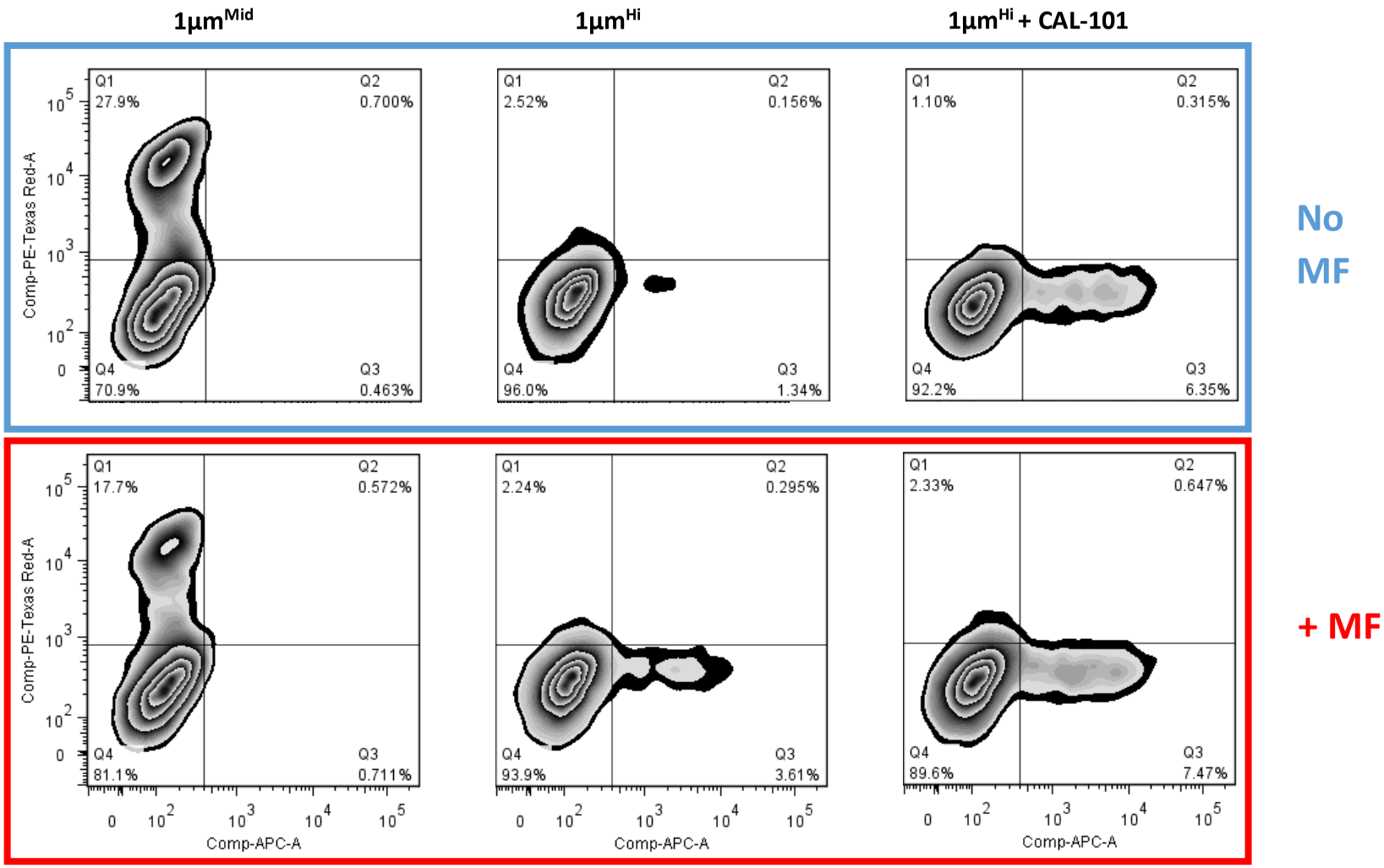


Figure 5.26 - Representative FACS plots from FoxP3 and IL-10 co-staining experiments described in figure 5.25. Co-staining for FoxP3 and IL-10 was performed as per 2.9.6, on CD4⁺ T cells stimulated as described in figure 5.25. FACS plots shown are from 1 independent experiment, representative of at least 2 independent repeats. Stimulation of CD4⁺ T cells with 1µm^{Hi} MNPs promotes low levels of IL-10 production, which is upregulated with 1 hour of magnetic force treatment. Treatment of 1µm^{Hi} MNP stimulated cells with 10nM CAL101 promoted a further upregulation of IL-10 expression.

Finally, we aimed to link the differential IL-10 expression profiles from each suppressor population to the ability of these cultures to modulate expression of proteins involved in the T cell activation machinery on the surface of APCs. It is known that IL-10 expression from suppressive $CD4^+$ T cell populations can induce a downregulation of CD80, CD86 and MHC-II expression of the surface of DCs and hence dampen the immune response within a given site of antigen recognition[324]. This property is a key mechanism in the initiation of bystander suppression[324,325]. To address this, we performed DC – putative suppressor co-cultures before analysing DC surface phenotype, as described in 2.15.2. Briefly, $CD11c^+$ cells were isolated from the spleens of B10.PL mice (see 2.3) as a source of DCs and were then co-cultured with each putative suppressor population for 24 hours in the presence or absence of 10µg/mL of the 4K peptide. After co-culture for 24 hours, surface expression levels of CD80 and CD86 were assessed on $CD11c^+$ $MHC\text{-}II^+$ populations.

This data indicates that in line with the low levels of IL-10 detected from each suppressor population at day 3 (figure 5.19), co-culture with any putative suppressor population at day 3 failed to prevent the upregulation of CD80 and CD86 on $CD11c^+$ $MHC\text{-}II^+$ cells in response to peptide (figure 5.27-A). However, when performing these experiments at day 7, where enhanced IL-10 production had been observed from suppressors stimulated with $1\mu m^{Hi}$ MNPs and CAL101, we found that co-culture of these suppressors with $CD11c^+$ DCs prevented the peptide dependent increase of CD80 and CD86 expression and induced a partial downregulation on CD80 on the surface on $CD11c^+$ DCs (figure 5.27-B). This data reaffirms the separate mechanisms of immune suppression from each suppressor culture, $1\mu m^{Mid}$ MNP stimulated suppressors induce immune suppression through mechanisms separate from IL-10 production, whereas suppression observed from $1\mu m^{Hi}$ and CAL101

stimulated putative suppressors can lead to induction of immune suppression potentially mediated by IL-10 expression.

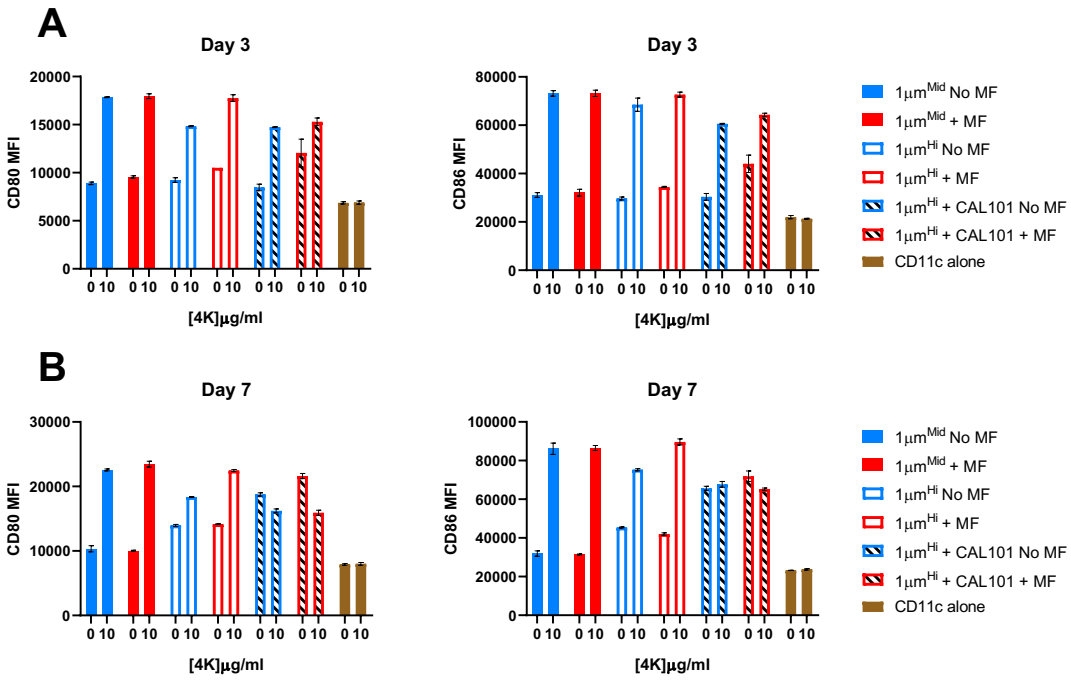


Figure 5.27 – Co-culture of 1µm^{Hi} and CAL101 treated putative suppressors with B10.PL CD11c$^+$ DCs at day 7 modulates DC surface expression of CD80 and CD86. Co-cultures of B10.PL CD11c$^+$ DCs and putative suppressor populations were performed at day 3 and day 7, as described in 2.15.2. Following co-culture for 24 hours, surface CD80 and CD86 expression was assessed on CD11c$^+$ MHC-II$^+$ cells as per 2.15.2. Bar graphs shown mean ± SD for one individual experiment, representative of 2 independent repeats.

5.7 Discussion

5.7.1 Signal 1 strength modulation of CD4$^+$ T cell phenotype

Whilst chapters 3 and 4 detail how force application to the TCR can promote T cell activation, the data presented in this chapter aims to monitor CD4$^+$ T cell phenotype and address how force application to the TCR and subsequent modulation of TCR signalling strength can affect CD4$^+$ T cell phenotype. Interestingly and in line with other reports[318,326], we find that increased TCR signal strength correlated with increased co-inhibitory receptor expression when measured 72 hours post force application. Here, use of functionalised

nanoparticles that can be considered to induce lower TCR signal 1 strength (250nm^{Mid} anti-CD3 MNPs and 1µm^{Mid} anti-CD3 MNPs) failed to induce robust co-inhibitory receptor expression, where co-inhibitory receptor expression on CD4^{+} T cells stimulated with these particles was entirely dependent on the presence of antigen at the point of restimulation (figures 5.3 – 5.4). However, stimulation of CD4^{+} T cells with high signal 1 strength MNPs (i.e., 1µm^{Hi} MNPs) induced robust expression of multiple co-inhibitory receptors by day 3. Co-inhibitory receptor expression under these conditions appeared independent of the presence of antigen at the point of restimulation (figure 5.5), indicating that their expression is ultimately driven by the particle mediated signal strength during the first round of stimulation. Importantly, additional increase in TCR signal strength by application of external force further increased co-inhibitory receptor expression on 1µm^{Hi} stimulated CD4^{+} T cells (figure 5.5), thereby supporting the link between TCR signal strength and co-inhibitory receptor expression.

Despite the link between TCR signal strength and co-inhibitory receptor expression, data suggests that expression of these receptors is not involved in the anergic phenotype observed when restimulating CD4^{+} T cells that had received treatment with 1µm^{Hi} MNPs with or without magnetic force (figure 5.9 and appendix figure 8.6). Instead, we find that the emergence of this anergic phenotype with restimulation antigen doses below 100µg/mL is more closely linked to TCR expression, where persistent TCR downregulation in 1µm^{Hi} stimulated CD4^{+} T cells gives rise to an anergic phenotype (figures 5.11 – 5.13).

Additionally, we observed a drastic effect on FoxP3 expression with increasing TCR signal strength. Previous work had described that extrathymic conversion of naïve CD4^{+} T cells into FoxP3^{+} CD4^{+} regulatory T cells in the periphery (pTregs) is achieved through administration

of low antigen doses and limited co-stimulation[319]. In this work, administration of low antigen dose induced robust expansion of a $CD25^+$ $CD4^+$ $FoxP3^+$ suppressive population, which was ultimately lost by either increasing the antigen dose or providing anti-CD40 agonistic antibodies to provide co-stimulatory signals. These observations are also in line with reports that show repeated administration of subimmunogenic doses of agonistic peptides in $Rag2^{-/-}$ models can induce suppressive $CD25^+$ $CD4^+$ $FoxP3^+$ peripheral Tregs[320], hereby providing further evidence for a link between TCR signalling strength and induction of peripheral $FoxP3^+$ Tregs. Our data aligns with these findings, where stimulation of $CD4^+$ T cells with high signal 1 strength $1\mu m^{Hi}$ MNPs fails to induce detectable FoxP3 expression by day 3 or day 7 (figures 5.15 and 5.20 respectively), whilst use of low signal 1 strength $1\mu m^{Mid}$ MNPs resulted in clearly detectable $CD4^+$ $FoxP3^+$ populations at both day 3 and 7. Finally, force application to these $1\mu m^{Mid}$ MNPs, known to increase TCR signalling strength as described in chapter 3, results in decreased FoxP3 expression at both days 3 and 7 (figures 5.15 and 5.20 respectively).

5.7.2 Distinct mechanisms of immune suppression linked to TCR signal strength

Given that force application to high signal 1 strength $1\mu m^{Hi}$ MNPs induced robust upregulation of multiple co-inhibitory receptors, and that use of low signal 1 strength $1\mu m^{Mid}$ MNPs promoted FoxP3 expression, we aimed to assess whether either of these potentially suppressive populations could mediate suppression of the naïve Tg4 $CD45.1^+$ $CD4^+$ response to antigen as per 2.15.1. Here, we aimed to address the following questions: Can co-inhibitory receptor high $CD4^+$ T cells suppress the response of naïve $CD4^+$ T cells via negative signalling or competition for co-stimulatory ligands? Can the $CD4^+$ $FoxP3^+$

population induced by stimulation with 1μm^{Mid} MNPs suppress the naive Tg4 CD45.1^{+} CD4^{+} response to antigen?

Firstly, we observed that CD4^{+} FoxP3^{+} T cells induced through stimulation with 1μm^{Mid} MNPs can mediate low levels of immune suppression, likely through mechanisms separate from IL-10 production given the low levels of IL-10 detected by ELISA (figures 5.19 and 5.23), ICCS staining (figure 5.24) and FoxP3 – IL-10 co-staining experiments (figures 5.25 – 5.26). Furthermore, supplementation with exogenous IL-2 appeared to partially recover cell proliferation by the naïve Tg4 CD45.1^{+} CD4^{+} population (figure 5.16), suggesting that the CD4^{+} FoxP3^{+} IL-10^{-} cells induced with 1μm^{Mid} MNPs may be mediating immune suppression via competition for IL-2[327]. However, whilst these experiments showed a trend toward recovery of naïve CD4^{+} T cell proliferation, it should be noted that this was not a complete recovery as the proliferation observed was still less than that of the no suppressor control (figure 5.16). This most likely reflects the complex mechanisms of FoxP3 Treg mediated suppression, and further work will be required to tease out other mechanisms by which 1μm^{Mid} induced FoxP3^{+} CD4^{+} T cells can mediate suppression[327,328].

Finally, data suggests that despite the robust expression of co-inhibitory receptors on CD4^{+} T cells treated with 1μm^{Hi} MNPs, these cells appear unable to mediate immune suppression through co-inhibitory receptor mediated mechanisms. When analysed at day 3, CD4^{+} T cells treated with these high signal 1 strength MNPs expressed very low levels of FoxP3 (approx. 5% of CD4^{+} cells were FoxP3^{+}, figure 5.15). However, despite their relatively low number, FoxP3^{+} CD4^{+} cells induced through stimulation with 1μm^{Hi} MNPs expressed higher levels of CTLA-4, PD-1 and Lag3 when compared to the low signal 1 strength 1μm^{Mid} MNP counterparts (figure 5.15). Use of these CD4^{+} T cells in suppression assays at day 3

showed no observable suppression of the naïve Tg4 CD45.1^{+} CD4^{+} response to peptide, when analysed by CTV dilution 3 days later, suggesting that despite the robust expression of co-inhibitory receptors on the 1µm^{Hi} MNP stimulated CD4^{+} population at this time point, they are unable to mediate immune suppression. However, use of this CD4^{+} population in suppression assays at day 7 began to allow for low levels of immune suppression to be observed (figure 5.22). This result can likely be attributed to the ability of these cells to produce low levels of the immunosuppressive cytokine IL-10 (figures 5.23 and 5.24), which we unexpectedly found was substantially increased by treatment of these CD4^{+} T cells with the PI3K inhibitor CAL101. In agreement with the suggestion that IL-10 secretion by these cells is driving the observed immune suppression when used at day 7, we found that where CAL101 treatment increases the expression of IL-10 by FoxP3^{-} CD4^{+} T cells, these cells are also then the most potent suppressor of the naïve Tg4 CD45.1^{+} CD4^{+} response and can also modulate expression of the T cell activation machinery on the surface of CD11c^{+} DCs (figures 5.22 and 5.27 respectively). To confirm this proposal, further work making use of IL-10 receptor (IL-10R) blocking antibodies will shed light on the dependence of IL-10 signalling on the observed immune suppression.

Therefore, taken together we observed two distinct mechanisms of immune suppression linked to the original signal 1 strength that the putative suppressor population was stimulated with. Stimulation of naïve CD4^{+} T cells with low signal 1 strength 1µm^{Mid} MNPs promoted the emergence of an inhibitory receptor low, IL-10^{-} FoxP3^{+} CD4^{+} population that could mediate low levels of suppression, whilst use of high signal 1 strength 1µm^{Hi} MNPs ultimately promoted IL-10 expression within FoxP3^{-} CD4^{+} populations that could also mediate immune suppression in part through suppression of the antigen-driven upregulation of costimulatory molecules on dendritic cells.

CHAPTER 6

6 General Discussion

6.1 Introduction

The data presented in this thesis fall into two main sections. Firstly, we aimed to investigate whether the TCR can function as a mechanosensor by way of responding to force application using our MNP based protocol. Within this we aimed to shed light on the mechanism behind force manipulation of the TCR to investigate the mechanisms that may promote T cell activation in response to force encountered through the TCR. Whilst growing in interest, this remains a relatively under studied area within the field of T cell biology. Despite this, investigation of how the TCR interprets different mechanical cues and environments is of importance due to the fascinating reports that T cell behaviour is modulated as a direct consequence of the mechanical environment within which antigen recognition takes place[190,240–242]. Therapeutically, this may enhance our understanding of why T cell function is often reduced in mechanically stiff environments such as tumours, whilst building our knowledge as to why environments that are mechanically soft are also poor for T cell activation. Indeed, multiple groups have studied this *in vitro* and described the possible existence of a mechanical 'sweet spot' for T cell activation[241].

When addressing these questions, we found that force application to the TCR is able to modulate TCR signalling strength, evidenced by the upregulation of a number of TCR signalling and T cell activation hallmarks such as Nr4a3, CD69 and CD25 expression together with subsequent T cell proliferation. Interestingly, we propose that this occurs through a mechanism dependent on force mediated TCR remodelling and reorganisation within the cellular membrane, where emergence of TCR clusters in response to magnetic force

application provide early evidence of force induced signalling events. Additionally, we observe a number of hallmarks of immune synapse formation, and therefore propose that force induced 'pseudo-synapse' structures on the T cell surface may promote sustained TCR signalling in response to force application leading to T cell activation. These hallmarks are TCR downregulation in response to force application (where flow cytometry analyses indicate that the emergence of force induced TCRlo Nr4a3^{+} populations) and loss of membrane CD45 intensity at areas of membrane-particle contact with force application. Importantly, perturbation of the actin cytoskeleton (a known critical mediator of TCR membrane remodelling and synapse formation), with Lat A, and blockade of active signalling, with PP2, prevents the emergence of both phenotypes.

Secondly, building on the force mediated modulation of TCR signal strength, we aimed to investigate whether this platform can be used to modify CD4^{+} T cell phenotype. Multiple lines of evidence are arising to support a role for strength of TCR signalling in CD4^{+} T cell fate[329]. Increased TCR signal strengths are known to promote dysfunctional T cell phenotypes (such as exhausted phenotypes[315,330]) and often correlate with expression of various co-inhibitory receptors[318,326], whilst weak TCR signals and TCR ligation in the absence of co-stimulatory signalling (resulting in TCR signalling of a lower functional avidity) are known to induce anergic T cell phenotypes[76–78]. In addition, it is well characterised that subimmunogenic *in vivo* administration of antigen can promote production of FoxP3^{+} regulatory CD4^{+} T cell phenotypes[319,320]. Interestingly, we provide evidence in line with other groups, suggesting that low TCR signalling strength promotes the emergence of FoxP3^{+} CD4^{+} T cell populations. However, we find that secretion of IL-10 from Tg4 CD4^{+} T cells is more closely associated with higher TCR signalling strength, resulting in a FoxP3^{-} IL-10^{+} phenotype. Finally, we provide evidence that despite this correlation between TCR

signal strength and IL-10 production, robust IL-10 secretion is only achieved when stimulation with high TCR signal strength MNPs (1μm^{Hi}) was combined with inhibition of the PI3K pathway via CAL101 treatment.

6.2 Force application to the TCR modulates TCR signalling strength and commits cells to T cell activation

6.2.1 Force application induces specific TCR triggering, reaching thresholds required for T cell activation

As previously discussed, multiple reports are emerging showing that T cells can initiate TCR triggering in response to force. To date, these experiments have largely focussed on single cell approaches, through the use of optical traps or micropipettes/biomembrane force pipettes (BFP) to apply force to TCRs for seconds-minutes time scales on a single cell basis[183,188,196,199]. Whilst mechanistically revealing, these approaches fail to assess T cell signalling and activation beyond the point of calcium signalling, which in itself may or may not reach thresholds required to commit T cells to activation.

Our approach utilised small, superparamagnetic nanoparticles (MNPs) that can be directed to cell surface receptors and proteins of interest through the crosslinking of biological reagents to the MNP surface via carbodiimide chemical crosslinking. This approach has been extensively utilised by the El Haj lab previously for the study of many other mechanosensitive cell surface receptors such as mechanically gated ion channels including TRPV4, TREK1 and Piezo-1[238,239,251,258]. In this thesis, use of MNPs functionalised with anti-CD3ε antibodies drove TCR signalling and T cell activation when subjected to external magnetic forces (as described in chapter 3).

However, with this approach there is indeed a concern surrounding off target effects. It is conceivable that tagging of an MNP to the TCR-CD3 complex and subsequent force application through exposure to external magnetic fields could induce localised membrane stresses which may cause non-specific opening of mechanically gated ion channels. On this note, T cells are known to express many of these mechanically gated ion channels, including Piezo-1[331,332] and TRPV4[333]. Therefore, non-specific activation of these receptors may permit calcium entry and triggering of TCR signalling pathways. To address this, we utilised off target antibodies (i.e., antibodies that bind $CD4^+$ T cell surface receptors not related to the propagation of the internal TCR signal) by functionalising MNPs with anti-MHC-I antibodies. Importantly, force application to MHC-I functionalised MNPs failed to induce TCR signalling, indicating that responses seen with anti-CD3ε functionalised antibodies were indeed specifically triggering via the TCR. Finally, use of the Src family kinase inhibitor PP2, which blocks the activity of Lck, Fyn and others (proteins responsible for initiating the earliest TCR signalling steps of ITAM phosphorylation) blocked force induced TCR signalling. These results provide confidence that our MNP approach specifically induces TCR signalling.

It should be noted that with this approach, we only observe approximately 10-50% of cells that signal across our experiments (as displayed throughout chapter 3). It is a possibility that this is a result of heterogeneity within the $CD4^+$ population in the non-transgenic Nr4a3-FT mouse. However, we have also investigated TCR signalling responses in the TCR transgenic Tg4 mouse, as well as in the Rag-deficient Tg4 TCR transgenic mouse (RTO). Investigation within these strains (figure 3.11) showed a slight increase in the percentage of cells signalling when compared to the Nr4a3-FT strain; however use of the RTO directly compared to Tg4 controls showed no observable benefit of investigating responses in the Rag deficient Tg4 TCR transgenic, suggesting that heterogeneity of the $CD4^+$ populations

between each strain does not contribute to the level of cells signalling in response to particle stimulation. Therefore, the physical constraints of the system are more likely to be responsible for this effect. It is conceivable that a cell-particle labelling efficiency below 100%, or small losses of particle binding through PBS washing after particle treatment on ice for 30 minutes will contribute to a lower detection of signalling in response to particle treatment.

However, we find that force application for 1 hour is sufficient to upregulate activation markers CD69, CD25 and Nr4a3 in $CD4^+$ T cells and promote increased cell proliferation. This is in agreement with other reports that use functionalised MNPs and external static magnetic fields which show increases in cell expansion with 1 hour of field application[265]. Additionally, we find that use of magnetic force for shorter time frames than this 60-minute period fails to induce robust $CD4^+$ T cell activation. This raises an interesting question as to why this level of force application is required to initiate sufficient TCR signalling required for Nr4a3 expression. We hypothesised that signalling events initiated downstream of force application to the TCR accumulate across the course of the 60-minute time course, and thus permit sufficient NFAT dephosphorylation required for nuclear entry and Nr4a3 translation. To address this, we performed experiments utilising a pulsatile magnet protocol coupled with cyclosporin mediated blockade of the calcineurin-calmodulin NFAT pathway displayed in figures 3.16 and 3.18. Here, we reveal that signalling events accumulate across the four pulses of 15 minutes to reach the threshold required for Nr4a3 expression across the course of 1 hour force application (figure 3.19).

Importantly, accumulation of signalling inputs to promote functional signalling output has been described elsewhere[334]. Here, authors have developed an optically controlled chimeric

antigen receptor (CAR) expressing T cell (Opto-CAR) which makes use of a synthetic receptor-ligand interaction. This CAR is formed of an extracellular ligand binding domain from the FK506-binding protein (FKBP), whose interaction with its binding partner FKBP12-rapamycin-binding (FRB) domain of mammalian target of rapamycin (mTOR) is dependent on addition of rapamycin, producing a druggable CAR – ligand interaction, giving temporal control over the initiation of receptor triggering[40]. James and colleagues, however, have utilised surface expression of FRB with a T2098L mutation in the Raji B cell line (henceforth called Raji-FRB), which allows for the use of the rapalog AP21967 as the druggable agent, which does not interfere with T cell activation in the way that rapamycin does[40,334].

This extracellular region is fused to the transmembrane domain of CD86, which in turn is fused to a CD3ζ domain to permit intracellular signal propagation upon FKBP-FRB interaction[40]. A light sensitive element, LOV2, was engineered into the CAR between the CD86 TM domain and intracellular CD3ζ chain to allow for receptor dissociation upon exposure to light, ensuring that signalling can only progress when cells are kept in a dark phase[334]. Use of this technology showed that when cells were persistently kept in the dark (≥6 hours) under stimulatory conditions (addition of Raji-FRB and rapalog), robust NFAT-GFP and CD69 expression was readily observed, with a minimum signalling duration of 30 minutes required for detectable signalling output[334].

Authors followed this up by utilising a pulsatile signalling system to investigate whether repeated shorter duration signals could accumulate and amount to substantial T cell signalling output. Here, short signalling durations of 15 minutes, 30 minutes, 60 minutes or 72 minutes were pulsed so that their total 'on' time totalled 6hrs (i.e., 15min x 24, 30min x12, 60min x 6 or 72min x 5)[334]. When compared to a sustained 6hr signal duration control,

authors observed that whilst a single 15 minute signal duration gave no detectable signalling output, pulsing of repeated 15 minute signal durations accumulated to allow for detectable signal output[334]. Here, authors showed that increasing the length of time between each pulse of signal (i.e., keeping the cells in light for longer between each signal inducing dark time frame) beyond the 10-15 minutes showed a loss of signal accumulation. Therefore, an obvious follow up experiment in our protocol will be to investigate whether increasing of the 15 minute breaks between each 15 minute force application pulse results in a similar loss of accumulation of signalling intermediates. It is conceivable that differences between the two systems may be found, which may arise through the use of synthetic CAR T cell interactions and primary $CD4^+$ T cells. However, since reports suggest that interactions between $CD4^+$ T cell and DCs are inherently short lived and that intervals between sequential T cell – DC interactions can be as long as 90 – 120 minutes[335], it will be important to define how long this accumulation along the NFAT pathway exists for.

Further experimentation is required to investigate the mechanism behind signal accumulation in our system. Firstly, it will be important to investigate signalling protein phosphorylation along the NFAT pathway (such as calcineurin phosphorylation) at the end of each 15 minute force pulse and 15 minute force 'break' in an attempt to directly observe an accumulation of signalling events. Alternatively, it may be possible that each 15 minute force pulse is sufficient to reach the level of NFAT dephosphorylation and nuclear entry, but that a certain level of nuclear NFAT is required to permit detectable Nr4a3 expression. This can be tested through producing nuclear extracts from cell suspensions after each period of treatment in the pulsatile magnet/CsA protocol. These nuclear extracts can then be probed via western blot or FACS for NFAT content, which may then reveal nuclear NFAT accumulation within this protocol. However, data presented in this part of the thesis clearly

show that in line with other groups[334], T cells are able to accumulate signalling events to reach the thresholds required for T cell activation.

6.2.2 Force application serves to modulate TCR signal strength

Another conclusion from the data presented in this thesis is that force application to the TCR serves to modulate $CD4^+$ TCR signal strength. Here, when original TCR signal 1 strength is low (achieved through use of particles functionalised with a lower level of anti-CD3 antibodies on the particle surface, $250nm^{Mid}$and $1\mu m^{Mid}$ anti-CD3 MNPs), force application serves to upregulate TCR signal strength evidenced through upregulation of activation markers CD69, CD25 and Nr4a3 together with an increase in cell proliferation ($250nm^{Mid}$ MNPs: figures 3.4 and 3.21. $1\mu m^{Mid}$ MNPs: figures 3.9 and 3.24). However, when original signal 1 strength was increased (using particles with an increased level of anti-CD3 on the particle surface, $1\mu m^{Hi}$ MNPs), we find that an increase in TCR signal strength achieved through magnetic force application served to downregulate Nr4a3, CD69 and CD25 expression when analysed 4 hours post force application, which correlated with an increase in co-inhibitory receptor expression at 72 hours. These findings are summarised in figure 6.1.

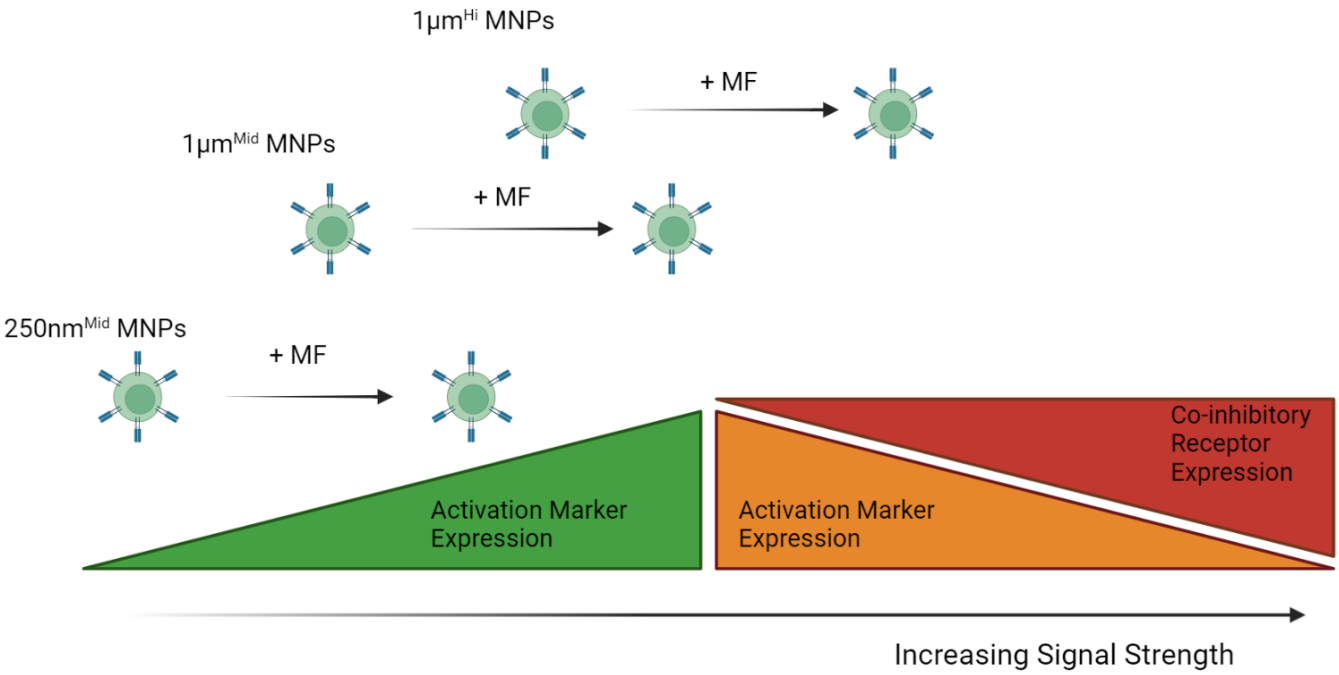


Figure 6.1 - Force application modulates TCR signal strength. Force application to MNPs that provide a low TCR signal strength (250nm^{Mid} anti-CD3 MNPs or 1µm^{Mid} MNPs), achieved through functionalisation with low doses of anti-CD3 antibodies, serves to promote T cell activation. Conversely, force application to MNPs that provide a high TCR signal strength (1µm^{Hi} MNPs), achieved through functionalisation with a high dose of anti-CD3 antibodies, increases TCR signal strengths to a point where T cell activation is negatively impacted. Image created in BioRender.

As postulated in chapter 3, this implies that perhaps these stronger TCR signals not only reach thresholds for T cell activation but also levels required for negative feedback mechanisms which may then act to downregulate T cell activation markers, which weaker signals may not reach even with force application. These ideas are summarised in figure 6.2.

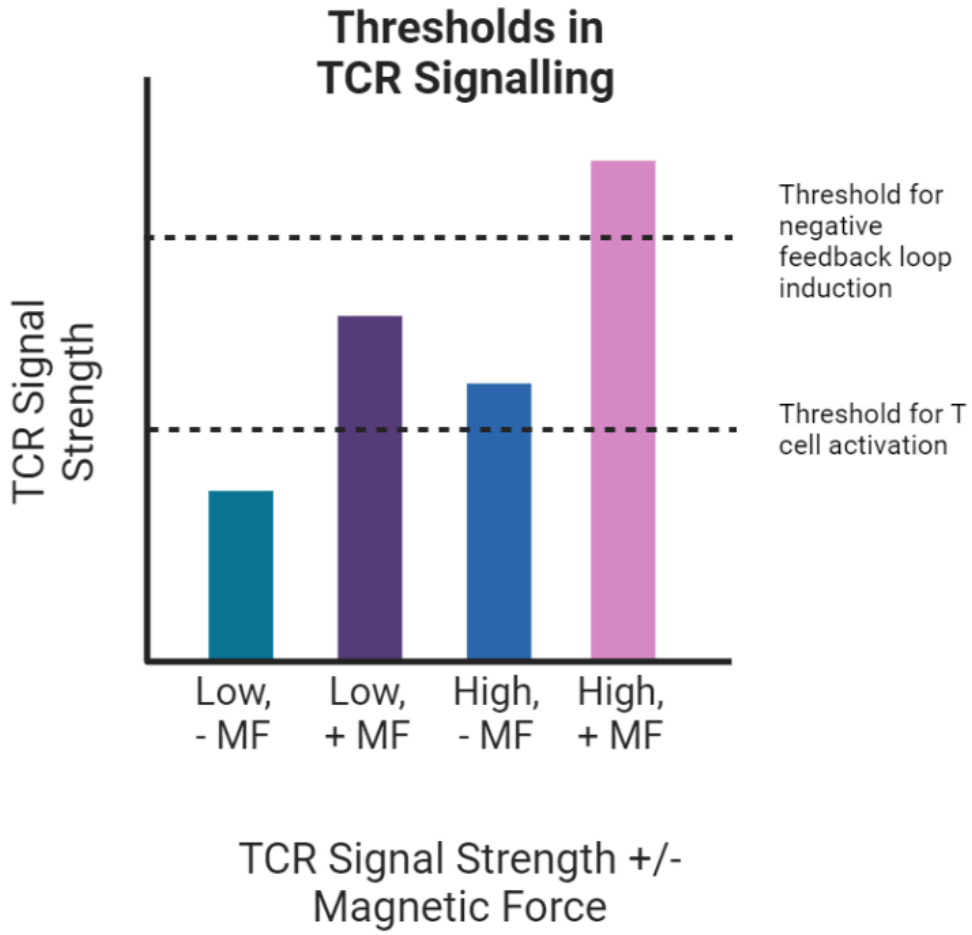


Figure 6.2 - Proposed threshold involved in TCR signalling and T cell activation. We have provided evidence that force application to 1μm^{Mid} MNPs results in accumulation of TCR signalling events within the NFAT pathway, promoting Nr4a3 expression and T cell activation. It may be possible that high signal strength MNPs (1μm^{Hi}) already provide signal that reach this threshold, and that force application to these particles induces an increase in TCR signalling strength that triggers negative feedback onto TCR signalling, and hence induces a downregulation of activation marker expression and cell proliferation.

Previous evidence has shown that persistent signals can drive negative feedback regulation of signalling pathways, including the MAPK/ERK pathway in HeLa cells[298]. Elsewhere, it has been proposed that pulsatile signalling inputs may alleviate the triggering of these pathways, preventing signalling induced negative feedback[336]. These results suggest that perhaps in these experiments, the observed signalling strength along the ERK pathway in NIH 3T3 mouse embryonic fibroblasts may oscillate between an activatory threshold and

negative feedback thresholds when signalling input was pulsed[336]. Further work is required to assess whether this is the case for $CD4^+$ T cells, however evidence exists that would otherwise support this hypothesis. In the Opto-CAR experiments described earlier, authors have also developed a similar optically controlled anti-CD19 CAR T cell and have begun to address the question in hand[334]. Here, activation of the anti-CD19 CAR T cell for either 6 hours continuously in the dark (to permit signalling), or with 24 x 15 minute pulses of dark to permit signalling, induced approximately a 3-fold increase in surface levels of CD137 expression when analysed as a measured of CAR T cell activation. These results indicate that when signalling input was pulsed, yet total signal input was identical (i.e., both treatments were given a 6-hour time period in the dark), the functional output was substantially increased by pulsatile inputs. We also see encouraging evidence of this in our own pulsatile magnetic force experiments, where 4 x 15-minute pulses induce an increased level of Nr4a3 expression when compared with a single 60-minute force treatment.

Further experimentation through the monitoring of negative feedback loops would shed light on the potential existence of these differential signalling induced thresholds. It would be interesting to assess phosphorylation of the protein phosphatases PTPN22[48], downstream of kinase (DOK) 1 and 2[337], and DUSP family proteins[65,297], as well as determining recruitment of ubiquitin ligases such as Cbl-b[75] to attempt to reveal any potential negative feedback mechanisms. Finally, simply performing the existing pulsatile magnetic force application protocol displayed in this thesis with the high signal strength $1\mu m^{Hi}$ MNPs would also reveal whether pulsatile signalling input in $CD4^+$ T cells can prevent induction of negative feedback loops. If negative feedback thresholds indeed exist within $CD4^+$ T cells, it may be expected that pulsatile force application for 4 x 15-minute pulses may prevent either the downregulation of activation markers, or upregulation of inhibitory

receptors, found with a single 60-minute force application to 1µm^{Hi} MNPs. In addition to this, preliminary experiments comparing the effect of a single 60 minute pulse, or 4x15 minute pulses on CTLA-4 expression in the context of 1µm^{Hi} MNPs (appendix show that with 1 hour of force application, expression of CTLA-4 is upregulated in the context of 1µm^{Hi} MNPs when compared with the no magnetic force control, yet this response in absent when force application was pulsed for 4 rounds of 15 minutes (appendix figure 8.10). Therefore, it appears that pulsing of the magnet force input prevents the triggering of negative feedback thresholds that may regulate expression of co-inhibitory receptors. However, since this is a preliminary experiment, further repeats are needed to be confident of this conclusion. Should this observation hold true, in would be of interest to investigate the phospho-proteome in these conditions to identify the pathways involved in permitting expression of these negative feedback associated proteins.

6.3 Pseudo Immune Synapse formation likely mediates the effects of magnetic force

6.3.1 Particle size is a key determinant in promoting TCR signalling

Within this thesis, we have utilised two different sized MNPs functionalised with anti-CD3ε (250nm MNPs vs 1µm MNPs). Use of a larger particle permits a larger force to be transferred to the TCR due to the larger body of magnetic material within the particle core. Therefore, we were able to determine whether the gradation of force magnitudes could affect TCR signalling by asking the following question: Does increasing the magnitude of force applied to the TCR increase the level of signalling observed?

As described in 2.7, force magnitudes transferred to 1µm MNPs by the MICA platform are estimated to be greater than those transferred to 250nm MNPs. Importantly, levels of anti-CD3 on the surface of these particles are estimated to be similar, when measured by FACS

(figure 3.10-B). Use of these particles in T cell activation assays measuring Nr4a3, CD69 and CD25 expression 4 hours post force application showed that whilst 1µm^{Mid} particles induce generally larger levels of T cell activation, this cannot be directly contributed to the increased force magnitude due to the fact background levels (i.e., no force application) of T cell activation also increase when using the larger 1µm particles. Interestingly, force application to both 250nm^{Mid} anti-CD3 and 1µm^{Mid} anti-CD3 MNPs induced approximately a 2-fold increase in the percentage of Nr4a3^{+} cells, as shown in figures 3.4 and 3.9 respectively (250nm^{Mid}: No MF average: 7.9%, + MF average: 13.9%, fold change: 1.75. 1µm^{Mid}: No MF average: 17.88%, + MF average: 32.15%, fold change: 1.79). Therefore, we cannot conclude from these data that increased levels of force application to the 1µm^{Mid} MNPs leads to more robust TCR signalling.

However, we do find that use of the 1µm particle, with a surface area approximately 16 times larger than that on the 250nm MNP induces greater levels of signalling than the 250nm MNP, both with and without magnet. This is important, as previous reports have shown that upon pMHC recognition, T cells undergo dramatic rearrangements during the formation of the immune synapse, within which physical symmetry between T cell and APC has been shown to be a critical factor in these rearrangements[270]. Here, Sims and colleagues have shown that PKC-θ may induce destabilisation of the IS, resulting in the breaking of symmetry within the pSMAC leading to increased cell motility and subsequent loss of stable synapse formation[338]. Symmetry breaking has been shown to be dependent on actin-myosin network reorganisation[339], which has led to an appealing scenario whereby PKCθ mediated phosphorylation of WASP interacting protein (WIP) may permit WASP-myosin II interaction, permitting contraction of the actin networks within the pSMAC and loss of IS stability[340,341].

Therefore, our results may suggest that use of particles with a larger surface area permit rearrangements required for IS formation to take place more successfully, and hence induce a larger degree of TCR signalling and T cell activation, explaining the increased levels of TCR signalling observed with 1µm^{Mid} MNPs compared to 250nm^{Mid} anti-CD3 MNPs at equivalent surface loadings of anti-CD3 (figure 3.10-B). This argument is further strengthened by the observation that production of artificial antigen presenting cells (aAPC) of different shape and topology, through the use of bodies of poly(ethylene glycol)-block-poly(D,L-lactide) (PEG-PDLLA) bodies tethered to anti-CD3 and anti-CD28 antibodies, showed that modulation of aAPC topology to promote an increased aAPC-T cell surface promoted increased T cell activation[342]. In our protocol, force application may therefore serve to manipulate TCRs and hence effect TCR membrane organisation, further promoting hallmarks of IS formation and promoting robust TCR signalling and T cell activation.

6.3.2 Hallmarks of immune synapse formation – Concurrent TCR downregulation and activation, and CD45 exclusion

As well as the intriguing effects arising from use of larger particles which provide larger degrees of symmetry between particle and T cell, we also provide evidence of further hallmarks of immune synapse formation in response to magnetic force application. Firstly, when analysing by confocal microscopy, we find that in areas of membrane – particle contact there is a loss of CD45 intensity within these regions of the membrane. Importantly, with force application this intensity is further reduced, indicating that force application for 60 minutes induces remodelling of proteins within the cell membrane that serve to exclude CD45 from areas of membrane – particle contact. This may serve to shift the balance of kinase – phosphatase activity at the site of actively engaged TCR-CD3 complexes in the favour of TCR signalling and T cell activation as reported by others[145,147,304].

Additionally, we find that the TCR itself is rapidly downregulated in response to force application. Importantly, we observe that TCR downregulation only occurs under conditions where T cell activation also takes place (figures 4.1, 4.2, 4.6), suggesting that the two processes are linked. Furthermore, we provide evidence that those cells that downregulate their TCRs in response to magnetic force application are predominantly those that are activated by force application, resulting in a population of $CD4^+$ T cells that become TCRlo and activation marker positive (figures 4.13-4.14).

Physiologically, TCRs are known to be downregulated in response to recognition of strong agonist pMHC molecules on the surface of APCs[108,115]. As described in the thesis introduction (1.6), TCR downregulation in the IS occurs at the central region of the structure, the cSMAC[104,108]. TCRs are shuttled along the cell surface, driven predominantly via actin retrograde flow from distal regions of the synapse[105,111]. In our system, we find that the induction of TCRlo activation marker positive $CD4^+$ T cells is prevented through the blockade of actin polymerisation, achieved through the use of Latrunculin A (which acts to sequester globular actin and hence prevent its incorporation into filamentous actin). This is an important finding, as it provides further support that TCR downregulation and T cell activation in response to magnetic force application are inherently linked, as where TCR downregulation in response to magnetic force is prevented, these cells do not simply become TCRhi whilst retaining activation marker expression.

Multiple lines of research have postulated whether IS formation is a cause, or a consequence of TCR signalling. In an attempt to address this question within our system, we again utilised the Src kinase inhibitor PP2 (figure 4.19). These experiments show that not only does use of PP2 block TCR signalling, but cells are also then unable to downregulate

their TCRs in response to magnetic field. These experiments suggest that TCR downregulation is dependent on TCR phosphorylation, which would support the notion that IS formation is a consequence, and not the initiating cause, of TCR signalling and serves as a mechanism to both promote robust signalling and activation. TCR downregulation could then be considered a negative feedback mechanism designed to limit TCR signalling. In line with these proposals is the fact that MNPs functionalised with typically non-activating antibodies that target the TCR-CD3 complex, failed to cause TCR downregulation in response to magnetic force (figure 4.1).

Continuing with this line of work, we performed single molecule localisation microscopy (SMLM) in order to look for the distribution of the TCR in the cell membrane in response to force application. In these experiments, we find that force application results in the emergence of TCR clusters (henceforth termed TCR microclusters, TCR-MCs) within 5-15 minutes of force application. Importantly, we also find that formation of these TCR-MCs is dependent on active TCR phosphorylation, as their formation is blocked by use of PP2. This again provides further support for the notion described earlier which suggests that TCR remodelling within the cell membrane requires TCR phosphorylation. Interestingly, this 5-15 minute time scale for TCR-MC formation strikes an intriguing parallel with the pulsatile magnet/CsA experiments descried earlier, which shows that accumulation of signalling events is induced within 15 minute pulses of magnetic force and this leads to robust TCR signalling required for T cell activation. Therefore, it is appealing to hypothesize that formation of these TCR-MCs is the driving factor behind initiation of these signalling events. Further experimentation may be required to prove this. For example, multi-colour STORM imaging experiments could be used to map the localisation of TCR molecules together with active signalling molecules such as pZAP-70 and negative signalling mediators such as CD45

to define the distribution and kinetics of 'signalling active' TCR molecules and their regulators. Finally, as described earlier (see 4.9.2), further experimentation comparing static and dynamic magnetic fields for force application may begin to address whether dynamic force application is able to induce upstream conformational changes in the TCR-CD3 complex that are able to govern TCR-MC formation.

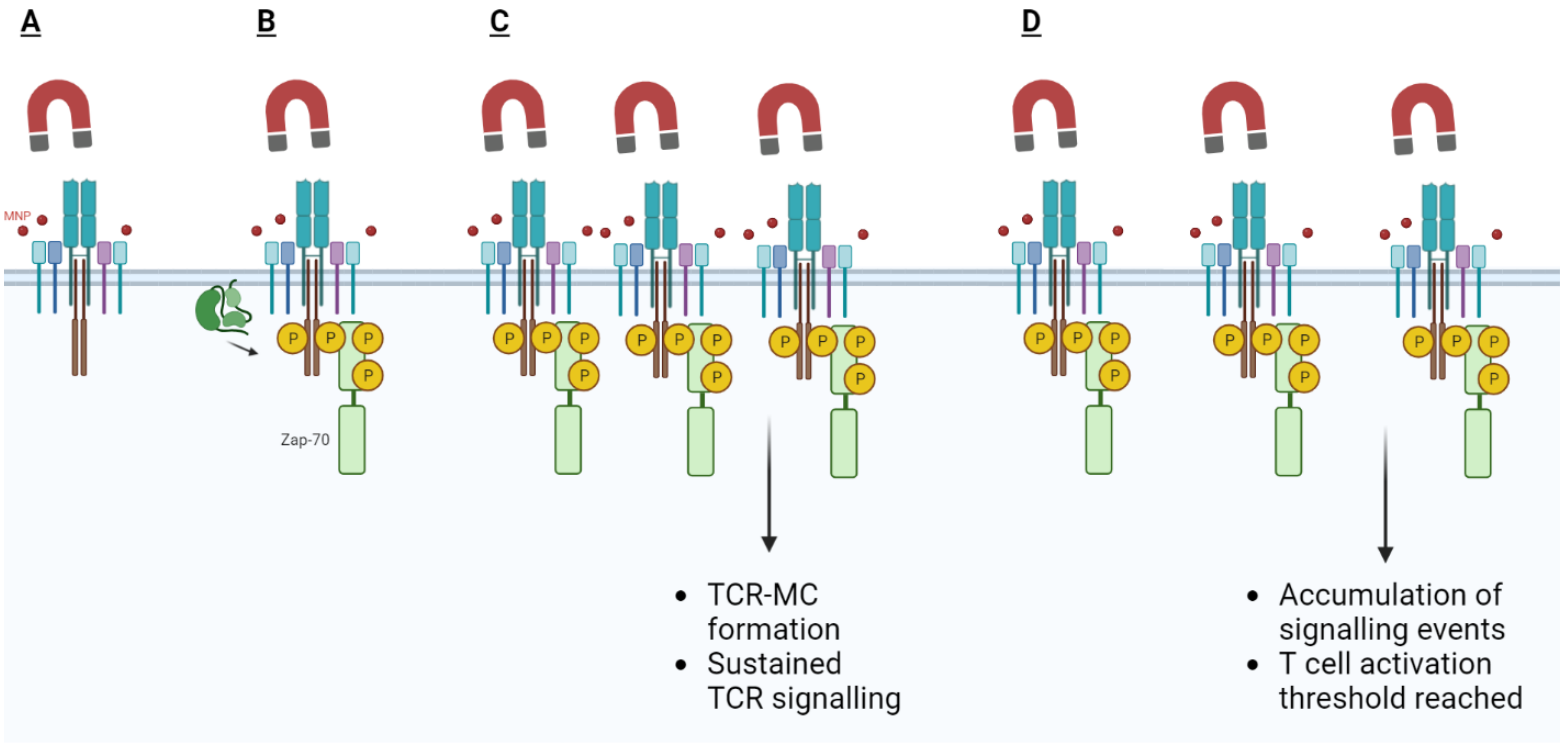


Figure 6.3 – A proposed mechanism of action for force mediated TCR signalling. A) TCRs are weakly phosphorylated in response to stimulation with MNPs alone, and hence only induce low levels of T cell activation. B) Force application to the TCR induces TCR phosphorylation, and force application for 5-15 minutes promotes formation of TCR microclusters (TCR-MCs) (C). D) Signalling events induced down stream of these TCR-MCs can promote accumulation of signalling events required to trigger thresholds for T cell activation, whilst TCR-MCs ultimately disassociate and are internalised from the cell surface.

Finally, we have observed that by 30 minutes of force application, TCR-MC formation is ultimately lost, whilst robust T cell activation appears to require an hour of force application. Interestingly, we provide evidence that TCR internalisation appears to accumulate across the time course of magnetic force application (whereby significant TCR

downregulation is observed with 30 minutes of force application, figures 4.1 and 4.8), which suggest a role for these internalised TCRs in promoting signal accumulation. This idea has been proposed elsewhere, where internalised plasma membrane derived CD3ζ molecules have been shown to be co-internalised in endosomes with active-Lck, which may promote continual ITAM phosphorylation within internalised endosomes[116]. Authors here also reported the interesting finding that endosomal CD3ζ molecules were phosphorylated more extensively than membrane bound CD3ζ[116], yet this does not answer whether this phosphorylation took place once the molecule was internalised and became endosomal, or whether this heavier phosphorylation is a result of phosphorylation and subsequent internalisation from the membrane. However, it has been reported that TCR triggering and subsequent TCR downregulation, can also mediate the downregulation of non-engaged receptors in a signal transduction dependent mechanism[117]. Therefore, taking these two findings together may provide support for a mechanism where signalling dependent internalisation of engaged receptors may also result in the increased proximity of co-internalised non-engaged TCRs with active Lck on endosomes and thus promote continual TCR signalling and subsequent signal accumulation.

6.4 Force modulation of CD4$^+$ T cell phenotype and therapeutic outlook

Data presented within this thesis indicate that force application to the TCR is able to modulate CD4$^+$ T cell phenotype. We indicate that force application to 1µm^{Hi} MNPs, which provide a high signal 1 strength when given in the absence of force, induces upregulation of co-inhibitory receptors Tigit, CTLA-4 and PD-1. In support of these findings is the fact that expression of co-inhibitory receptors has been widely reported to correlate with TCR signalling strength[318,326]. However, we identify that use of these CD4$^+$ T cells in suppression

assays fails to induce robust immune suppression, likely through a lack of robust IL-10 expression, since treatment with CAL101 was found to promote IL-10 expression and subsequently mediated immune suppression of the naïve $CD4^+$ T cell response. However, we do observe that by day 7, when analysing IL-10 expression from $CD4^+$ T cells treated with $1\mu m^{Hi}$ MNPs, these cells were capable of producing higher levels of IL-10 than compared with cells stimulated with $1\mu m^{Mid}$ MNPs (figures 5.23 and 5.24). Interestingly, we also find a small effect of force application on this level of IL-10 production from cells stimulated with $1\mu m^{Hi}$ MNPs (figures 5.24 – 5.26). These results are important when put into context with the results of IL-2 and IFNγ production when measured via peptide rechallenge of these cells at day 3. Broadly, we find that when cells are restimulated with peptide at day 3, cells that were originally stimulated with $1\mu m^{Mid}$ MNPs secreted high levels of IL-2 and intermediate levels of IFNγ in response to peptide, whilst cells originally stimulated with $1\mu m^{Hi}$ MNPs lost the ability to secrete IL-2 in response to peptide rechallenge yet secreted IFNγ largely in a peptide-independent manner (figure 5.2). These results suggest that TCR signal strength alters the cytokine secretion profile of Tg4 $CD4^+$ T cells via the Th1 pathway, as previously reported through the use of altered peptide ligands for the Tg4 TCR[343]. This previous work has shown that use of the 4K/4A/4Y analogues of the Ac1-9 MBP peptide, which have an increasing affinity for the Tg4 TCR, produced a shift in the cytokine secretion profile from IL-2, to IFNγ and finally to IL-10 secretion correlating with increasing peptide affinity[343], and induction of a suppressive phenotype[344]. We therefore conclude that whilst TCR signalling strength is able to control the cytokine secretion profile of $CD4^+$ T cells, magnetic force application under the conditions tested induces only small effects of eventual IL-10 production, and that without further chemical perturbation of these $CD4^+$ T cells, these cells do not induce robust immune suppression. It will be interesting to interrogate through

further experimentation whether TCR signalling strengths with our MNP approach can reach sufficient levels to promote robust IL-10 secretion required for immune suppression.

Additionally, we also find that TCR signal strength correlates with the emergence of an anergic phenotype (figures 5.1 and 5.8), which we identify as potentially being mediated through persistent TCR downregulation in response to strong TCR signalling (figure 5.13). These findings are in line with other studies which show that *in vivo* stimulation with high affinity antigens for $CD4^+$ T cells in both *M. tuberculosis* infection models[314,316] and transgenic models using TCRs specific for MCC peptide[315] induces a prolonged loss of TCR expression compared to stimulation with lower affinity antigens, and associated with loss of effector functions.

Finally, we found that in line with other reports, low TCR signalling strengths induces an outgrowth of $FoxP3^+$ expressing $CD4^+$ T cells *in vitro*, which was reduced upon force application. Whilst these cells were found to induce low levels of immune suppression, we again failed to observe robust IL-10 production from these $CD4^+$ T cells. However, as CAL101 treatment was performed in an effort to reinstate FoxP3 expression where it was otherwise lost in $1\mu m^{Hi}$ stimulated cultures, $1\mu m^{Mid}$ stimulated conditions were not treated with CAL101. Therefore, it will be important to assess whether a combination of $1\mu m^{Mid}$ MNP and CAL101 treatment can induce a population of $FoxP3^+$ $CD4^+$ T cells which express IL-10 to higher levels and may induce greater immune suppression.

We conclude that the data presented in this thesis supports the concept that force application to the TCR promotes TCR signalling, membrane remodelling and has subsequent downstream consequences on $CD4^+$ T cell responses.

CHAPTER 7

7 References

1. Arstila, T. P. *et al.* A direct estimate of the human αβ T cell receptor diversity. *Science (80-.).* **286**, 958–961 (1999).
2. Davis, M. M. & Bjorkman, P. J. The T cell receptor genes and T cell recognition. *Nature* **334**, 395–402 (1988).
3. Krangel, M. Mechanics of T cell receptor gene rearrangement. *Curr. Opin. Immunol.* **21**, 133–139 (2009).
4. Krangel, M. S. Gene segment selection in V(D)J recombination: accessibility and beyond. *Nat. Immunol. 2003 47* **4**, 624–630 (2003).
5. Jackson, K. J. L., Kidd, M. J., Wang, Y. & Collins, A. M. The shape of the lymphocyte receptor repertoire: Lessons from the B cell receptor. *Front. Immunol.* **4**, 1–12 (2013).
6. Takaba, H. & Takayanagi, H. The Mechanisms of T Cell Selection in the Thymus. *Trends Immunol.* **38**, 805–816 (2017).
7. Anderson, G. & Takahama, Y. Thymic epithelial cells: Working class heroes for T cell development and repertoire selection. *Trends Immunol.* **33**, 256–263 (2012).
8. Takahama, Y. Journey through the thymus: stromal guides for T-cell development and selection. *Nat. Rev. Immunol.* **6**, 127–135 (2006).
9. Palmer, E. Negative selection - Clearing out the bad apples from the T-cell repertoire. *Nat. Rev. Immunol.* **3**, 383–391 (2003).
10. Liston, A., Lesage, S., Wilson, J., Peltonen, L. & Goodnow, C. C. Aire regulates negative selection of organ-specific T cells. *Nat. Immunol.* **4**, 350–354 (2003).
11. Borgulya, P., Kishi, H., Muller, U., Kirberg, J. & Von Boehmer, H. Development of the CD4 and CD8 lineage of T cells: instruction versus selection. *EMBO J.* **10**, 913–918 (1991).
12. Maloy, K. J. & Powrie, F. Regulatory T cells in the control of immune pathology. *Nat. Immunol.* **2**, 816–822 (2001).
13. Hsieh, C. S., Lee, H. M. & Lio, C. W. J. Selection of regulatory T cells in the thymus. *Nat. Rev. Immunol.* **12**, 157–167 (2012).
14. Van Der Merwe, P. A. & Davis, S. J. Molecular Interaction Mediating T Cell Antigen Recognition. *Annu. Rev. Immunol* **21**, 659–84 (2003).
15. Pishesha, N., Harmand, T. J. & Ploegh, H. L. A guide to antigen processing and presentation. *Nat. Rev. Immunol.* **26**, (2022).
16. Lieberman, J. The ABCs of granule-mediated cytotoxicity: New weapons in the arsenal. *Nat. Rev. Immunol.* **3**, 361–370 (2003).

17. Voskoboinik, I., Whisstock, J. C. & Trapani, J. A. Perforin and granzymes: function, dysfunction and human pathology. *Nat. Rev. Immunol. 2015 156* **15**, 388–400 (2015).

18. Russell, J. H. & Ley, T. J. Lymphocyte-Mediated Cytotoxicity. *Annu. Rev. Immunol* **20**, 323–370 (2003).

19. Cox, M. A., Harrington, L. E. & Zajac, A. J. Cytokines and the inception of CD8 T cell responses. *Trends Immunol.* **32**, 180–186 (2011).

20. Russ, B. E., Prier, J. E., Rao, S., Turner, S. J. & Galvan, S. C. T cell immunity as a tool for studying epigenetic regulation of cellular differentiation. **4**, 1–10 (2013).

21. Malterer, M. B., Glass, S. J. & Newman, J. P. Interferon-stimulated genes: A complex web of host defenses. *Annu. Rev. Immunol.* **44**, 735–745 (2014).

22. Luckheeram, R. V., Zhou, R., Verma, A. D. & Xia, B. CD4 +T cells: Differentiation and functions. *Clin. Dev. Immunol.* **2012**, (2012).

23. Swain, S. L., McKinstry, K. K. & Strutt, T. M. Expanding roles for CD4 + T cells in immunity to viruses. *Nat. Rev. Immunol.* **12**, 136–148 (2012).

24. Dong, D. *et al.* Structural basis of assembly of the human T cell receptor–CD3 complex. *Nature* **573**, 546–552 (2019).

25. Brazin, K. N. *et al.* Structural features of the aβTCR mechanotransduction apparatus that promote pMHC discrimination. *Front. Immunol.* **6**, (2015).

26. Harrison, D. L., Fang, Y. & Huang, J. T-cell mechanobiology: Force sensation, potentiation, and translation. *Front. Phys.* **7**, 1–18 (2019).

27. Deseke, M. & Prinz, I. Ligand recognition by the γδ TCR and discrimination between homeostasis and stress conditions. *Cellular and Molecular Immunology* vol. 17 914–924 (2020).

28. Oettinger, M. A., Schatz, D. G., Gorka, C. & Baltimore, D. RAG-1 and RAG-2, Adjacent Genes That Synergistically Activate V(D)J Recombination. *Science (80-.).* **248**, 1517–1523 (1990).

29. Schatz, D. G., Oettinger, M. A. & Schlissel, M. S. V(D)J RECOMBINATION: Molecular Biology and Regulation. *Annu. Rev. Immunol* **10**, 359–383 (1992).

30. Schatz, D. G. & Ji, Y. Recombination centres and the orchestration of V(D)J recombination. *Nat. Rev. Immunol.* **11**, 251–263 (2011).

31. Cowell, L. G., Kim, H.-J., Humaljoki, T., Berek, C. & Kepler, T. B. Enhanced Evolvability in Immunoglobulin V Genes Under Somatic Hypermutation. *J. Mol. Evol.* **49**, 23–26 (1999).

32. Wong, W. K., Leem, J. & Leem, J. Comparative Analysis of the CDR Loops of Antigen Receptors. *Front. Immunol.* **10**, 1–11 (2019).

33. Xu, X., Li, H. & Xu, C. Structural understanding of T cell receptor triggering. *Cell. Mol. Immunol.* **17**, 193–202 (2020).

34. Mariuzza, R. A., Agnihotri, P. & Orban, J. The structural basis of T-cell receptor (TCR)

activation: An enduring enigma. *J. Biol. Chem.* **295**, 914–925 (2020).

35. He, Y. *et al.* Identification of the docking site for CD3 on the T cell receptor β chain by solution NMR. *J. Biol. Chem.* **290**, 19796–19805 (2015).

36. Birnbaum, M. E. *et al.* Molecular architecture of the αβ T cell receptor-CD3 complex. *Proc. Natl. Acad. Sci. U. S. A.* **111**, 17576–17581 (2014).

37. Gascoigne, N. R. J., Casas, J., Brzostek, J. & Rybakin, V. Initiation of TCR phosphorylation and signal transduction. *Front. Immunol.* **2**, 1–8 (2011).

38. Call, M. E., Pyrdol, J. & Wucherpfennig, K. W. Stoichiometry of the T-cell receptor-CD3 complex and key intermediates assembled in the endoplasmic reticulum. *EMBO J.* **23**, 2348–2357 (2004).

39. Wucherpfennig, K. W., Gagnon, E., Call, M. J., Huseby, E. S. & Call, M. E. Structural biology of the T-cell receptor: insights into receptor assembly, ligand recognition, and initiation of signaling. *Cold Spring Harb. Perspect. Biol.* **2**, (2010).

40. James, J. R. Tuning ITAM multiplicity on T cell receptors can control potency and selectivity to ligand density. *Sci. Signal.* **11**, (2018).

41. Natarajan, A. *et al.* Structural Model of the Extracellular Assembly of the TCR-CD3 Complex. *Cell Rep.* **14**, 2833–2845 (2016).

42. Call, M. E. & Wucherpfennig, K. W. Molecular mechanisms for the assembly of the T cell receptor–CD3 complex. *Mol. Immunol.* **40**, 1295 (2004).

43. Alarcon, B., Berkhout, B., Breitmeyer, J. & Terhorst, C. Assembly of the human T cell receptor-CD3 complex takes place in the endoplasmic reticulum and involves intermediary complexes between the CD3-γ·δ·ε core and single T cell receptor α or β chains. *J. Biol. Chem.* **263**, 2953–2961 (1988).

44. Sušac, L. *et al.* Structure of a fully assembled tumor-specific T cell receptor ligated by pMHC. *Cell* **185**, 3201–3213 (2022).

45. Reth, M. Antigen receptor tail clue. *Nature* **338**, 383–384 (1989).

46. Love, P. E. & Hayes, S. M. ITAM-mediated signaling by the T-cell antigen receptor. *Cold Spring Harb. Perspect. Biol.* **2**, 1–11 (2010).

47. Li, Y.-C. *et al.* Cutting Edge: Mechanical Forces Acting on T Cells Immobilized via the TCR Complex Can Trigger TCR Signaling. *J. Immunol.* **184**, 5959–5963 (2010).

48. Gaud, G., Lesourne, R. & Love, P. E. Regulatory mechanisms in T cell receptor signalling. *Nat. Rev. Immunol.* **18**, 485–497 (2018).

49. Balagopalan, L., Kortum, R. L., Coussens, N. P., Barr, V. A. & Samelson, L. E. The linker for activation of T Cells (LAT) signaling hub: From signaling complexes to microclusters. *J. Biol. Chem.* **290**, 26422–26429 (2015).

50. Casas, J. *et al.* Ligand-engaged TCR is triggered by Lck not associated with CD8 coreceptor. *Nat. Commun.* **5**, (2014).

51. Balagopalan, L., Coussens, N. P., Sherman, E., Samelson, L. E. & Sommers, C. L. The

LAT Story : A Tale of Cooperativity , Coordination , and Choreography. *Cold Spring Harb. Perspect. Biol.* 1–22 (2010).

52. Yi, J., Balagopalan, L., Nguyen, T., Mcintire, K. M. & Samelson, L. E. TCR microclusters form spatially segregated domains and sequentially assemble in calcium-dependent kinetic steps. *Nat. Commun.* 1–13 doi:10.1038/s41467-018-08064-2.

53. Conley, J. M., Gallagher, M. P., Rao, A. & Berg, L. J. Activation of the Tec Kinase ITK Controls Graded IRF4 Expression in Response to Variations in TCR Signal Strength. *J. Immunol.* **205**, 335–345 (2020).

54. Feske, S. Ca2+ influx in T cells: How many Ca2+ channels? *Front. Immunol.* **4**, 1–4 (2013).

55. Feske, S. Calcium signalling in lymphocyte activation and disease. *Nat. Rev. Immunol.* **7**, 690–702 (2007).

56. Shah, K., Al-Haidari, A., Sun, J. & Kazi, J. U. T cell receptor (TCR) signaling in health and disease. *Signal Transduct. Target. Ther.* **6**, (2021).

57. Hwang, J. R., Byeon, Y., Kim, D. & Park, S. G. Recent insights of T cell receptor-mediated signaling pathways for T cell activation and development. *Exp. Mol. Med.* **52**, 750–761 (2020).

58. Hebeisen, M. *et al.* SHP-1 phosphatase activity counteracts increased T cell receptor affinity. *J. Clin. Invest.* **123**, 1044–1065 (2013).

59. Lorenz, U. SHP-1 and SHP-2 in T cells: two phosphatases functioning at many levels. *Immunol. Rev.* **228**, 342–359 (2009).

60. Zhang, Z., Shen, K., Lu, W. & Cole, P. A. The Role of C-terminal Tyrosine Phosphorylation in the Regulation of SHP-1 Explored via Expressed Protein Ligation*. *J. Biol. Chem.* **278**, 4668–4674 (2002).

61. Moogk, D. *et al.* Constitutive Lck Activity Drives Sensitivity Differences between CD8 + Memory T Cell Subsets . *J. Immunol.* **197**, 644–654 (2016).

62. Liu, Y., Kruhlak, M. J., Hao, J.-J. & Shaw, S. Rapid T cell receptor-mediated SHP-1 S591 phosphorylation regulates SHP-1 cellular localization and phosphatase activity. *J. Leukoc. Biol.* **82**, 742–751 (2007).

63. Chiang, G. G. & Sefton, B. M. Specific Dephosphorylation of the Lck Tyrosine Protein Kinase at Tyr-394 by the SHP-1 Protein-tyrosine Phosphatase. *J. Biol. Chem.* **276**, 23173–23178 (2001).

64. Caunt, C. J., Armstrong, S. P., Rivers, C. A., Norman, M. R. & McArdle, C. A. Spatiotemporal regulation of ERK2 by dual specificity phosphatases. *J. Biol. Chem.* **283**, 26612–26623 (2008).

65. Bertin, S. *et al.* Dual-specificity phosphatase 6 regulates CD4+ T-cell functions and restrains spontaneous colitis in IL-10-deficient mice. *Mucosal Immunol. 2015 83* **8**, 505–515 (2014).

66. Buckler, J. L., Liu, X. & Turka, L. A. Regulation of T-cell responses by PTEN. *Immunol.*

Rev. **224**, 239–248 (2008).

67. Stambolic, V. *et al.* Negative regulation of PKB/Akt-dependent cell survival by the tumor suppressor PTEN. *Cell* **95**, 29–39 (1998).

68. Kliza, K. & Husnjak, K. Resolving the Complexity of Ubiquitin Networks. *Front. Mol. Biosci.* **7**, (2020).

69. Li, X., Gong, L. & Gu, H. Regulation of immune system development and function by Cbl-mediated ubiquitination. *Immunol. Rev.* **291**, 123–133 (2019).

70. Fang, D. *et al.* Cbl-b, a RING-type E3 Ubiquitin Ligase, Targets Phosphatidylinositol 3-Kinase for Ubiquitination in T Cells. *J. Biol. Chem.* **276**, 4872–4878 (2001).

71. Fang, D. & Liu, Y. C. Proteolysis-independent regulation of PI3K by Cbl-b–mediated ubiquitination in T cells. *Nat. Immunol. 2001 29* **2**, 870–875 (2001).

72. Bevington, S. L. *et al.* Chromatin Priming Renders T Cell Tolerance-Associated Genes Sensitive to Activation below the Signaling Threshold for Immune Response Genes. *Cell Rep.* **31**, 107748 (2020).

73. Fathman, C. G. & Lineberry, N. B. Molecular mechanisms of CD4+ T-cell anergy. *Nat. Rev. Immunol.* **7**, 599–609 (2007).

74. Chiang, Y. J. *et al.* Cbl-b regulates the CD28 dependence of T-cell activation. *Nat. 2000 4036766* **403**, 216–220 (2000).

75. Bachmaier, K. *et al.* Negative regulation of lymphocyte activation and autoimmunity by the molecular adaptor Cbl-b. *Nature* **403**, 211–216 (2000).

76. Schwartz, R. H. T cell anergy. *Annu. Rev. Immunol.* **21**, 305–334 (2003).

77. Schwartz, R. H. A cell culture model for T lymphocyte clonal anergy. *Science (80-.).* **248**, 1349–1356 (1990).

78. This, S., Valbon, S. F., Lebel, M. È. & Melichar, H. J. Strength and numbers: The role of affinity and avidity in the 'quality' of t cell tolerance. *Cells* **10**, 1–21 (2021).

79. Jenkins, M. K. & Schwartz, R. H. Antigen presentation by chemically modified splenocytes induces antigen-specific T cell unresponsiveness in vitro and in vivo. *J. Exp. Med.* **165**, 302–319 (1987).

80. Lamb, J. R., Skidmore, B. J., Green, N., Chiller, J. M. & Feldmann, M. Induction of tolerance in influenza virus-immune T lymphocyte clones with synthetic peptides of influenza hemagglutinin. *J. Exp. Med.* **157**, 1434–1447 (1983).

81. Ragazzo, J. L., Ozaki, M. E., Karlsson, L., Peterson, P. A. & Webb, S. R. Costimulation via lymphocyte function-associated antigen 1 in the absence of CD28 ligation promotes anergy of naive CD4+ T cells. *Proc. Natl. Acad. Sci.* **98**, 241–246 (2001).

82. Beverly, B., Kang, S. mo, Lenardo, M. J. & Schwartz, R. H. Reversal of in vitro T cell clonal anergy by IL-2 stimulation. *Int. Immunol.* **4**, 661–671 (1992).

83. Wells, A. D., Bluestone, J. A. & Turka, L. A. Signaling through CD28 and CTLA-4 controls two distinct forms of T cell anergy. *J Clin Invest* **108**, (2001).

84. Tanchot, C., Barber, D. L., Chiodetti, L. & Schwartz, R. H. Adaptive Tolerance of CD4+ T Cells In Vivo: Multiple Thresholds in Response to a Constant Level of Antigen Presentation. *J. Immunol.* **167**, 2030–2039 (2001).

85. Liu, S. *et al.* Recruitment of Grb2 and SHIP1 by the ITT-like motif of TIGIT suppresses granule polarization and cytotoxicity of NK cells. *Cell Death Differ. 2013 203* **20**, 456–464 (2012).

86. Stamper, C. *et al.* Crystal structure of the B7-1/CTLA-4 complex that inhibits human immune responses. *Nature* **410**, 608–611 (2001).

87. Schwartz, J.-C. D., Zhang, X., Fedorov, A., Nathenson, S. G. & Almo, S. C. Structural basis for co-stimulaton by the human CTLA-4/B7-2 complex. *Nature* **410**, 604–608 (2001).

88. Arasanz, H. *et al.* PD1 signal transduction pathways in T cells. *Oncotarget* **8**, 51936–51945 (2017).

89. Leach, D. R., Krummel, M. F. & Allison, J. P. Enhancement of antitumor immunity by CTLA-4 blockade. *Science (80-.).* **271**, 1734–1736 (1996).

90. Hamanishi, J. *et al.* Safety and antitumor activity of Anti-PD-1 antibody, nivolumab, in patients with platinum-resistant ovarian cancer. *J. Clin. Oncol.* **33**, 4015–4022 (2015).

91. Rowshanravan, B., Halliday, N. & Sansom, D. M. CTLA-4: a moving target in immunotherapy. *Blood* **131**, 58–67 (2018).

92. Qin, W. *et al.* The Diverse Function of PD-1/PD-L Pathway Beyond Cancer. *Front. Immunol.* **10**, 2298 (2019).

93. Sharpe, A. H. & Pauken, K. E. The diverse functions of the PD1 inhibitory pathway. *Nat. Rev. Immunol.* **18**, 153–167 (2018).

94. Yokosuka, T. *et al.* Programmed cell death 1 forms negative costimulatory microclusters that directly inhibit T cell receptor signaling by recruiting phosphatase SHP2. *J. Exp. Med.* **209**, 1201–1217 (2012).

95. Harjunpää, H. & Guillerey, C. TIGIT as an emerging immune checkpoint. *Clin. Exp. Immunol.* **200**, 108–119 (2020).

96. Yu, X. *et al.* The surface protein TIGIT suppresses T cell activation by promoting the generation of mature immunoregulatory dendritic cells. *Nat. Immunol. 2008 101* **10**, 48–57 (2008).

97. Chauvin, J.-M. & Zarour, H. M. TIGIT in cancer immunotherapy. *J Immunother Cancer* **8**, (2020).

98. Graydon, C. G., Mohideen, S. & Fowke, K. R. LAG3's Enigmatic Mechanism of Action. *Front. Immunol.* **11**, (2021).

99. Maruhashi, T. *et al.* Binding of LAG-3 to stable peptide-MHC class II limits T cell function and suppresses autoimmunity and anti-cancer immunity. *Immunity* **55**, 912-924.e8 (2022).

100. Workman, C. J., Dugger, K. J. & Vignali, D. A. A. Activation Gene-3 Lymphocyte Negative Regulatory Function of Cutting Edge: Molecular Analysis of the. *J Immunol* **169**, 5392–5395 (2002).

101. Workman, C. J. & Vignali, D. A. A. Negative Regulation of T Cell Homeostasis by Lymphocyte Activation Gene-3 (CD223). *J. Immunol.* **174**, 688–695 (2005).

102. Monks, C. R. F., Freiberg, B. A., Kupfer, H., Sciaky, N. & Kupfer, A. Three-dimensional segregation of supramolecular activation clusters in T cells. *Nature* **395**, 82–86 (1998).

103. Bromley, S. K. *et al.* THE IMMUNOLOGICAL SYNAPSE. *Annu. Rev. Immunol* **19**, 375–396 (2001).

104. Alarcón, B., Mestre, D. & Martínez-Martín, N. The immunological synapse: A cause or consequence of T-cell receptor triggering? *Immunology* **133**, 420–425 (2011).

105. Krummel, M. F., Sjaastad, M. D., Wulfing, C. W. & Davis, M. M. Differential clustering of CD4 and CD3ζ during T cell recognition. *Science (80-.).* **289**, 1349–1352 (2000).

106. Lillemeier, B. F. *et al.* TCR and Lat are expressed on separate protein islands on T cell membranes and concatenate during activation. *Nat. Immunol.* **11**, 90–96 (2010).

107. Beck-García, K. *et al.* Nanoclusters of the resting T cell antigen receptor (TCR) localize to non-raft domains. *Biochim. Biophys. Acta - Mol. Cell Res.* **1853**, 802–809 (2015).

108. Onnis, A. & Baldari, C. T. Orchestration of Immunological Synapse Assembly by Vesicular Trafficking. *Front. Cell Dev. Biol.* **7**, 1–12 (2019).

109. Schamel, W. W. A. *et al.* Coexistence of multivalent and monovalent TCRs explains high sensitivity and wide range of response. *J. Exp. Med.* **202**, 493–503 (2005).

110. Krummel, M. F. & Davis, M. M. Dynamics of the immunological synapse: Finding, establishing and solidifying a connection. *Curr. Opin. Immunol.* **14**, 66–74 (2002).

111. Varma, R., Campi, G., Yokosuka, T., Saito, T. & Dustin, M. L. T Cell Receptor-Proximal Signals Are Sustained in Peripheral Microclusters and Terminated in the Central Supramolecular Activation Cluster. *Immunity* **25**, 117–127 (2006).

112. Vardhana, S., Choudhuri, K., Varma, R. & Dustin, M. L. Essential Role of Ubiquitin and TSG101 Protein in Formation and Function of the Central Supramolecular Activation Cluster. *Immunity* **32**, 531–540 (2010).

113. Naramura, M. *et al.* C-Cbl and Cbl-b regulate T cell responsiveness by promoting ligand-induced TCR down-modulation. *Nat. Immunol.* **3**, 1192–1199 (2002).

114. Williams, R. L. & Urbé, S. The emerging shape of the ESCRT machinery. *Nat. Rev. Mol. Cell Biol. 2007 85* **8**, 355–368 (2007).

115. Martínez-Martín, N. *et al.* T Cell Receptor Internalization from the Immunological Synapse Is Mediated by TC21 and RhoG GTPase-Dependent Phagocytosis. *Immunity* **35**, 208–222 (2011).

116. Yudushkin, I. A. & Vale, R. D. Imaging T-cell receptor activation reveals accumulation of tyrosine-phosphorylated CD3ζ in the endosomal compartment. *Proc. Natl. Acad.*

Sci. U. S. A. **107**, 22128–22133 (2010).

117. San José, E., Borroto, A., Niedergang, F., Alcover, A. & Alarcón, B. Triggering the TCR complex causes the downregulation of nonengaged receptors by a signal transduction-dependent mechanism. *Immunity* **12**, 161–170 (2000).

118. Campi, G., Varma, R. & Dustin, M. L. Actin and agonist MHC-peptide complex-dependent T cell receptor microclusters as scaffolds for signaling. *J. Exp. Med.* **202**, 1031–1036 (2005).

119. Sykulev, Y., Joo, M., Vturina, I., Tsomides, T. J. & Eisen, H. N. Evidence that a single peptide-MHC complex on a target cell can elicit a cytolytic T cell response. *Immunity* **4**, 565–571 (1996).

120. Huang, J. *et al.* A Single peptide-major histocompatibility complex ligand triggers digital cytokine secretion in CD4+ T Cells. *Immunity* **39**, 846–857 (2013).

121. Irvine, D. J., Purbhoo, M. A., Krogsgaard, M. & Davis, M. M. Direct observation of ligand recognition by T cells. *Nature* **419**, 845–849 (2002).

122. Valitutti, S. The serial engagement model 17 years after: From TCR triggering to immunotherapy. *Front. Immunol.* **3**, 272 (2012).

123. Rossy, J., Owen, D. M., Williamson, D. J., Yang, Z. & Gaus, K. Conformational states of the kinase Lck regulate clustering in early T cell signaling. *Nat. Immunol.* **14**, 82–89 (2013).

124. Trautmann, A. & Randriamampita, C. Initiation of TCR signalling revisited. *Trends Immunol.* **24**, 425–428 (2003).

125. Choudhuri, K. & van der Merwe, P. A. Molecular mechanisms involved in T cell receptor triggering. *Semin. Immunol.* **19**, 255–261 (2007).

126. Dushek, O., Acuto, O., Alarcon, B. & Dunn, W. Elementary steps in T cell receptor triggering. *Front. Immunol.* **2**, (2012).

127. Junghans, V., Jönsson, P., Santos, A., Lui, Y. & Davis, S. Dimensions and Interactions of Large T-Cell Surface Proteins. *Front. Immunol.* **9**, (2018).

128. Davis, S. J. & van der Merwe, P. A. The kinetic-segregation model: TCR triggering and beyond. *Nat. Immunol.* **7**, 803–809 (2006).

129. Davis, S. J. & van der Merwe, P. A. Lck and the nature of the T cell receptor trigger. *Trends Immunol.* **32**, 1–5 (2011).

130. Van Der Merwe, P. A. & Dushek, O. Mechanisms for T cell receptor triggering. *Nat. Rev. Immunol.* **11**, 47–55 (2011).

131. Locksley, R. M., Reiner, S. L., Hatam, F., Littman, D. R. & Killeen, N. Helper T cells without CD4: Control of leishmaniasis in CD4-deficient mice. *Science (80-.).* **261**, 1448–1451 (1993).

132. Krogsgaard, M., Juang, J. & Davis, M. M. A role for 'self' in T-cell activation. *Semin. Immunol.* **19**, 236–244 (2007).

133. Štefanoví, I., Dorfman, J. R. & Germain, R. N. Self-recognition promotes the foreign antigen sensitivity of naive T lymphocytes. *Nature* **420**, 429–434 (2002).

134. van der Merwe, P. A. Do T cell receptors do it alone? *Nat. Immunol.* **3**, 1122–1123 (2002).

135. Krogsgaard, M. *et al.* Agonist/endogenous peptide-MHC heterodimers drive T cell activation and sensitivity. *Nature* **434**, 238–243 (2005).

136. Wülfing, C. *et al.* Costimulation and endogenous mhc ligands contribute to t cell recognition. *Nat. Immunol.* **3**, 42–47 (2002).

137. Brameshuber, M. *et al.* Monomeric TCRs drive T cell antigen recognition. *Nat. Immunol.* **19**, 487–496 (2018).

138. Choudhuri, K. *et al.* Peptide-major histocompatibility complex dimensions control proximal kinase-phosphatase balance during T cell activation. *J. Biol. Chem.* **284**, 26096–26105 (2009).

139. Davis, S. J. & Van Der Merwe, P. A. The structure and ligand interactions of CD2: Implications for T-cell function. *Immunol. Today* **17**, 177–187 (1996).

140. Chang, V. T. *et al.* Initiation of T cell signaling by CD45 segregation at 'close contacts'. *Nat. Immunol.* **17**, 574–582 (2016).

141. Nika, K. *et al.* Constitutively active lck kinase in T cells drives antigen receptor signal transduction. *Immunity* **32**, 766–777 (2010).

142. O'Shea, J. J., Mcvicar, D. W., Bailey, T. L., Burns, C. & Smyth, M. J. Activation of human peripheral blood T lymphocytes by pharmacological induction of protein-tyrosine phosphorylation. *Proc. Natl. Acad. Sci. U. S. A.* **89**, 10306–10310 (1992).

143. Secrist, J. P., Burns, L. A., Karnitz, L., Koretzky, G. A. & Abraham, R. T. Stimulatory effects of the protein tyrosine phosphatase inhibitor, pervanadate, on T-cell activation events. *J. Biol. Chem.* **268**, 5886–5893 (1993).

144. Anton van der Merwe, P., McNamee, P. N., Davies, E. A., Barclay, A. N. & Davis, S. J. Topology of the CD2-CD48 cell-adhesion molecule complex: implications for antigen recognition by T cells. *Curr. Biol.* **5**, 74–84 (1995).

145. Chen, K. Y. *et al.* Trapping or slowing the diffusion of T cell receptors at close contacts initiates T cell signaling. *Proc. Natl. Acad. Sci. U. S. A.* **118**, (2021).

146. Dustin, M. L. The immunological synapse. *Cancer Immunol. Res.* **2**, 1023–1033 (2014).

147. Cordoba, S. P. *et al.* The large ectodomains of CD45 and CD148 regulate their segregation from and inhibition of ligated T-cell receptor. *Blood* **121**, 4295–4302 (2013).

148. Choudhuri, K., Wiseman, D., Brown, M. H., Gould, K. & Van Der Merwe, P. A. T-cell receptor triggering is critically dependent on the dimensions of its peptide-MHC ligand. *Nature* **436**, 578–582 (2005).

149. Mckeithan, T. W. Kinetic proofreading in T-cell receptor signal transduction. *Proc.*

Natl. Acad. Sci. U. S. A. **92**, 5042–5046 (1995).

150. Yousefi, O. S. *et al.* Optogenetic control shows that kinetic proofreading regulates the activity of the t cell receptor. *Elife* **8**, (2019).

151. Tischer, D. K. & Weiner, O. D. Light-based tuning of ligand half-life supports kinetic proofreading model of T cell signaling. *Elife* **8**, 1–25 (2019).

152. Carreño, L. J., Bueno, S. M., Bull, P., Nathenson, S. G. & Kalergis, A. M. The half-life of the T-cell receptor/peptide-major histocompatibility complex interaction can modulate T-cell activation in response to bacterial challenge. *Immunology* **121**, 227–237 (2007).

153. Kersh, G. J., Kersh, E. N., Fremont, D. H. & Allen, P. M. High-and Low-Potency Ligands with Similar Affinities for the TCR: The Importance of Kinetics in TCR Signaling. *Immunity* **9**, 817–826 (1998).

154. Kalergis, A. M. *et al.* Efficient T cell activation requires an optimal dwell-time of interaction between the TCR and the pMHC complex. *Nat. Immunol.* **2**, 229–234 (2001).

155. Aleksic, M. *et al.* Dependence of T Cell Antigen Recognition on T Cell Receptor-Peptide MHC Confinement Time. *Immunity* **32**, 163–174 (2010).

156. Pettmann, J. *et al.* The discriminatory power of the t cell receptor. *Elife* **10**, 1–42 (2021).

157. Au-Yeung, B. B., Shah, N. H., Shen, L. & Weiss, A. ZAP-70 in Signaling, Biology, and Disease. *Annu. Rev. Immunol.* **36**, 127–156 (2018).

158. Swamy, M. ZAP70 holds the key to kinetic proofreading for TCR ligand discrimination. *Nat. Immunol.* **23**, 1293–1302 (2022).

159. Voisinne, G. *et al.* Kinetic proofreading through the multi-step activation of the ZAP70 kinase underlies early T cell ligand discrimination. *Nat. Immunol. 2022 239* **23**, 1355–1364 (2022).

160. Rangarajan, S. *et al.* Peptide–MHC (pMHC) binding to a human antiviral T cell receptor induces long-range allosteric communication between pMHC- and CD3-binding sites. *J. Biol. Chem.* **293**, 15991–16005 (2018).

161. Beddoe, T. *et al.* Antigen Ligation Triggers a Conformational Change within the Constant Domain of the αβ T Cell Receptor. *Immunity* **30**, 777–788 (2009).

162. Kjer-Nielsen, L. *et al.* The 1.5 Å crystal structure of a highly selected antiviral T cell receptor provides evidence for a structural basis of immunodominance. *Structure* **10**, 1521–1532 (2002).

163. Natarajan, K. *et al.* An allosteric site in the T-cell receptor Cβ domain plays a critical signalling role. *Nat. Commun.* **8**, 1–14 (2017).

164. Rossjohn, J. *et al.* T Cell Antigen Receptor Recognition of Antigen-Presenting Molecules. *Annu. Rev. Immunol.* **33**, 169–200 (2015).

165. Yang, X. & Mariuzza, R. A. Pre-T-cell receptor binds MHC: Implications for thymocyte signaling and selection. *Proc. Natl. Acad. Sci. U. S. A.* **112**, 8166–8167 (2015).

166. Dutta, A., Zhao, B. & Love, P. E. New insights into TCR β-selection. *Trends Immunol.* **42**, 735–750 (2021).

167. Brazin, K. N., Mallis, R. J., Das, D. K. & Feng, Y. Structural features of the αβ TCR mechanotransduction apparatus that promote pMHC discrimination. *Front. Immunol.* **6**, (2015).

168. Garboczi, D. N. *et al.* Structure of the complex between human T-cell receptor, viral peptide and HLA-A2. *Nature* **384**, 134–141 (1996).

169. Wang, J. H. *et al.* Atomic structure of an αβ T cell receptor (TCR) heterodimer in complex with an anti-TCR Fab fragment derived from a mitogenic antibody. *EMBO J.* **17**, 10–26 (1998).

170. Das, D. K. *et al.* Force-dependent transition in the T-cell receptor β-subunit allosterically regulates peptide discrimination and pMHC bond lifetime. *Proc. Natl. Acad. Sci. U. S. A.* **112**, 1517–1522 (2015).

171. Sasada, T. *et al.* Involvement of the TCR Cβ FG loop in thymic selection and T cell function. *J. Exp. Med.* **195**, 1419–1431 (2002).

172. Kim, S. T. *et al.* Distinctive CD3 Heterodimeric Ectodomain Topologies Maximize Antigen-Triggered Activation of αβ T Cell Receptors. *J. Immunol.* **185**, 2951–2959 (2010).

173. DeFord-Watts, L. M. *et al.* The CD3 ζ Subunit Contains a Phosphoinositide-Binding Motif That Is Required for the Stable Accumulation of TCR–CD3 Complex at the Immunological Synapse. *J. Immunol.* **186**, 6839–6847 (2011).

174. Zhang, H., Cordoba, S. P., Dushek, O. & Van Der Merwe, P. A. Basic residues in the T-cell receptor ζ cytoplasmic domain mediate membrane association and modulate signaling. *Proc. Natl. Acad. Sci. U. S. A.* **108**, 19323–19328 (2011).

175. Li, L. *et al.* Ionic CD3−Lck interaction regulates the initiation of T-cell receptor signaling. *Proc. Natl. Acad. Sci. U. S. A.* **114**, E5891–E5899 (2017).

176. Xu, C. *et al.* Regulation of T Cell Receptor Activation by Dynamic Membrane Binding of the CD3ε Cytoplasmic Tyrosine-Based Motif. *Cell* **135**, 702–713 (2008).

177. Guo, X. *et al.* Lipid-dependent conformational dynamics underlie the functional versatility of T-cell receptor. *Cell Res.* **27**, 505–525 (2017).

178. Borroto, A. *et al.* Relevance of Nck–CD3ε Interaction for T Cell Activation In Vivo. *J. Immunol.* **192**, 2042–2053 (2014).

179. Gagnon, E., Schubert, D. A., Gordo, S., Chu, H. H. & Wucherpfennig, K. W. Local changes in lipid environment of TCR microclusters regulate membrane binding by the CD3 □ cytoplasmic domain. *J. Exp. Med.* **209**, 2423–2439 (2012).

180. Fernandes, R. A. *et al.* What Controls T Cell Receptor Phosphorylation? *Cell* **142**, 668–669 (2010).

181. DeFord-Watts, L. M. *et al.* The Cytoplasmic Tail of the T Cell Receptor CD3 ε Subunit Contains a Phospholipid-Binding Motif that Regulates T Cell Functions. *J. Immunol.* **183**, 1055–1064 (2009).

182. Fernandes, R. A., Huo, J., Lui, Y., Felce, J. H. & Davis, S. J. On the control of TCR phosphorylation. *Front. Immunol.* **3**, 1–4 (2012).

183. Kim, S. T. *et al.* The αβ T cell receptor is an anisotropic mechanosensor. *J. Biol. Chem.* **284**, 31028–31037 (2009).

184. Tacke, M., Hanke, G., Hanke, T. & Hünig, T. CD28-mediated induction of proliferation in resting T cells in vitro and in vivo without engagement of the T cell receptor: Evidence for functionally distinct forms of CD28. *Eur. J. Immunol.* **27**, 239–247 (1997).

185. Evans, E. J. *et al.* Crystal structure of a soluble CD28-Fab complex. *Nat. Immunol.* **6**, 271–279 (2005).

186. Beyersdorf, N., Hanke, T., Kerkau, T. & Hünig, T. Superagonistic anti-CD28 antibodies: Potent activators of regulatory T cells for the therapy of autoimmune diseases. *Ann. Rheum. Dis.* **64**, 91–95 (2005).

187. Lühder, F. *et al.* Topological requirements and signaling properties of T cell-activating, anti-CD28 antibody superagonists. *J. Exp. Med.* **197**, 955–966 (2003).

188. Feng, Y. *et al.* Mechanosensing drives acuity of αβ T-cell recognition. *Proc. Natl. Acad. Sci. U. S. A.* **114**, E8204–E8213 (2017).

189. Al-Aghbar, M. A., Jainarayanan, A. K., Dustin, M. L. & Roffler, S. R. The interplay between membrane topology and mechanical forces in regulating T cell receptor activity. *Commun. Biol.* **5**, 1–16 (2022).

190. Basu, R. *et al.* Cytotoxic T Cells Use Mechanical Force to Potentiate Target Cell Killing Cytotoxic T Cells Use Mechanical Force to Potentiate Target Cell Killing. *Cell* **165**, 100–110 (2016).

191. Basu, R. & Huse, M. Mechanical Communication at the Immunological Synapse. *Trends Cell Biol.* **27**, 241–254 (2017).

192. Connor, R. S. O. *et al.* Substrate Rigidity Regulates Human T Cell Activation and Proliferation. *J. Immunol.* **189**, 1330–1339 (2012).

193. Judokusumo, E., Tabdanov, E., Kumari, S., Dustin, M. L. & Kam, L. C. Mechanosensing in T lymphocyte activation. *Biophys. J.* **102**, L5–L7 (2012).

194. Saitakis, M. *et al.* Different TCR-induced T lymphocyte responses are potentiated by stiffness with variable sensitivity. *Elife* 1–29 (2017) doi:10.7554/eLife.23190.

195. Iii, R. H. P. & Abel, S. M. Catch Bonds at T Cell Interfaces : Impact of Surface Reorganization and Membrane Fluctuations. *Biophysj* **113**, 120–131 (2017).

196. Liu, B., Chen, W., Evavold, B. D. & Zhu, C. Accumulation of dynamic catch bonds between TCR and agonist peptide-MHC triggers T cell signaling. *Cell* **157**, 357–368 (2014).

197. Pryshchep, S., Zarnitsyna, V. I., Hong, J., Evavold, B. D. & Zhu, C. Accumulation of Serial Forces on TCR and CD8 Frequently Applied by Agonist Antigenic Peptides Embedded in MHC Molecules Triggers Calcium in T Cells. *J. Immunol.* **193**, 68–76 (2014).

198. Wu, P., Zhang, T., Liu, B., Zhu, C. & Chen, W. Mechano-regulation of Peptide-MHC Class I Conformations Determines TCR Antigen Article Mechano-regulation of Peptide-MHC Class I Conformations Determines. *Mol. Cell* **73**, 1015–1027 (2019).

199. Zhao, X. *et al.* Tuning T cell receptor sensitivity through catch bond engineering. *Science (80-.).* **376**, (2022).

200. Linette, G. P. *et al.* Cardiovascular toxicity and titin cross-reactivity of affinity-enhanced T cells in myeloma and melanoma. *Blood* **122**, 863–871 (2013).

201. Cameron, B. J. *et al.* Identification of a titin-derived HLA-A1-presented peptide as a cross-reactive target for engineered MAGE A3-directed T cells. *Sci. Transl. Med.* **5**, (2013).

202. Rotherham, M., Nahar, T., Broomhall, T. J., Telling, N. D. & El Haj, A. J. Remote magnetic actuation of cell signalling for tissue engineering. *Curr. Opin. Biomed. Eng.* **24**, 100410 (2022).

203. Jin, P., Jan, L. Y. & Jan, Y. N. Mechanosensitive Ion Channels: Structural Features Relevant to Mechanotransduction Mechanisms. *Annu. Rev. Neurosci.* **43**, 207–229 (2020).

204. Wang, N., Butler, J. P. & Ingber, D. E. Mechanotransduction Across the Cell Surface and Through the Cytoskeleton. *Science (80-.).* **260**, 1124–1127 (1993).

205. Hogg, N., Laschinger, M., Giles, K. & McDowall, A. T-cell integrins: More than just sticking points. *J. Cell Sci.* **116**, 4695–4705 (2003).

206. Kong, F., García, A. J., Mould, A. P., Humphries, M. J. & Zhu, C. Demonstration of catch bonds between an integrin and its ligand. *J. Cell Biol.* **185**, 1275–1284 (2009).

207. Chen, Y., Ju, L., Rushdi, M., Ge, C. & Zhu, C. Receptor-mediated cell mechanosensing. *Mol. Biol. Cell* **28**, 3134–3155 (2017).

208. Arnaout, M. A., Mahalingam, B. & Xiong, J.-P. Integrin Structure, Allostery, and Bidirectional Signaling. *Annu. Rev. Cell Dev. Biol* **21**, 381–410 (2005).

209. Chen, W. & Zhu, C. Mechanical regulation of T-cell functions. *Immunol. Rev.* **256**, 160–176 (2013).

210. Chen, W., Lou, J. & Zhu, C. Forcing switch from short- to intermediate- and long-lived states of the αA domain generates LFA-1/ICAM-1 catch bonds. *J. Biol. Chem.* **285**, 35967–35978 (2010).

211. Choi, Y. I. *et al.* Dynamic control of β1 integrin adhesion by the plexinD1-sema3E axis. *Proc. Natl. Acad. Sci. U. S. A.* **111**, 379–384 (2014).

212. Rosetti, F. *et al.* A Lupus-Associated Mac-1 Variant Has Defects in Integrin Allostery and Interaction with Ligands under Force. *Cell Rep.* **10**, 1655–1664 (2015).

213. Chen, Y., Lee, H., Tong, H., Schwartz, M. & Zhu, C. Force regulated conformational change of integrin αVβ3. *Matrix Biol.* **60**–**61**, 70–85 (2016).

214. Elosegui-Artola, A. *et al.* Mechanical regulation of a molecular clutch defines force transmission and transduction in response to matrix rigidity. *Nat. Cell Biol.* **18**, 540–548 (2016).

215. Schmidt, C., Pommerenke, H., Dürr, F., Nebe, B. & Rychly, J. Mechanical stressing of integrin receptors induces enhanced tyrosine phosphorylation of cytoskeletally anchored proteins. *J. Biol. Chem.* **273**, 5081–5085 (1998).

216. Pommerenke, H. *et al.* Stimulation of integrin receptors using a magnetic drag force device induces an intracellular free calcium response. *Eur* **70**, 157–164 (1996).

217. Coste, B. *et al.* Piezo1 and Piezo2 are essential components of distinct mechanically-activated cation channels. *Science (80-.).* **330**, 55–60 (2010).

218. Martinac, B. & Cox, C. D. *Mechanosensory Transduction: Focus on Ion Channels ☆. Reference Module in Life Sciences* (2017). doi:10.1016/b978-0-12-809633-8.08094-8.

219. Wang, L. *et al.* Structure and mechanogating of the mammalian tactile channel PIEZO2. *Nature* **573**, 225–229 (2019).

220. Cox, C. D. *et al.* Removal of the mechanoprotective influence of the cytoskeleton reveals PIEZO1 is gated by bilayer tension. *Nat. Commun.* **7**, 1–13 (2016).

221. Lewis, A. H. & Grandl, J. Mechanical sensitivity of Piezo1 ion channels can be tuned by cellular membrane tension. *Elife* **4**, 1–17 (2015).

222. Lin, Y. C. *et al.* Force-induced conformational changes in PIEZO1. *Nature* **573**, 230–234 (2019).

223. Albuisson, J. *et al.* Dehydrated hereditary stomatocytosis linked to gain-of-function mutations in mechanically activated PIEZO1 ion channels. *Nat. Commun.* **4**, (2013).

224. Lukacs, V. *et al.* Impaired PIEZO1 function in patients with a novel autosomal recessive congenital lymphatic dysplasia. *Nat. Commun.* **6**, 1–7 (2015).

225. Fotiou, E. *et al.* Novel mutations in PIEZO1 cause an autosomal recessive generalized lymphatic dysplasia with non-immune hydrops fetalis. *Nat. Commun.* **6**, (2015).

226. Martinac, B. & Cox, C. D. Mechanosensory Transduction: Focus on Ion Channels ☆. in *Module in Life Sciences* (2017). doi:10.1016/b978-0-12-809633-8.08094-8.

227. Michalick, L. & Kuebler, W. M. TRPV4—A Missing Link Between Mechanosensation and Immunity. *Front. Immunol.* **11**, 1–9 (2020).

228. Cheng, W., Yang, F., Takanishi, C. L. & Zheng, J. Thermosensitive TRPV channel subunits coassemble into heteromeric channels with intermediate conductance and gating properties. *J. Gen. Physiol.* **129**, 191–207 (2007).

229. Wu, S. *et al.* Genetically magnetic control of neural system via TRPV4 activation with magnetic nanoparticles. *Nano Today* **39**, 101187 (2021).

230. Wu, S. *et al.* Genetically magnetic control of neural system via TRPV4 activation with

magnetic nanoparticles. *Nano Today* **39**, 101187 (2021).

231. Liu, L. *et al.* Role of Transient Receptor Potential Vanilloid 4 in Vascular Function. *Front. Mol. Biosci.* **8**, 1–11 (2021).

232. Hamanaka, K. *et al.* TRPV4 channels augment macrophage activation and ventilator-induced lung injury. *Am. J. Physiol. - Lung Cell. Mol. Physiol.* **299**, 353–362 (2010).

233. Narita, K. *et al.* TRPV4 regulates the integrity of the blood-cerebrospinal fluid barrier and modulates transepithelial protein transport. *FASEB J.* **29**, 2247–2259 (2015).

234. Yin, J. *et al.* Role of transient receptor potential vanilloid 4 in neutrophil activation and acute lung injury. *Am. J. Respir. Cell Mol. Biol.* **54**, 370–383 (2016).

235. Hughes, S. *et al.* Expression of the mechanosensitive 2PK+ channel TREK-1 in human osteoblasts. *J. Cell. Physiol.* **206**, 738–748 (2006).

236. Hughes, S., McBain, S., Dobson, J. & El Haj, A. J. Selective activation of mechanosensitive ion channels using magnetic particles. *J. R. Soc. Interface* **5**, 855–863 (2008).

237. Henstock, J. R., Rotherham, M. & El Haj, A. J. Magnetic ion channel activation of TREK1 in human mesenchymal stem cells using nanoparticles promotes osteogenesis in surrounding cells. *J. Tissue Eng.* **9**, (2018).

238. Henstock, J. R., Rotherham, M., Rashidi, H., Shakesheff, K. M. & El Haj, A. J. Remotely Activated Mechanotransduction via Magnetic Nanoparticles Promotes Mineralization Synergistically With Bone Morphogenetic Protein 2: Applications for Injectable Cell Therapy. *Stem Cells Transl. Med.* **3**, 1363–1374 (2014).

239. Markides, H. *et al.* Translation of remote control regenerative technologies for bone repair. *npj Regen. Med.* **3**, (2018).

240. Blumenthal, D., Chandra, V., Avery, L. & Burkhardt, J. K. Mouse t cell priming is enhanced by maturation-dependent stiffening of the dendritic cell cortex. *Elife* **9**, 1–44 (2020).

241. Meng, K. P., Majedi, F. S., Thauland, T. J. & Butte, M. J. Mechanosensing through YAP controls T cell activation and metabolism. *J. Exp. Med.* **217**, (2020).

242. Pageon, S. V., Govendir, M. A., Kempe, D. & Biro, M. Mechanoimmunology: Molecular-scale forces govern immune cell functions. *Mol. Biol. Cell* **29**, 1919–1926 (2018).

243. Lekka, M. Discrimination Between Normal and Cancerous Cells Using AFM. *Bionanoscience* **6**, 65–80 (2016).

244. Swaminathan, V. *et al.* Mechanical Stiffness Grades Metastatic Potential in Patient Tumor Cells and in Cancer Cell Lines. *Cancer Res.* **71**, 5075–5080 (2011).

245. Nicolas-Boluda, A. *et al.* Tumor stiffening reversion through collagen crosslinking inhibition improves t cell migration and anti-pd-1 treatment. *Elife* **10**, (2021).

246. Chakraborty, M. *et al.* Mechanical Stiffness Controls Dendritic Cell Metabolism and

Function. *Cell Rep.* **34**, (2021).

247. Meli, V. S. *et al.* YAP-mediated mechanotransduction tunes the macrophage inflammatory response. *Sci. Adv.* **6**, 1–14 (2020).

248. Du, H. *et al.* Tuning immunity through tissue mechanotransduction. *Nat. Rev. Immunol.* 1–15 (2022) doi:10.1038/s41577-022-00761-w.

249. Atcha, H. *et al.* Mechanically activated ion channel Piezo1 modulates macrophage polarization and stiffness sensing. *Nat. Commun.* **12**, 1–14 (2021).

250. Morikis, V. A., Masadeh, E. & Simon, S. I. Tensile force transmitted through LFA-1 bonds mechanoregulate neutrophil inflammatory response. *J. Leukoc. Biol.* **108**, 1815–1828 (2020).

251. Unnithan, A. R. *et al.* Remotely Actuated Magnetic Nanocarpets for Bone Tissue Engineering: Non-Invasive Modulation of Mechanosensitive Ion Channels for Enhanced Osteogenesis. *Adv. Funct. Mater.* (2022) doi:10.1002/adfm.202201311.

252. Hu, K. H. & Butte, M. J. T cell activation requires force generation. *J. Cell Biol.* **213**, 535–542 (2016).

253. Dustin, M. L. & Kam, L. C. Tapping out a mechanical code for T cell triggering. *J. Cell Biol.* **213**, 501–503 (2016).

254. Hoffmann, S. *et al.* Single cell force spectroscopy of T cells recognizing a myelin-derived peptide on antigen presenting cells. *Immunol. Lett.* **136**, 13–20 (2011).

255. Zhu, C., Chen, W., Lou, J., Rittase, W. & Li, K. Mechanosensing through immunoreceptors. *Nat. Immunol.* **20**, 1269–1278 (2019).

256. Liu, G. Y. *et al.* Low avidity recognition of self-antigen by T cells permits escape from central tolerance. *Immunity* **3**, 407–415 (1995).

257. Bending, D. *et al.* A timer for analyzing temporally dynamic changes in transcription during differentiation in vivo. *J. Cell Biol.* **217**, 2931–2950 (2018).

258. Hughes, S., McBain, S., Dobson, J. & El Haj, A. J. Selective activation of mechanosensitive ion channels using magnetic particles. *J. R. Soc. Interface* **5**, 855–863 (2008).

259. Pankhurst, Q., Connolloy, J., Jones, S. & Dobson, J. Applications of magnetic nanoparticles in biomedicine. *J. Phys. D. Appl. Phys.* **36**, R167–R181 (2003).

260. Baun, O. & Blümler, P. Permanent magnet system to guide superparamagnetic particles. *J. Magn. Magn. Mater.* **439**, 294–304 (2017).

261. Pageon, S. V. *et al.* Functional role of T-cell receptor nanoclusters in signal initiation and antigen discrimination. *Proc. Natl. Acad. Sci. U. S. A.* **113**, E5454–E5463 (2016).

262. Shepard, E. R. *et al.* The Mechanism of Action of Antigen Processing Independent T Cell Epitopes Designed for Immunotherapy of Autoimmune Diseases. *Front. Immunol.* **12**, 1–14 (2021).

263. Clayton, L. K. *et al.* T-cell receptor ligation by peptide/MHC induces activation of a

caspase in immature thymocytes: The molecular basis of negative selection. *EMBO J.* **16**, 2282–2293 (1997).

264. Perica, K. *et al.* Nanoscale artificial antigen presenting cells for T cell immunotherapy. *Nanomedicine Nanotechnology, Biol. Med.* **10**, 119–129 (2014).

265. Perica, K. *et al.* Magnetic field-induced t cell receptor clustering by nanoparticles enhances t cell activation and stimulates antitumor activity. *ACS Nano* **8**, 2252–2260 (2014).

266. Kosmides, A. K., Necochea, K., Hickey, J. W. & Schneck, J. P. Separating T Cell Targeting Components onto Magnetically Clustered Nanoparticles Boosts Activation. *Nano Lett.* **18**, 1916–1924 (2018).

267. Reinherz, E. L. αβ TCR-mediated recognition: Relevance to tumor-antigen discovery and cancer immunotherapy. *Cancer Immunol. Res.* **3**, 305–312 (2015).

268. Wang, J. huai & Reinherz, E. L. A new angle on TCR activation. *Immunity* **35**, 658–660 (2011).

269. Sims, T. N. *et al.* Opposing Effects of PKCθ and WASp on Symmetry Breaking and Relocation of the Immunological Synapse. *Cell* **129**, 773–785 (2007).

270. Fritzsche, M. What Is the Right Mechanical Readout for Understanding the Mechanobiology of the Immune Response? *Front. Cell Dev. Biol.* **9**, 2018–2022 (2021).

271. Hanke, J. H. *et al.* Discovery of a novel, potent, and Src family-selective tyrosine kinase inhibitor: Study of Lck- and FynT-dependent T cell activation. *J. Biol. Chem.* **271**, 695–701 (1996).

272. Dienz, O. *et al.* Accumulation of NFAT mediates IL-2 expression in memory, but not naïve, CD4+ T cells. *Proc. Natl. Acad. Sci. U. S. A.* **104**, 7175–7180 (2007).

273. Zikherman, J. & Au-Yeung, B. The role of T cell receptor signaling thresholds in guiding T cell fate decisions. *Curr. Opin. Immunol.* **33**, 43–48 (2015).

274. Jennings, E. *et al.* Nr4a1 and Nr4a3 Reporter Mice Are Differentially Sensitive to T Cell Receptor Signal Strength and Duration. *Cell Rep.* **33**, 1–10 (2020).

275. Walsh, C. T., Zydowsky, L. D. & McKeon, F. D. Cyclosporin A, the cyclophilin class of peptidylprolyl isomerases, and blockade of T cell signal transduction. *J. Biol. Chem.* **267**, 13115–13118 (1992).

276. Jenkins, M., Schwartz, R. & Pardoll, D. Effects of cyclosporine A on T cell development and clonal deletion. *Science (80-.).* **241**, 1655–1658 (1988).

277. Liu, J. *et al.* Calcineurin is a common target of cyclophilin-cyclosporin A and FKBP-FK506 complexes. *Cell* **66**, 807–815 (1991).

278. Jin, L. & Harrison, S. C. Crystal structure of human calcineurin complexed with cyclosporin A and human cyclophilin. *Proc. Natl. Acad. Sci. U. S. A.* **99**, 13522–13526 (2002).

279. Ai, W., Li, H., Song, N., Li, L. & Chen, H. Optimal Method to Stimulate Cytokine

Production and Its Use in Immunotoxicity Assessment. *Int. J. Environ. Res. Public Health* **10**, 3834 (2013).

280. Chatila, T., Silverman, L., Miller, R. & Geha, R. Mechanisms of T cell activation by the calcium ionophore ionomycin. *J. Immunol.* **143**, (1989).

281. Le Borgne, M. *et al.* Real-Time Analysis of Calcium Signals during the Early Phase of T Cell Activation Using a Genetically Encoded Calcium Biosensor. *J. Immunol.* **196**, 1471–1479 (2016).

282. Arrol, H. P., Church, L. D., Bacon, P. A. & Young, S. P. Intracellular calcium signalling patterns reflect the differentiation status of human T cells. *Clin. Exp. Immunol.* **153**, 86–95 (2008).

283. Christo, S. N. *et al.* Scrutinizing calcium flux oscillations in T lymphocytes to deduce the strength of stimulus. *Sci. Reports 2015 51* **5**, 1–8 (2015).

284. Palin, A. *et al.* A TCR mechanotransduction signaling loop induces negative selection in the thymus. *Nat. Immunol.* **19**, (2018).

285. Saitakis, M., Dellaporta, A. & Gizeli, E. Measurement of two-dimensional binding constants between cell-bound major histocompatibility complex and immobilized antibodies with an acoustic biosensor. *Biophys. J.* **95**, 4963–4971 (2008).

286. Xie, Z.-R., Chen, J. & Wu, Y. Linking 3D and 2D binding kinetics of membrane proteins by multiscale simulations. *Protein Sci.* **23**, 1789–1799 (2014).

287. Tolentino, T. P. *et al.* Measuring diffusion and binding kinetics by contact area FRAP. *Biophys. J.* **95**, 920–930 (2008).

288. Dam, T., Chouliara, M., Junghans, V. & Jönsson, P. Supported Lipid Bilayers and the Study of Two-Dimensional Binding Kinetics. *Front. Mol. Biosci.* **9**, (2022).

289. Schodin, B. A., Tsomides, T. J. & Kranz, D. M. Correlation Between the Number of T Cell Receptors Required for T Cell Activation and TCR – Ligand Affinity. **5**, 137–146 (1996).

290. Valitutti, S. & Lanzavecchia, A. Serial triggering of TCRs: A basis for the sensitivity and specificity of antigen recognition. *Immunol. Today* **18**, 299–304 (1997).

291. Valitutti, S., Miller, S., Cella, M., Padovan, E. & Lanzavecchia, A. Serial triggering of many T-cell receptors by a few peptide-MHC complexes. *Nature* **375**, 148–151 (1995).

292. Lanzavecchia, A., Iezzi, G. & Viola, A. From TCR engagement to T cell activation: A kinetic view of T cell behavior. *Cell* **96**, 1–4 (1999).

293. Au-Yeung, B. B. *et al.* Quantitative and Temporal Requirements Revealed for Zap-70 Catalytic Activity During T Cell Development. *Nat. Immunol.* **15**, 687–694 (2014).

294. Au-Yeung, B. B. *et al.* A sharp T-cell antigen receptor signaling threshold for T-cell proliferation. *Proc. Natl. Acad. Sci. U. S. A.* **111**, E3679–E3688 (2014).

295. Moogk, D. *et al.* Constitutive Lck Activity Drives Sensitivity Differences between CD8 + Memory T Cell Subsets . *J. Immunol.* **197**, 644–654 (2016).

296. Snook, J. P., Kim, C. & Williams, M. A. TCR signal strength controls the differentiation of CD4+ effector and memory T cells. *Sci. Immunol.* **3**, (2018).

297. Li, J. P. *et al.* The phosphatase JKAP/DUSP22 inhibits T-cell receptor signalling and autoimmunity by inactivating Lck. *Nat. Commun.* **5**, 1–13 (2014).

298. Amit, I. *et al.* A module of negative feedback regulators defines growth factor signaling. *Nat. Genet. 2007 394* **39**, 503–512 (2007).

299. Huang, F. *et al.* Establishment of the major compatibility complex-dependent development of CD4+ and CD8+ T cells by the Cbl family proteins. *Immunity* **25**, 571–581 (2006).

300. Naramura, M., Kole, H. K., Hu, R. J. & Gu, H. Altered thymic positive selection and intracellular signals in Cbl-deficient mice. *Proc. Natl. Acad. Sci. U. S. A.* **95**, 15547–15552 (1998).

301. Hao, Y. K., Charras, G. T., Mitchison, T. J. & Brieher, W. M. Actin disassembly by cofilin, coronin, and Aip1 occurs in bursts and is inhibited by barbed-end cappers. *J. Cell Biol.* **182**, 341–353 (2008).

302. Spector, I., Shochet, N. R., Kashman, Y. & Groweiss, A. Latrunculins: Novel marine toxins that disrupt microfilament organization in cultured cells. *Science (80-.).* **219**, 493–495 (1983).

303. van der Donk, L. E. H. *et al.* Separate signaling events control TCR downregulation and T cell activation in primary human T cells. *Immunity, Inflamm. Dis.* **9**, 223–238 (2021).

304. Razvag, Y., Neve-Oz, Y., Sajman, J., Sherman, E. & Reches, M. Nanoscale kinetic segregation of TCR and CD45 in engaged microvilli facilitates early T cell activation. *Nat. Commun.* **9**, (2018).

305. Hashimoto-Tane, A. *et al.* T-Cell Receptor Microclusters Critical for T-Cell Activation Are Formed Independently of Lipid Raft Clustering. *Mol. Cell. Biol.* **30**, 3421–3429 (2010).

306. Hashimoto-Tane, A. & Saito, T. Dynamic regulation of TCR-microclusters and the microsynapse for T cell activation. *Front. Immunol.* **7**, 1–8 (2016).

307. Kumar, R. *et al.* Article Increased Sensitivity of Antigen-Experienced T Cells through the Enrichment of Oligomeric T Cell Receptor Complexes. (2011) doi:10.1016/j.immuni.2011.08.010.

308. Castro, M. *et al.* Receptor pre-clustering and T cell responses: Insights into molecular mechanisms. *Front. Immunol.* **5**, 132 (2014).

309. Mannix, R. J. *et al.* Nanomagnetic actuation of receptor-mediated signal transduction. *Nat. Nanotechnol.* **3**, 36–40 (2008).

310. Sušac, L. *et al.* Structure of a fully assembled tumor-specific T cell receptor ligated by pMHC. *Cell* **185**, 3201–3213 (2022).

311. Ma, Z., Discher, D. & Finkel, T. H. Mechanical force in T cell receptor signal initiation. *Front. Immunol.* **3**, 1–3 (2012).

312. Evnouchidou, I., Caillens, V., Koumantou, D. & Saveanu, L. The role of endocytic trafficking in antigen T cell receptor activation. *Biomed. J.* **45**, 310–320 (2022).

313. Shakiba, M. *et al.* TCR signal strength defines distinct mechanisms of T cell dysfunction and cancer evasion. *J. Exp. Med.* **219**, (2021).

314. Gallegos, A. M. *et al.* Control of T cell antigen reactivity via programmed TCR downregulation. *Nat. Immunol.* **17**, 379–386 (2016).

315. Trefzer, A. *et al.* Dynamic adoption of anergy by antigen-exhausted CD4+ T cells. *Cell Rep.* **34**, (2021).

316. Gallegos, A. M., Pamer, E. G. & Glickman, M. S. Delayed protection by ESAT-6–specific effector CD4+ T cells after airborne M. tuberculosis infection. *J. Exp. Med.* **205**, 2359–2368 (2008).

317. Gallegos, A. M. *et al.* A Gamma Interferon Independent Mechanism of CD4 T Cell Mediated Control of M. tuberculosis Infection in vivo. *PLOS Pathog.* **7**, (2011).

318. Elliot, T. A. E. *et al.* Antigen and checkpoint receptor engagement recalibrates T cell receptor signal strength. *Immunity* **54**, 2481–2496 (2021).

319. Kretschmer, K. *et al.* Inducing and expanding regulatory T cell populations by foreign antigen. *Nat. Immunol.* **6**, 1219–1227 (2005).

320. Apostolou, I. & Von Boehmer, H. In vivo instruction of suppressor commitment in naive T cells. *J. Exp. Med.* **199**, 1401–1408 (2004).

321. Sauer, S. *et al.* T cell receptor signaling controls Foxp3 expression via PI3K, Akt, and mTOR. *Proc. Natl. Acad. Sci. U. S. A.* **105**, 7797–7802 (2008).

322. Han, J. M., Patterson, S. J. & Levings, M. K. The Role of the PI3K Signaling Pathway in CD4+ T Cell Differentiation and Function. *Front. Immunol.* **3**, (2012).

323. Garçon, F. *et al.* CD28 provides T-cell costimulation and enhances PI3K activity at the immune synapse independently of its capacity to interact with the p85/p110 heterodimer. *Blood* **111**, 1464–1471 (2008).

324. Richardson, N. & Wraith, D. C. Advancement of antigen-specific immunotherapy: knowledge transfer between allergy and autoimmunity. *Immunother. Adv.* **1**, 1–16 (2021).

325. Schurgers, E. & Wraith, D. C. Induction of Tolerance to Therapeutic Proteins With Antigen-Processing Independent T Cell Epitopes: Controlling Immune Responses to Biologics. *Front. Immunol.* **12**, (2021).

326. Künzli, M., Reuther, P., Pinschewer, D. D. & King, C. G. Opposing effects of T cell receptor signal strength on CD4 T cells responding to acute versus chronic viral infection. *Elife* **10**, (2021).

327. Akkaya, B. & Shevach, E. M. Regulatory T cells: Master thieves of the immune system. *Cell. Immunol.* **355**, 104160 (2020).

328. Shevach, E. M. Mechanisms of Foxp3+ T Regulatory Cell-Mediated Suppression.

Immunity **30**, 636–645 (2009).

329. Bhattacharyya, N. D. & Feng, C. G. Regulation of T Helper Cell Fate by TCR Signal Strength. *Front. Immunol.* **11**, 1–14 (2020).

330. Han, S., Asoyan, A., Rabenstein, H., Nakano, N. & Obst, R. Role of antigen persistence and dose for CD4+ T-cell exhaustion and recovery. *Proc. Natl. Acad. Sci. U. S. A.* **107**, 20453–20458 (2010).

331. Liu, C. S. C. *et al.* Cutting Edge: Piezo1 Mechanosensors Optimize Human T Cell Activation. *J. Immunol.* **200**, 1255–1260 (2018).

332. Jairaman, A. *et al.* Piezo1 channels restrain regulatory T cells but are dispensable for effector CD4+ T cell responses. *Sci. Adv.* **7**, (2021).

333. Majhi, R. K. *et al.* Functional expression of TRPV channels in T cells and their implications in immune regulation. *FEBS J.* **282**, 2661–2681 (2015).

334. Harris, M. J., Fuyal, M. & James, J. R. Quantifying persistence in the T-cell signaling network using an optically controllable antigen receptor. *Mol. Syst. Biol.* **17**, 1–20 (2021).

335. Gunzer, M. *et al.* Antigen presentation in extracellular matrix: Interactions of T cells with dendritic cells are dynamic, short lived, and sequential. *Immunity* **13**, 323–332 (2000).

336. Wilson, M. Z., Ravindran, P. T., Lim, W. A. & Toettcher, J. E. Tracing Information Flow from Erk to Target Gene Induction Reveals Mechanisms of Dynamic and Combinatorial Control. *Mol. Cell* **67**, 757–769 (2017).

337. Acuto, O., Bartolo, V. Di & Michel, F. Tailoring T-cell receptor signals by proximal negative feedback mechanisms. *Nat. Rev. Immunol.* **8**, 699–712 (2008).

338. Sims, T. N. *et al.* Opposing Effects of PKCθ and WASp on Symmetry Breaking and Relocation of the Immunological Synapse. *Cell* **129**, 773–785 (2007).

339. Yam, P. T. *et al.* Actin-myosin network reorganization breaks symmetry at the cell rear to spontaneously initiate polarized cell motility. *J. Cell Biol.* **178**, 1207–1221 (2007).

340. Arsenio, J., Metz, P. J. & Chang, J. T. Asymmetric Cell Division in T Lymphocyte Fate Diversification. *Trends Immunol.* **36**, 670–683 (2015).

341. Dustin, M. L. The Cellular Context of T Cell Signaling. *Immunity* **30**, 482–492 (2009).

342. Wauters, A. C. *et al.* Artificial Antigen-Presenting Cell Topology Dictates T Cell Activation. *ACS Nano* **16**, 15072–15085 (2022).

343. Gabryšová, L. & Wraith, D. C. Antigenic strength controls the generation of antigen-specific IL-10-secreting T regulatory cells. *Eur. J. Immunol.* **40**, 1386–1395 (2010).

344. Burton, B. R. *et al.* Sequential transcriptional changes dictate safe and effective antigen-specific immunotherapy. *Nat. Commun.* **5**, (2014).

CHAPTER 8

8 Appendix

8.1 TCR Downregulation Kinetics with 1µm^{Mid} MNPs

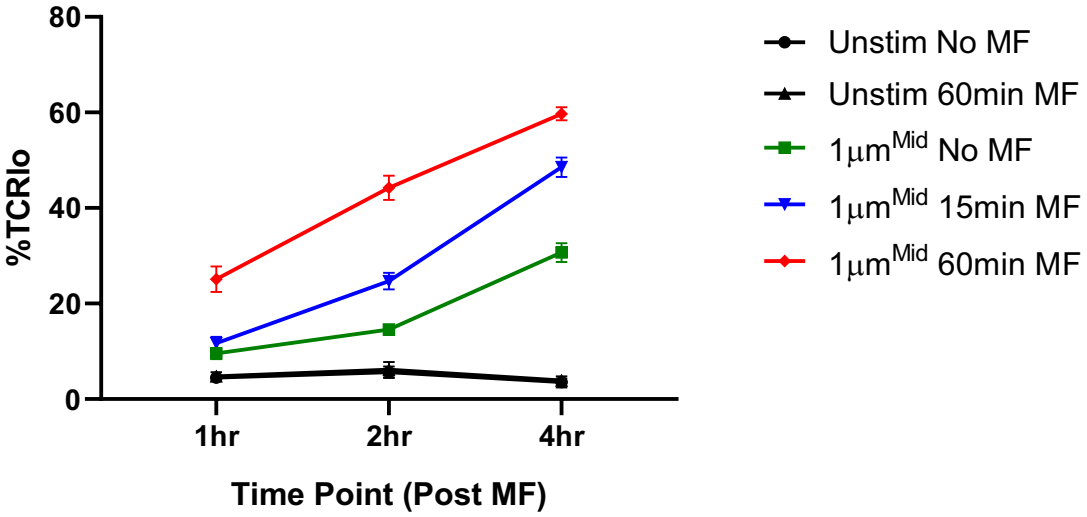


Figure 8.1 - TCR downregulation kinetics in response to 1µm^{Mid} MNPs and magnetic force application. Purified CD4^{+} T cells from Nr4a3-FT mice were treated with 1µm^{Mid} MNPs as described in 2.6, before being stimulated with magnetic force as per 2.7. Cells were analysed for TCR downregulation by flow cytometry at 1, 2 and 4 hour time points post force application. Data shown from 1 experiment containing 2 biological replicates.

8.2 Inhibition of Calmodulin with Cyclosporin A Does Not Inhibit TCR Downregulation

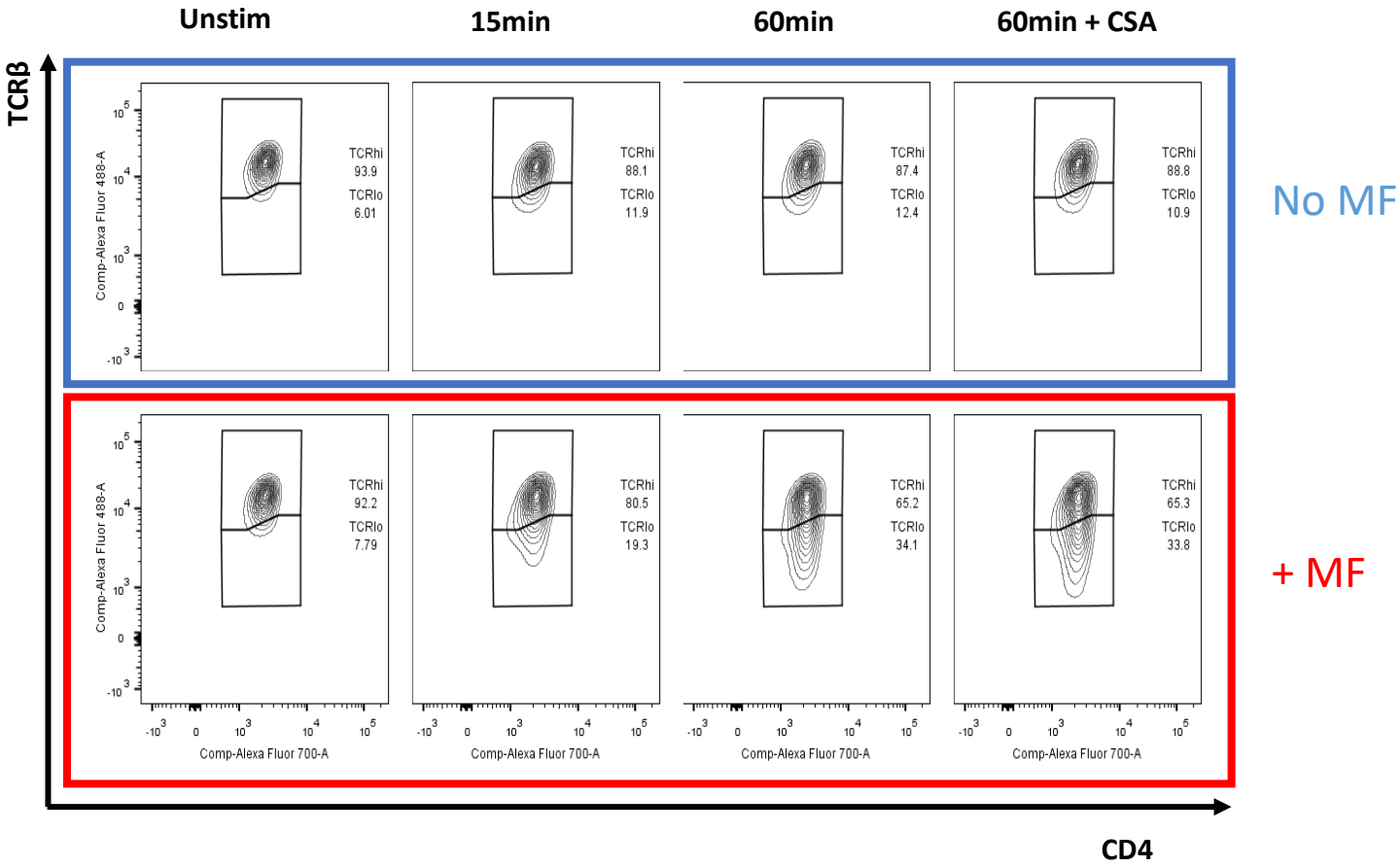


Figure 8.2 - Blockade of the NFAT pathway with CsA does not prevent force induced TCR downregulation. $CD4^+$ Nr4a3-FT T cells were treated with $1\mu m^{Mid}$ MNPs, or left unstimulated, and subjected to magnetic force for time frames shown. Where indicated, cells were also pre-treated with CsA to a final concentration of 1µM which was maintained throughout the culture. Plots representative of 3 independent experiments.

8.3 Halbach Array Calcium Signalling Experiments

To assess calcium signalling in response to shear force application with the Halbach array, purified $CD4^+$ T cells from the Tg4 mouse were loaded with the Fura-2 AM calcium indicator dye, treated with functionalised MNPs ($250nm^{Mid}$ anti-CD3:CD28, or $1\mu m^{Mid}$ / $1\mu m^{Hi}$ CD3, or irrelevant off target controls as shown) on ice as previously described and subjected to

shear forces with the Halbach array whilst monitoring calcium influx by live microscopy as per 2.11.3.

Appendix figure 8.3 shows normalised calcium signalling signatures in response to shear forces, when cells were either not treated with particles (unstimulated) or were bound to 250nm^{Mid} MNP particles functionalised with anti-CD3 and CD28 antibodies as previously described. To assess the specificity of any observed calcium signalling, cells were also treated with either 50µg/mL Nifedipine (a non-specific calcium channel blocker) or 10µM PP2. Use of the Src kinase inhibitor PP2 has previously been shown to significantly inhibit calcium signalling downstream of TCR ligation[47]. Calcium signatures were significantly increased in response to shear forces when cells were treated with 250nm^{Mid} anti-CD3:CD28 MNPs when compared to unstimulated controls, and whilst this increase in calcium signalling appeared to be partially blocked by treatment with Nifedipine, pre-treatment with 10µM PP2 appeared to have less of an effect (appendix figure 8.3A). Additionally, 250nm MNPs functionalised with CD28 alone as an off-target control also produced the same increase in calcium signalling in response to shear force application (appendix figure 8.3B). Experiments targeting the TCR-CD3 complex alongside off target controls with 1µm MNPs produce similar results (appendix figure 8.4). Taken together, these results suggest that shear force application via the Halbach array does not induce TCR specific signalling and instead may induce localised membrane stresses resulting in partial membrane deformation and subsequent calcium entry. The fact that treatment with PP2 does not block this response provides support for this hypothesis.

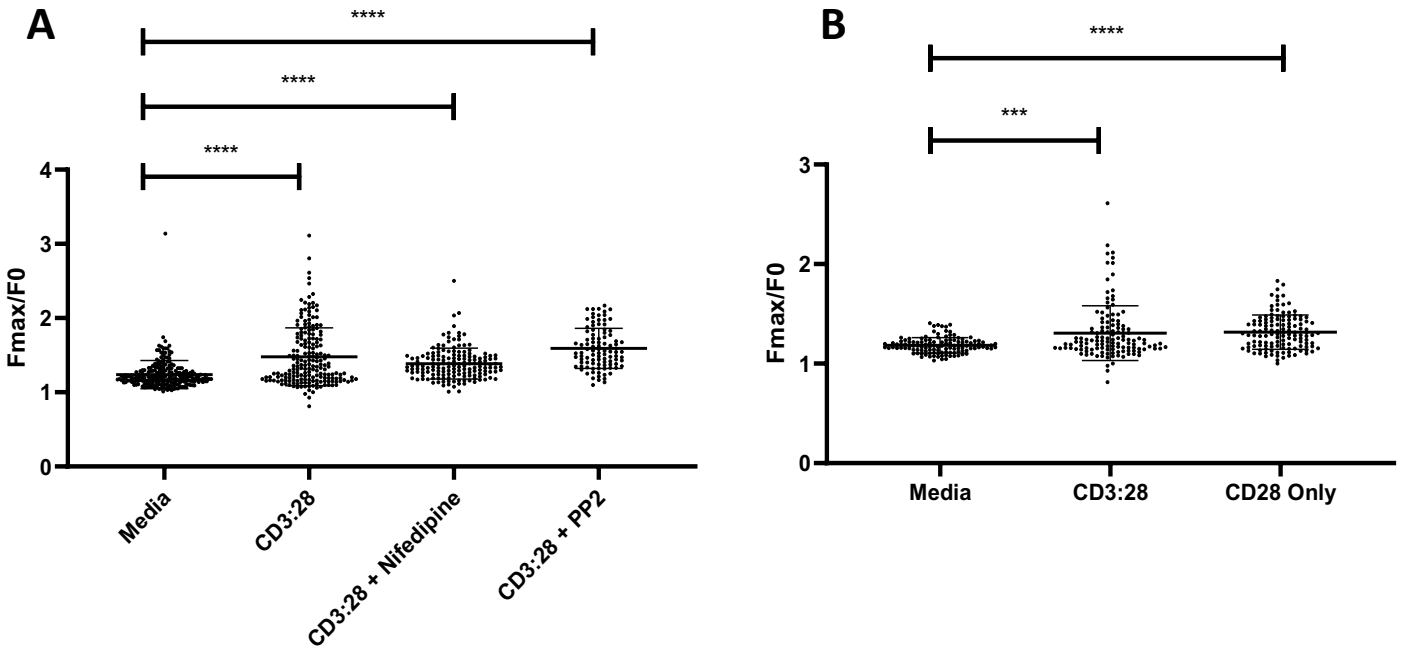


Figure 8.3 – Calcium signalling with shear force application – 250nm^{Mid} MNPs. Calcium signalling responses from CD4^{+} T cells isolated from Tg4 mice were assessed as described in section 2.11. Calcium signalling responses to shear force application were observed to be non-TCR specific, evidenced through the inability of PP2 to block the signal (A) and calcium signalling induction when using non-TCR targeting coated MNPs (B).

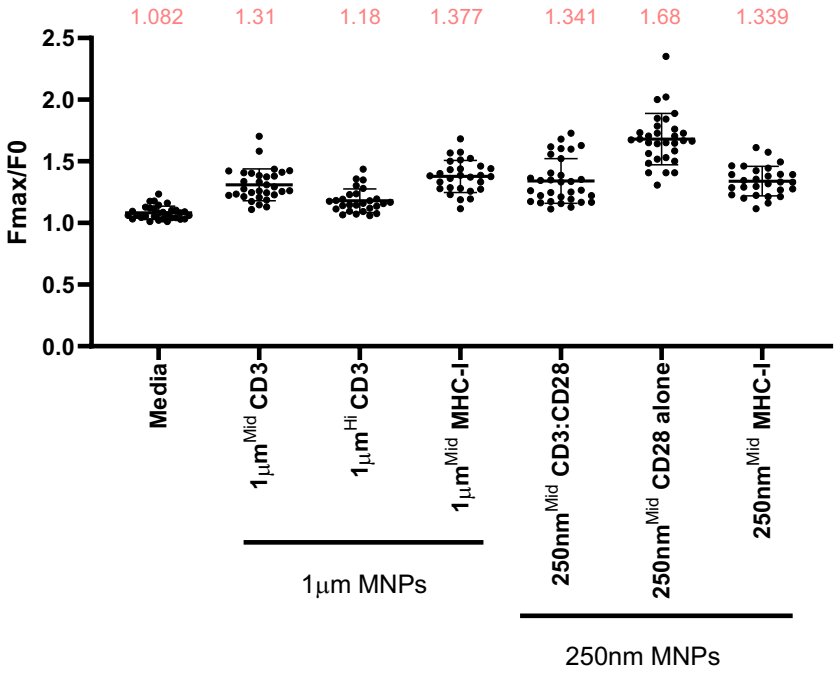


Figure 8.4 – Calcium signalling with shear force application – 1μm MNPs. Calcium signalling responses as per section 2.11 with both 1μm^{Mid} and 250nm^{Mid} MNPs were found to be induced when particles were functionalised with irrelevant, off target antibody controls. Red text indicates the mean Fmax/F0 for each condition.

8.4 Magnetic Force Application to Tg4 Th1 cells Fails to Upregulate T Cell Activation Marker CD69

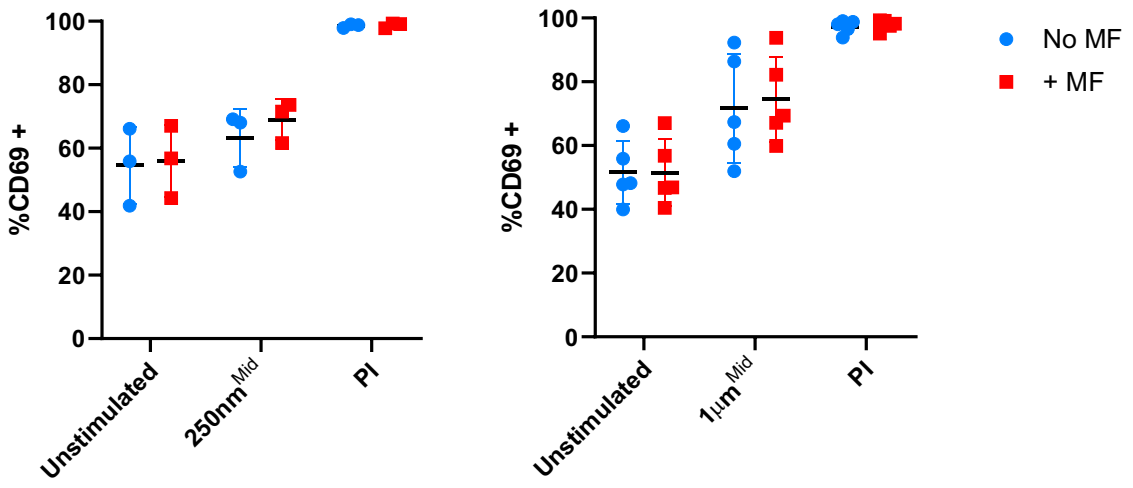


Figure 8.5 - Magnetic force application to Tg4 Th1 cells fails to induce upregulation of CD69. Th1 cells from the Tg4 mouse were produced *in vitro* as per 2.16, before use in a magnetic force application experiment with MICA as described in 2.7. Briefly, cells were treated with either 250nm^{Mid} or 1µm^{Mid} anti-CD3 MNPs as per 2.6 and treated with +/- 1 hour of magnetic force (MF) as per 2.7. CD69 expression was measured by flow cytometry 4 hours post force application. MF application to either particle fails to induce upregulation of CD69 expression of Tg4 Th1 cells. Data shown from 3 (250nm^{Mid} MNPs) or 5 (1µm^{Mid} MNPs) independent experiments.

8.5 Surface Expression of Antigen Presentation Machinery Proteins by PL8 Cells

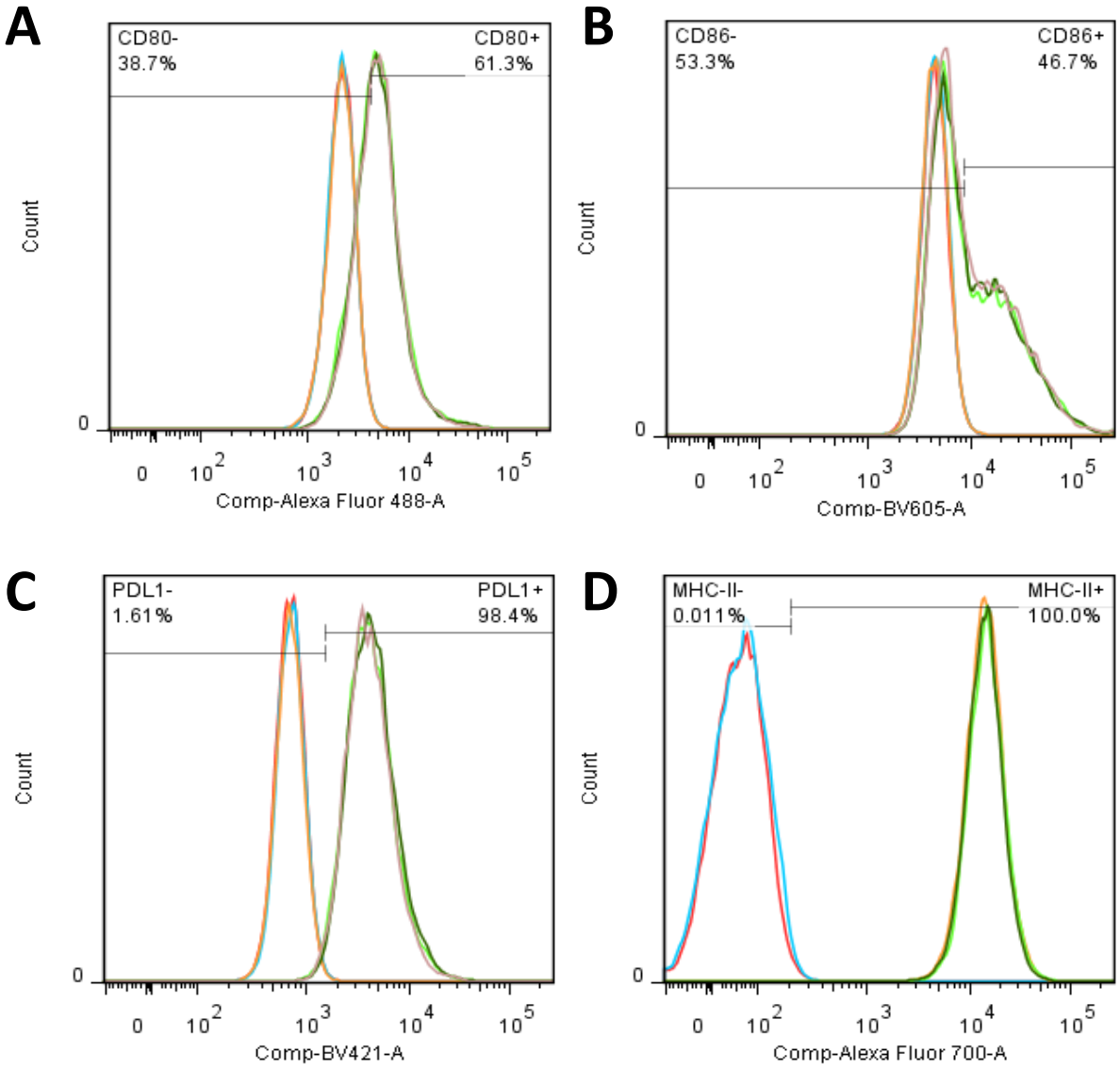


Figure 8.6 - Cell surface expression of proteins involved in the antigen presentation machinery by PL8 cells. PL8 cells were surface stained as per 2.9.1 for CD80 (A), CD86 (B), PD-L1 (C) or MHC-II (D). Representative FACS plots shown detail histograms for samples stained in triplicate overlayed onto FMO (fluorescence minus one) controls for each target.

8.6 Blockade of CTLA-4 and PD-1 does not reverse the anergic phenotype observed in 1µm^{Hi} MNP stimulated cells

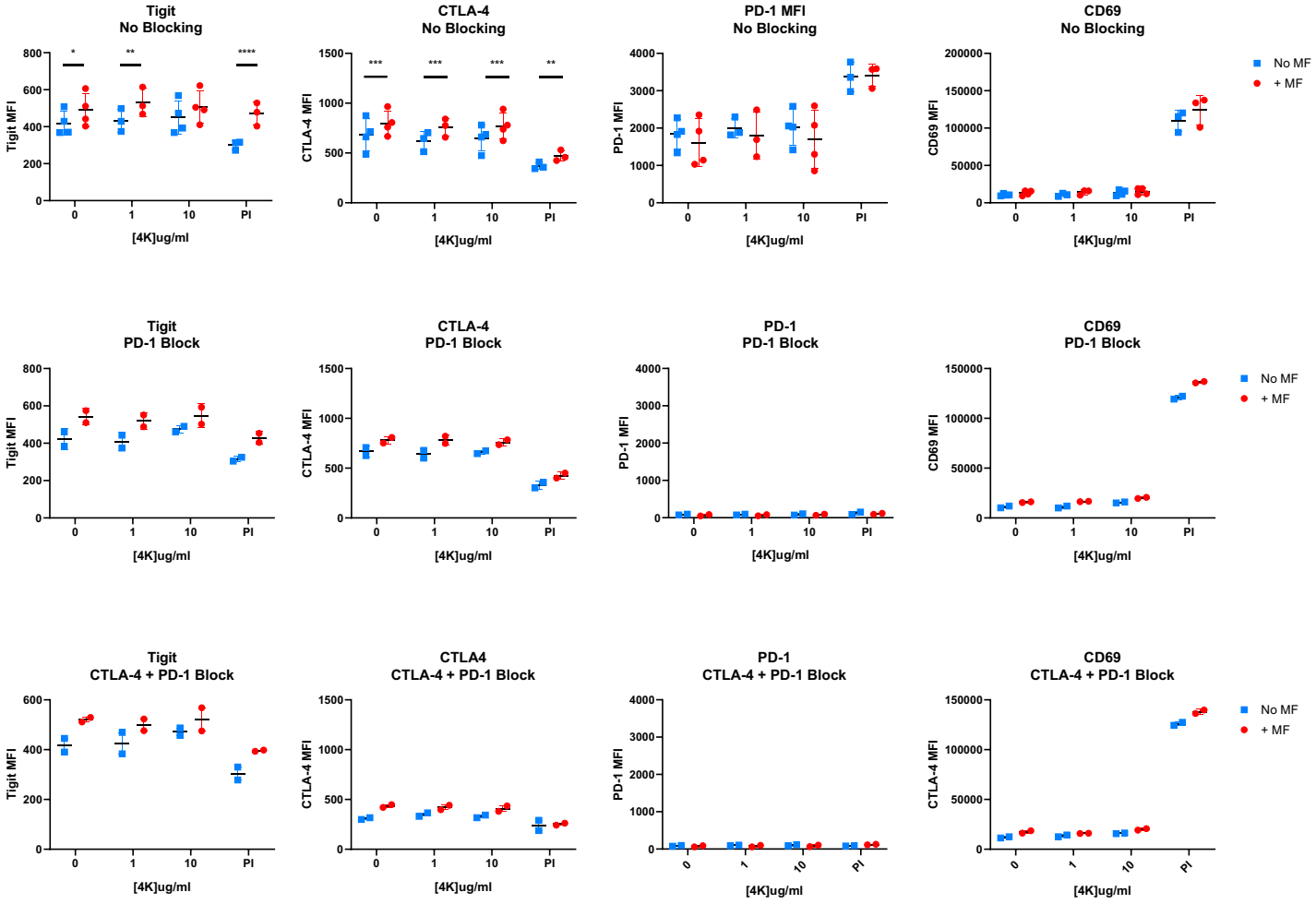


Figure 8.7 - PD-1 blockade or dual CTLA-4 and PD-1 blockade does not restore TCR dependent CD69 expression. CD4^{+} T cells were stimulated with 1µm^{Hi} MNPs +/- magnetic force for 1 hour as previously described and maintained in culture for 72 hours in the presence of 20U/mL IL-2 before restimulation as per 2.13. At the point of restimulation, the effect of CTLA-4 and/or PD-1 blocking antibodies were assessed as described in 2.13.1. Data shown from 2 independent experiments.

8.7 Surface Phenotype of CD4⁺ FoxP3- T cells in Suppression Assays

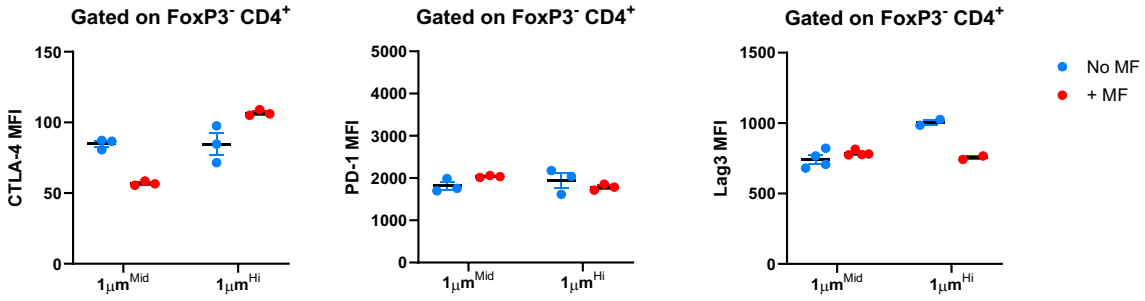


Figure 8.8 - Cell surface co-inhibitory receptor expression on 1µm MNP stimulated FoxP3⁻ CD4⁺ T cells at 72 hours. CD4⁺ T cells stimulated with 1µm^{Mid} or 1µm^{Hi} MNPs were stained for FoxP3⁺ expression at 72 hours as per 2.9.6, together with surface staining for various co-inhibitory receptors as per 2.9.1. Graphs show co-inhibitory receptor expression on CD4⁺ FoxP3⁻ populations. Data shown from one individual experiment, representative of at least 3 independent repeats.

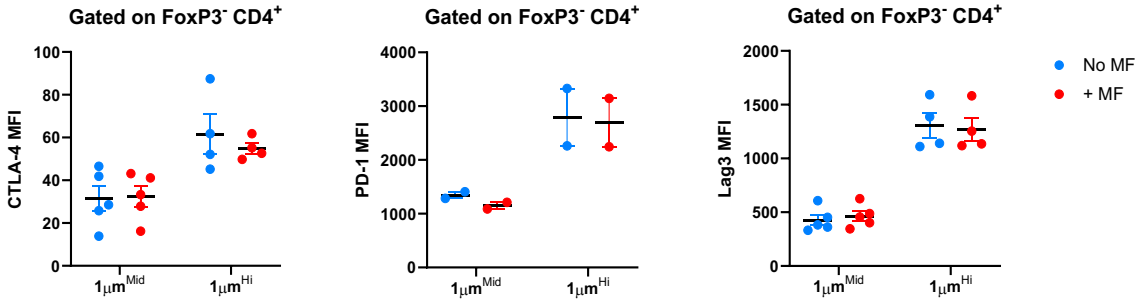


Figure 8.9 - Cell surface co-inhibitory receptor expression on 1µm MNP stimulated FoxP3⁻ CD4⁺ T cells at day 7. CD4⁺ T cells stimulated with 1µm^{Mid} or 1µm^{Hi} MNPs were stained for FoxP3⁺ expression at day 7 as per 2.9.6, together with surface staining for various co-inhibitory receptors as per 2.9.1. Graphs show co-inhibitory receptor expression on CD4⁺ FoxP3⁻ populations. Data shown from one individual experiment, representative of at least 3 independent repeats.

8.8 Pulsatile Magnetic Force Application to 1µm^{Hi} MNPs Appears to Prevent CTLA-4 Upregulation

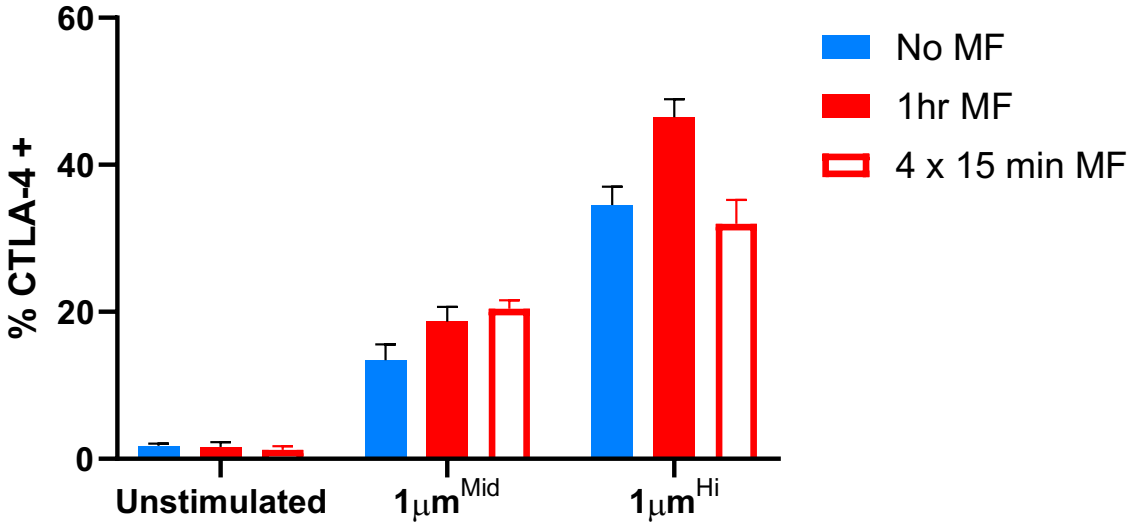


Figure 8.10 - Pulsatile magnetic force application to 1µm^{Hi} MNPs prevents upregulation of CTLA-4. Nr4a3-FT CD4^{+} T cells were treated with 1µm^{Mid} or 1µm^{Hi} MNPs as described in 2.6 and subjected to either a 1 hour pulse of magnetic force (MF), or 4 rounds of 15 minutes of MF each separated by a 15 minute gap so that total 'ON' time equalled 1 hour. CTLA-4 expression was assessed by flow cytometry 4 hours post force application. CTLA-4 was found to be upregulated with 1 hour MF to 1µm^{Hi} MNPs (solid red bars), an effect which was absent when force application was pulsed for 4 rounds of 15 minutes (hollow red bars). Bar graphs shown mean ± SD for 2 biological repeats from 1 independent experiment.